DESIGN OF A 3 AXIS WEAR TESTING DEVICE TO EVALUATE THE EFFECT OF SLIDE TO ROLL RATIO ON ULTRA HIGH MOLECULAR WEIGHT POLYETHYLENE WEAR IN TOTAL KNEE REPLACEMENTS

A thesis

submitted in partial fulfillment

of the requirements for the Degree

of

Master of Engineering in Mechanical Engineering

in the

University of Canterbury

by

Benjamin Low

Department of Mechanical Engineering

University of Canterbury

Christchurch

New Zealand

August 2005

ABSTRACT

Multidirectional motion occurs in total knee replacements (TKR), is a major factor in ultra high molecular weight polyethylene (UHMWPE) wear and is a requirement for wear tester and simulators. There are three ways the femoral component can move relative to the tibial component; sliding, rolling and gliding and these are defined by the slide to roll ratio. Previous wear tester research has investigated the effects of multidirectional motion and slide to roll ratio, individually but not combined. The project aim was to design a machine that combined multidirectional motion with variable slide to roll ratio. A three station wear testing machine was designed and built featuring flexion extension, variable anterior posterior translation, variable internal external rotation and a 2KN load per station. The TKR was simplified to a cylinder on flat. Lubrication was 25% bovine serum and each station had its own recirculation system.

A million cycle validation test was successfully carried out on non-irradiated UHMWPE samples using a slide to roll ratio of 1 : 0.5 and the mean wear rate was 14.7mg/10^6 cycles. Polished areas and scratches from 3rd body abrasion were observed. Magnification revealed a fine ripple pattern with a 1-2μm periodicity. Ripples were randomly oriented, perpendicular to the primary direction of motion and a small number were running parallel to the primary direction of motion, indicative of rolling motion. The results from the validation study show that the knee joint wear tester is capable of producing wear rates and wear mechanisms similar to those observed in other wear testers and knee joint simulators and has met the aim of the project.

ACKNOWLEDGEMENTS

I would like to thank all the people who have helped me throughout the course of this project. My supervisor Dr Milo Kral for his supervision, support, patience, materials advice and behind the scenes work to ensure the knee joint wear tester got build. The Mechanical Engineering Department for the resources they put into this project. Drs Shayne Gooch and Keith Alexander for their expert advice and help with some of the design work. Drs Mark Staiger and John Smaill for their help on some materials matters. I would like to thank the technical staff of the Department of Mechanical Engineers, in particular Scott Amies for managing the construction of the device and building some of the components, and Paul Wells for answering my silly questions with a smile and "of course we can do it Ben". Julian Murphy and Julian Phillips for their fast and efficient wiring up of the machine and its instrumentation. Most importantly I would like to thank Ken Brown, for the months of work spent constructing the machine and the highly accurate job performed.

I would like to thank Paul Morrison and Enztec Ltd for their financial contribution to the construction of the wear tester and for the opportunity they provided me to work on interesting projects in the bio-engineering field. I would also like to thank Dr James Burn for getting me started in this area of replacement knee joint research.

I would like to thank Perplas Medical and Zimmer for the donation of UHMWPE samples.

I would like to thank the other postgraduate students with whom I have shared my time completing this degree. Your presence and friendship has been highly valued. In particular I would like to thank Dr Iain McMillian, who has now completed, for his design advice and discussions about this project. I would also like to thank my flatmates over the course of this project. Steve, Emily and a large number of short term exchange students. You have all been easy to get along with and fun to have around.

Finally I would like to thank my family for all the support and encouragement they have given me.

TABLE OF CONTENTS

LIST OF FIGURES

LIST OF TABLES

1 INTRODUCTION

1.1

Arthritis is a degenerative disease of the cartilage and articular structures in joints, causing pain, loss of mobility and function for millions of people world wide. There are two forms: the more common osteoarthritis or “old age wear and tear on the joints” and rheumatoid arthritis, which is an immune system disorder that destroys the joints. It can often be treated with analgesics, but more serious cases require replacement of the joint surfaces to restore mobility and give freedom from pain. The hip and knee are the joints most often replaced.

The standard total knee replacement (TKR) consists of a very hard, polished cobalt chrome femoral component fitted over the distal (bottom) end of the femur articulating against an ultra high molecular weight polyethylene (UHMWPE) tibial component that resurfaces the proximal (top) end of the tibia. This material combination provides a low friction joint, low wear rates and generally excellent results for the short and medium term. Long term, the sub micron sized UHMWPE wear debris produces an inflammatory immune system response that can lead to resorption of the bone supporting the implant, leading to pain, loosening of the implant and the requirement for revision surgery to replace the TKR.

Numerous industry and academic groups are carrying out research into cobalt chrome on UHMWPE and other bearing combinations, to gain a better understanding of the wear properties and wear mechanisms that occur in vivo. Their objective is to increase the survival rates and to extend the functional lives of TKR, through a reduction in the number of inflammatory wear debris particles produced.

This research was originally carried out using linear reciprocating test rigs with a polyethylene pin on a cobalt chrome disc. These simple rigs have since been shown to produce erroneous results as the motions experienced by TKR in vivo are multidirectional rather than linear and UHMWPE exhibits anisotropic properties under multidirectional motion. At the other end of the spectrum are full knee joint simulators, often costing over $US300,000, that test commercially available TKR and apply physiologically accurate loads and motions. Of intermediate complexity are knee joint wear testers that use a CoCr or stainless steel cylinder or sphere on a UHMWPE flat to represent the TKR and have a simplified motion profile. These devices are used for the preliminary investigations into new materials and for research into the wear mechanisms of TKR.

As a TKR undergoes flexion during walking, the motion between the two components is initially rolling, but this changes to a sliding motion during greater flexion angles. Previous research on linear test rigs has shown the wear mechanisms for rolling differ from those of sliding. Other researchers have carried out experiments on

multidirectional knee joint wear testers, but have only investigated one slide to roll ratio.

The aim of this project is to develop a low cost knee joint wear testing machine capable of filling this gap in the research, by combining a variable slide to roll ratio with multidirectional motion.

1.2 THESIS ORGANISATION

Chapter two is a literature review covering the anatomy of the knee and the loads and motions of the joint, followed by a brief explanation of arthritis and current TKR. It then goes into more detail covering knee joint simulators and wear testers that have been used to develop theories on UHMWPE wear mechanisms, with a special emphasis on the importance of multi-directional motion and slide to roll ratio. Chapter three is the design specification, discussing the load, motions, contact conditions and other factors required to meet the project aim. Chapter four covers the design process of the knee joint wear tester, the rationale for the chosen solution and presents the final design. Chapter five is the validation of the machine, including the results from a one million cycles wear test. Conclusions and recommendations for future work are included in chapter six.

2 LITERATURE REVIEW

2.1 THE KNEE JOINT

2.1.1 STRUCTURE OF THE KNEE JOINT

The knee is a complicated synovial hinge type joint between the femur and tibia with an intermediate articulation between the femur and the patella. The synovial joint is defined by a joint cavity, articular cartilage and an articular capsule consisting of a fibrous capsule lined with synovial membrane. Lubrication of the joint is provided by synovial fluid from the synovial membrane, giving nearly frictionless motion.

The main surfaces of the joint, which are covered in articular cartilage, are the convex medial and lateral condyles of the femur, the medial and lateral condyles of the tibia, also known as the tibial plateau, and the posterior surface of the patella. The femoral condyles sit in the slightly concave tibial condyles while the patella sits in front of the femur, in the groove between the femoral condyles. Figure 2-1 shows the knee in flexion with the patella removed for clarity.

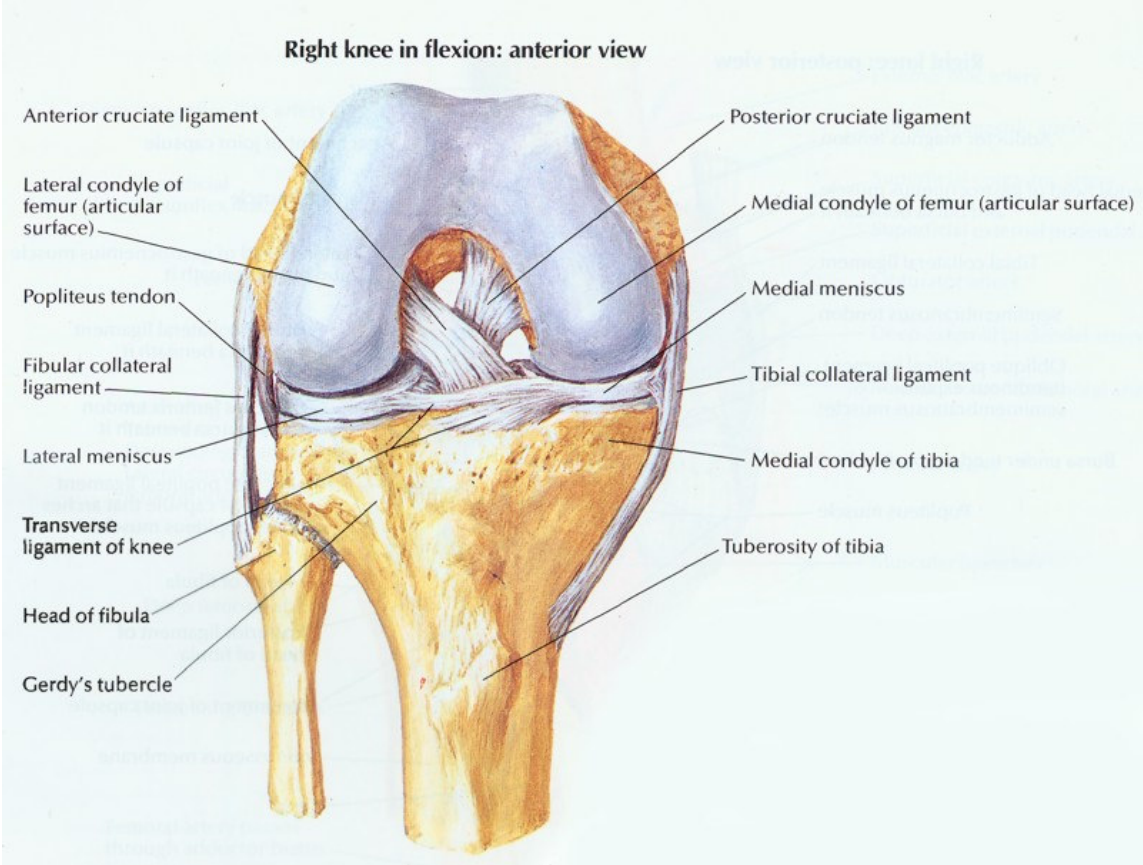

Figure 2-1 Right knee in flexion: anterior view [1]

The tibial condyles are partially covered by the medial and lateral menisci, crescent shaped pieces of fibrocartilage. The menisci are firmly attached round the outside of the tibial plateau but are unattached nearer the center. These act as shock absorbers for the knee joint and fill in some of the gaps between the incongruent femoral and tibial condyles.

The knee joint is mechanically rather weak due to the configuration of the articular surfaces, most of the stability being provided by muscles and ligaments running

between the femur and the tibia. The major ligaments of the knee are the two cruciates, the two collateral ligaments and the patella ligament, which is also known as the patella tendon. The anterior and posterior cruciate ligaments (ACL and PCL) attach between the medial and lateral condyles and form a cross which controls the anterior-posterior displacement of the tibia relative to the femur. The fibular and tibial collateral ligaments are on the medial and lateral sides of the knee respectively. The patella ligament attaches the patella to the tibia and transmits the motion and forces from the quadriceps. The menisci of the knee and the cruciate ligaments are shown in Figure 2-2 and Figure 2-3 is a cross section through the knee showing the general layout of the joint.

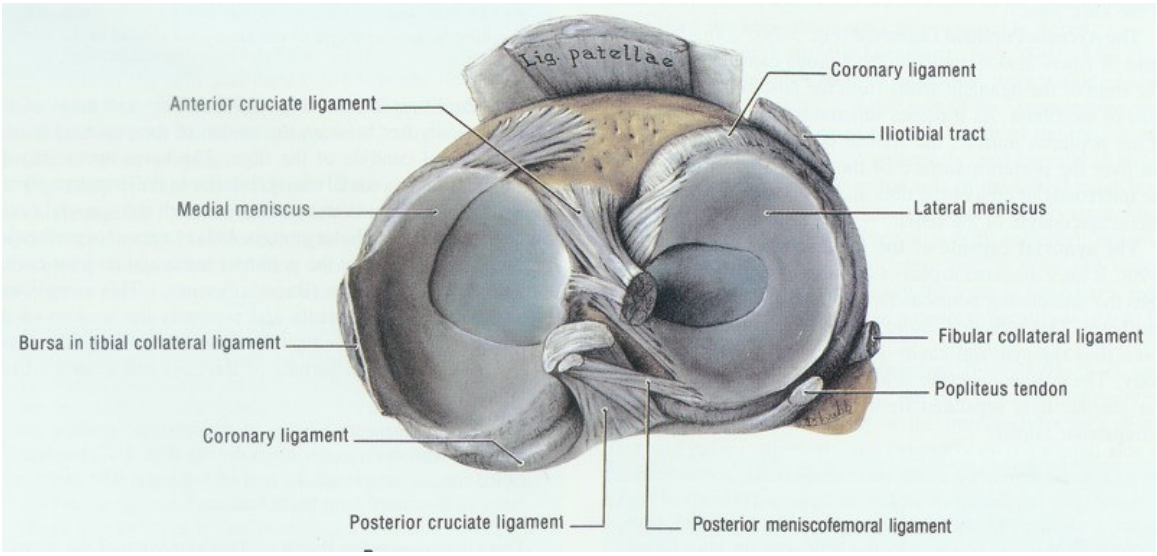

Figure 2-2 Tibial plateau: superior view [1]

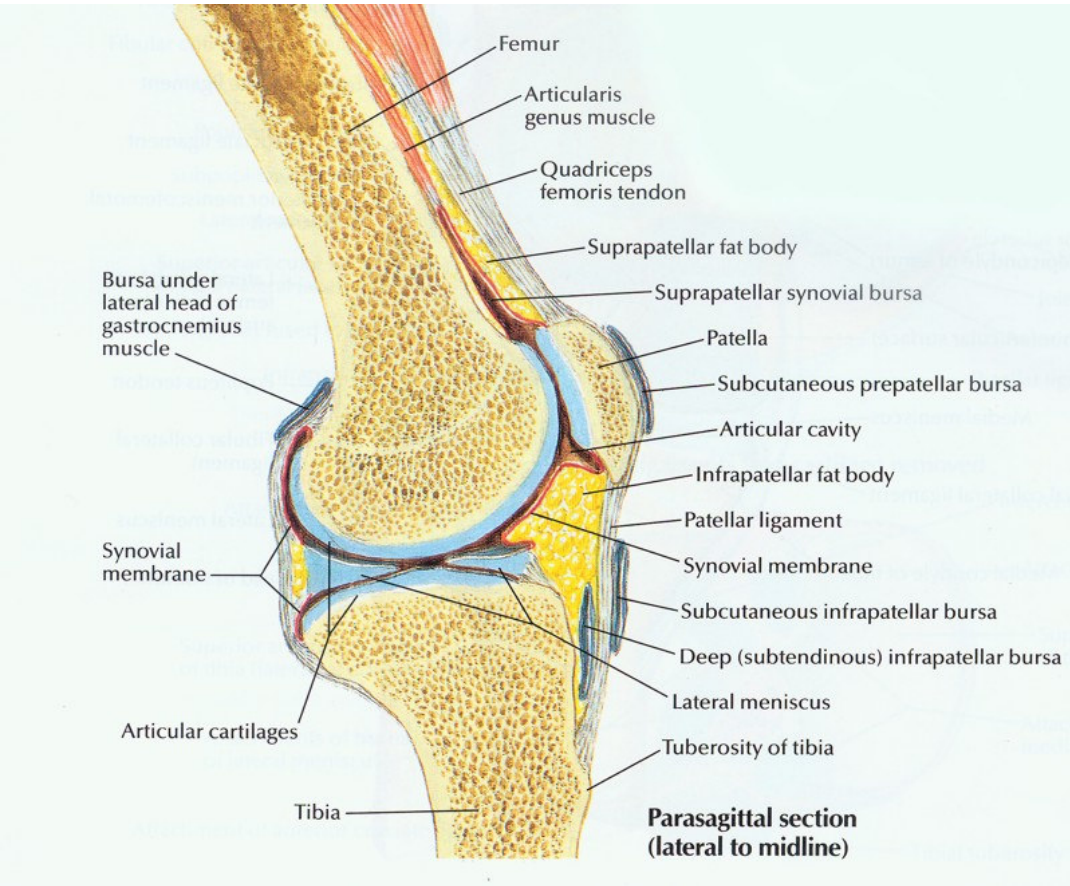

Figure 2-3 Parasagittal section of the knee [1]

2.1.2 MOTION OF THE KNEE

Every joint has 6 degrees of freedom, three translations and three rotations, although some of the degrees of freedom are larger and therefore more significant than others. The three rotations are flexion extension (FE), internal external tibial rotation (IE) and abduction adduction and the three translations are anterior posterior (AP) displacement, medial lateral shift and compression distraction.

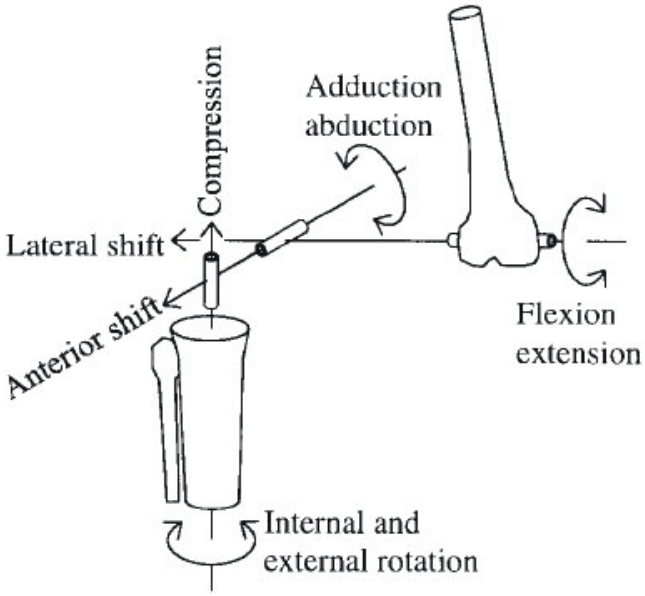

Figure 2-4 The six degrees of freedom of the knee [2]

The primary motion of the knee is flexion and extension, with ligament tension causing the knee to lock at full extension and full flexion being constrained by the calf hitting the thigh, giving an approximate range of motion of 165 degrees. Internal/external rotation is the rotation of the tibia about the long (vertical) axis of the bone and internal rotation occurs when the foot is pointed inwards. Abduction of the tibia occurs when it rotates laterally about a horizontal anterior posterior axis, away from the median plane and adduction is the reverse when the tibia rotates medially. Anterior/posterior displacement is the forward and back translation of the tibia relative to the femur. Its motion is closely linked to the flexion angle, with posterior displacement occurring with increasing flexion angle. Medial lateral shift is another small motion of the knee

joint involving the medial or lateral displacement of the tibia relative to the femur. Compression/distraction is the proximal/distal (up and down) motion of the tibia relative to the femur. It is not often reported in the literature and is primarily included for completeness.

There is still no consensus on what constitutes the normal kinematics of the knee, since all of the motions apart from flexion extension are small and difficult to measure. Neither is there full agreement on the method of defining the joint axes [2]. One widely reported aspect of motion is the “screw home” or screw axis mechanism of the knee, where internal/external rotation is coupled to flexion /extension [3]. As the knee is flexed the tibia rotates internally and extension produces external rotation. Wilson [4] has shown in a cadaver study that the passive knee joint has only one degree of freedom despite moving in six different axes and can be defined by the angle of flexion. The degree of internal/external rotation, abduction/adduction, anterior/posterior displacement, medial/lateral shift and compression/distraction are constrained along a unique path by the ACL, PCL, medial collateral ligament and the shape of the medial and lateral compartments.

The problem with cadaver studies is that they only report the passive rather than the active motion of the knee, which is affected by muscle, ground reaction and inertial forces that are encountered during walking and other daily activities. Numerous investigators have carried out active knee joint motion studies, the majority involving either multiple video cameras recording the positions of skin makers [5] or

goniometers, devices attached above and below the joint with between one and six potentiometers connected to each other by rigid links. The six linkage goniometers are also known as instrumented spatial linkages (ISL). Both these methods suffer from two problems. The markers or goniometer are attached externally. Movement between the skin and bone causes positional uncertainty between the markers and the bony anatomical landmarks of the knee, resulting in errors these measurements. For subjects running this error has been calculated as 21% for flexion extension, 63% for internal external rotation and 70% for adduction abduction [6].

The author found two studies in the literature that have used markers attached to the femur and tibia to generate knee joint motion profiles without the skin movement errors. However one of them [7] used seated rather than walking subjects, the knee was therefore unloaded and results supported the existence of the "screw home" mechanism.

The other article by Lafortune [8] is regarded as the definitive source on knee joint motion during walking, despite showing significant differences from the majority of other researchers. Intercortical tractions pins were inserted into five subjects who were captured on calibrated high speed cine cameras. It found 65 degrees of flexion during level walking and posterior displacement linked to flexion angle, in general agreement with the literature. The result for FE is shown in Figure 2-5, AP translation in Figure 2-6 and IE rotation in Figure 2-7. The thin motion profile in each graph is the result from each individual subject and the bold line is the average.

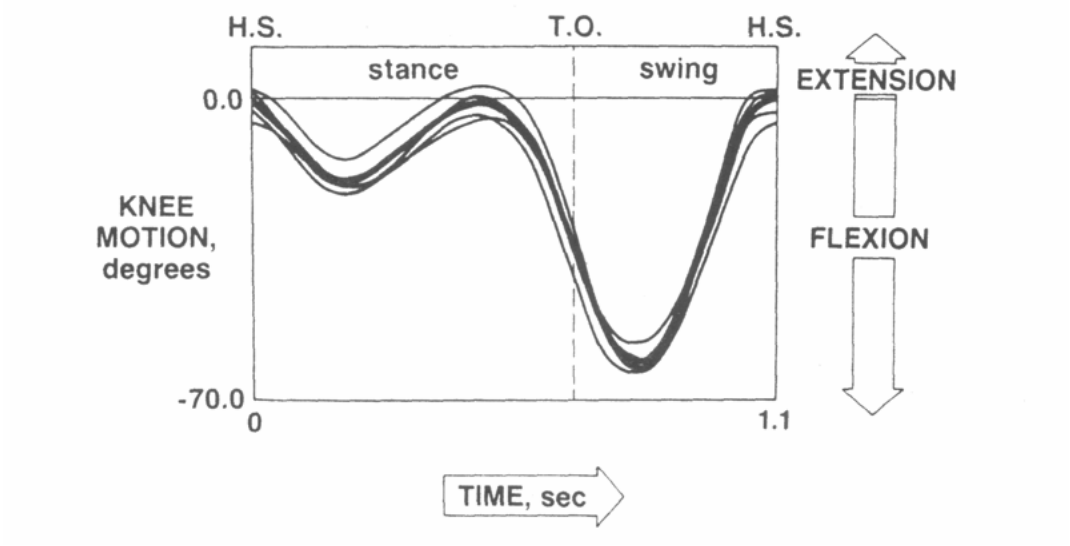

Figure 2-5 Flexion Extension [8]

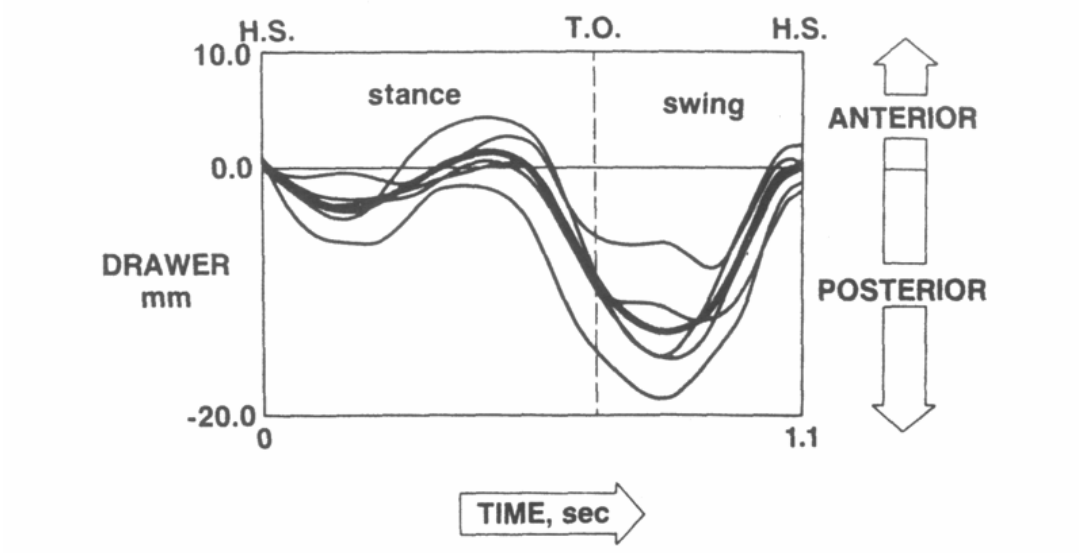

Figure 2-6 Anterior posterior translation [8]

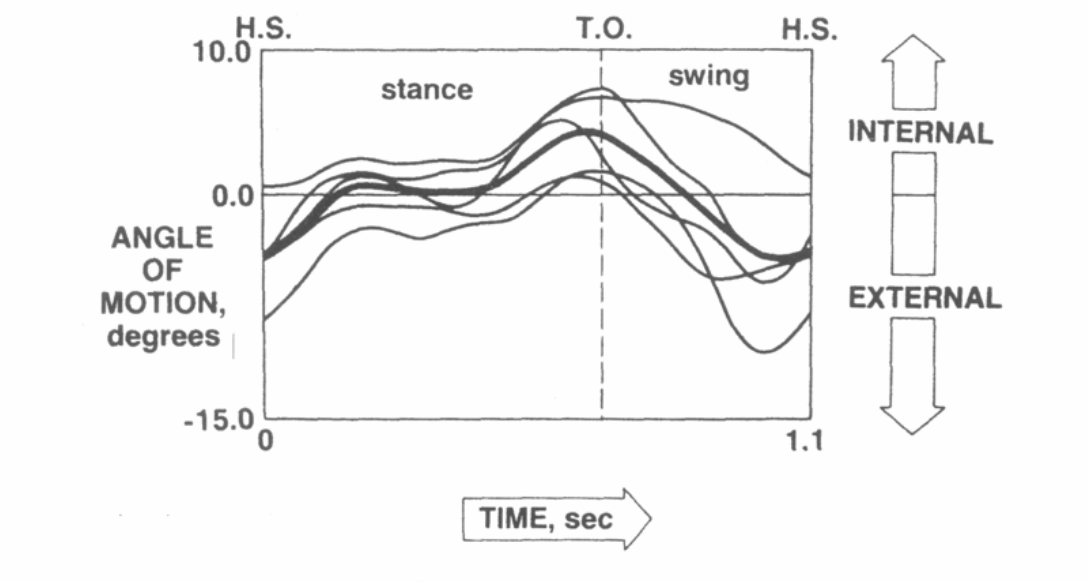

Figure 2-7 Internal external rotation [8]

The results for internal/external rotation did not show a fixed path for both flexion and extension and differed considerably from the widely reported screw mechanism. It is unlikely that there are major flaws in the work of either Lafortune or all the screw mechanism researchers; rather they were measuring different aspects of knee motion. Lafortune's measurements were made during active walking whereas the majority of the other work was a static, passive or unloaded analysis using cadavers or stationary or non-walking subjects. When the graph of IE rotation Vs FE from Lafortune et al [8](Figure 2-8) is compared to Wilson et al [4] (Figure 2-9), the difference is clearly obvious.

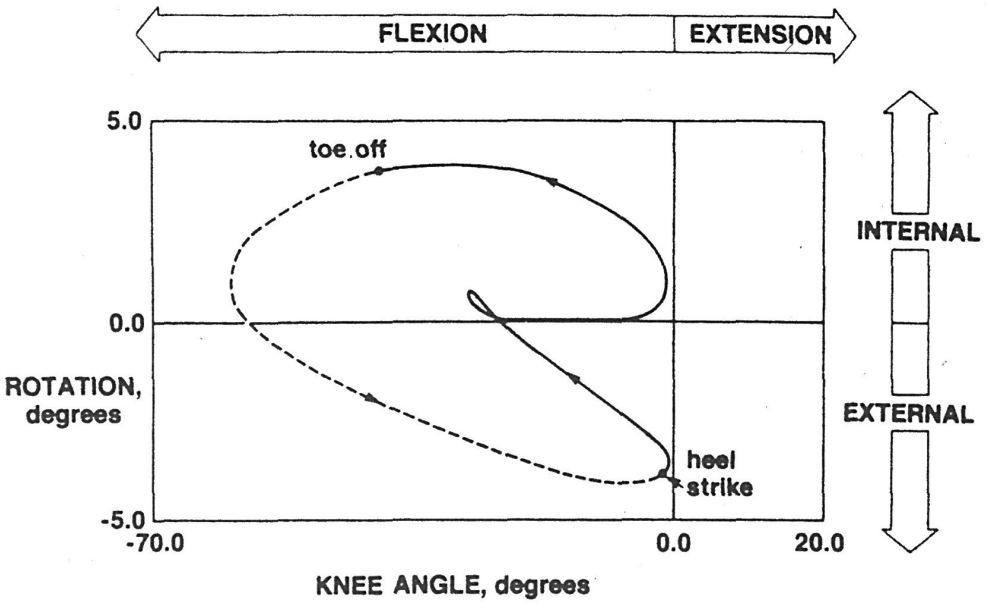

Figure 2-8 IE rotation as defined by FE – Lafortune et al [8]

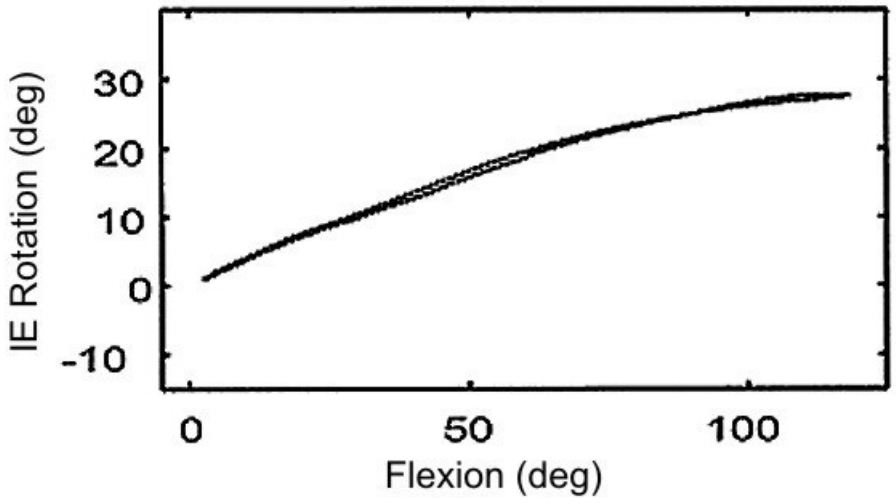

Figure 2-9IE rotation as defined by FE – Wilson et al [4]

The dependence on the condition of the knee and conditions under which its motion is measured is further highlighted by an ISL study by Ishii [9] which found significant differences between the motions of patients with TKR when compared to healthy controls. The TKR group showed reduced flexion extension, internal external rotation and increased anterior posterior translation. The variability of TKR motion is further highlighted by a study using a force controlled knee joint simulator that simulated the soft tissue structures. Nine different TKR were tested, with the shape of the implant the only variable, and IE rotation was found to vary from 5º to 20º [10].

2.1.3 KNEE JOINT LOADS

The knee is the most heavily loaded joint in the body, with peak reported loads of 7.1 times body weight for level walking [11], which translates to 5KN for a 70Kg person. The largest force through the joint is due to muscle contractions and ligament tension, but the impact loading that occurs during heel strike or walking down stair also makes a significant contribution [12]. The two most commonly used load profiles for knee joint simulators are Paul [13] and Seireg & Arvikar [11], with maximum forces of 3.4 and 7.1 times body weight respectively. These load profiles were calculated by analyzing the lower limbs through a series of quasi-static walking positions. Muscle, gravity, joint reaction and ligament forces were accounted for but inertial forces and impact loading were not. The large difference in the peak load between the two studies is attributed to

Seireg and Arvikar including antagonistic muscle activity (contraction of opposing muscles at the same time) and Paul omitting it. These load profiles are shown in Figure 2-10 and Figure 2-11.

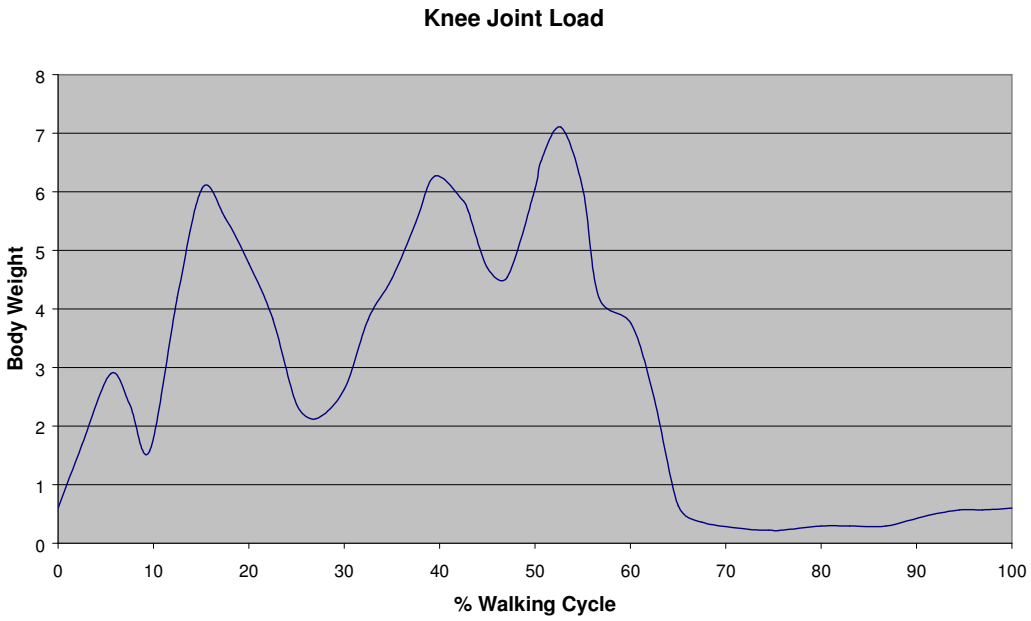

Figure 2-10 Knee joint loads during normal walking – Seireg & Arvikar [11]

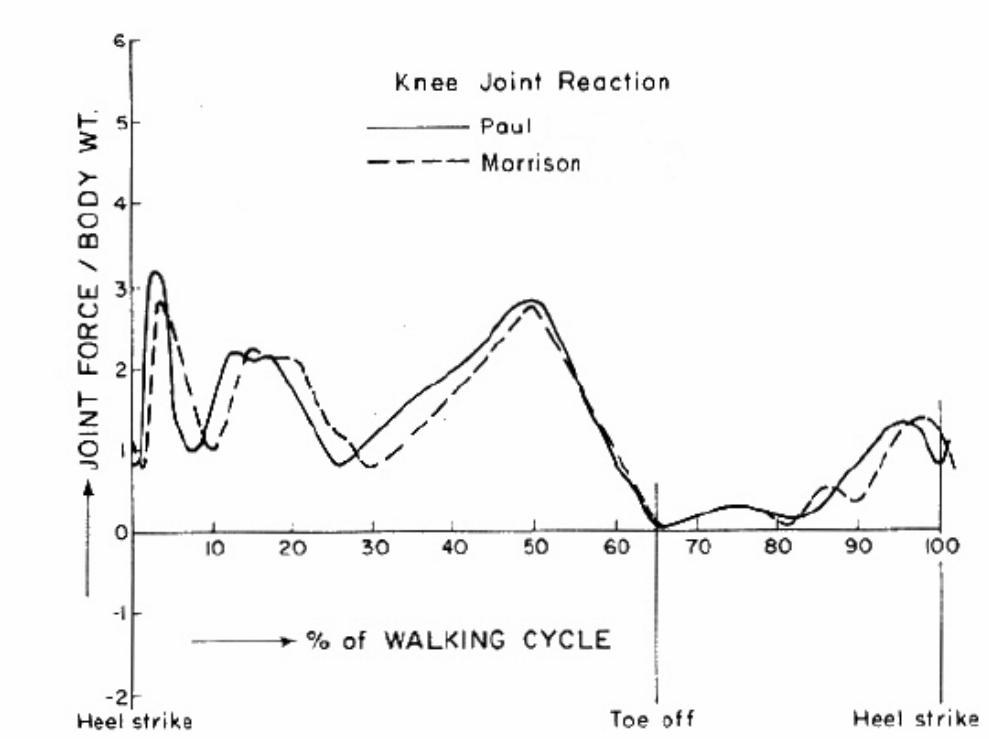

Figure 2-11 Knee joint load during normal walking – Paul [13]

2.1.4 ARTHRITIS OF THE KNEE

Arthritis is one of the leading cause of disability in the United States where there are approximately 70 Million sufferers of arthritis and other rheumatic conditions [14]. It is a degenerative disease of the cartilage and articular structures in joints, causing pain, stiffness and loss of mobility. Figure 2-12 is an X-ray with evidence of arthritis on the medial side of the knee, shown by the loss of joint space indicated by the black arrow. The most common type is osteoarthritis (OA) that is sometimes referred to as “old age wear and tear on the joints” although it can affect people of all ages. Rheumatoid

arthritis (RA) is the second most common and is an immune system disorder that attacks the cartilage and other structures in the joints. There is a genetic propensity for OA to run in families, although previous injuries such as rupturing the ACL or tearing of the meniscus greatly increase the chance of developing the condition later in life. Since cartilage is largely avascular (without blood supply), the rate of regeneration or repair is negligible and the disease progresses, resulting in a gradual loss of cartilage and joint space. In the more severe stages of arthritis there is bone on bone contact, causing considerable pain and requiring replacement of the joint with a prosthesis.

Figure 2-12 X-ray of arthritis in the medial compartment of the knee

2.2 TOTAL KNEE REPLACEMENT

The first knee replacement, performed in 1952, was a custom hinge joint made of a dental acrylic polymer and stainless steel and was hinged about a nylon axle [15]. It survived for 1 year before the skin over the joint failed due to over stretching and the final result was an above the knee amputation. In the ensuing five decades there have been numerous improvements to TKR and this procedure now provides relief from pain and greatly improved mobility for approximately 130,000 patients every year in the United States [16]. In the short and medium term, TKR is a very successful procedure with 15 year survival rates as high as 98.9% [17], although not all implants are this successful. Beyond this the survival rate can drop significantly, as Ultra High Molecular Weight Polyethylene (UHMWPE) wear debris from the articulating surface provokes an inflammatory response that leads to osteolysis (bone loss) around the implant, followed by pain and loosening and failure of the implant. Despite the significant improvements in the understanding of UHMWPE and its processing and manufacturing, late aseptic loosening caused by wear debris induced osteolysis has now replaced fixation loosening as the main cause of failure of long term implants. [18]

2.2.1 CURRENT TKR

Today's TKR consists of a cobalt chrome (CoCr) femoral component, replacing the condyles of the distal end of the femur and a slightly concave or dished UHMWPE tibial component covering the tibial plateau. A photo of a TKR is shown in Figure 2-13 and schematic of an implanted TKR is shown in Figure 2-14. CoCr is used because of its excellent biocompatibility, corrosion resistance and high hardness. UHMWPE, a linear homopolymer is used because of its good biocompatibility in the bulk form, low friction, low wear rate and good creep resistance. Tibial components often have a titanium base plate with an integral stem to improve the fixation. The components are attached by either bone cement or a press fit, with a roughened or porous surface to promote osteointegration (bone ingrowth) to enhance long term stability. In some cases where there are problems with the patello-femoral joint the surgeon will also resurface the underside of the patella with a UHMWPE component.

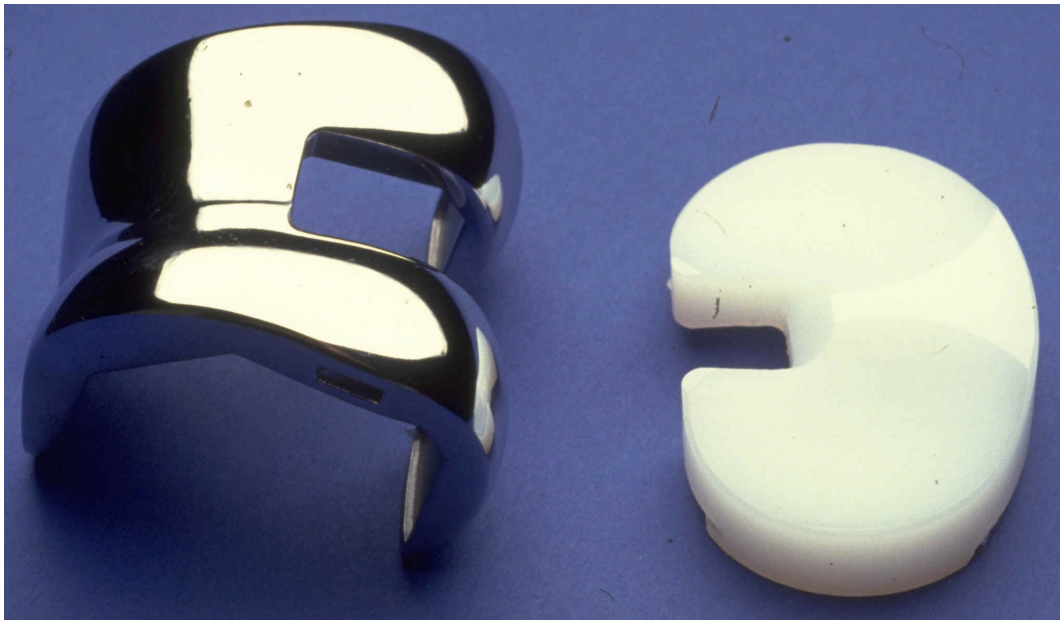

Figure 2-13 A total knee replacement. Femoral component (left) and tibial component (right)

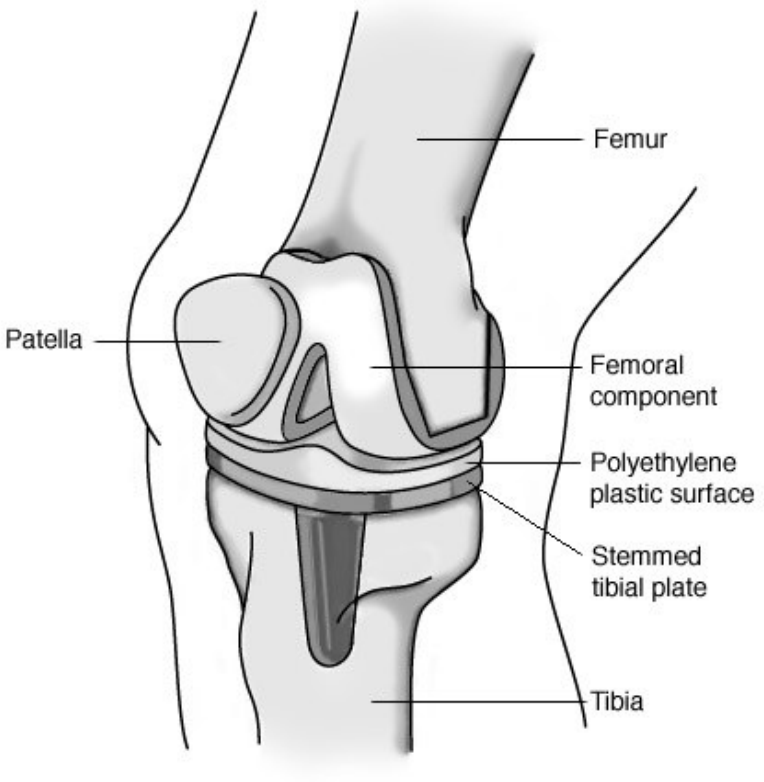

Figure 2-14 Location of the TKR in a knee

Improvements in component and surgical tooling design and better surgical techniques have resulted in improved primary fixation (component attachment to the bone directly after surgery), lower stresses in the UHMWPE tibial component, better component positioning and soft tissue (ligaments and tendons) balancing, resulting in better TKR survival rates and more natural joint kinematics for the patient. The advances in component sterilisation techniques and infection control during surgery have greatly reduced the early failure rate due to infections.

2.2.2 OSTEOLYSIS AND IMPLANT FAILURE

The majority of research done on the role of UHMWPE wear, osteolysis and total joint replacement failure has been carried out on total hip replacements (THR), but most of it is transferable to TKR as they both use the same materials, a cobalt chrome convex surface articulating on a concave UHMWPE surface and similar methods of attachment to the bone.

The mechanisms involved in late asceptic loosening caused by osteolysis are highly complex and not fully understood, but a simplified explanation follows. In its bulk form, UHMWPE is a bio-inert material, but when millions of small wear particles are released during articulation they provoke an immune system response whereby they are phagocytosed by macrophages. The macrophages then release pro-inflammatory cytokines (chemical messengers) and other mediators of inflammation that stimulate osteoclastic bone resorption, However the macrophages are unable to digest the polyethylene wear particles and this creates a state of continuous inflammation, leading to osteolysis and eventual loosening of the prosthesis. [19]. From TKR the UHMWPE wear debris ranges in size from sub micron to over one hundred microns [20], but particles in the 0.1-0.8um size range have been shown to provoke the strongest response and therefore have the greatest osteolytic potential [19] [21].

Bone loss is restricted to areas where the UHMWPE wear debris can migrate and cause the inflammatory response. Osteolysis is only a major concern if it is in the periprosthetic bone. Cases of revision surgery have shown the UHMWPE tibial tray having severe wear, chronic inflammatory response and resorption of surrounding bone, but the components were still firmly attached. Good bone ingrowth into the porous coating of the implant had effectively sealed the periprosthetic bone from wear debris and prevented osyeolysis there [20]. One of these retrieved implants is shown in Figure 2-15.

Figure 2-15 Retrieved TKR components showing severe UHMWPE wear [20]

2.3 KNEE JOINT SIMULATOR, WEAR TESTERS AND UHMWPE WEAR

2.3.1 INTRODUCTION

This section of the literature review, covering the mechanisms of UHMWPE wear and the joint simulators and wear testers that were used to investigate these properties, forms a central part of the thesis. It starts with the early research and the effects of surface finish and third body wear, followed by the discovery of the importance of accurately reproducing the joint kinematics by Bragdon et al and Wang et al. and the multidirectional motion induced anisotropy theory developed by Wang. Existing knee joint simulators are briefly covered and the need for low cost wear testers explained. This leads to the wear tester work done by Blunn et al, Cornwall et al, Saikko et al and McGoulin et al on the different kinematic conditions that occur in the TKR, namely sliding, rolling and gliding and the effect of varying the slide to roll ratio. A gap in the literature is identified and this leads to the motivation for this project.

2.3.2 EARLY UHMWPE WEAR RESEARCH

Early classifications of UHMWPE wear were descriptive and did not give good insight into how the properties of the polymer related to the observed damage. The wear of UHMWPE was originally classified as abrasive, adhesive or fatigue. [22] Abrasive wear is the cutting of the polymer by roughness on the counter surface or third body debris. Adhesive wear occurs during boundary or mixed lubrication when asperity contact occurs and the interfacial strength between the metallic component and the polymer is greater than the bulk strength of the UHMWPE. Fatigue wear is caused by repeated cyclic loading creating and then propagating cracks in the polymer. It is found in retrieved implants as either surface micro-cracking or sub-surface delamination. The ball in socket configuration of the hip joint gives a much larger contact area and lower stress than the point or line contact in a knee joint. As a result, delamination fatigue wear is almost exclusively found in TKR and most commonly in designs with thin polyethylene tibial components and non-conforming geometry that create high sub-surface stresses [18]. Later research has shown that in addition to high sub-surface stresses, sterilization by irradiation in air and then aging of the polyethylene is required to produce the sub-surface embrittlement that leads to delamination and fatigue wear. [23]

For several decades in vitro research into THR and TKR materials was carried out using simple reciprocating wear test rigs. The use of distilled water for lubrication

caused a UHMWPE transfer layer to form on the metallic counter surface, a phenomenon not observed with retrieved implants. The results these linear wear testers produced showed little resemblance to clinical data in terms of wear rates, mechanisms or ranking of materials [18]. Another factor that can create errors in the wear rates is the hydroscopic nature of polyethylene. It absorbs water during testing and gains weight that offsets the mass loss due to wear. This can be corrected by soak controls, samples being subjected to the same fluids, temperatures and sometimes load as the test piece without the motion to create wear. However errors can still arise if the soak controls don't have the same absorption rate as the test samples. This is particularly relevant if the wear rate is small, as some studies have reported negative wear rates. [23]

2.3.3 THE IMPORTANCE OF MULTIDIRECTIONAL MOTION

The major discovery of the importance of correctly reproducing the joint kinematics and multidirectional motion came when Bragdon & O'Connor [24] from Advanced Mechanical Testing Inc ran tests on a new hip simulator with physiological loading, ±23 deg flexion extension and a mechanically linked ±10 deg internal external rotation and found no measurable wear after 7 million cycles and the UHMWPE surface was

lacking the polished appearance that is commonly found on explanted acetabular cups. Scanning electron microscope (SEM) and atomic force microscope (AFM) revealed a rippled surface perpendicular to the direction of motion. A 3D loci analysis of multiple points on the femoral head revealed that the simulator motion produced a series of linear paths, which was strikingly different to clinical data that produced quasi-elliptical or roughly rectangular paths. Not only did each path cross itself at an acute angle, but adjacent points would cross the paths of multiple other adjacent points on the femoral head. The AMTI simulator was modified by decoupling the internal external rotation from the flexion extension and abduction adduction was added. The new simulator produced results that closely matched successful THR retrieved at autopsy: a wear rate of 24.8mg/10^6 cycles and a polished polyethylene surface, which on SEM investigation revealed fibrils oriented in multiple directions.

Shortly after Bragdon and O'Connor's discovery, Wang et al published a series of papers [18], [25], [26], [27] that provided a theoretical basis for the results observed by Bragdon & O'Connor, along with supporting experimental evidence. The molecular chain structure of the UHMWPE at the articulating surface of the implant is reorganized as a result of strain accumulation caused by surface traction. The linear polymer chains align in the direction of motion, resulting in an anisotropic structure. This microstructure has higher strength along the axis of motion but is considerably weaker off axis. The production of wear debris caused by on-axis motion requires the tensile rupture of strong polymer chains, but off-axis motion only needs to break the weaker bonds that bind one chain to another. A TJR experiences a continuously

variable tractive force, both in direction and magnitude. In this situation the polymer chains align to the direction of motion at maximum stress during the walking cycle, and at all other parts of the cycle the aligned chains are experiencing an off axis loading. Under these conditions the traction forces are at an angle to the chains for most of the cycle and this breaks the weaker bonds between the polymer chains, leading to the pulling out of the fibres (fibrils) and wear debris [18]. The polymer chain reorientation theory is backed by many experiments that have shown that the wear rates from linear wear testers are commonly two or three orders of magnitude lower than joint simulators and clinical results. [26], [24], [27]

Gamma irradiation is commonly used to sterilize medical implants, which also causes cross linking of the linear polymer chains by creating covalent bonds between the chains. This restricts the chains' movement and reorganization under tractive forces and also reduces some physical properties such as UTS and ductility. Under linear wear testing, UHMWPE that has been gamma irradiated shows a higher wear rate than non-irradiated UHMWPE, as the lack of chain mobility means that they can't align to the direction of motion and some of the polymer chains will experience an off axis loading and fibre pull out. However the results are reversed for multidirectional motion where irradiation induced cross linking has been shown in joint simulators and clinical studies, to significantly reduce UHMWPE wear. This is caused by the 3D network of chains created by irradiation being more resistant to inter-fibre splitting and fibre pull out from off axis loading.

Experimental results from Wang et al [18] on a hip simulator with multidirectional motion showed that the unirradiated UHMWPE cup had a wear rate three times greater than the irradiated one. This finding has been backed up by clinical findings, where lower wear rates have been reported in radiation sterilized components, compared to unirradiated ethylene oxide sterilized ones. A test on a knee simulator showed that the addition of IE rotation to change the motion from linear to multidirectional, increased the wear rate three times [18].

These previous studies show the importance of joint kinematics and multidirectional motion. Any study that does not consider these issues will produce results that are not relevant to clinical practice, giving incorrect wear rates and incorrect rankings of materials.

2.3.4 CURRENT KNEE JOINT SIMULATORS

Knee joint simulators are complex machines that reproduce the physiological loads and motions of the knee to evaluate the performance of TKR prior to the start of clinical trials and to investigate wear properties and patterns. Some have been developed by universities with large bio-tribology laboratories [28],[29],[30] but the majority are produced by commercial manufacturers such as AMTI, MTS and Instron Stanmore. The KS2-6-1000 by AMTI, shown in Figure 2-16 and costing $US350,000 is given as

an example, but the other commercial simulators have similar features. It is servo-hydraulically controlled on four axes, with the other two having free movement. There is an option of having the medial lateral shift force controlled. Force measurements for each TKR are carried out using 6 axis strain gauges and each test station has its own fluid circulation and temperature control system. The maximum load and motions of the AMTI simulator are shown in Table 2-1.

Figure 2-16 The AMTI KS2-6-1000 six station knee joint simulator

Table 2-1 Specifications of the AMTI knee joint simulator

Load	4500 N
FE Angle	134 deg
AP Translation	50mm
IE Rotation	40 deg
ML Shift	7.5mm force controlled
Abduction Adduction	3 deg free rotation

Due to the high cost of the full knee joint simulators and the length of tests, commonly 1-5 million cycles, it is often impractical or impossible to use them to investigate numerous new bearing material combinations, processing techniques or examine the effects of different kinematic conditions. This is where multi-axis knee joint wear testers have application, between the knee simulators and simple but inaccurate linear sliding test rigs. The knee joint wear testers have two or three of the following motions: FE, AP translation and IE rotation, being able to create motions more complex than simple sliding. The motions are usually driven by mechanical linkages, meaning they can only be a basic approximation of the motions experienced by in vivo TKR, but some have been shown to produce results comparable to joint simulators [31]. The components in the knee joint wear testers are also a simplification of TKR, aiming to recreate the line or point contact conditions that occur in the implant, without the significant cost of the components. The femoral component is substituted by a sphere or cylinder and the tibial component is replaced by a flat UHMWPE disk.

2.3.5 THE EFFECT OF CONTACT CONDITIONS AND KINEMATICS ON UHMWPE WEAR IN TKR

The motions occurring in a TKR are complex. In addition to multidirectional motion, the kinematic conditions change during each step and can include sliding, rolling and gliding. These different conditions are shown in Figure 2-17. Sliding occurs when the surface of the femoral component rotates against a stationary point on the polymer. This is the only kind of motion in the hip joint and occurs in the knee, typically when it is flexed 20 degrees or more [32]. Rolling is when the contact point of the metallic and polymer components both move at the same surface speed, so there is no relative surface motion. It usually occurs in the first 20 degrees of flexion in the TKR. Gliding occurs when a fixed point on the metallic component moves over the polymer surface. It does not usually occur in modern TKR, but can take place in designs with insufficient conformity or patients with excessive ligament laxity.

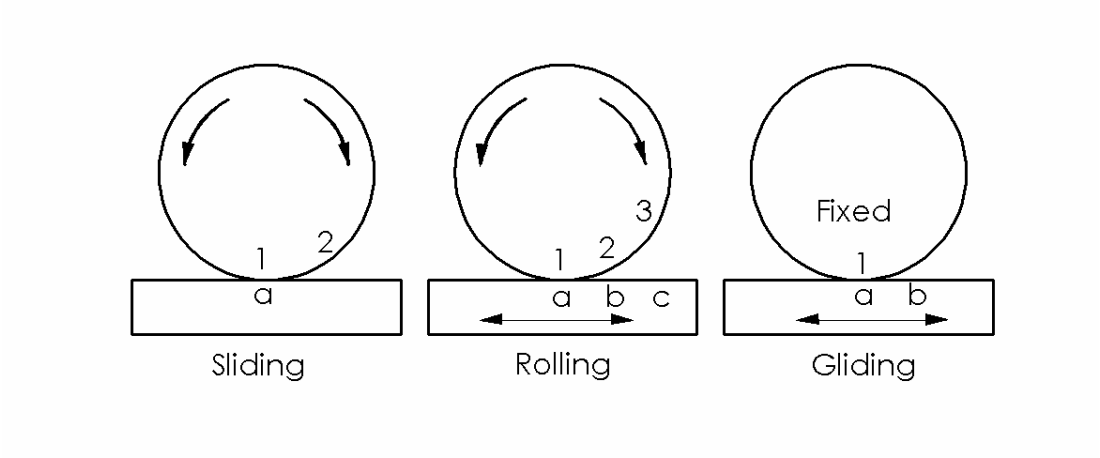

Figure 2-17 Sliding, rolling and gliding from Cornwall et al [33]

Blunn et al [34] proposed that one of the reasons for the greatly differing clinical wear rates that can occur with identical TKR is the variability in patient to patient kinematic conditions and other researchers have found different wear rates and patterns under different kinematic conditions [33], [23], [35], [32]. During linear wear testing using distilled water and a 10Hz cyclic load, Blunn et al [34] found that the gliding condition (this was reported as sliding, but the actual kinematics were identical to gliding) produced severe wear, sub-surface cracking and delamination whereas the damage from rolling was far less severe and did not include delamination or sub-surface cracking.

Cornwall et al [33] investigated sliding, rolling and gliding on a linear reciprocating test rig with a constant load and bovine serum lubrication. Sliding was carried out using a polymer pin on a CoCr disk, rolling used a CoCr sphere on polymer disk and gliding a spherical ended CoCr pin on a polymer disk. Gliding and rolling produced similar

wear rates, two orders of magnitude higher than the sliding tests. Although the load was constant in this series of tests, the contact stresses varied considerably due to the different test components used. The reported stress for the two sliding tests were 3MPa (ASTM) and 32 MPa, 32MPa for gliding and 22-32MPa for rolling.

Wang et al [31] developed a biaxial line contact wear machine to investigate bearing materials for TKR. It consisted of a CoCr disk with flexion extension that represented the femoral component and a flat tibial component of UHMWPE that had IE rotation. This configuration only produced the sliding condition and results from this study showed that as the angle of internal / external rotation increased, the effect of UHMWPE irradiation dose became more apparent. Under linear sliding conditions the irradiation dose, from 2.5 – 10Mrad had no effect on the wear rate. As internal / external rotation was added the wear rates increased across the board, but were far higher for samples with lower irradiation doses. These results were compared with those of a six station, 3 axis knee joint simulator investigating the effect of irradiation dose and were comparable. This showed that the use of simplified contact mechanics can still produce the same rankings of bearing materials, wear surface and particle morphology and similar wear rates to the considerably more complicated and expensive joint simulators. This bi-axial line contact wear tester is shown in Figure 2-18.

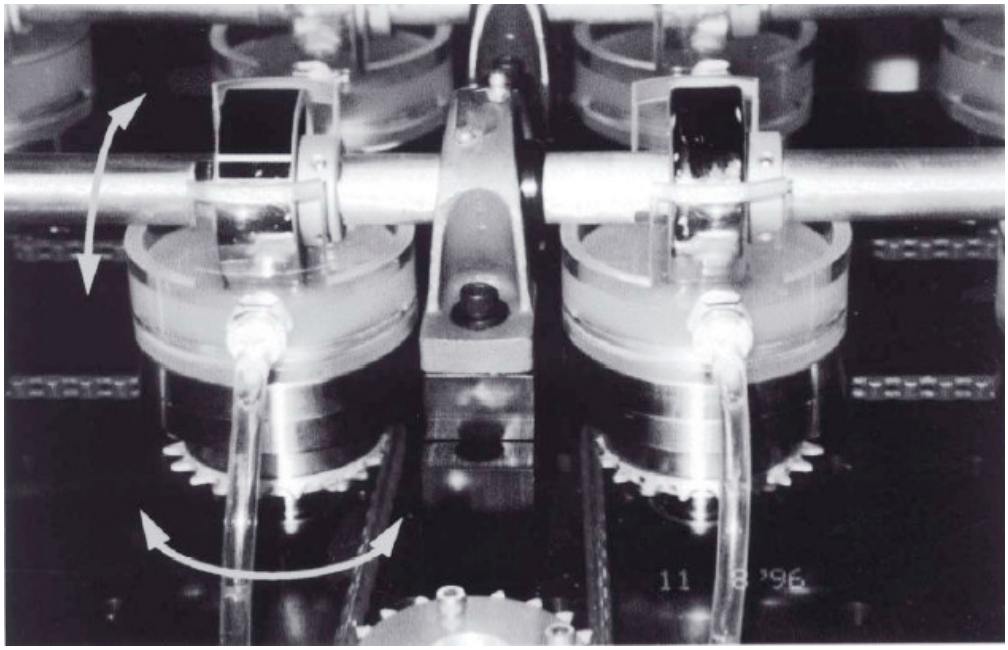

Figure 2-18 Close up of Wang et al's 12 station knee joint wear tester [31]

A five station, 3 axis, sphere on flat knee joint wear tester was used by Saikko et al [36], [37] to investigate the effect of gamma irradiation and aging on UHMWPE wear. This test rig had a static load of 2KN, 42.2 deg FE, 10mm AP translation and 10 deg IE rotation. The surface translation of the 54mm diameter CoCr ball was 20mm, giving a slide to roll ratio of 1 : 0.5. Results showed a 2.5-4 Mrad irradiation gave a 17% decrease in wear compared to non-irradiated polyethylene but simulated ageing and oxidation of irradiated samples produced wear rates up to approximately five times that of the non-irradiated or irradiated non-aged samples. Despite very high contact stresses and tests run for 5 million cycles, no delamination or fatigue wear was observed in any of the samples. A test sample machined from a tibial component that had been air

irradiated and shelf aged for 10 years, failed due to severe delamination after 500 cycles.

A three station, two axis knee joint wear tester with variable AP translation was developed by Mcgoulin et al [23] to investigate the effect of varying the slide to roll ratio. Wear rates increased as the motion changed from pure sliding, to a combination of sliding and rolling but then dropped as the slide to roll ratio approached 1 : 1. The lack of IE rotation and therefore no multidirectional motion gave unrealistically low wear rates and the finding of a negative wear rate indicated that there were problems with the soak controls.

The experimental parameters and results of these four investigations into the kinematic condition, plus the experimental parameters of this study are summarized in Table 2-2. Cornwall tested sliding, rolling and gliding without IE rotation whereas Wang et al included IE rotation but omitted AP translation, only investigating the sliding condition. Saikko et al included AP translation as well as IE rotation, but only tested one slide to roll ratio and McGoulin investigated sliding, rolling and three intermediate slide to roll ratios, but did not include IE rotation. It can be seen that there are no studies that combine IE rotation with a range of slide to roll ratios and so producing a machine capable of filling this gap in the literature is the motivation for the project.

Table 2-2 Specifications of knee joint wear testers

	Cornwall	Wang	Saikko	McGoulin	This Study
Load KN	0.2	1.1	2	1	2
AP Translation mm	21	NA	10	Variable 25 max	Variable 25 max
FE Surface Translation mm	21	38	20	25	25
IE Rotation deg	NA	15	10	NA	15
Slide:Roll Ratio	0 : 1 gliding 1 : 1 rolling 1: 0 sliding	1 : 0	1 : 0.5	1 : 0 1: 0.25 1: 0.5 1:0.75 1 : 1	1 : 0 1: 0.25 1: 0.5 1 : 1
Femoral Component	Different shapes. See text above	Cylinder 71.9mm dia	54mm dia sphere	20 x 30mm radius elliptical	50mm cylinder

3 DESIGN SPECIFICATION

3.1 INTRODUCTION

This chapter details the process and rationale used in the creation of a design specification. It shows how the initial concept of the wear tester, a device having a variable slide to roll ratio and multidirectional motion, was developed into a fully defined design specification. The most critical aspect of this is the contact conditions between the femoral and tibial components, which are determined by the load, the motion, and the size and shape of the test components. The contact stress experienced by the UHMWPE is determined by the applied load and the size and shape of the femoral component. Other important factors that were considered were the number of test stations, the choice of material, lubrication conditions and temperature and friction measurement.

3.2 LOAD

As discussed in section 2.1.3 the load fluctuates considerably during each walking cycle and this alternating stress has been shown to greatly increase wear [38]. However during AP translation, the point or line of contact moves, so the polyethylene would

experience a fluctuating compressive stress field. In cases where there is a slide to roll ratio of less than 1 : 1 an additional stress field perpendicular to the first stress field would be created in the UHMWPE by the frictional force from the femoral component. It was decided to use a constant load because it creates the required stress reversals in the polyethylene and eliminates the potential for loading or fatigue artifacts to affect the wear results, when the aim of the tests is to examine the effects of motion. Using a physiological loading would have greatly increased the cost and complexity of the machine.

Higher loads can be used to create larger wear rates without increasing contact stress by increasing the area of the polyethylene under load, which is beneficial as it reduces the effect of errors associated with fluid absorption. Existing wear testers used loads between 200N and 2KN, as shown in Table 2-2. It was decided to use a load of 2KN per test station and to design the femoral components so that they would give the required contact stress. This load was expected to provide sufficient wear and is the minimum load specified in ASTM F1715-00.

3.3 TEST COMPONENTS

Since the aim of the project was to develop a knee joint wear tester to investigate the wear rates and mechanisms of varying slide to roll ratio under multidirectional motion, it was decided to use a simplified geometry for the test components rather than actual implants. The reasons for this are twofold; simplified geometry would isolate the effects of the motion from the TKR design and the high cost of obtaining three commercially available TRK per test was prohibitive.

Since the tibial components of TKR typically have a large radius, the most appropriate simplification of this shape would be a flat. The thickness of the polyethylene is another important consideration. Examination of revised implants, as well as finite element analysis (FEA) and theoretical contact mechanics studies have shown tibial components thinner than 6mm are at a greater risk of fatigue and delamination failure [39, 40]. It was decided to make the tibial component 10mm thick to avoid this potential problem and this is also a common dimension used in current TKR.

The two most promising shapes identified for the femoral component were a sphere and a cylinder; both of which have been previously used in other knee joint wear testers. Depending on the geometry of the particular TKR, the contact conditions are either a line or point contact [31]. Table 3-1 shows the femoral component radii for 9 TKR in the sagittal and coronal planes. TKR with flat on flat or the same radius in the

coronal plane in both the femoral and tibial components have line contact, whereas the others have point contact.

Table 3-1 Femoral Profile Measurements [10]

Implant Type	Sagittal Radius At 0º Flexion (mm)	Sagittal Radius At 60º Flexion (mm)	Coronal Radius At 0º Flexion (mm)	Coronal Radius At 60º Flexion (mm)
IB	46	20	14	14
NGL	43	20	23	23
MBK	25	25	25	25
SML	40	40	Flat	Flat
HOWD	40	23	18	55/35
NGCR 30	30	20	40	40
SPROlat	30/50	20	30	30
SPROmed	30/50	20	Flat	Flat
JJPFC 34	34	20	8/48	8/48

The reported contact stresses in TKR range from 18 – 40 MPa, with the large variation attributed to different TKR designs, the applied load and angle of flexion as well as the method of calculation. FEA, contact area, pressure sensitive film, pressure transducers and theoretical contact mechanics have all been used [39-43]. The majority of papers

found in this area show the contact stresses exceeding the 21 MPa yield strength of UHMWPE [44], especially in low conformity designs and at high angles of flexion where the femoral component's radius reduces to allow a more anatomical motion.

Table 3-2 Loads, contact stresses and femoral components for existing knee wear tester

	Cornwall	Wang	Saikko	McGoulin	This Study
Load KN	0.2	1.1	2	1	2
Max Contact Pressure MPa	3-32 Varied between tests	19	57	48	25
Femoral Component	Sliding CoCr Flat Rolling 32mm Ø sphere Gliding – 25mm Ø sphere	Cylinder 71.9mm Ø x 25.4mm	Sphere 54mm Ø	Elliptical 20mm x 30mm radii	Cylinder 50mm Ø x 30mm

As can be seen in Table 3-2 a wide range in contact stresses have been used in knee joint wear testers. The maximum contact stresses shown in the table were calculated using the Hertzian contact equations from the component sizes and shapes and the applied load. In some cases they differ considerably from the values reported in the

journal article. For example, Saikko et al [37] reported a maximum contact pressure (P_O) of 18.7 MPa, based on a 14.3mm width of the wear tracks (a,b=7.15mm), a 2KN (P=2000N) load and an elliptical stress distribution, whereas the Hertzian contact equation gives a maximum contact pressure of 57MPa. It appears that Saikko et al used Equation (3.1) developed by Stewart et al [39], but neglected the assumption that the stresses within the polymer were within the elastic region.

$$P_O = \frac{3P}{2\pi ab} \qquad (3.1)$$

The Hertzian contact stress for a sphere pressed into a flat is given in Equation (3.2) The variables and the values used are given in Table 3-3

Table 3-3 Variables and values for calculating Hertzian contact stress for a sphere on flat

Item	**Symbol**	**Value**
Load	P	2KN
Radius of sphere	R	27mm
Poisson's ratio CoCr	v_1	0.3
Poisson's ratio UHMWPE	v_2	0.4 [39]
Young's modulus CoCr	E_1	200GPa
Young's modulus UHMWPE	E_2	500MPa [45]

$$P_O = \frac{1}{\pi}\left(\frac{6P}{R^2\left(\frac{1-\nu_1^{\,2}}{E_1}+\frac{1-\nu_2^{\,2}}{E_2}\right)^2}\right)^{\frac{1}{3}} \qquad (3.2)$$

While a contact stress of 18.7 MPa may be correct at the end of the wear test, at the start the yield strength of the polyethylene would have been grossly exceeded and plastic flow and wear occurred to increase the contact area to the reported value, with the concomitant reduction in contact stress to a value the polyethylene can withstand. While it is acknowledged that using the Hertzian contact equation where the yield of the polyethylene is exceeded will result in the calculated contact stress values being higher than they really are, they still provide a useful comparison and they avoid the need to perform non-linear elastic-plastic analysis. The true contact stress in this example would lie somewhere between the two calculated values of 18.7MPa and 57MPa.

It was decided to use a 25 MPa contact stress as this is slightly greater that the yield of the polyethylene and would be representative of a conforming design under normal, rather than extreme usage conditions. It was also identified that there was the potential for further research into the effect of contact stress on knee joint wear and the creation

of femoral components that would generate stresses around 40 MPa, as calculated by Hertzian contact theory.

The radius of the femoral component is another important factor in the wear of UHMWPE, with the large variation shown in Table 3-1. Taking the mean of these values, the radius in the sagittal plane was 38mm at 0 deg flexion and 23mm at 60 deg flexion. It was desired to have a femoral component radius of 30mm, halfway between these two values, but at the time of design the largest bar of medical grade CoCr available was 2 inches diameter, limiting the radius of the component to 25mm. While this is slightly less than ideal, it is still within the range of clinically used TKR.

With the radius limited to 25mm and a 2KN load it was calculated that a spherical femoral component would produce contact stresses of 60MPa and so it was decided to use a cylindrical component. The contact stress with a cylindrical femoral component is determined by its length (*L*). Sharp edges of a cylinder would cut and scratch the UHMWPE, so rounding them would be needed to avoid this. Using the equation for line contact (3.3), it was found that a 30mm long cylinder with an 8mm radius on each corner produced line contact length of 24.5mm and a Hertzian contact stress of 24.8MPa. It is shown in Figure 3-1.

$$P_O = \sqrt{\frac{P}{\pi RL\left(\frac{1-\nu_1^{\,2}}{E_1}+\frac{1-\nu_2^{\,2}}{E_2}\right)}} \qquad (3.3)$$

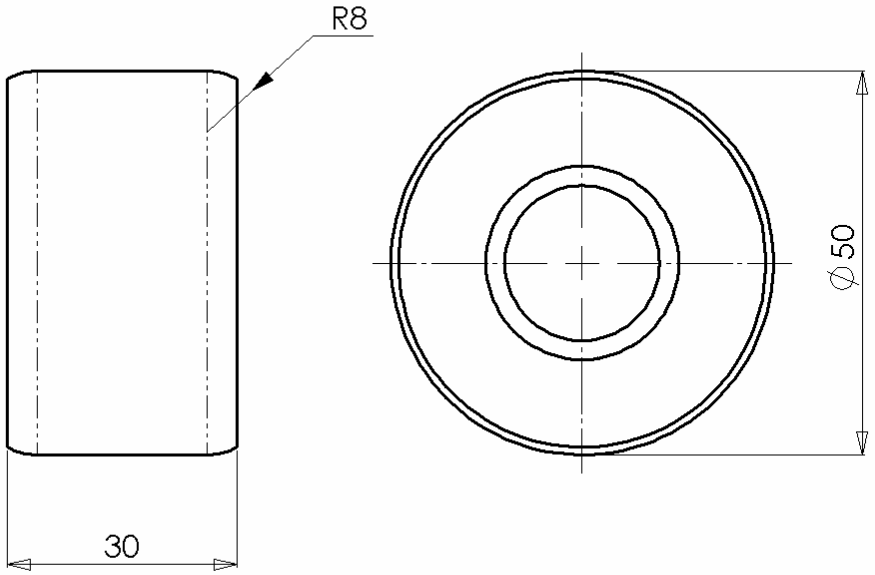

Figure 3-1 The femoral component

3.4 MOTION

As discussed in section 2.1.2, the motion of the knee joint is highly complex and dependent on the individual and the shape and condition of their knee. The motion profile published by Lafortune is commonly used by other researchers in TKR simulators, despite other research showing differences between healthy knees and TKR. The different designs of TKR have a range of motion profiles and varying slide to roll ratios. To minimize the design complexity and thus construction, it was decided to use a simple motion profile rather than a physiological profile. To be able to produce a range of slide to roll ratios and incorporate multi-directional motion, the machine would need to include flexion / extension, anterior / posterior translation and internal / external rotation.

The magnitude of the AP translation was based on the work of McGoughlin [23] and the clinical retrievals by Blunn et al [46] where the wear tracks varied in length between 15 and 35mm, with an average of 24mm. This was very close to the 25mm radius of the femoral component and so the maximum AP translation was set at 25mm, with intermediate translations of 12.5, 6.25 and 0mm to create slide to roll ratios of 1:1, 1:0.5, 1:0.25 and 1:0 respectively.

Unlike the femoral component of a TKR with a changing radius in the sagittal plane, using a single radius femoral component means that the actual flexion / extension angle

is largely unimportant and the surface sliding distance is the important parameter. It was decided to define the FE angle such that the surface translation of the femoral component equals the AP translation at a slide to roll ratio of 1:1. A surface translation of 25mm on a 50mm diameter cylinder requires a rotation of 1 radian or 57º.

The angle of IE rotation was specified at 15º as this was very close to the 14.2º found by Lafortune et al [8], the same as used by Wang et al [18] and falls within the range found by DesJardins [10]. The requirement for IE rotation has been discussed earlier, but the phase relationship between the IE rotation and AP translation is also important to create the required multidirectional motion. If the IE rotation is in phase, the resulting motion on the UHMWPE will be curve-linear, the femoral component's movement relative to the tibial component will be in an arc, but any given point on the polyethylene will only experience a linear reciprocating motion. Putting the IE rotation 90º out of phase moves the tibial component in a narrow figure-eight motion generating the required multidirectional motion that creates strain induced anisotropy. This is the same motion used by Saikko et al [36] to create multidirectional motion. The phase requirement is also backed up the different results from two TKR simulator studies. Wang et al [18] found adding physiological IE rotation caused a three-fold increase in wear, whereas Ash et al [30] found that adding IE rotation mechanically linked to AP translation caused no change in wear rate. Shown in Figure 3-2 is the required motion of the 3 axes of the knee joint wear tester at a 1 : 1 slide to roll ratio. When the FE angle is converted to a distance on the circumference on the femoral component it is the same as the AP translation.

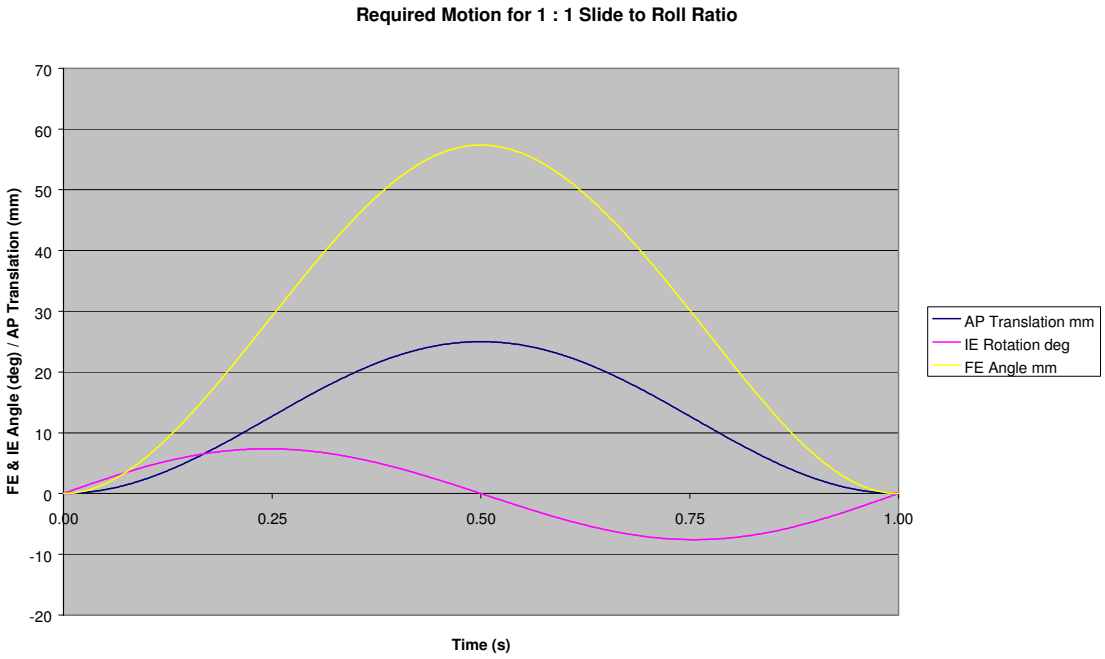

Figure 3-2 Required motion profile for 1 : 1 slide to roll ratio

3.5 TEST CHAMBER CONDITIONS

3.5.1 TEMPERATURE

There are two opposing factors to consider in selecting the temperature at which to run the experiments. The human body's normal temperature is 37ºC and it is reported that there is a significant decrease in the Young's modulus of polyethylene from body temperature to room temperature (24ºC) [33]. The other factor is that higher temperatures such as body temperature, greatly accelerate the degradation of the bovine serum lubricant, with the precipitation of proteins forming a protective layer on the bearing surfaces, adversely affecting the results. It was decided to run the test at 25ºC as there is a large body of evidence, including a multi-laboratory trial [47], that supported the idea of serum degradation causing artifacts in the results. While it was previously common to heat the bovine serum to body temperature, some laboratories now run cooling equipment or fluid circulation systems to counter the effects of friction induced heating [47], [31].

3.5.2 LUBRICATION

It is now well established that water and saline solution do not recreate the in vivo wear mechanisms and to date, diluted bovine serum is the medium that most accurately reproduces clinical wear. While there is some debate about the optimum concentration of proteins and the ratio between albumin and globulin in the lubricating fluid, the majority of researchers use the ASMT standard F1715, which recommends the use of filtered sterilized bovine serum, diluted with up to 75% deionized water. It was decided to also follow the standard and many other researchers and use filtered sterilized bovine serum diluted with 75% deionized water [47], [18].

An initial test run of 82,000 cycles revealed that the volume of the test chamber was too small and total evaporation of the bovine serum invalidated the test. As a result an additional design specification was added; a fluid recirculation system capable of pumping 100ml per minute and holding a minimum of 200ml of bovine serum. To minimize the risk of cross contamination of wear debris between samples, each test chamber would require its own system including pump.

3.5.3 NUMBER OF TEST STATIONS

To differentiate between two different experimental parameters to a level that reaches statistical significance requires the experiment to be repeated. Wear tests for TKR and their materials are usually run for 1-5 million cycles, taking between two weeks and two months for each test, making repeating the experiment a very time consuming and tedious process. To get around this problem, it is common to have multiple test stations, all applying identical loading and motion to a number of samples. The AMTI knee simulator has 6 stations and a hip simulator manufactured by the same company has 12 stations. While having a greater number of test stations would produce better results, they also cost more to manufacture. It was decided to incorporate three test stations into the knee joint wear tester, since cost was a significant factor in this project and it was thought that three stations was the minimum number that could produce valid results.

3.5.4 FINAL DESIGN SPECIFICATIONS

Load: 2000N

Tibial Component: 10mm thick UHMWPE

Femoral Component: 50mmØ cylinder, 30mm long with 8mm radius

Contact Stress: 25MPa as calculated by Hertzian contact equations

AP Translation: 0-25mm

FE: 57º

IE Rotation: 15º. 90º out of phase from AP translation

Temperature: 25 deg C

Lubrication: Sterile filtered bovine serum 25% : distilled water 75%

Lubrication System: 3 x 200ml capacity

Fluid Pumps: 100ml per minute

Number of test stations: 3

4 THE DESIGN

4.1 INTRODUCTION

This chapter starts with the conceptual design of methods to create the required motions and load and then gives a description of the knee joint wear tester, its major sub-assemblies and a more detailed description of how the motions are created. It is followed by the detail design of the FE shaft. It was decided to present this as an example of the detail design process. Detail design of the knee joint wear tester formed the major aspect of the project, but the reader gains very little from the rationale and calculations behind the sizing, selection and dimensions of every bearing, bolt and manufactured component. What is of more interest is how the machine performs.

4.2 CONCEPTUAL DESIGN

4.2.1 MOTION

The first task in the design process was selecting the method of driving the specified motions. Servo hydraulics are commonly used in knee joint simulators for their high forces and accurate control, but the cost was prohibitive. While stepper or DC servo motors, associated power electronics and gearboxes are cheaper than servo hydraulics, they were still outside the project's budget. The remaining option would be to use mechanical linkages to create the required motions. This certainly would reduce the cost of externally purchased components, a major driving factor in the design, but it would also add considerable complexity to the design task and to the number and complexity of components the workshop staff had to build. Generating each motion with a different motor would have simplified the design of the linkages, but would have required electronic synchronisation of the motors, which is only one step away from servo motors. For this reason it was decided to drive the three motions from a single motor.

The easiest way to convert rotary motion to reciprocating motion was a slider crank mechanism and so this was chosen as the means of generating the AP translation. It was decided to have a variable crank radius to give a variable AP translation distance

and therefore provide a variable slide to roll ratio. In machine design, the four bar linkage is one of the most common mechanisms and this was chosen to convert rotary motion to the FE oscillating angular motion as shown in Figure 4-1

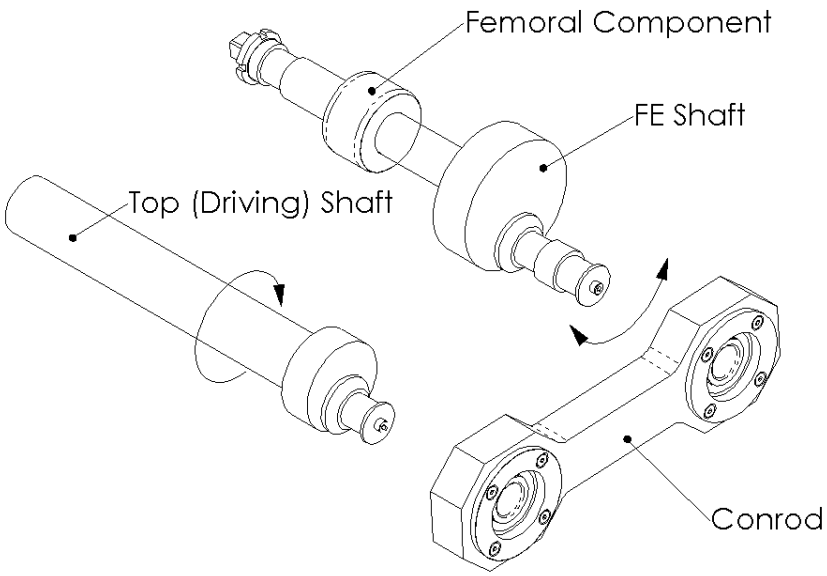

Figure 4-1 The FE drive mechanism

The next decision was to select the component, femoral or tibial, to which the AP translation would be applied. As the femoral component already had the FE motion, adding AP translation to the femoral component would require a more complex drive mechanism for FE, as the center distances between the driving shaft and the femoral component shaft would be moving back and forward. For this reason the AP translation was put on the tibial component.

A similar decision followed for the IE rotation. Due to the nature of FE drive mechanism, it was deemed near impossible to accommodate IE rotation on the femoral component so this was placed on the tibial component, with the IE rotation to be superimposed on top of the AP translation. The motions and load of the femoral and tibial components are shown in Figure 4-2.

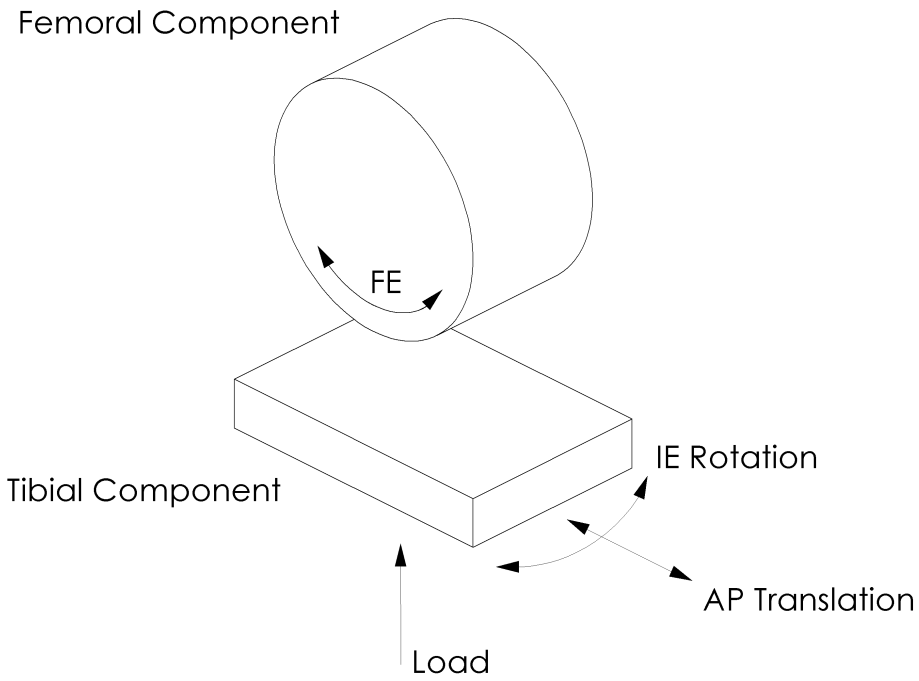

Figure 4-2 Schematic of the simplified TKR components and their motions and loading

Like FE, IE rotation is an oscillating angular rotation and so the mechanism chosen was similar; a short radius driving crankshaft, a conrod and a longer radius crank on the IE rotation shaft. As the driving crankshaft and the IE rotation shaft were perpendicular it was necessary to use spherical joints to allow the motion in two different planes. Computer simulations were used to work out the settings for the IE rotation drive mechanism, as it proved to be slightly more difficult than the previous two motions, due to the 90º phase shift required and the axis of IE rotation moving as a result of AP translation. Solidworks, a 3D computer aided design software package was used to quickly model the conceptual designs and COSMOS Motion, a kinematics package was used to simulate the motion created by the different linkages. Simulation was required at this early stage of the development to ensure that the proposed mechanism was actually capable of creating the desired motion. An early simulation model is shown in Figure 4-3

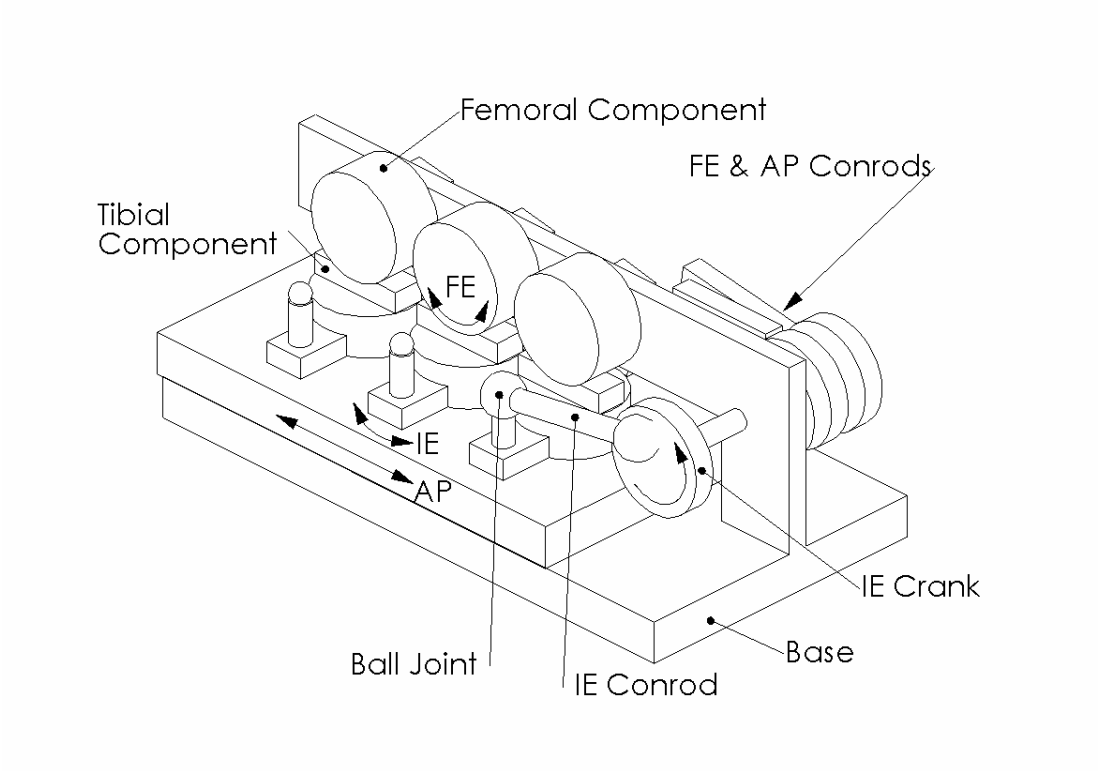

Figure 4-3 Early SolidWorks model for simulating the motion of the knee joint wear tester

4.2.2 LOADING

The load could be applied to either the femoral or tibial component, but adding another motion to the FE shaft to allow the loading, in this case a vertical translation, would stop the FE drive mechanism working correctly and so the load would be applied through the tibial component. To avoid the same problem occurring with the tibial components' drive mechanisms, it was decided to place the loading mechanism after

AP translation and IE rotation drive systems. Pneumatics were quickly identified as a cheap and compact method of providing the required 2KN force and air bellows were chosen over pneumatic cylinders as they were half the price and more compact, despite one minor disadvantage. Under constant air pressure, the force from the bellows decreases as they extend. From the manufacturer's data sheet it was calculated that the expected load variation would be less than 1% and ASTM F1715-00, the standard for testing TKR allows 3%. One of the air bellows is shown in Figure 4-4. The metal thread is used for location as well as the connection for the air supply.

Figure 4-4 The air bellows used to provide the load

4.3 THE KNEE JOINT WEAR TESTER

Compared to many linear wear testing devices, the three axis wear tester developed for this project is relatively large and complex, being approximately 950mm long, 700mm wide and 600mm high and weighing 250kg. It is constructed from just over 1000 separate parts, with approximately 130 unique components. Figure 4-5 shows a photo of the device covered by the safety guard and mounted on its pedestal. The sub-assembly drawing of the bottom shaft shown in Figure 4-6 is given as an example. A full set of manufacturing drawings, including assembly and sub-assembly drawings is included in Appendix A.

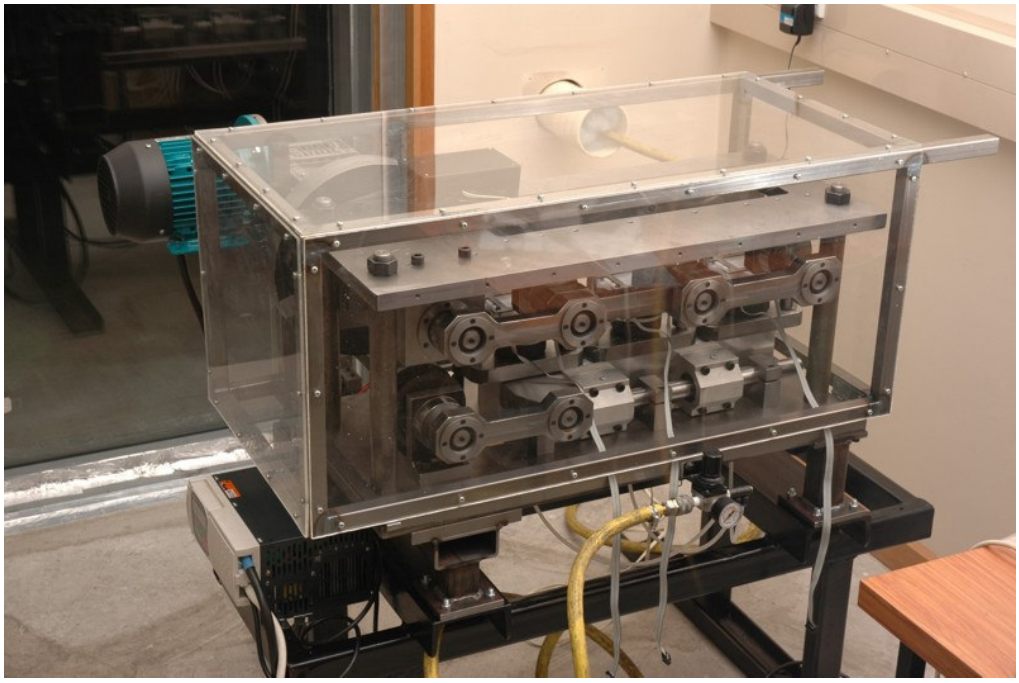

Figure 4-5 The assembled knee joint wear tester

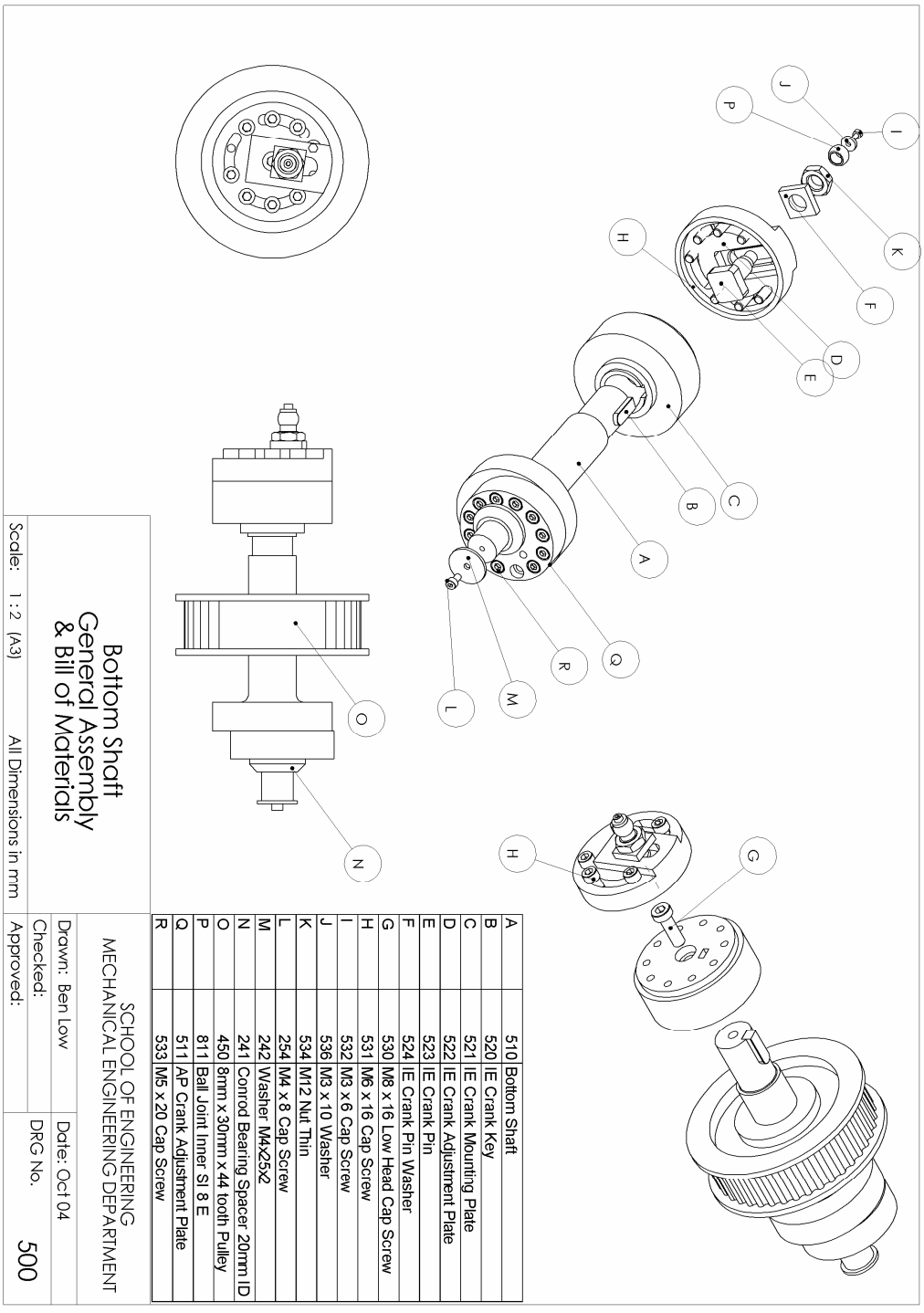

Figure 4-6 Manufacturing sub-assembly drawing 500: Bottom shaft general assembly and bill of materials

4.3.1 DESCRIPTION OF THE KNEE JOINT WEAR TESTER

The top and bottom of the frame was constructed from 24mm steel plates, held together by four 40mm vertical columns. The large slots in the top and bottom plates are for access to the test components and the pneumatic hoses respectively. A regulator and pressure gauge attached to the bottom plate supplies air at a constant pressure to the air bellows. A 3 phase, 0.55KW motor and 25:1 reduction worm gearbox are mounted out to the left of the machine on a rectangular hollow steel (RHS) frame. Motion from the gearbox is transferred via a short shaft through a soft coupling (Figure 4-10) to the top shaft where a flywheel is used to smooth out fluctuations experienced by the gearbox from the reciprocating load of the machine. Power from the top shaft is transferred to the bottom shaft via two synchronous pulleys and a belt (Figure 4-10). The pulley ratio is 1:1. On the right hand end of the top shaft is a 12mm radius crank that drives the flexion extension motion of the FE shaft (Figure 4-9) via a conrod and a 25mm radius crank that is part of the FE shaft. This motion is transferred to the other two FE shafts via two more conrods, (these are called joining rods in the manufacturing drawings)(Figure 4-9). A femoral component (Figure 4-11) is mounted at the center of each FE shaft and location and drive is provided by a Morse taper.

Two 30mm diameter shafts attached to the bottom plate are the rails for the linear bearings (Figure 4-7) that allow the AP translation. The four linear bearings are in pillow blocks that are bolted to the AP carriage (Figure 4-7) , a large aluminum block

that moves the tibial component back and forward. In the AP carriage are the angular contact bearings (Figure 4-7) that allow the internal external rotation of the IE shaft. The top of the IE shaft is pressed into the base of the “dieset”, so named as it is similar to a press tool dieset, with two vertical ground rods pressed into a base plate and a top plate that can move up and down on linear bushings. The 2KN load is provided by air bellows placed between the top and bottom plates of the dieset. The air supply for the air bellows runs through the hollow IE shaft. On top of the dieset top plate is the UHMWPE tibial test component and its holder (Figure 4-7). The test component sits on a flat ground 316L stainless plate with a polyacetal sample holder constraining motion in the horizontal directions and containing the bovine serum. These two components attached together are known as the tibial tray.

There is a 6mm quick connect fitting and attached hose in each end of the polyacetal sample holder that is part of the fluid recirculation system. One hose is for bovine serum delivery from the peristaltic pump (Omega FPU-116) and the other for drainage to a reservoir below the machine. Each reservoir consists of a 1000ml plastic container with sealed lid and three hoses. The last hose is attached to a suction pump, to initiate siphoning on the drainage line. The fluid recirculation system is shown in Figure 4-8

A conrod (Figure 4-9) attaches the adjustable radius crank on the right hand end of the bottom shaft drives to the AP carriage, creating the anterior posterior motion. The radius of this crank can be set between 0 and 12.5mm, giving an AP translation of 0 to 25mm. On the left hand end of the bottom shaft is the IE crank (Figure 4-10) that is

adjustable in both phase and radius that controls the internal external rotation of the diesets and therefore the tibial components. Ball joints on the IE crank and dieset base plate are connected by the IE conrod, converting rotary motion of the IE crank to oscillatory motion of the first dieset with a 90° phase shift. This motion is then transferred to the other two dieset via joining rods. A Perspex safety guard covers the machine to keep observers from getting too close and getting injured. The electronic motor control is interlocked to the safety guard so that if the guard is raised the motor cuts out. The safety guard has the secondary function of reducing atmospheric dust getting into the machine.

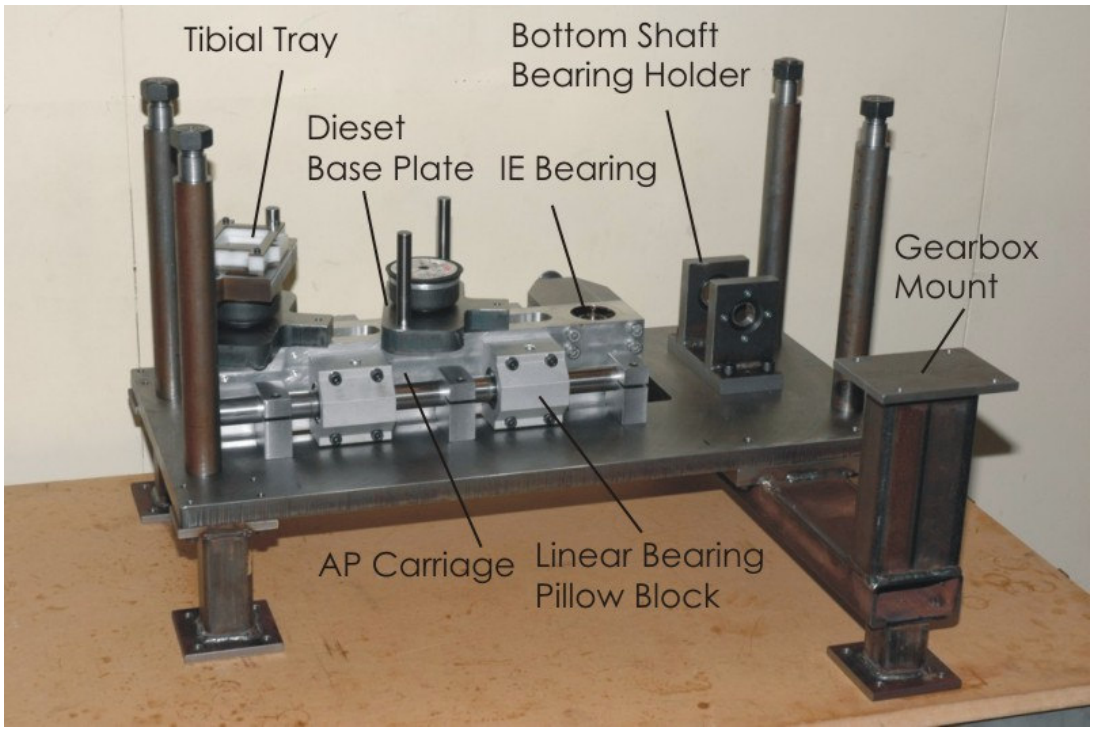

Figure 4-7 The knee joint wear tester during assembly

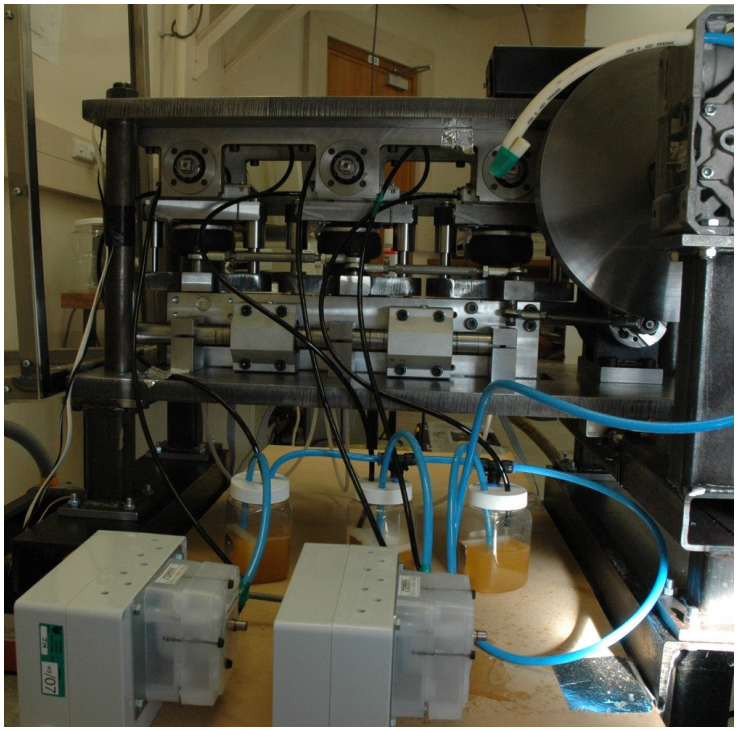

Figure 4-8 Fluid recirculation system

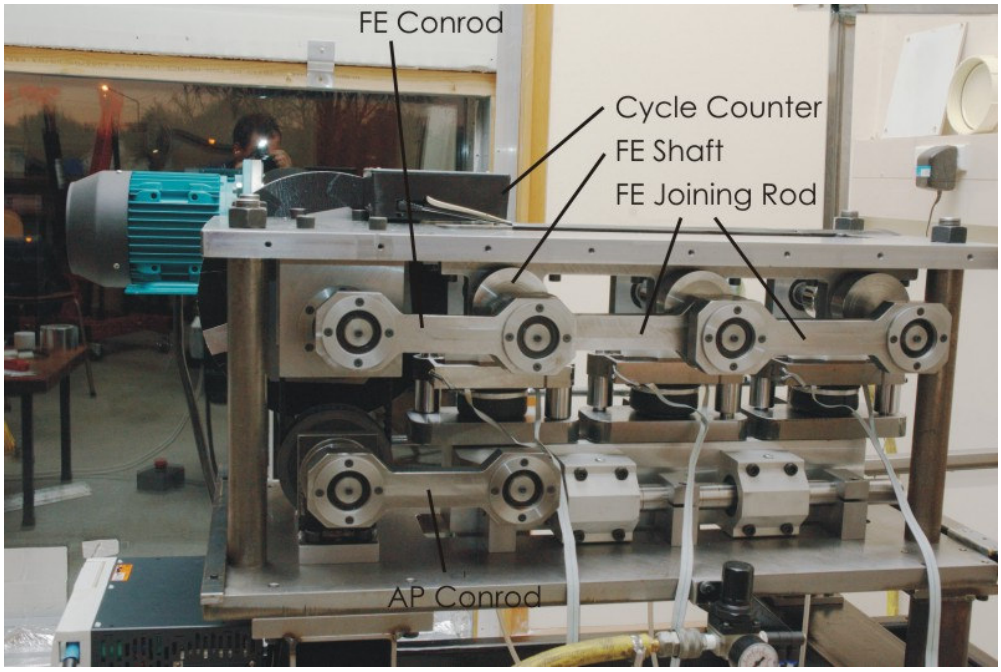

Figure 4-9 Right side view of the knee joint wear tester

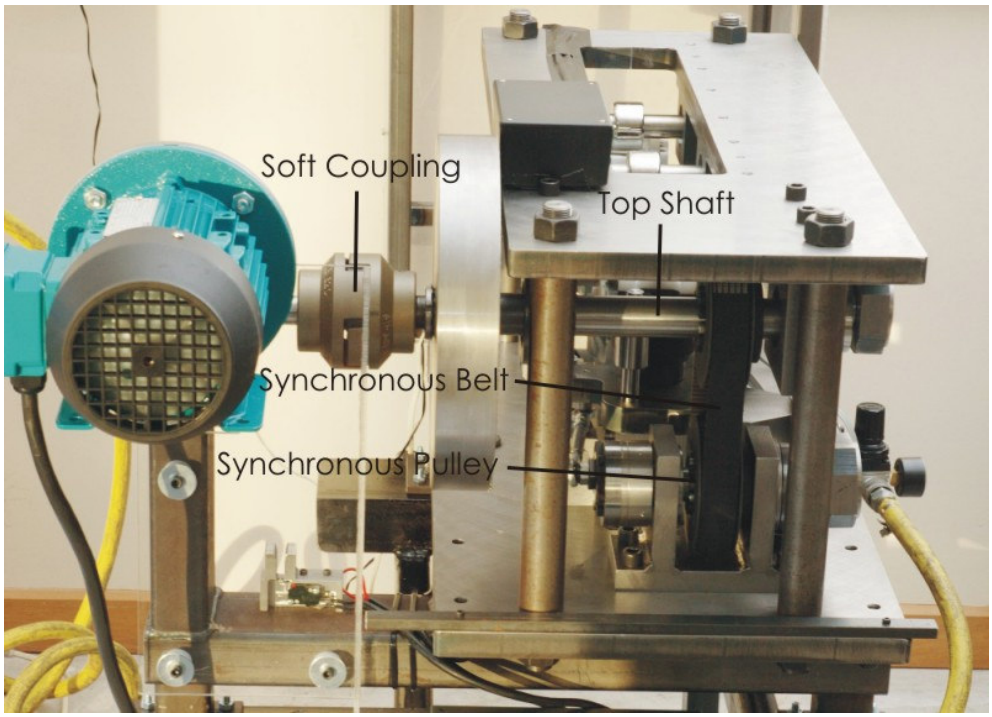

Figure 4-10 Front view of the knee wear tester

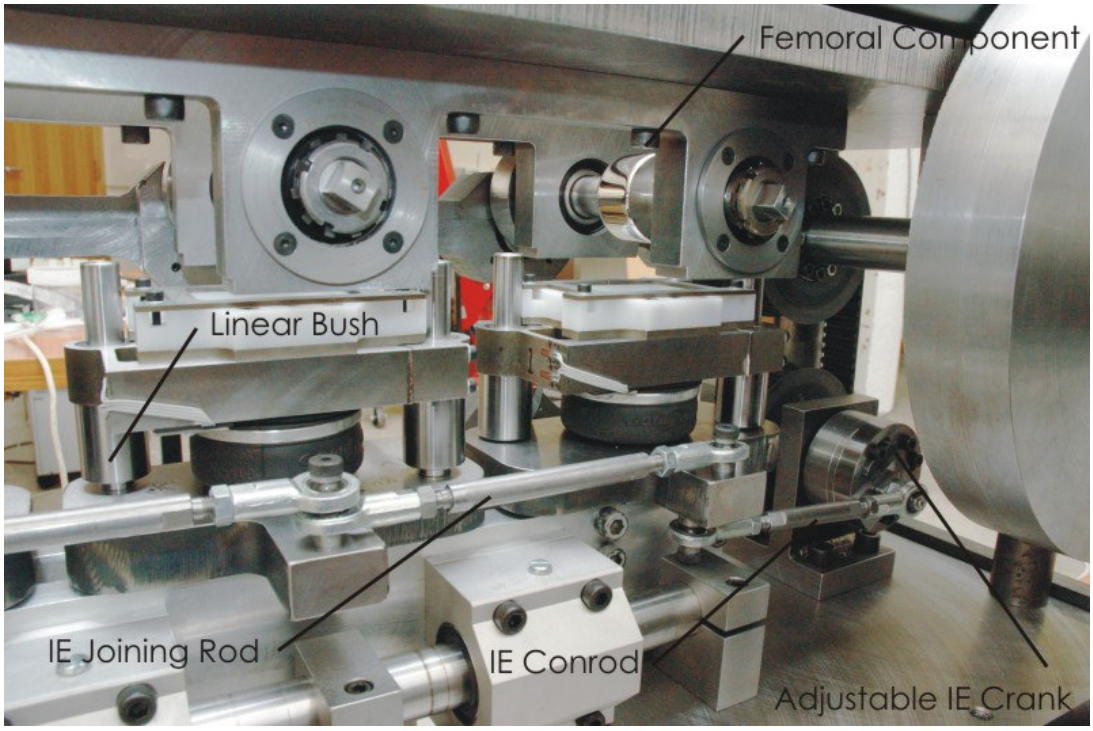

Figure 4-11 Left side view of the knee joint wear tester

Simulation of the final machine design showed the tibial tray moving in the correct figure-eight profile. Examining the graph of the motion showed that the IE rotation was 90º out of phase with FE and the AP translation and had the desired slide to roll ratio. The 3 axis motion output from the simulation with a slide to roll ratio of 1 : 0.5 is shown in Figure 4-12

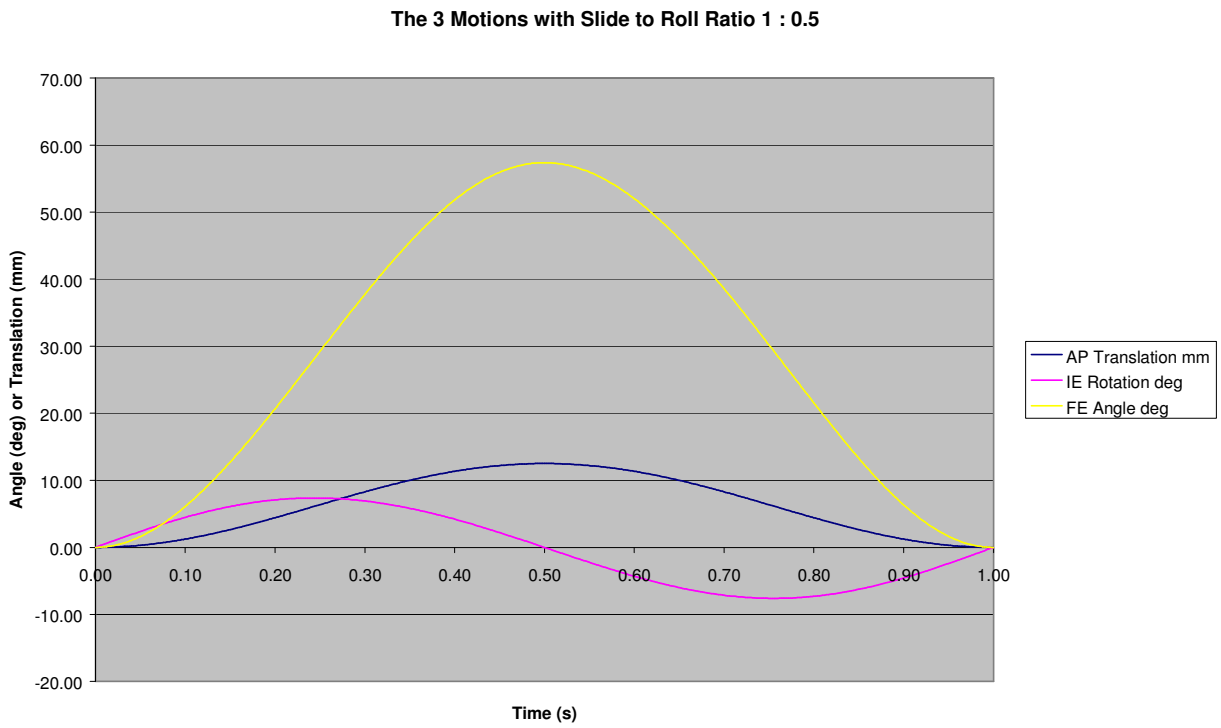

Figure 4-12 Motion simulation results for a slide to roll ratio of 1 : 0.5

4.4 DETAIL DESIGN – FE SHAFT

The device was designed to last a minimum of 20 million cycles, so fatigue was a major design consideration. While no problems were encountered with the frame and other stationary parts, the cyclic stresses in the shafts were near the fatigue limit of the 4340 steel used, necessitating careful design. This steel was chosen due to its high strength in the "as machined" form and availability. It was intended to use a material that would not need heat treatment, as this would add to the cost and would require post heat treatment grinding to achieve the required accuracy. The most challenging was the FE shaft and so the design process is given as an example. The top and bottom shafts were designed using the same method. The challenge for the FE shaft came from its diameter being constrained by the size of the femoral component and the need to provide clearance between the shaft and the tibial tray holding the bovine solution. The femoral component also needed be attached to the shaft at the point of the highest bending moment. From calculations it was found that using keyways, shoulders or threaded fasteners would create stress concentrations in the shaft that would lead to fatigue failure. A Morse taper was used as this would only introduce a small stress concentration at the start of the taper. A free-body-diagram of the FE shaft is shown in Figure 4-13.

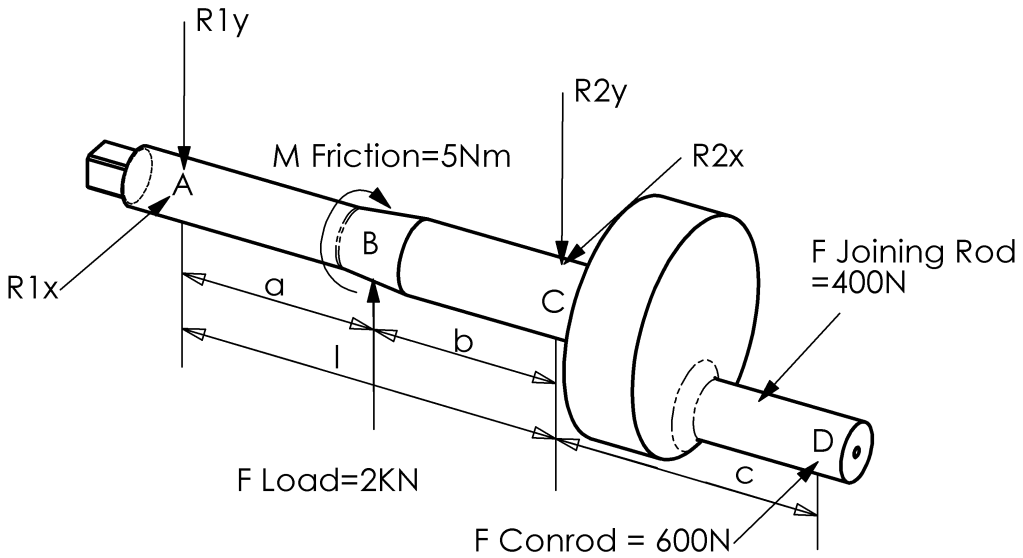

Figure 4-13 Free Body Diagram of FE Shaft Showing Forces and Bearing Reactions

The four R forces are the horizontal and vertical reactions of the two bearings supporting the FE shaft. A, B, C and D are the positions of the left hand bearing, the femoral component, the right hand bearing and the conrod bearing respectively. The frictional force between the femoral and tibial components was calculated using the applied load and a dynamic coefficient of friction of 0.1 [32], the highest found for TKR. The moment from this force was also calculated.

$$F_{Friction} = \mu F_{Load} = 0.1 \times 2000 = 200N \quad (4.1)$$

$$M_{Friction} = r_{Femoral\_component} \times F_{Friction} = 0.025 \times 200 = 5Nm \quad (4.2)$$

The friction from the bearings was ignored since it was insignificant compared to the other frictional forces involved. Since the crank arm length on the FE shaft was the same as the femoral component radius, 25mm, the force on the crank arm required to rotate the shaft would be the same as the frictional force. The conrod provided this force for all three stations, so would be 600N. The joining rod transferred a force of 400N to the remaining two test stations. This force was included for completeness of the diagram but was omitted in the bending moment and stress calculations, as it reduced the stress experienced in the shaft and due to a small amount of play in the joining rod bearings, there were two instances per cycle when the joining rod force was not acting.

The bending moments from the 2KN Load were calculated using Equation (4.3) for section AB and Equation (4.4) for section BC. The bending moment from the 600N conrod force was calculated using Equation (4.5) for section AC and Equation (4.6) for section CD [48]

$$M_{AB} = \frac{F_{Load} bx}{l} \quad (4.3)$$

$$M_{BC} = \frac{F_{Load} a}{l}(l - x) \qquad (4.4)$$

$$M_{AC} = -\frac{F_{Conrod} cx}{l} \qquad (4.5)$$

$$M_{CD} = F_{Conrod}(x - l - c) \qquad (4.6)$$

The two bending moments were evaluated at 13 separate points along the FE shaft, including areas where there were stress concentrations and points of application of load. The two bending moments were perpendicular and so the magnitude of the combined bending moment was calculated by adding their vectors together.

$$M_{Combined} = \sqrt{M_{Load}{}^2 + M_{Conrod}{}^2} \qquad (4.7)$$

The individual and combined bending moments down the length of the FE shaft are shown in Figure 4-14. A – D marked on the graph correspond to the position shown in Figure 4-13

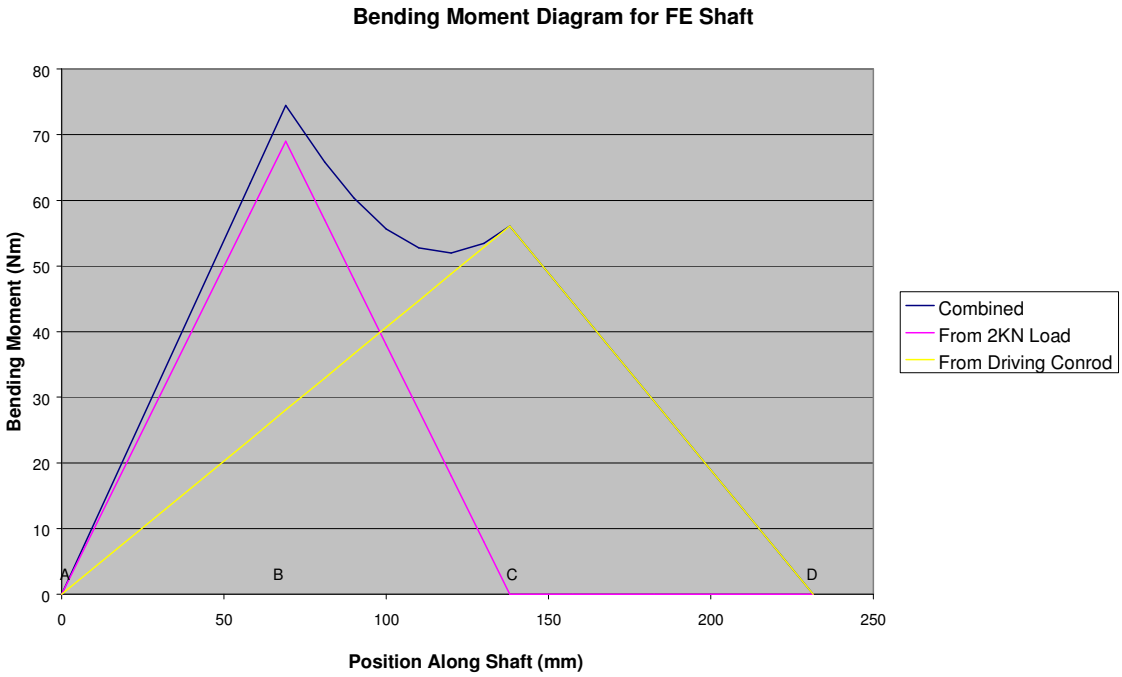

Figure 4-14 Bending moment diagram for FE shaft

Maximum shear stress theory was used in Equation (4.8) [48] to calculate the minimum required diameter along the shaft. The variables used in the equation were: d =required diameter, n = safety factor, T_a = alternating torque, S_e = modified endurance limit of the material, T_m = mean torque, S_y = modified yield strength of material, M_a = alternating bending moment, M_m = mean bending moment. The modified yield strength and endurance limit took into account stress concentrations, surface finish, size factors and reliability factors.

$$d = \left\{ \frac{32n}{\pi} \left[\left(\frac{T_a}{S_e} + \frac{T_m}{S_y} \right)^2 + \left(\frac{M_a}{S_e} + \frac{M_m}{S_y} \right)^2 \right]^{1/2} \right\}^{1/3} \qquad (4.8)$$

The finished FE shaft with femoral component is shown in Figure 4-15 The completed FE shaft with femoral component

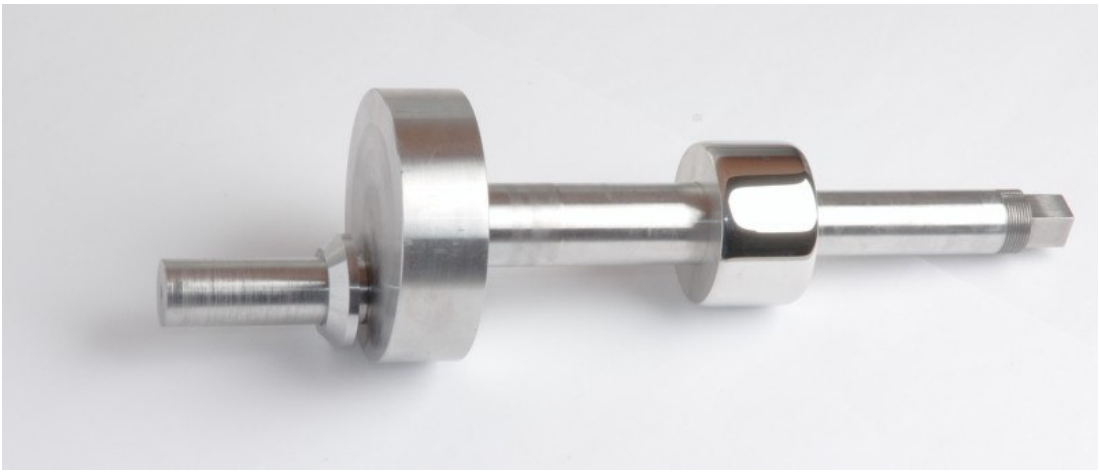

Figure 4-15 The completed FE shaft with femoral component

4.5 TEST COMPONENTS

Nine tibial components measuring 10 x 40 x 60mm were manufactured from a block of unirradiated GUR 1050 UHMWPE (Perplas Medical). To minimize 3rd body contamination the mill and the cutting tool were thoroughly cleaned before machining the test samples.

To avoid the cost of purchasing 2" CoCr bar, and the required special tooling to cut it, it was decided to manufacture the first femoral components out of 316L stainless steel. While this is not ideal, stainless steel was commonly used in THR for many years and other researchers have used it for preliminary investigations [McGoulin].

Polishing was carried out with the femoral component mounted on the FE shaft which was mounted in a lathe. It was then polished using a buffing wheel attached to a drill. The polishing media used was metal polish, 9μ diamond paste, 1μ diamond paste and finally colloidal silica. A new buffing wheel was used for each grade of media. The finished femoral component is shown in Figure 4-16. Despite thoroughly cleaning the lathe, FE shaft and ultrasonically cleaning the samples between each media, contamination of the buffing wheels always left scratches on the femoral component. The polishing was carried out in a machine shop and it is believed that the contamination came from the dusty and dirty environment. To obtain an implant grade polish will require facilities in a cleaner environment.

Figure 4-16 The polished femoral component

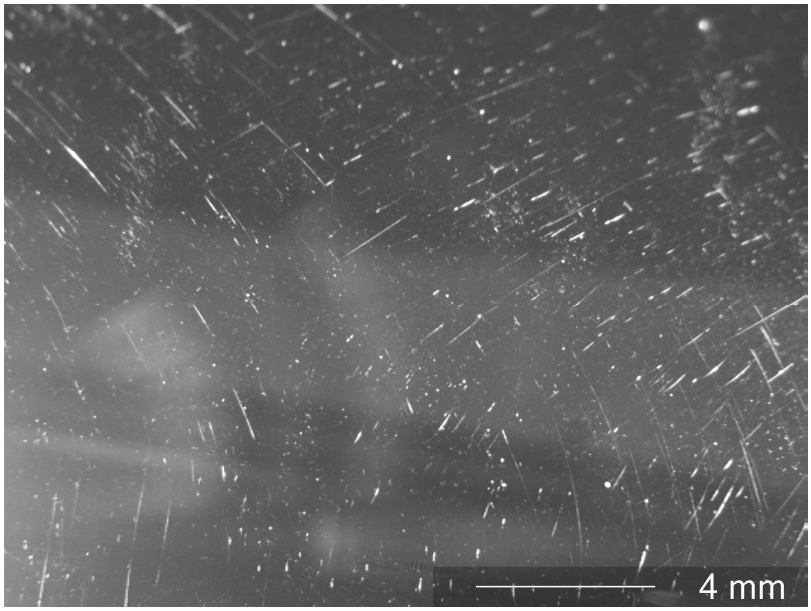

Figure 4-17 Close up of the femoral component

5 VALIDATION

To validate the performance of the knee joint wear tester a number of tests were performed, initially ranging from a few cycles to check the machines operation to a preliminary test of 82,000 cycles that had to be prematurely stopped due to fluid evaporation. The final experiment performed was a 1 million cycle wear test carried out at 1Hz. The machine performed as designed, without any component failures and the only stoppages were performed for weight loss measurements. The results showed wear rates and morphology similar to other wear testers and joint simulators.

5.1 PRELIMINARY TEST

This test was carried out using a 1 : 0.5 slide to roll ratio, so the results could be compared to those of Saikko et al [36, 37]. A 25% bovine serum (South Pacific Sera) solution was made up and 30ml added to each of the tibial trays. Since the water content in the bovine serum would evaporate during the test it was intended to manually top it up with deionised water every day. Unfortunately the rate of evaporation was much faster than this and the test ran dry after 82,000 cycles and was stopped. Figure 5-1 shows the polymer transfer layer on the femoral component that occurred under dry sliding conditions and was highly unrepresentative of in vivo knee wear conditions. Despite the fluid evaporation problem, the mechanical side of the device showed that it was capable of creating wear in the UHMWPE, as can be seen in Figure 5-2. A close up of the wear track in Figure 5-3 shows the scratches crossing each other at a narrow angle, indicating multidirectional motion. As a result of this test, the requirements for a fluid recirculation system were added to the design specification and the machine modified to accommodate the peristaltic pumps and associated hardware.

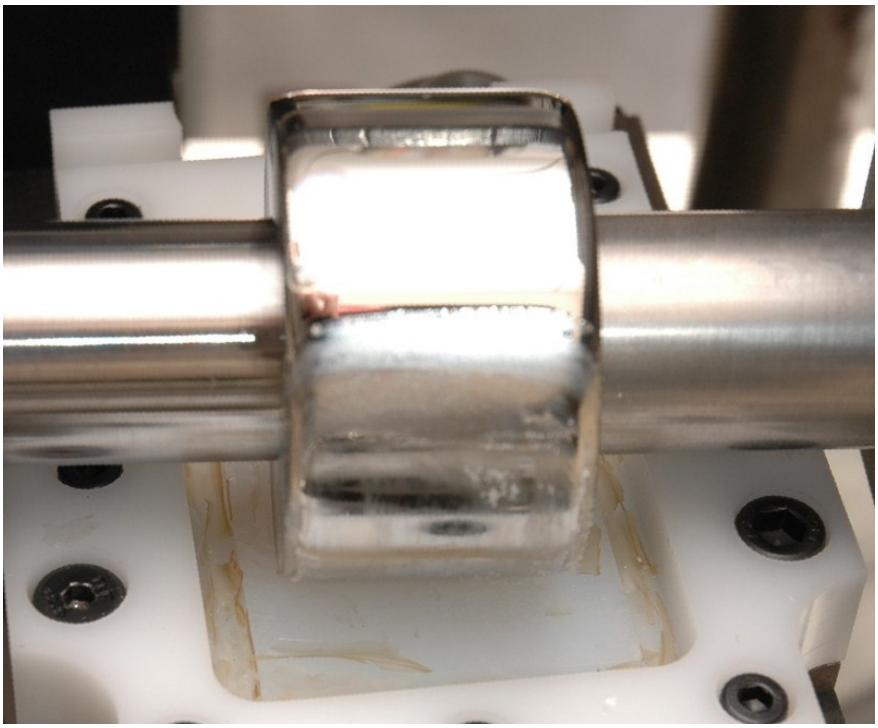

Figure 5-1 Polymer transfer layer on the femoral component

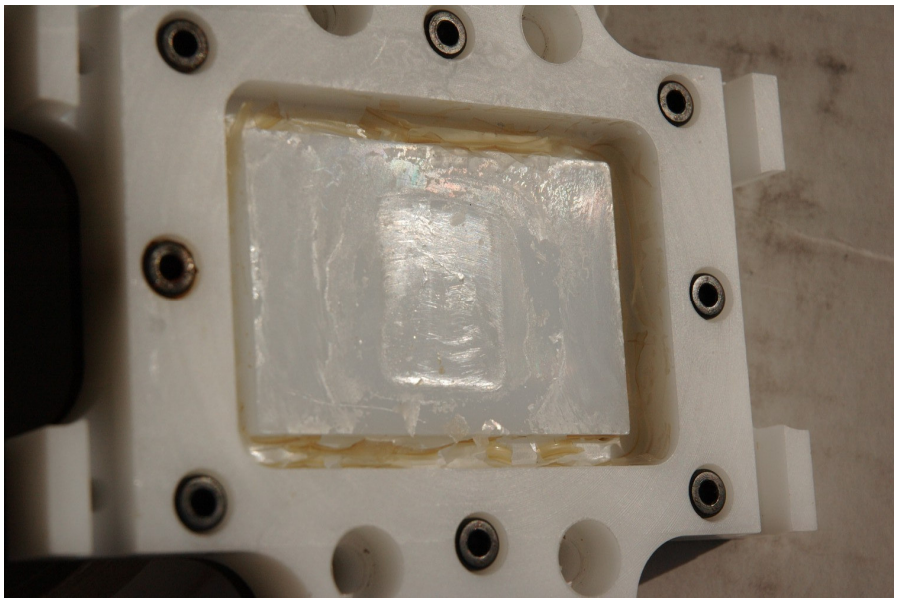

Figure 5-2 Wear tracks in the UHMWPE surface

Figure 5-3 Close up of the wear track. Note the wear marks crossing each other

5.2 MILLION CYCLE WEAR TEST - METHOD

Three UHMWPE test samples and three identical UHMWPE soak controls were soaked in a 25% bovine serum solution for nine months to minimise fluid uptake during the test. These were cleaned, dried and weighed as follows:

Rinse H_2O
5 min ultrasonic clean H_2O + detergent
Rinse H_2O
5 min ultrasonic clean H_2O + detergent

Rinse H_2O
Rinse ethanol
5 min ultrasonic clean ethanol
Rinse ethanol
Vacuum dry @ 0.001mm Hg for 30 min
Weigh - 5 times per sample - Sartorius balance (0.1mg resolution)

While handling samples during the weighing procedure the operator was always earthed to the balance, and samples not being weighed were stored on a metal plate that was earthed to the balance. The purpose of these procedures was to minimise the effects of static electricity on the measured mass of the samples.

The machine and safety guard were wiped down and the femoral components, sample holders and fluid recirculation system were ultrasonically cleaned and rinsed before being assembled with the UHMWPE test samples. 200ml of bovine serum solution was added to each of the three reservoirs and the soak controls were stored in distilled water. The test was commenced using a 1 : 0.5 slide to roll ratio, ±7.5º IE rotation and a load of 2KN.

Two minor modifications to the test rig were carried out during the test; shortly after starting the experiment the covers of the peristaltic pumps were removed to allow better cooling and at ¼ million cycles the fluid reservoirs were increased in size from 400ml to 1000ml. The recirculation of the bovine serum caused bubbles to form in the reservoir and some of the serum was lost as the foam escaped down the vacuum line. Increasing the reservoir size stopped the foam loss and also allowed the soak controls to be stored in the same solution as the test samples. For the remaining ¾ million cycles the soak controls were stored in the bovine serum.

The cleaning and weighing was performed at 251,000 cycles, 540,000 cycles, 765,000 cycles and 1,003,000 cycles and the bovine serum was also replaced at 540,000 cycles.

The knee joint wear tester took just over two weeks to complete a million cycles and at the end of the test, after cleaning and weighing, two of the three samples were gold coated for SEM examination and the other retained for optical microscopy.

5.3 RESULTS

5.3.1 WEIGHT LOSS

The mean wear rate for the UHMWPE tibial components was 14.7mg/10^6 cycles, with a range of 13.9 to 16.1mg/10^6 cycles. A graph of the weigh loss over the test is shown in Figure 5-4. The error bars shown are the maximum variation in the weight measurement of the individual samples.

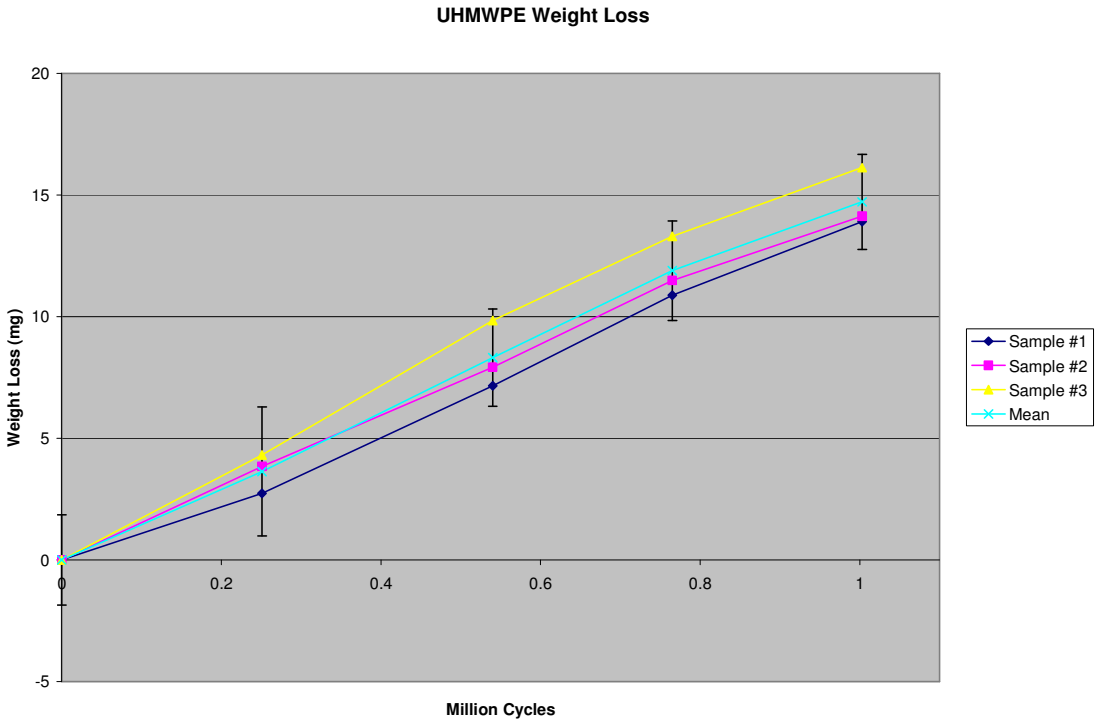

Figure 5-4 UHMWPE weight loss

5.3.2 VISUAL EXAMINATION

The wear tracks in the UHMWPE samples show an indented area 27mm wide by 17.5mm long with a polished or burnished appearance and the removal of machining marks left from manufacture. There are a number of scratches or gouges in the surface that have had their edges smoothed over and the majority of them tend to be near the edges of the wear track. Figure 5-5 displays a "v" shaped scratch showing the path of motion of a scratch on the femoral component relative to the motion of the UHMWPE sample. Perpendicular to the AP direction are two lines 10.5mm apart that are deeper than the other parts of the wear track. These two areas of high wear are called tractive[1] rolling zones, for reasons discussed later.

Visual examination of the 316 stainless steel femoral components revealed numerous fine scratches in a very thin elliptical pattern covering the area in contact with the UHMWPE. A large proportion of the scratches were running along the FE direction, with the ends of the FE motion defined by an area of tightly curved scratches, created in this location as the majority of the IE rotation occurred near each end of the FE travel. There were several deeper scratches of the surfaces of the cylinders, as shown in Figure 5-6 of the femoral component from test station 1. The femoral components are shown on a black cloth to maximize the visibility of the scratches. When viewed in conjunction with Figure 5-7 of the corresponding UHMWPE component, it can be seen that the location of the large scratch on the femoral component (shown by arrow) matches the gouge in the UHMWPE test component. There was no appreciable difference in the number of scratches between femoral components 1 and 2, but number three had a higher level of fine scratches as shown in Figure 5-8.

[1] The evidence for these two deep wear tracks 10.5mm apart being caused by tractive rolling is not conclusive. Gliding motion could instead be the cause. Further investigation is required to determine which wear mechanism caused the observed damage.

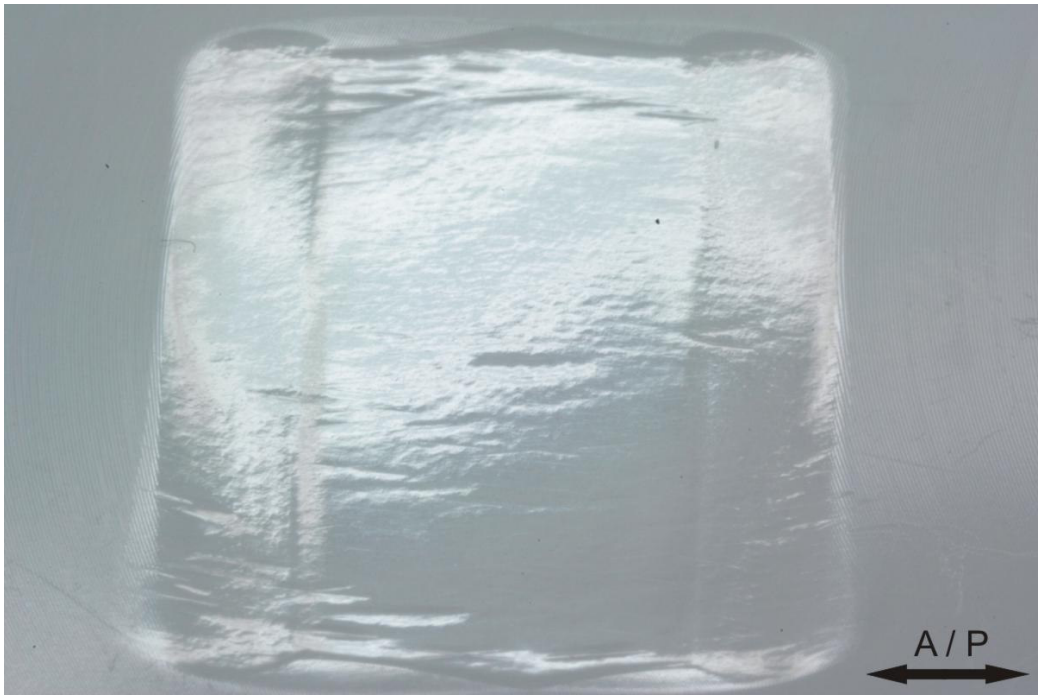

Figure 5-5 UHMWPE sample #2

L to R: End section, tractive rolling zone, middle section, tractive rolling zone, end section

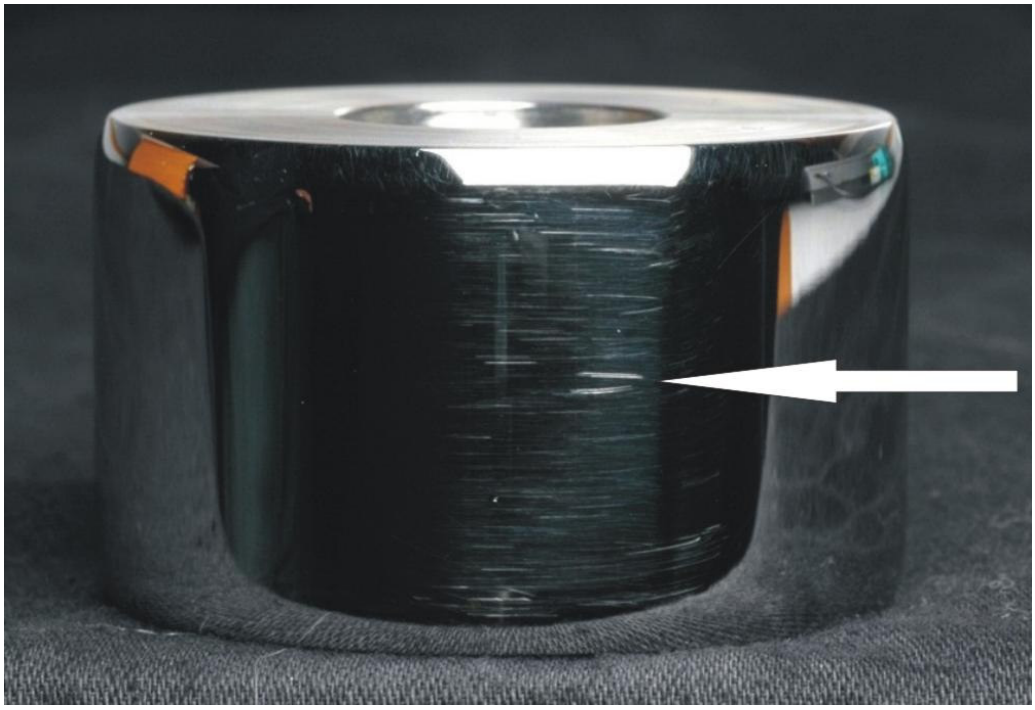

Figure 5-6 Femoral component #1.

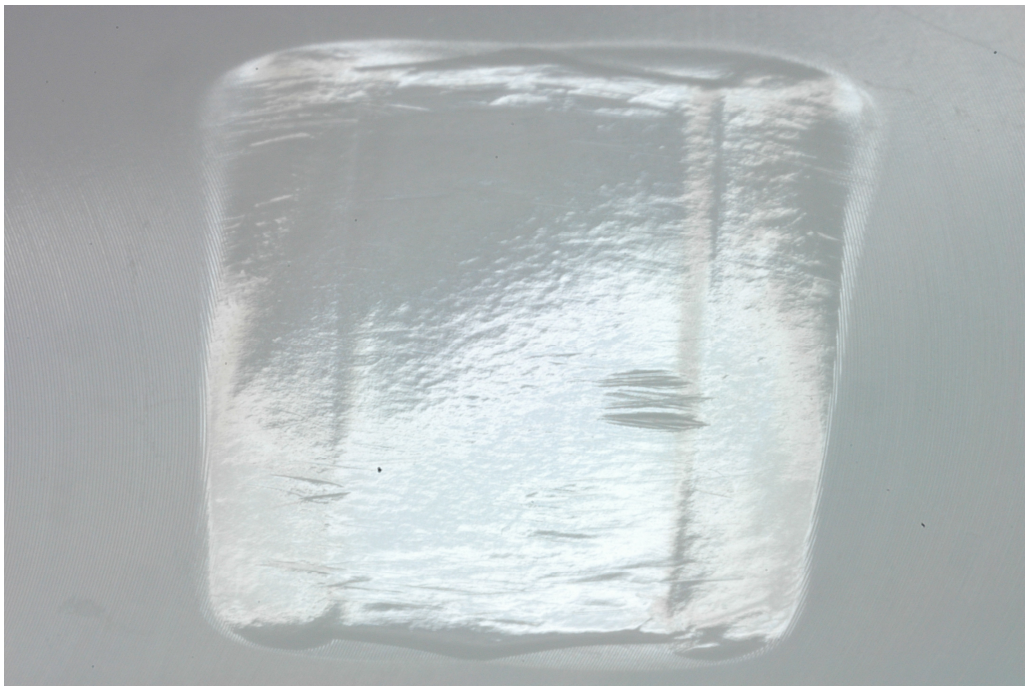

Figure 5-7 UHMWPE sample #1.

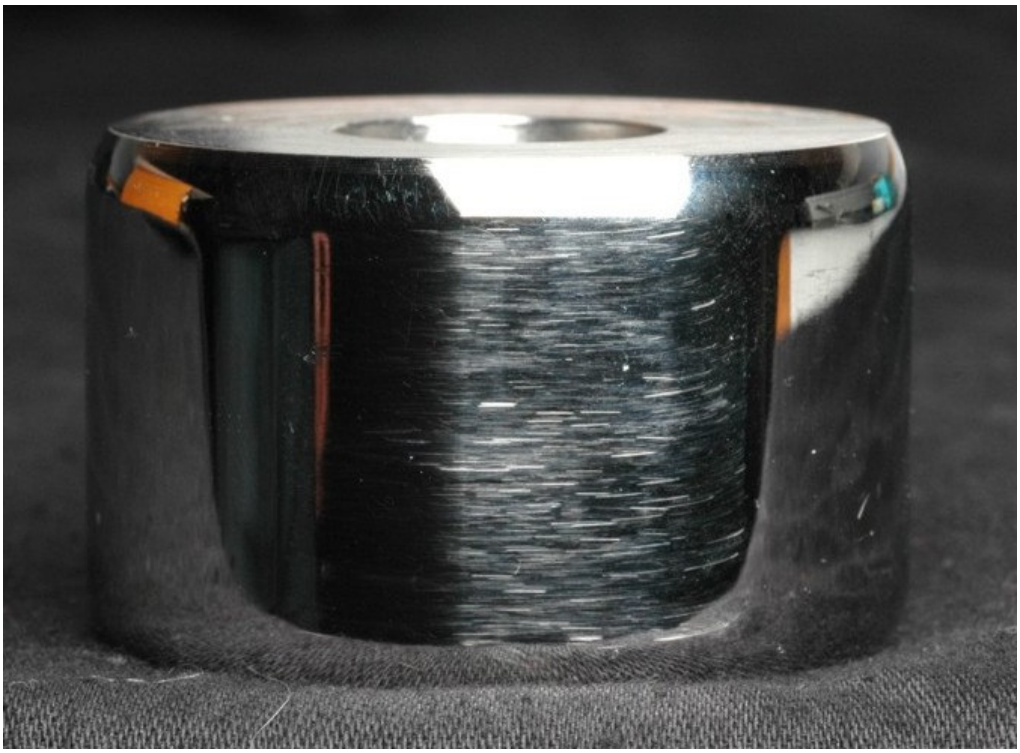

Figure 5-8 Femoral component #3.

5.3.3 OPTICAL MICROSCOPY

Low magnification showed the scratches visible to the naked eye, along with large smooth areas that had some gentle undulations. 1000x magnification of the polished or burnished areas revealed a densely packed rippled texture, with the majority of ripples between the tractive rolling zones running approximately perpendicular to the AP direction. Some areas of this zone had randomly oriented ripples as shown in Figure 5-10 and near the middle of the wear track a number of ripple free areas were observed that were completely devoid of features at 1000x magnification. In two places near the tractive rolling line, small areas of ripples were found that ran nearly parallel to the AP direction. These ripples, shown in Figure 5-11 were much straighter and more uniform than others observed in other areas. Figure 5-9 shows the large gouge in UHMWPE sample #1 at 5x magnification. The same area is shown in Figure 5-13 at 500x magnification with densely packed ridges adjacent to the gouge and on this occasion they are running approximately perpendicular to the direction of the scratch.

At 1000x magnification the regions at either end of the wear track appeared to be made up of three types of areas; ripples aligned 45º to the left of the AP direction, 45º to the right of the AP direction as well as randomly oriented. Some of the 45º oriented ripples are shown in Figure 5-12. Figure 5-14 at 1000x magnification shows one of the tractive rolling zones. The typical ripples can be seen, but these abruptly end and an unusual wear pattern is observed. The wear damage in this area is deeper than the surrounding ripples, being approximately 5µm below the main rippled surface. It appears that this small area of the surface has delaminated and left behind a network of random cracks. For the purpose of giving this feature a name in this thesis it will be called micro-delamination to distinguish it from the larger scale delamination that is commonly found in UHMWPE that has been air irradiated and aged or is suffering from consolidation defects [49]. This surface feature continues for 2-3mm in a wavy line 10-20µm wide that runs perpendicular to the AP direction, meaning that it only covers

approximately 0.01% of the total wear track area. Generally the orientation of the ripples on one side of the micro-delamination are quite different to the orientation of the ripples on the other side. Due to the depth of field limitations of optical microscopy, the photo does not fully show the differences in surface morphology between the common ripples and the micro-delamination area.

Figure 5-9 Gouge from sample 1. Original magnification 5x

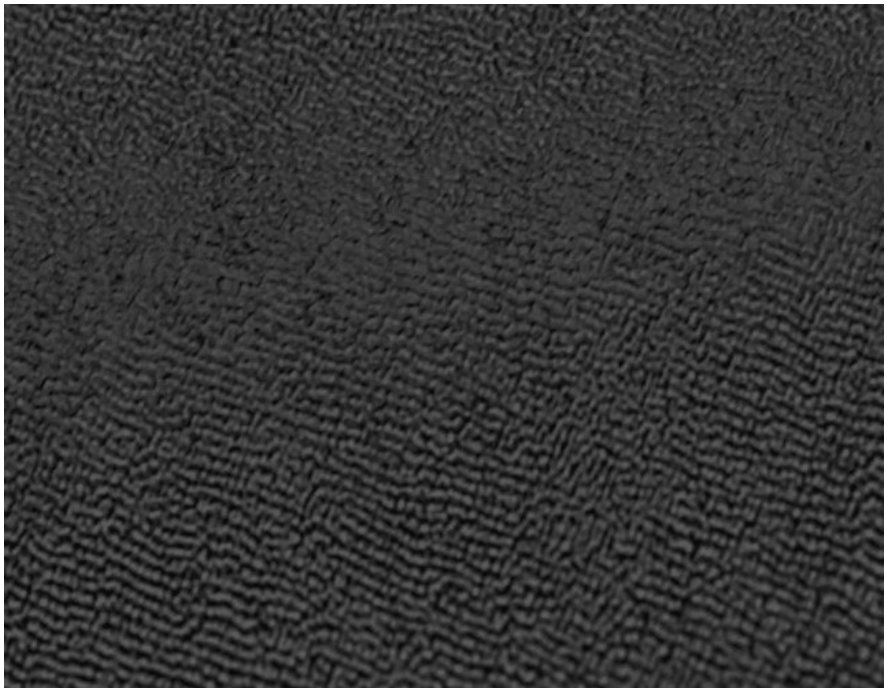

Figure 5-10 Randomly orientated ripples. 500x cropped to equal 1000x

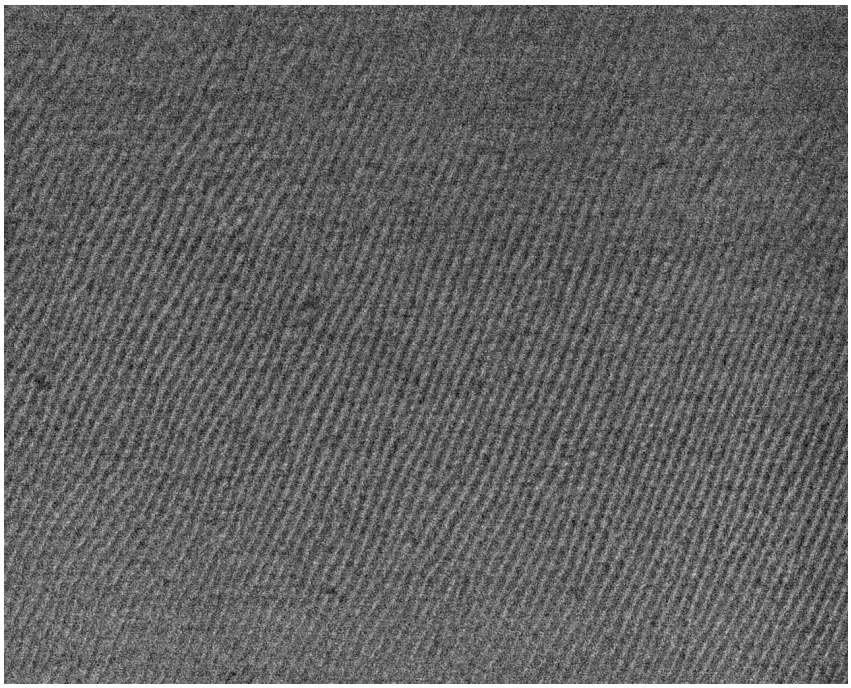

Figure 5-11 Ripples running almost parallel to the AP direction. Original magnification 1000x

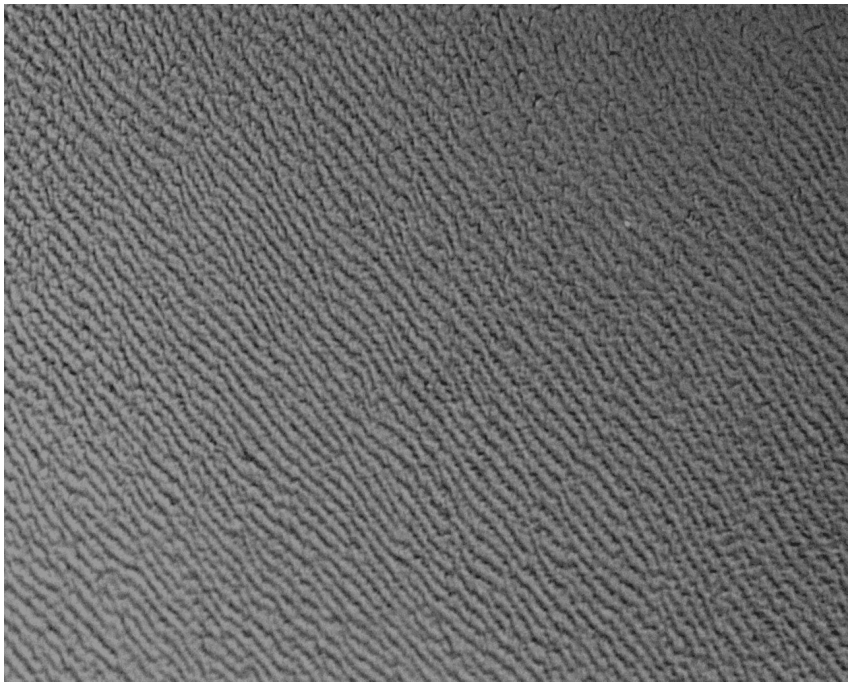

Figure 5-12 Rippled texture from the IE zone running 45º to the AP motion. Original magnification 1000x

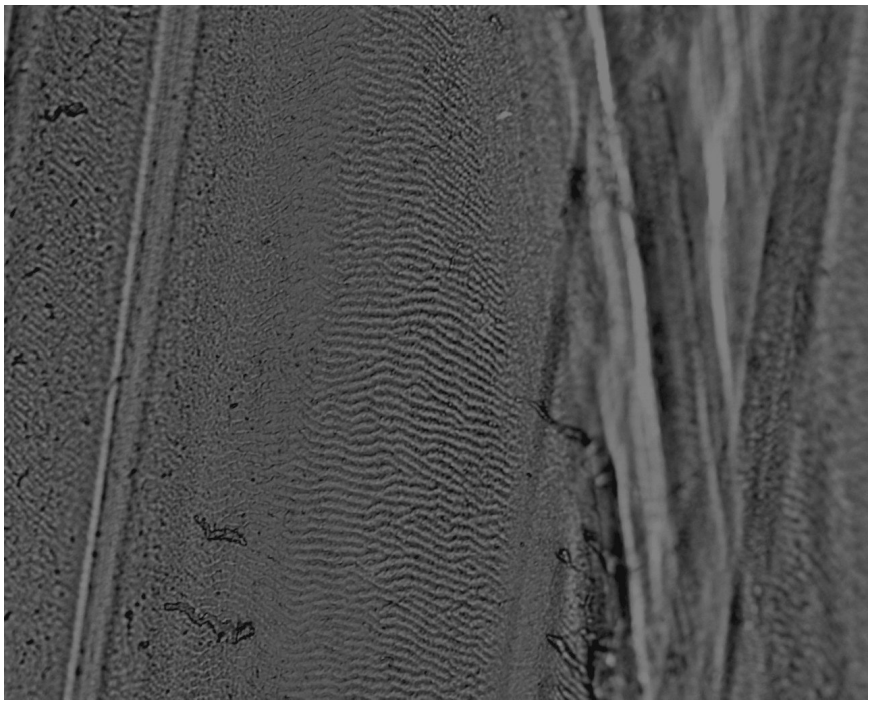

Figure 5-13 Ripples perpendicular to a major scratch. 500x original magnification

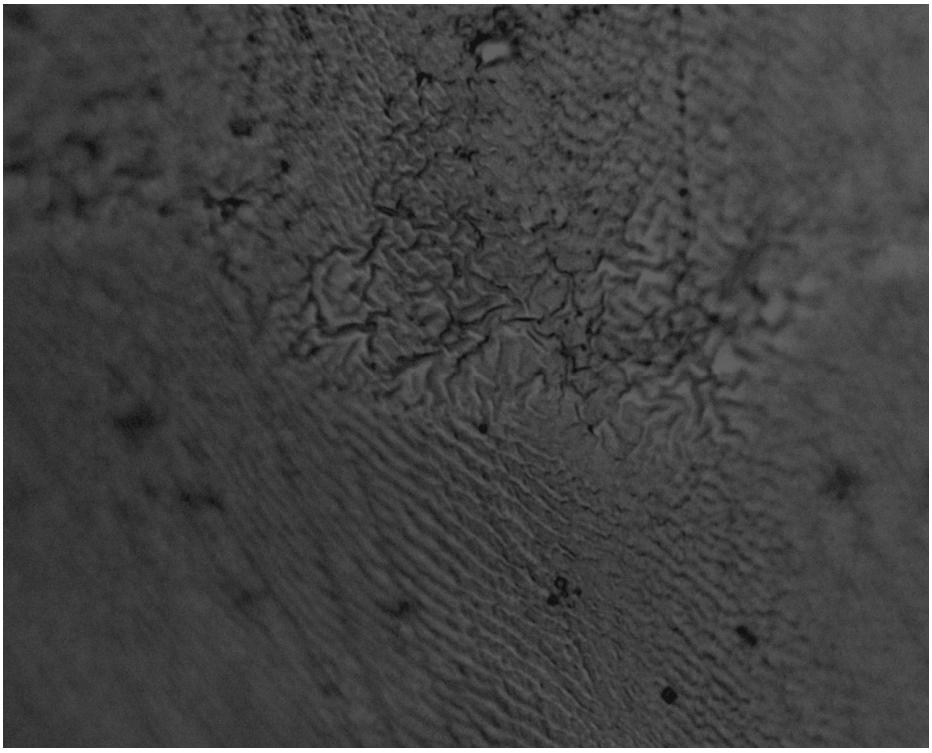

Figure 5-14 Wear patterns from tractive rolling. Original magnification 1000x

5.3.4 SCANNING ELECTRON MICROSCOPY

The scanning electron microscope (JEOL JSM 6100) revealed further details of the typical ripple pattern of the worn UHMWPE surface as shown in Figure 5-15. The remains of a hard 3rd body particle that had been shattered and embedded in the UHMWPE is shown in Figure 5-16. The curved path that the particles lie on, show the direction of motion the femoral component took while traversing this area. Figure 5-17 shows the ripple pattern in more detail. The rough edges of the ripples are an indication of the formation of fibrils, but the resolution is not high enough to confirm this. The ripple pattern has a periodicity of 1-2μm. Figure 5-18 and Figure 5-19 show large wear debris particles that are either in the process of being removed from or embedded into the surface of the UHMWPE. These particles are fairly elongated, being approximately 15μm long and 0.5μm wide.

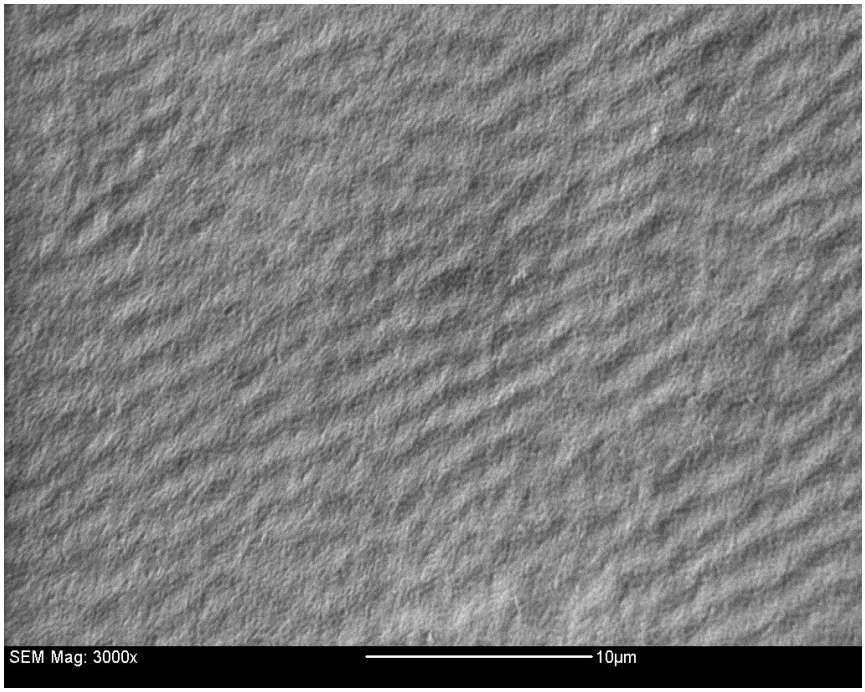

Figure 5-15 Rippled texture of the worn UHMWPE surface

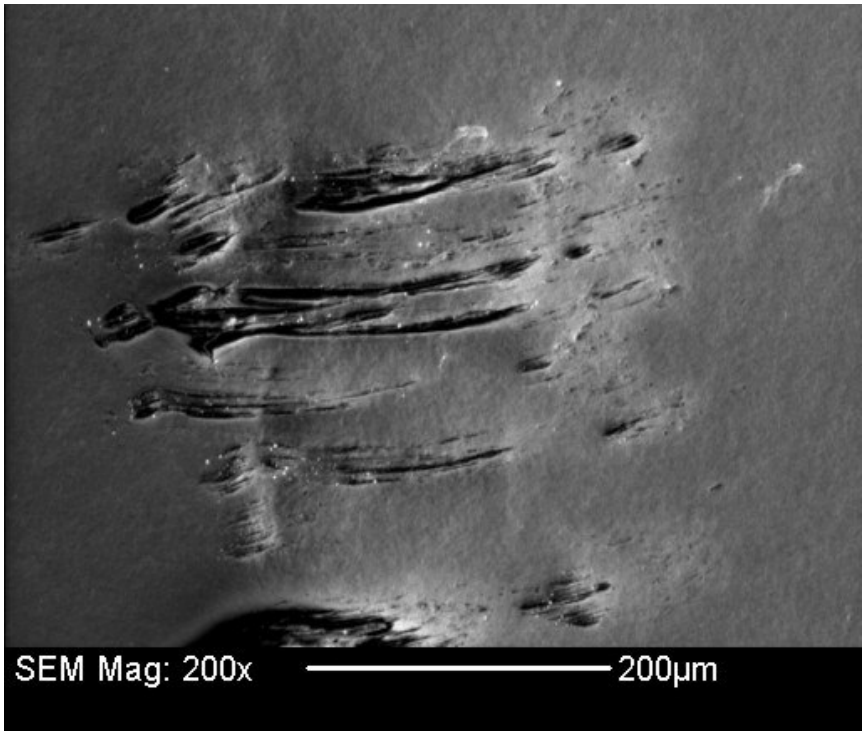

Figure 5-16 Third body debris embedded into the UHMWPE surface

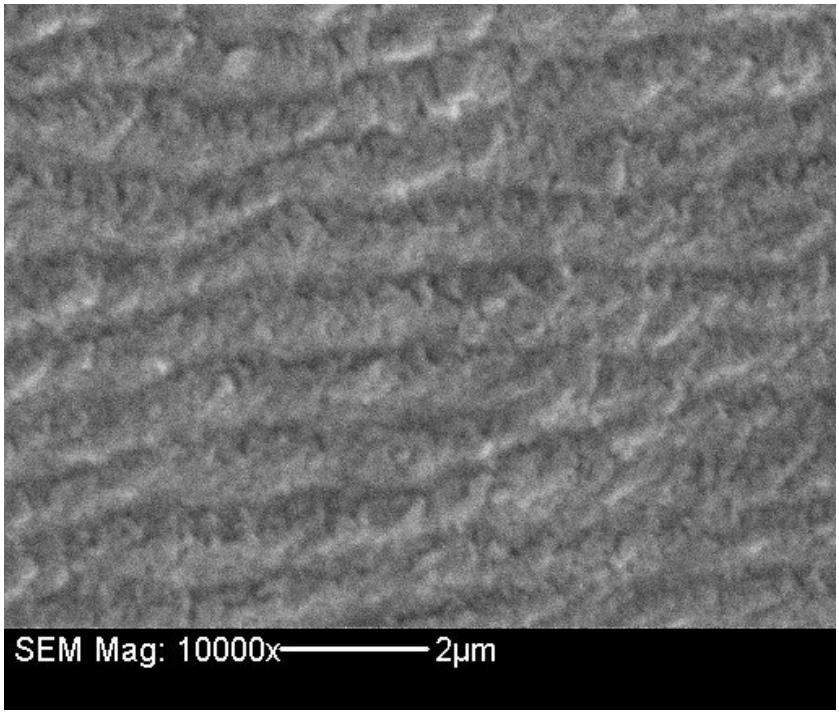

Figure 5-17 Rippled surface texture at 10,000x

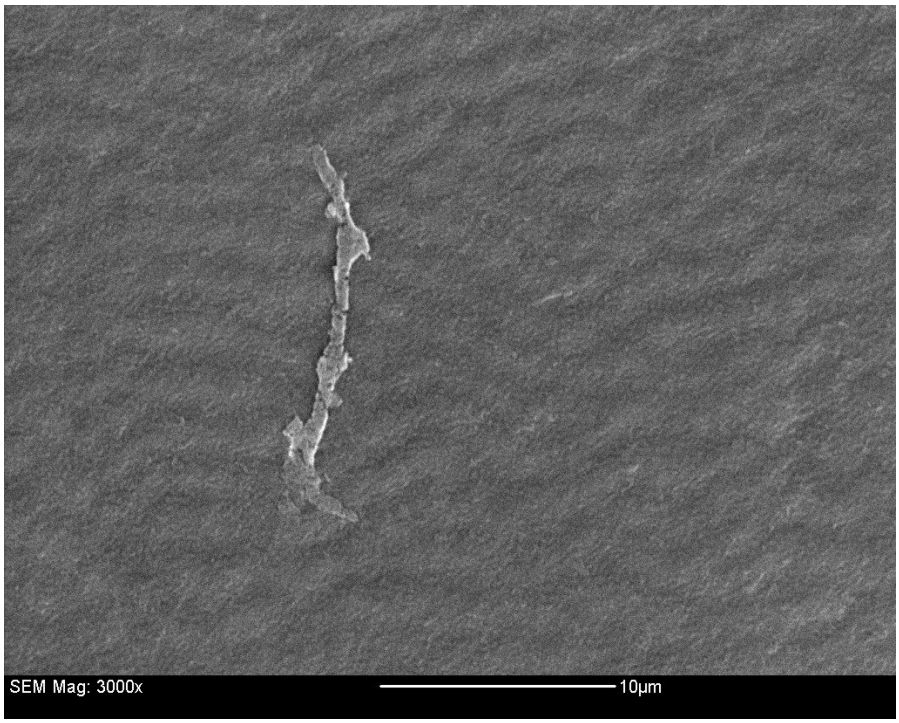

Figure 5-18 Embedded wear debris

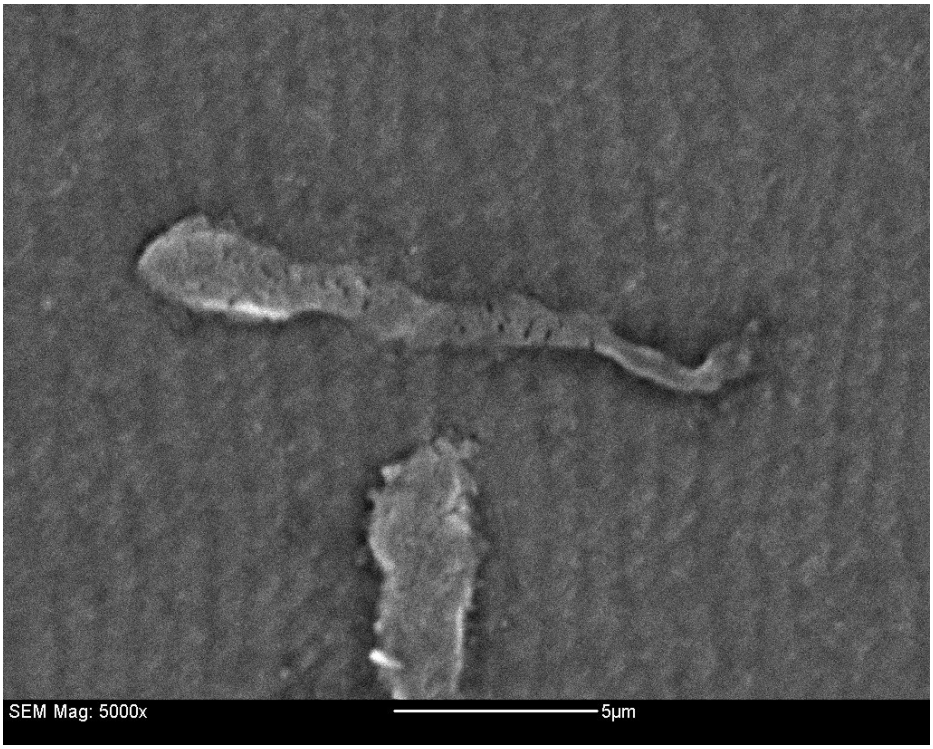

Figure 5-19 Embedded wear debris

5.4 DISCUSSION

5.4.1 WEIGHT LOSS

The slide to roll ratio of 1 : 0.5 for this test was selected as it gave conditions very similar to those reported by Saikko et al [37] and would serve as a useful comparison. The mean weight loss for this experiment of 14.7mg/million cycles was close to the 14.5mg/million cycles reported by Saikko et al. The two main differences between the tests were as follows; scratches to the femoral components showed that 3rd body wear occurred in this test but was not reported in Saikko et al's experiment, and Saikko et al used a sphere rather than a cylinder as a femoral component which had the effect of creating higher peak contact stresses but a smaller width of wear track. The net effect

of these differences could not be fully quantified, however results from Mcgoulin et al [23] suggested that they were small when compared to such things as the effect of IE rotation. For the same slide to roll ratio, McGoulin's group found a wear rate of only 3mg / million cycles despite the occurrence of third body wear and higher contact stresses, although the load was lower. The primary difference here was a lack of IE rotation.

There was a large range of knee joint simulator wear rates reported in the literature, due to a lack of universally agreed conditions to test the implants under, as well as different implant designs and materials. Earlier studies had values ranging from less than 2mg/10^6 cycles to over 70mg/10^6 cycles [23] but the range has now decreased as some of the previous variables, such as distilled water or bovine serum for lubrication have now been largely standardized. Wang et al [18] obtained a wear rate of 13.4mg/10^6 cycles using a Duracon TKR with a 2.5Mrad irradiated UHMWPE tibial component, and Kawanabe et al [50] found wear rates of 15.1±2.6mg/10^6 cycles and 18.8 ±2.7mg/10^6 cycles with Biomet AGCs. The effect of the 2.5Mrad irradiation dose on the wear of the TKR was not thought to be huge, as Saikko et al [37] also tested material irradiated at 2.5-4Mrad and found a wear rate 17% lower than non-irradiated UHMWPE. While there were many differences between these simulator studies and the wear test described here, the use of simplified TKR components, loads, motions and materials have produced similar wear rates.

Despite ultrasonic cleaning of components and other equipment and careful handling of the samples, external debris got into the bovine serum. It was then embedded in the UHMWPE surface where it scratched the 316 stainless steel femoral components and these in turn scratched and gouged the UHMWPE surface. This is known as third body wear and the majority of this debris was thought to have come from construction activity of another project using the same room that involved cutting and dust generation. Femoral component number three had the most scratches and this test station also recorded the highest wear rate of 16.1mg /10^6 cycles. To reduce or

eliminate 3rd body wear and obtain more accurate results, future tests should be carried out in a considerably cleaner environment and the 316 stainless steel femoral components should instead be made of the considerably harder cobalt chrome.

To minimise the use of bovine serum, the soak controls were stored in distilled water for the first 251,000 cycles. This mistake of treating the soak controls differently to the actual wear samples became apparent at the first weigh in at ¼ million cycles where all the samples were cleaned and weighed. Some of the soak controls showed a larger weight loss than some of the wear samples, whereas no change or a very small weight gain was expected. As a consequence of treating the soak controls differently from the test samples, their use in correcting the fluid absorption of the test samples was no longer valid and so were not used. However the effect of not using soak controls was expected to be minimal as the UHMWPE samples had been pre-soaking in bovine serum for nine months, which should have left them very close to a fully saturated equilibrium state. This error was shown to be reasonably small, as during the remaining ¾ million cycles in the reservoirs with bovine serum, the soak controls showed a weight change of less than 1 mg.

5.4.2 WEAR DEBRIS

The fibrils and other wear debris particles retrieved from TKR are generally larger than those retrieved from THR, with one study finding the mean sizes being 1.7μm and 0.6μm respectively. Predominantly the shape of the TKR debris was spherical with occasional fibrillar attachments and flakes. The largest particle reported was 22μm [51]. The flat and elongated wear debris identified in this thesis, measuring approximately 15μm long, was considerably larger than the above mean and the shape was also quite different. It was most likely the difference in morphology was caused by the particles becoming embedding in the UHMWPE surface and then being repeatedly flattened and elongated by the action of the femoral component. These few random wear particles embedded in the UHMWPE sample were highly unlikely to be

representative of the particle size distribution produced during this wear test. Proper wear debris isolation using potassium hydroxide digestion of the bovine serum was hampered by the unavailability of 0.2μm polycarbonate filters and by the not totally unexpected failure of 0.22μm nitro-cellulose filters due to the potassium hydroxide solution. Future debris isolation should be carried out using the correct filters.

5.4.3 UHMWPE WEAR SURFACE

Visual examination of the wear surfaces showed the typical polished surface that is usually found in retrieved implants as well as from knee joint simulator tests. Unlike some older implants, no large scale delamination or cracking was observed, but this was not expected as high quality UHMWPE was used and it had not been air irradiated and aged. The fine scratches from 3rd body wear that were observed on the surface of the femoral component are reasonably common [23], [52], although the larger scratches and gouges in the UHMWPE are less so.

Optical microscope examination of the polished surface revealed ripples running perpendicular to the main direction of motion in the middle section, as well as ripples with random orientations. These are common features of both worn replacement hip and knee UHMWPE components [18], [37], [26] and are the typical wear surface produced by sliding wear [35]. The ripples at both ends of the wear track showed a more random orientation, with a reasonable proportion running ±45° to the AP direction. This was thought to be caused by the greater rate of IE rotation in these areas leading to a complex pattern of wear tracks that crossed each other in multiple directions. The ripples found in the tractive rolling zone that were almost parallel with the AP direction were thought to be caused by the rolling motion in this area. Similar ripples with a very uniform and straight appearance had also been found by Tamura et al [35] in areas of UHMWPE that have undergone rolling in TKR joint simulator

studies, and these had also been reported in retrieval studies [53] in areas where rolling was thought to have occurred.

The two lines 10.5mm apart that ran perpendicular to the AP direction were thought to be the result of tractive rolling. Based on visual examination of the depth of the wear tracks, these two lines had the highest wear rate on the surface of the UHMWPE, with the exception of large 3rd body gouges. The mechanisms by which tractive rolling is thought to occur and how it may relate to the "micro-delamination" found within the tractive rolling zone seen in Figure 5-14 is discussed below. For an instant at the start and half way through each cycle, both the AP translation and FE rotation are stationary. Even though the wear tester was set to a slide to roll ratio of 1 : 0.5, the initial motion would be pure rolling (1:1) as the "play" in the mechanisms would allow the frictional force between the femoral and tibial components to cause rolling. Once the "play" in the system was taken up, the tangential force between the two components would increase until it exceeded the frictional force and then sliding with a slide to roll ratio of 1: 0.5 would occur. This period where tangential forces exist while pure rolling occurs is known as tractive rolling [32] and has been shown to cause deeper wear tracks [54] as the shear stresses induced in the UHMWPE are higher than when sliding occurs. In the experiment reported here the two tractive rolling lines are approximately 1mm from each end of the AP translation, which fits with Schwenke et al's [54] findings of tractive rolling damage occurring just after pure rolling.

Knowing that tractive rolling occurs during the initiating or breaking of rolling [32] and gait analysis has shown this to occur two times per cycle [54], it could be expected to be a common phenomenon in TKR. However such a pronounced line or micro-delamination has not been observed in retrieved implants and although not exhaustive, searches in the literature for photos or a description of micro-delamination have not returned any positive results. However that is not to say this phenomenon does not exist. The lack of a well defined tractive rolling line in retrieved TKR is caused by the slide to roll transition point changing due to variations in the patients gait and the lack

of micro-delamination can be explained by the more common sliding wear mechanisms removing the tractively rolled surface before the micro-delamination has a chance to occur. While Saikko et al [36], [37] did not report this phenomenon, photos from their experiment of a UHMWPE sample show greater wear depth near the ends of the wear track, similar to this experiment. Since micro-delamination was only observed over 0.01% of the total wear trackin this experiment, it would be quite easy to miss it during microscope examination.

The depth of the micro-delamination surface below the adjacent rippled surface and the sudden drop to the lower surface suggests that it was unlikely to be caused by the common sliding wear mechanisms of abrasive wear or ripple formation followed by fibril pullout (previously known as adhesive wear), as it is hard to envisage how the surface of the femoral component could actually reach the surface of the micro-delamination without causing significant rounding the corners of the surrounding rippled surface.

It is thought that the micro-delamination found here is the most extreme form of tractive rolling damage and will only occur in joint simulators under high stresses and where the slide to roll transition point is constant and repeatable. Consolidation defects are a known cause of large scale delamination (>0.5mm) [49] and may also be a contributing factor for micro-delamination by providing a sub-surface crack initiation point that is then grown by the tractive rolling shear stresses. Although the lubrication mechanisms were not explicitly studied, the lower component velocities near the tractive rolling zones (as opposed to the middle of the wear track) are more likely to result in boundary lubrication, asperity contact and associated higher wear rates and transmission of tangential forces.

While multidirectional motion has been proven to be a major factor in the wear rates and mechanism of adhesive type wear, its effect on tractive rolling induced micro-delamination is unknown. It occurred during this experiment where IE rotation was

included, but further research will need to be carried out to determine the importance of multidirectional motion on this wear mechanism.

The aim of research in this area is to gain a better understanding of the mechanisms and processes of UHMWPE wear in THR and from this to develop improved products and ultimately better clinical outcomes. Further investigation is required to either prove or disprove micro-delamination wear in a non-irradiated UHMWPE and in the process may yield insight into the mechanisms of higher wear rates in tractive rolling zones. This could be confirmed by a more detailed surface examination, monitoring the frictional force throughout the cycle and adding displacement transducers to the axes of motion to determine if tractive rolling is occurring.

6 CONCLUSIONS AND RECOMMENDATIONS

6.1 CONCLUSIONS

From the literature it was found that multidirectional motion occurs in TKR and is an important aspect for recreating UHMWPE wear similar to in vivo conditions. It was also found that the type of motion of the femoral component relative to the tibial component, namely sliding, rolling or gliding produced different wear rates and mechanisms. Other researchers using wear testers had investigated each of these phenomenon individually but had not investigated the two combined and this led to the aim of the project, the design of a 3 station knee joint wear tester capable of investigating the effects of slide to roll ratio on UHMWPE wear in total knee replacements.

A full design specification was created and the machine designed and manufactured to meet this. The device has 3 individual test stations that have 57º flexion extension, variable anterior posterior translation from 0 to 25mm and internal external rotation of 15º that is 90º out of phase from the other two motions. Each test station has its own fluid reservoir and recirculation system and the load per station can be set at any force up to 2KN.

A million cycle validation test was successfully carried out on non-irradiated UHMWPE samples using a 2KN load with a slide to roll ratio of 1 : 0.5. The mean

wear rate was 14.7mg/10^6 cycles which was in good agreement with the 14.5mg/10^6 cycles reported by Saikko et al, who used a very similar load and motion profile. Examination of the wear tracks by visual, optical and SEM methods revealed a surface morphology similar to other reported wear testers, knee joint simulator and retrieved total knee replacements. The surface featured some scratches caused by 3rd body debris as well as polished areas. Under magnification these polished areas revealed a fine ripple pattern, with a periodicity of approximately 1-2μm. Some of these areas showed randomly oriented ripples, while others showed an orientation perpendicular to the primary direction of motion. Small areas of uniform ripples running parallel to the primary direction of motion were also observed which are indicative of rolling motion. The results from the validation study show that the knee joint wear tester is capable of producing wear rates and wear mechanisms similar to those observed in other wear testers and knee joint simulators. Therefore this machine is suitable for further investigations into the effects of slide to roll ratio on UHMWPE wear under multidirectional motion and met the major aim of the project.

Although not a specific design requirement, an interesting and unexpected phenomenon of tractive rolling was identified near each end of the AP motion. This was shown as a line of wear that was deeper than the surrounding wear track, and within this tractive rolling zone micro-delamination approximately 5μm deep was observed. While large scale delamination is a regular occurrence in aged air irradiated tibial components as well as poorly consolidated UHMWPE, delamination on such a small scale is not.

6.2 RECOMMENDATIONS AND FUTURE WORK

There are a number of changes that could be made to the knee joint wear tester to improve its accuracy in recreating UHMWPE wear and measuring the factors that influence this wear. Possible future work is discussed below.

6.2.1 FEMORAL COMPONENT

The femoral components should be made from cobalt chrome (ASTM F75 or F1537) and polished to an implant grade surface finish of 0.05μm Ra. The greater hardness of the cobalt chrome would give it considerably better resistance to 3rd body scratching than the 316 stainless steel. The combined effect of these two factors would greatly reduce abrasive wear and gouging and therefore would be more representative of an in vivo TKR.

6.2.2 TESTING ENVIRONMENT

While the Perspex cover over the machine provided some protection against dust in the room, it was not sufficient to prevent debris from getting into the bovine serum which in turn caused 3rd body wear. Ideally, further experiments would be carried out in a temperature controlled clean room, but the lack of availability of such a facility leads to the more practical solution of installing a continuous supply of filtered air into the Perspex safety guard to act as a mini clean room. Thorough cleaning of the room before the test and careful handling of the components during setup, cleaning and weighing would also help minimize the chance of getting debris in the test chambers.

6.2.3 WEIGHING PROCEDURE

The effects that static electricity had on the weight measurements were reduced by earthing the samples to the balance, but it is thought that repeatability of the measurements could be further improved by performing the weighing in a high humidity, temperature controlled room.

6.2.4 WEAR DEBRIS ISOLATION

The purchase of 0.2μm polycarbonate filters specifically designed for imaging of particles extracted from fluids would allow proper wear debris isolation and analysis.

6.2.5 COEFFICIENT OF FRICTION MEASUREMENT

Measurement of coefficient of friction at a high sampling rate would provide useful data that could be used to help determine when tractive rolling was occurring and the tangential forces involved. It may also give some insight into the lubrication conditions, by comparing the coefficient of friction to the velocity of the components at different positions during the cycle. The dieset top plate, which is attached to the tibial tray, has a thin section with strain gauges attached. The intention was to use these integrated "load cells" for friction measurements, but initial tests showed significant hysteresis as the direction of motion changed. Therefore a non-linear calibration is required to obtain meaningful data.

6.2.6 FE, AP AND IE ROTATION MEASUREMENT

The motions of the three axes were determined with Solidworks and Cosmos Motion based on ideal mechanisms with no slop or play in them. In reality there is some play in the bearings and linkages and although not large, is thought to be one of the factors that

caused tractive rolling. Attaching rotary and linear encoders to the appropriate axes would give the exact motion of the test components which could be used to determine the location and length of the tractive rolling zones. This data could then be compared with the friction results and surface examination.

6.3 FUTURE WORK

Further validation of the wear tester could be carried out by testing UHMWPE that has been air irradiated and aged, as well as other samples that have been irradiated in an inert atmosphere. Based on clinical experience, it is expected that the air irradiated and aged UHMWPE would show large scale delamination wear and the highest wear rate, followed by the non-irradiated material and finally inert atmosphere irradiated UHMWPE with the lowest wear rate. If the knee joint wear tester produced these results, the confidence in future experiments performed on the machine would be enhanced.

A series of three experiments should be carried out to investigate the effects of slide to roll ratio under multidirectional motion. This should be carried out using UHMWPE irradiated in an inert atmosphere as the majority of tibial components are irradiated for sterilization and cross-linking and a typical dose would be between 2.5-4MRad. Throughout all these experiments, further investigations into tractive rolling and micro-delamination could be performed to gain a better understand of the factors influencing this wear mechanism, how it relates to in vivo tractive rolling and its associated higher wear rate.

7 REFERENCES

[1]F. H. Netter, *Atlas of Human Anatomy*. Basle, Switzerland: Ciba-Geigy Limited, 1989.

[2]A. M. J. Bull and A. A. Amis, "Knee joint motion: Description and measurement," *Proceedings of the Institution of Mechanical Engineers, Part H: Journal of Engineering in Medicine*, vol. 212, pp. 357-372, 1998.

[3]S. C. Shoemaker, D. Adams, D. M. Daniel, and S. L. Woo, "Quadriceps/anterior cruciate graft interaction. An in vitro study of joint kinematics and anterior cruciate ligament graft tension," *Clin Orthop Relat Res*, pp. 379-90, 1993.

[4]D. R. Wilson, J. D. Feikes, A. B. Zavatsky, and J. J. O'Connor, "Components of passive knee movement are coupled to flexion angle," *Journal of Biomechanics*, vol. 33, pp. 465-473, 2000.

[5]K. N. An, E. Growney, and E. Y. S. Chao, "Measurement of joint kinematics using ExpertVision system," presented at Proceedings of the 28th Annual Rocky Mountain Bioengineering Symposium and the 28th International ISA Biomedical Sciences Instrumentation Symposium, Apr 12-13 1991Apr 12-13 1991, RochesterRochester, MNMN, USAUSA, 1991.

[6]C. Reinschmidt, A. J. van den Bogert, B. M. Nigg, A. Lundbergt, and N. Murphy, "Effect of skin movement on the analysis of skeletal knee joint motion during running," *Journal of Biomechanics*, vol. 30, pp. 729-732, 1997.

[7]Y. Ishii, K. Terajima, S. Terajima, K. Imura, S. Imaizumi, K. Koga, T. Hara, and H. E. Takahashi, "In Vivo Three-Dimensional Kinematics of the Human Knee - Instrumented Spatial Linkage Fixed with Intra-Cortical Kirschner Wires," *Transactions of the 41st Annual Meeting of the Orthopaedic Research Society, 1995*, pp. 692, 1995.

[8]M. A. Lafortune, P. R. Cavanagh, H. J. I. Sommer, and A. Kalenak, "Three-dimensional kinematics of the human knee during walking," *Journal of Biomechanics*, vol. 25, pp. 347-357, 1992.

[9]Y. Ishii, K. Terajima, K. Koga, H. E. Takahashi, J. E. Bechtold, and R. B. Gustilo, "Gait analysis after total knee arthroplasty. Comparison of posterior cruciate retention and substitution," *Journal of Orthopaedic Science*, vol. 3, pp. 310-317, 1998.

[10] J. D. DesJardins, P. S. Walker, H. Haider, and J. Perry, "Use of a force-controlled dynamic knee simulator to quantify the mechanical performance of total knee replacement designs during functional activity," *Journal of Biomechanics*, vol. 33, pp. 1231-1242, 2000.

[11] A. Seireg and R. J. Arvikar, "PREDICTION OF MUSCULAR LOAD SHARING AND JOINT FORCES IN THE LOWER EXTREMITIES DURING WALKING.," vol. 8, pp. 89-102, 1975.

[12] A. Hoshino and W. A. Wallace, "Impact-absorbing properties of the human knee," *J Bone Joint Surg Br*, vol. 69, pp. 807-11, 1987.

[13] J. P. Paul, "Forces transmitted by joints in human body," *Institution of Mechanical Engineers -- Proceedings of Lubrication and Wear in Living and Artificial Human Joints*, vol. 181, pp. 8-15, 1966.

[14] American Academy of Orthopaedic Surgeons: http://orthoinfo.aaos.org/fact/thr_report.cfm?Thread_ID=142&topcategory=General%20Information, 27/6/05.

[15] J. N. Wilson, A. W. Lettin, and J. T. Scales, "20 Years of Evolution of the Stanmore Hinged Total Knee Replacement," 1974.

[16] emedicine, "No. of TKR per year in USA," http://www.emedicine.com/orthoped/topic347.htm, 15/6/05.

[17] E. M. Keating, J. B. Meding, P. M. Faris, and M. A. Ritter, "Long-term followup of nonmodular total knee replacements," *Clin Orthop Relat Res*, pp. 34-9, 2002.

[18] A. Wang, C. Stark, and J. H. Dumbleton, "Mechanistic and morphological origins of ultra-high molecular weight polyethylene wear debris in total joint replacement prostheses," *Proceedings of the Institution of Mechanical Engineers, Part H: Journal of Engineering in Medicine*, vol. 210, pp. 141-155, 1996.

[19] E. Ingham and J. Fisher, "Biological reactions to wear debris in total joint replacement," *Proceedings of the Institution of Mechanical Engineers, Part H: Journal of Engineering in Medicine*, vol. 214, pp. 21-37, 2000.

[20] M. A. McGee, D. W. Howie, S. D. Neale, D. R. Haynes, and M. J. Pearcy, "Role of polyethylene wear in joint replacement failure," *Proceedings of the*

Institution of Mechanical Engineers, Part H: Journal of Engineering in Medicine, vol. 211, pp. 65-72, 1997.

[21] J. Fisher, J. Bell, P. S. M. Barbour, J. L. Tipper, J. B. Matthews, A. A. Besong, M. H. Stone, and E. Ingham, "A novel method for the prediction of functional biological activity of polyethylene wear debris," *Proceedings of the Institution of Mechanical Engineers, Part H: Journal of Engineering in Medicine*, vol. 215, pp. 127-132, 2001.

[22] J. M. Dowling, J. R. Atkinson, D. Dowson, and J. Charnley, "The characteristics of acetabular cups worn in the human body," *J Bone Joint Surg Br*, vol. 60-B, pp. 375-82, 1978.

[23] T. M. McGloughlin, D. M. Murphy, and A. G. Kavanagh, "A machine for the preliminary investigation of design features influencing the wear behaviour of knee prostheses," *Proceedings of the Institution of Mechanical Engineers, Part H: Journal of Engineering in Medicine*, vol. 218, pp. 51-62, 2004.

[24] C. R. Bragdon, D. O. O'Connor, J. D. Lowenstein, M. Jasty, and W. D. Syniuta, "Importance of multidirectional motion on the wear of polyethylene," *Proceedings of the Institution of Mechanical Engineers, Part H: Journal of Engineering in Medicine*, vol. 210, pp. 157-165, 1996.

[25] A. Wang, A. Essner, V. K. Polineni, C. Stark, and J. H. Dumbleton, "Lubrication and wear of ultra-high molecular weight polyethylene in total joint replacements," *Tribology International*, vol. 31, pp. 17-33, 1998.

[26] A. Wang, D. C. Sun, S.-S. Yau, B. Edwards, M. Sokol, A. Essner, V. K. Polineni, C. Stark, and J. H. Dumbleton, "Orientation softening in the deformation and wear of ultra-high molecular weight polyethylene," *Wear Proceedings of the 1997 11th International Conference on Wear of Materials, Apr 20-23 1997*, vol. 203-204, pp. 230-241, 1997.

[27] A. Wang, "A unified theory of wear for ultra-high molecular weight polyethylene in multi-directional sliding," *Wear*, vol. 248, pp. 38-47, 2001.

[28] H. M. J. McEwen, P. I. Barnett, C. J. Bell, R. Farrar, D. D. Auger, M. H. Stone, and J. Fisher, "The influence of design, materials and kinematics on the in vitro wear of total knee replacements," *Journal of Biomechanics*, vol. 38, pp. 357-365, 2005.

[29] I. C. Burgess, M. Kolar, J. L. Cunningham, and A. Unsworth, "Development of a six station knee wear simulator and preliminary wear results," *Proceedings of the Institution of Mechanical Engineers, Part H: Journal of Engineering in Medicine*, vol. 211, pp. 37-47, 1997.

[30] H. E. Ash, I. C. Burgess, and A. Unsworth, "Long-term results for Kinemax and Kinematic knee bearings on a six-station knee wear simulator," *Proceedings of the Institution of Mechanical Engineers, Part H: Journal of Engineering in Medicine*, vol. 214, pp. 437-447, 2000.

[31] A. Wang, A. Essner, C. Stark, and J. H. Dumbleton, "Biaxial line-contact wear machine for the evaluation of implant bearing materials for total knee joint replacement," *Wear*

Proceedings of the 1999 12th International Conference on Wear of Materials, WOM-99, Apr 25-Apr 29 1999, vol. 225-229, pp. 701-707, 1999.

[32] M. A. Wimmer and T. P. Andriacchi, "Tractive forces during rolling motion of the knee: Implications for wear in total knee replacement," *Journal of Biomechanics*, vol. 30, pp. 131-137, 1997.

[33] G. B. Cornwall, J. T. Bryant, and C. M. Hansson, "The effect of kinematic conditions on the wear of ultra-high molecular weight polyethylene (UHMWPE) in orthopaedic bearing applications," *Proceedings of the Institution of Mechanical Engineers, Part H: Journal of Engineering in Medicine*, vol. 215, pp. 95-106, 2001.

[34] G. W. Blunn, P. S. Walker, A. Joshi, and K. Hardinge, "The dominance of cyclic sliding in producing wear in total knee replacements," *Clin Orthop Relat Res*, pp. 253-60, 1991.

[35] J. Tamura, I. C. Clarke, K. Kawanabe, M. Akagi, V. D. Good, P. A. Williams, T. Masaoka, D. Schroeder, and H. Oonishi, "Micro-wear patterns on UHMWPE tibial inserts in total knee joint simulation," *Journal of Biomedical Materials Research*, vol. 61, pp. 218-225, 2002.

[36] V. Saikko, T. Ahlroos, and O. Calonius, "A three-axis knee wear simulator with ball-on-flat contact," *Wear*, vol. 249, pp. 310-315, 2001.

[37] V. Saikko and O. Calonius, "Simulation of wear rates and mechanisms in total knee prostheses by ball-on-flat contact in a five-station, three-axis test rig," *Wear*, vol. 253, pp. 424-429, 2002.

[38] P. A. Revell, B. Weightman, M. A. Freeman, and B. V. Roberts, "The production and biology of polyethylene wear debris," *Arch Orthop Trauma Surg*, vol. 91, pp. 167-81, 1978.

[39] T. Stewart, Z. M. Jin, D. Shaw, D. D. Auger, M. Stone, and J. Fisher, "Experimental and theoretical study of the contact mechanics of five total knee joint replacements," *Proceedings of the Institution of Mechanical Engineers, Part H: Journal of Engineering in Medicine*, vol. 209, pp. 225-231, 1995.

[40] J. P. Collier, M. B. Mayor, J. L. McNamara, V. A. Surprenant, and R. E. Jensen, "Analysis of the failure of 122 polyethylene inserts from uncemented tibial knee components," *Clin Orthop Relat Res*, pp. 232-42, 1991.

[41] R. E. Bristol, D. C. Fitzpatrick, T. D. Brown, and J. J. Callaghan, "Non-uniformity of contact stress on polyethylene inserts in total knee arthroplasty," *Clinical Biomechanics*, vol. 11, pp. 75-80, 1996.

[42] E. A. Reeves, D. C. Barton, D. P. FitzPatrick, and J. Fisher, "Two-dimensional model of cyclic strain accumulation in ultra-high molecular weight polyethylene knee replacements," *Proceedings of the Institution of Mechanical Engineers, Part H: Journal of Engineering in Medicine*, vol. 212, pp. 189-198, 1998.

[43] M. L. Harris, P. Morberg, W. J. M. Bruce, and W. R. Walsh, "Improved method for measuring tibiofemoral contact areas in total knee arthroplasty: A comparison of K-scan sensor and Fuji film," *Journal of Biomechanics*, vol. 32, pp. 951-958, 1999.

[44] Perplas Medical Ltd, "Test Certificate Perplas PUR 1050 Medical Grade UHMWPE," 2004.

[45] S. D. Waldman, G. B. Cornwall, R. Kiss, T. N. Moore, and A. J. Bowe, "Vibration monitoring in wear testing of orthopaedic biomaterials," *ASTM Special Technical Publication*

Proceedings of the Symposium on Effects of Mechanical Stiffness and Vibration on Wear, May 18 1994, pp. 46-61, 1995.

[46] G. W. Blunn, A. B. Joshi, R. J. Minns, L. Lidgren, P. Lilley, L. Ryd, E. Engelbrecht, and P. S. Walker, "Wear in retrieved condylar knee arthroplasties. A comparison of wear in different designs of 280 retrieved condylar knee prostheses," *J Arthroplasty*, vol. 12, pp. 281-90, 1997.

[47] I. C. Clarke, F. W. Chan, A. Essner, V. Good, C. Kaddick, R. Lappalainen, M. Laurent, H. McKellop, W. McGarry, D. Schroeder, M. Selenius, M. C. Shen, M. Ueno, A. Wang, and J. Yao, "Multi-laboratory simulator studies on effects of serum proteins on PTFE cup wear," *Wear*, vol. 250-251, pp. 188-198, 2001.

[48] J. E. Shigley and L. D. Mitchell, *Mechanical engineering design*, 4th ed. New York: McGraw-Hill, 1983.

[49] R. M. Gul, F. J. McGarry, C. R. Bragdon, O. K. Muratoglu, and W. H. Harris, "Effect of consolidation on adhesive and abrasive wear of ultra high molecular weight polyethylene," *Biomaterials*, vol. 24, pp. 3193-3199, 2003.

[50] K. Kawanabe, I. C. Clarke, J. Tamura, M. Akagi, V. D. Good, P. A. Williams, and K. Yamamoto, "Effects of A-P translation and rotation on the wear of UHMWPE in a total knee joint simulator," *Journal of Biomedical Materials Research*, vol. 54, pp. 400-406, 2001.

[51] A. S. Shanbhag, H. O. Bailey, D.-S. Hwang, C. W. Cha, N. G. Eror, and H. E. Rubash, "Quantitative analysis of ultrahigh molecular weight polyethylene (UHMWPE) wear debris associated with total knee replacements," *Journal of Biomedical Materials Research*, vol. 53, pp. 100-110, 2000.

[52] T. M. McGloughlin and A. G. Kavanagh, "Wear of ultra-high molecular weight polyethylene (UHMWPE) in total knee prostheses: a review of key influences," *Proceedings of the Institution of Mechanical Engineers, Part H (Journal of Engineering in Medicine)*, vol. 214, pp. 349-59, 2000.

[53] M. A. Wimmer, T. P. Andriacchi, R. N. Natarajan, J. Loos, M. Karlhuber, J. Petermann, E. Schneider, and A. G. Rosenberg, "A striated pattern of wear in ultrahigh-molecular-weight polyethylene components of Miller-Galante total knee arthroplasty," *J Arthroplasty*, vol. 13, pp. 8-16, 1998.

[54] T. Schwenke, L. L. Borgstede, E. Schneider, T. P. Andriacchi, and M. A. Wimmer, "The influence of slip velocity on wear of total knee arthroplasty," *Wear*, vol. 259, pp. 926-32, 2005.

APPENDICES

APPENDIX A LINEAR BEARINGS

Model used was SSE PB M30 DD

SSEPB 2

APPLICATION ENGINEERING DATA

Super Smart Pillow Blocks

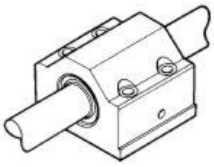

Closed type

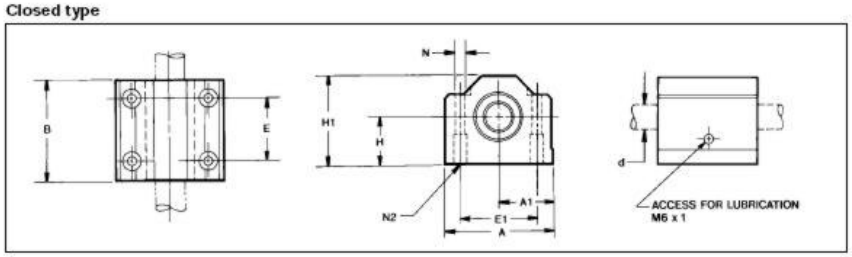

Part Number	Dimensions (mm)										Mass (Kg)	Dynamic Load W[1][2] (N)	Load Limit W[2] (N)
	d[2]	H ±0,020	H1	A	A1 ±0,020	B	E ±0,1	E1 ±0,1	N Dia.	N2			
SP PB M08	8	15	28	35	17,5	32	20	25	3,3	M4	0,07	310	340
SP PB M12	12	18	35	43	21,5	39	23	32	4,3	M5	0,13	650	715
SSE PB M16 DD	16	22	42	53	26,5	43	26	40	5,3	M6	0,21	2200	2400
SSE PB M20 DD	20	25	50	60	30,0	54	32	45	6,6	M8	0,35	4000	4400
SSE PB M25 DD	25	30	60	78	39,0	67	40	60	8,4	M10	0,67	6700	7300
SSE PB M30 DD	30	35	71	87	43,5	79	45	68	8,4	M10	0,99	8300	9100
SSE PB M40 DD	40	45	91	108	54,0	91	58	86	10,5	M12	1,84	13700	15000

[1]For rated travel life of 100 km. For longer travel lives, reduce load to W • (100/L)$^{1/3}$ where L (km) is the required travel life. Do not exceed the Dynamic Load Rating for travel life of less than 100km.

[2]The Load Limit is the maximum load that may be applied to a bearing/shaft. It is important to analyze the application so the peak and/or shock loads do not exceed the Load Limit.

[3]For bearing diametral clearances, see Table 1.

NOTE: For additional technical data, see Engineering Support section.

Table 1 –Standard Diametral Clearances Closed Type

Nominal Size d (mm)	Diametral Clearance (µm)
8	+23 +2
12	+26 +3
16	+26 +3
20	+30 +4
25	+30 +4
30	+30 +4
40	+35 +5

For pillow blocks used with LinearRace* Shaft, h6 tolerance

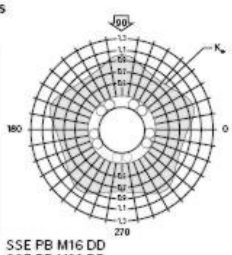

SSE PB M16 DD
SSE PB M20 DD
SSE PB M25 DD
SSE PB M30 DD
SSE PB M40 DD

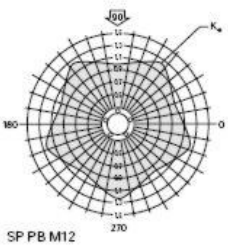

SP PB M12

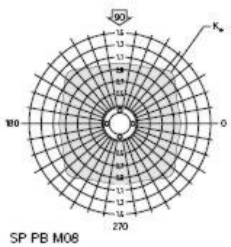

SP PB M08

THOMSON
First in Linear Motion and Control Technology

For assistance call: 1-800-554-8466

APPENDIX B AIR BELLOWS

1S3-013

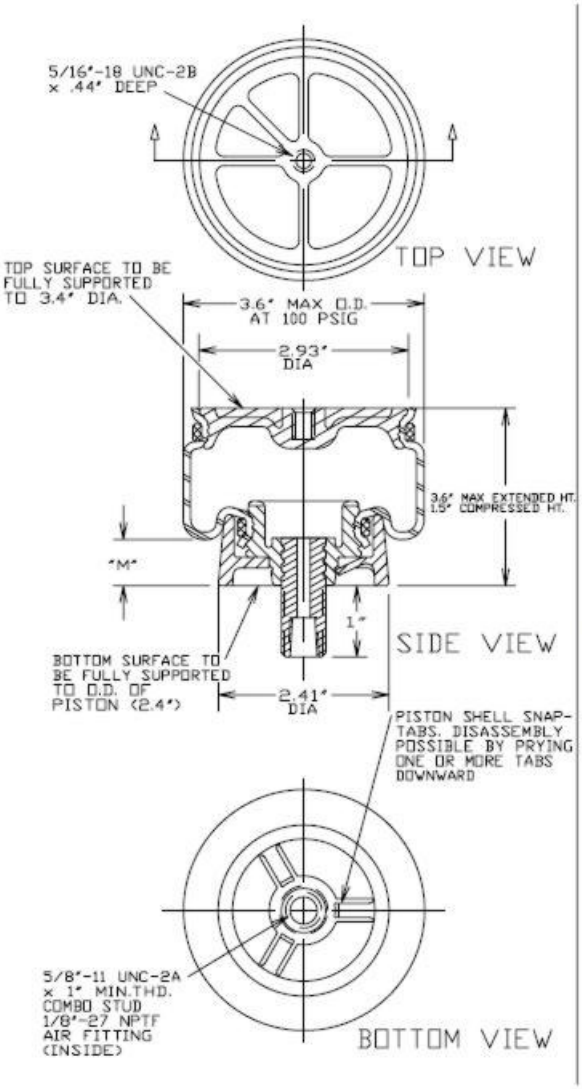

ASSEMBLY NUMBER	ELASTOMER	AIR FITTING	BUMPER INCLUDED
1S3-013	WINGPRENE	1/8"-27 NPTF COMBO STUD	NO

SPRING FEATURES:

- LOAD RANGE (ISOLATOR).....90-580 lb
- DESIGN HEIGHT RANGE (ISOLATOR).....2.0-3.0 in
- USEABLE STROKE (ACTUATOR).....2.1 in
- ASSEMBLY WEIGHT.....0.6 lb
- TEMPERATURE RANGE*.....
- FORCE TO COMPRESS AT 0 PSIG.....6 lb
- LIGHT WEIGHT END RETAINERS (REINFORCED THERMOPLASTIC)
- ABUSE RESISTANT STEEL STUD

* NOTE: PRODUCT LIFE MAY BE SHORTENED WHEN OPERATING AT OR NEAR EXTREME TEMPERATURES. SEE TEMPERATURE RANGE GUIDELINES SECTION.

RECOMMENDED MAX. TORQUE VALUES

5/16"-18 UNC BLIND TAP	5/8"-11 UNC COMBO STUD	1/8"-27 UNC AIR FITTING
30-50 in-lb 2.5-4 ft-lb	300 in-lb 25 ft-lb	180 in-lb 15 ft-lb

NOTE: SEE GUIDELINES FOR PROPER APPLICATION OF THIS PRODUCT

1S3-013

GRAPHS FOR REFERENCE ONLY - USE THE CHART DATA BELOW FOR DESIGN WORK

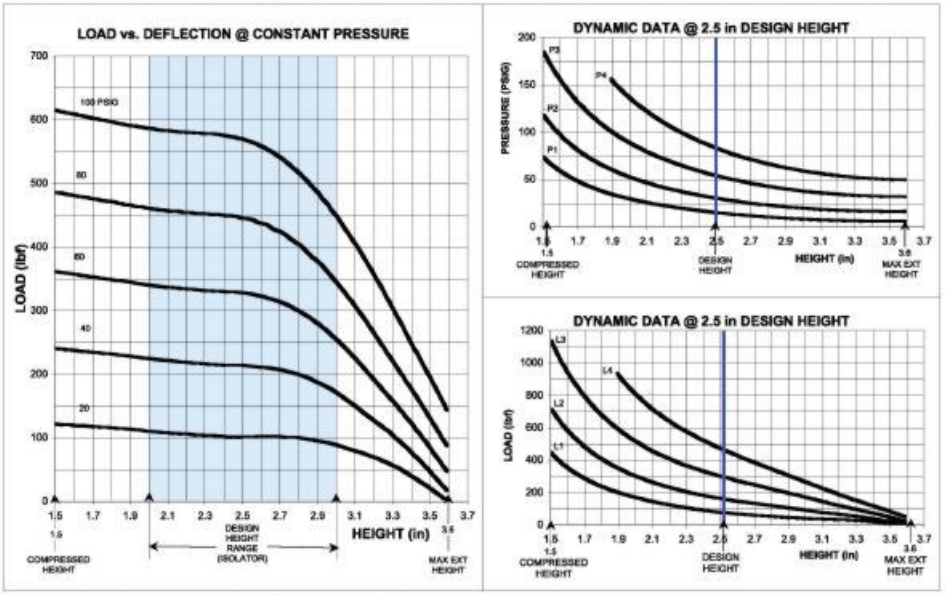

**NOTE: MAXIMUM INFLATION PRESSURE IS 100 PSIG. MAXIMUM JOUNCE PRESSURE IS 200 PSIG. IF YOUR APPLICATION WILL EXCEED THESE LIMITS, CONSULT A GOODYEAR REPRESENTATIVE FOR APPLICATION ASSISTANCE.

CONSTANT PRESSURE CHARACTERISTICS

Assembly Height (in)	Meniscus Height "M" Dim. @ 100 PSIG	Volume @ 100 PSIG (in³)	Nominal Force (lb)				
			@ 20 PSIG	@ 40 PSIG	@ 60 PSIG	@ 80 PSIG	@ 100 PSIG
3.6	1.03	14.8	10	30	40	80	120
3.5	1.02	14.3	20	50	90	140	180
3.0	0.98	12.3	90	170	260	340	440
2.5	0.78	9.6	100	220	320	440	560
2.0	0.45	6.5	110	230	340	460	580
1.5	0.16	3.4	120	240	360	480	600

DYNAMIC CHARACTERISTICS

Design Height (in)	Load (lb)	Pressure (PSIG)	Spring Rate (lb/in)	Natural Frequency	
				cpm	Hz
3.0	80	21	160	236	3.93
	160	43	300	230	3.83
	300	77	495	223	3.72
2.5	80	18	145	224	3.73
	160	35	225	202	3.37
	300	61	370	194	3.23
	460	88	520	191	3.18
2.0	80	17	190	258	4.30
	160	34	300	231	3.85
	300	60	470	216	3.60
	460	85	610	208	3.47
	570	100	720	207	3.45

APPENDIX C PERISTALTIC PUMP

Model was FPU-116-Dual-240V

OMEGAFLEX® OEM STYLE PERISTALTIC PUMPS

FPU101
$78

1 YEAR WARRANTY MADE IN USA

FPU101 pump, $78, shown smaller than actual size, supplied with Norprene tubing and mounting panel.

FPU4500, $209, shown smaller than actual size.

- UL Listed AC or DC Motor
- Suitable for Fluids Carrying Small Particles
- Easy to Maintain
- Mounting Panel Standard
- Benchtop Case Optional
- New High Flow FPU4500 Series has the Capability of 2000 mL/Min

FPU100 Series peristaltic pumps offer exceptional simplicity at a very low cost. The UL listed AC or DC motor turns the rollers, which squeeze fluid through the precision-bore high tolerance tubing in a wave-like motion, acting like a positive displacement pump. The fluid doesn't touch the pump only comes into contact with the tubing. This makes the pump suitable for fluids carrying small particles. FPU100 pumps continuously overocclude the tubing, which makes the pump self-priming and non-siphoning. They are easy to maintain, with few moving parts and no seals or valves to clog, clean or replace. As one section of tube fatigues, just move the tubing to a section which hasn't been under the rollers and continue pumping. Or simply replace the supplied tubing. The replacement 230 mm (9") lengths of precision-bore tubing insure repeatable pumping rates time after time. The pumps are supplied with tubing that has polyethylene union connectors for hooking up your system tubing. The replacement 230 mm (9") lengths of tubing come without connectors. The pumps are supplied standard with a mounting panel. The AC powered pumps are also available in a rugged polycarbonate enclosure for bench mounting. Maximum backpressure is 15 psi without derating (up to 25 psi @ 75% of maximum flow). Maximum suction head is 8.5 m (28'). Flow rate repeatability from one pump to the next or when replacing tubing is within 8% of maximum flow rate listed. Shipping weight is 1.6 kg (3.5 lb) for all sizes. These pumps are ideal for metering/dosing, repetitive dispensing, and general liquid/gas transfer, and they have a 100% duty cycle for continuous operation.

SPECIFICATIONS (FPU100 Series)

Mounting Plate: 94 L x 130 W x 109 mm D (3.74 x 5.12 x 4.28") the 5.6 mm (0.22") diameter holes are centered 76 x 110 mm (3.0 x 4.34") on the plate.
For units with rear fan: 130 L x 130 W x 135 mm D (5.11 x 5.12 x 5.28") overall
Case: 152 H x 152 W x 102 mm D (6 x 6 x 4")
Shipping Weight: 1.6 kg (3.5 lb)
Ambient Temp. Range: 20 to 30°C (68 to 86°F)
Max Liquid Viscosity: 8,500 cp

SPECIFICATIONS (FPU4500 Series)

Electrical: 115 Vac/60 Hz
Flow Rate: 2000 mL/min (78.6 oz)
Mounting: 12 gauge zinc-plated steel mounting plate
Dimensions: 140 H x 116 W x 191 mm D (5.5 x 4.6 x 7.5")
Shipping Weight: 2.4 kg (5.3 lb)

Benchtop Case Available
The AC powered pumps are also available in a rugged polycarbonate enclosure with ON/OFF switch, power indicator lamp and rubber feet for benchtop use. Each is supplied with a 1.8 m (6'), 115 Vac, three-wire cord. To order, select the desired pump. Add suffix "**-CASE**" to model number and add **$75** to price. For 240 Vac models with European plug, consult OMEGA's Flow Department. An optional 24-hour timer with momentary ON switch for priming the pump is also available for the case unit. The timer is settable up to 24 hours in increments of 15 minutes by internal DIP switches. To order case unit with timer for 115 Vac, add suffix "**-CASE-CT**" to model number and add **$95** to price.

Replacement 230 mm (9") Tubing Lengths

Model No.	Price	Description (I.D. x O.D.)
FPU116-S	$6	1/16" x 3/8" silicone tubing*
FPU18-N	4	1/8" x 3/8" Norprene tubing
FPU18-S	4	1/8" x 3/8" silicone tubing
FPU316-N	4	3/16" x 3/8" Norprene tubing
FPU316-S	4	3/16" x 3/8" silicone tubing
FPU14-N	4	1/4" x 7/16" Norprene tubing
FPU14-S	4	1/4" x 7/16" silicone tubing

** Tubes are supplied inserted into 3/16" x 3/4" tubes. Connection is made to the 1/16" x 1/4" internal tubing.*

Brushless 115 Vac, 60 Hz induction motors; flowrates based on pumping water.

Accessory

Model No.	Price	Description
CM-4441	$112	Reference Book: Systematic Methods of Chemical Process Design

For a complete selection of OMEGAFLEX® tubing and accessories, see Section T

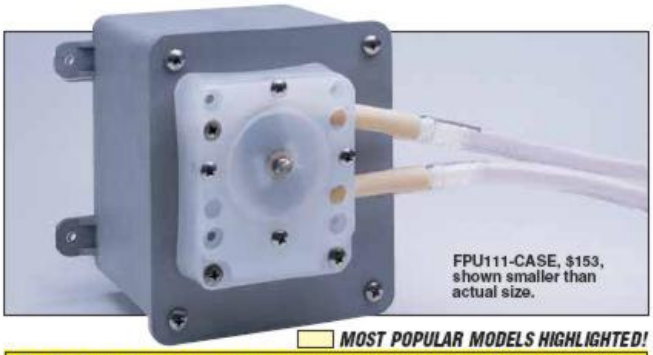

MOST POPULAR MODELS HIGHLIGHTED!

To Order *(Specify Model Number)* Norprene Tube Standard†

Model No.	Price	Approx. Flow Rate @ 60 Hz. mL/Min	Approx. Flow Rate @ 60 Hz. GPM	Tube ID	Average Tube Life Silicone Hours†	Average Tube Life Norprene Hours†	RPM	Amperage**
FPU101	$78	3	0.0008	1/16"	2600	5200	14	0.37
FPU102	78	5	0.0013	1/16"	1600	3200	23	0.42
FPU103	78	6	0.0016	1/16"	1300	2600	28	0.75
FPU104	78	12	0.0032	1/8"	2600	5200	14	0.37
FPU105	78	20	0.0052	1/8"	1600	3200	23	0.42
FPU106	78	25	0.0065	1/8"	1300	2600	28	0.75
FPU107	78	30	0.008	3/16"	2600	5200	14	0.37
FPU108	78	45	0.012	3/16"	1600	3200	23	0.42
FPU109	78	50	0.013	1/4"	2600	5200	14	0.37
FPU110	78	55	0.015	3/16"	1300	2600	28	0.75
FPU111	78	70	0.018	3/16"	1000	2000	36	0.90
FPU112	78	80	0.022	1/4"	1600	3200	23	0.42
FPU113	78	100	0.026	3/16"	750	1500	48	1.00
FPU114	78	100	0.026	1/4"	1300	2600	28	0.75
FPU115	78	115	0.030	3/16"	600	1200	58	1.20
FPU116	78	130	0.034	1/4"	1000	2000	36	0.90
FPU117	95	150	0.040	3/16"	500	1000	75	1.50
FPU118	95	165	0.044	1/4"	750	1500	49	1.00
FPU119	95	195	0.052	1/4"	600	1200	58	1.20
FPU120	95	250	0.066	1/4"	500	1000	75	1.50
FPU121	95	360	0.095	1/4"	350	700	108	1.90
FPU122	95	425	0.110	1/4"	300	600	129	2.20
FPU123	125	635	0.168	1/4"	200	400	172	2.20
FPU124	125	750	0.200	1/4"	180	360	203	2.20
FPU125	125	1000	0.265	1/4"	130	260	282	2.20
FPU4500*	209	2000	0.528	3/8"	500	1000	154	3.80

Comes with complete operator's manual.
** The FPU4500 comes with Norprene tubing.*

(FPU100 Series)

Note: *DC powered versions have a 500 hr life; for long-term or continuous applications, use the standard 115 Vac powered models.*
For units powered by 12 to 30 Vdc *add "**-12VDC**" or "**-24VDC**" to the model number and add **$20** to the price.*
For units powered by 240 Vac @ 50 Hz, *add suffix "**-240VAC**" to model number and add **$10** to price. 50 Hz units have approximately 5/6 of the capacity of standard 60 Hz units.*
For dual head units *with two separate outputs, add suffix "**-DUAL**" to model number and add **$45** to price, for **FPU101** through **FPU120**. For **FPU121** through **125-DUAL**, add **$70**.*
Ordering Example: FPU119-240VAC-DUAL*, 240 Vac, 50 Hz powered, dual head unit with a total flow of 3/4 x 2,000 ml/min. = 1,666 ml/min, **$95 + 10 + 45 = $150**.*
*** 240 Vac amperage is 1/2 that for 115 Vac; 24 Vdc amperage, 0.8 amps nominal max. For dual head units, consult OMEGA's Flow Engineering Department.*
*† Pumps are supplied with Norprene tubes standard. For silicone tubing add suffix "**-SL**" to model number; no additional charge.*
Ordering Example: FPU119-SL*, 195 ml/min. pump with silicone tube, **$95. FPU107-CASE**, pump with polycarbonate enclosure, $78 + 75 = **$153**.*

APPENDIX D MANUFACTURING DRAWINGS

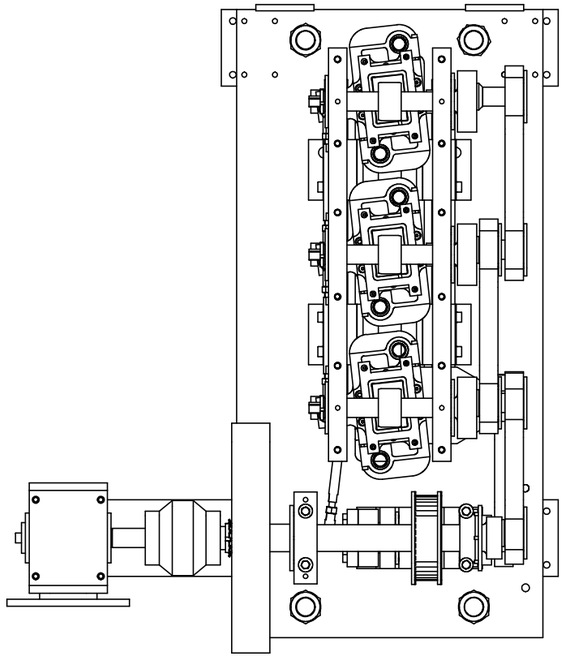

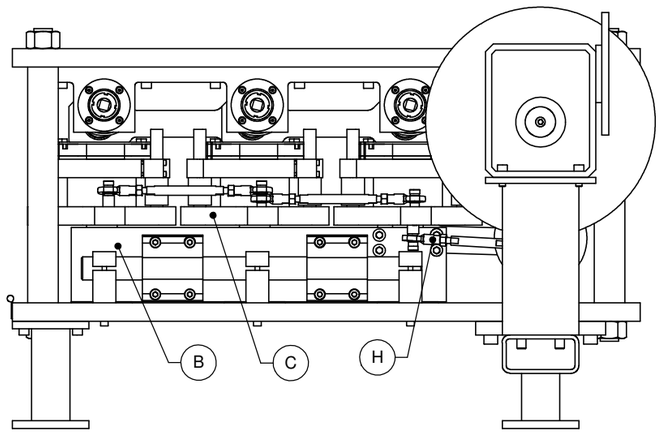

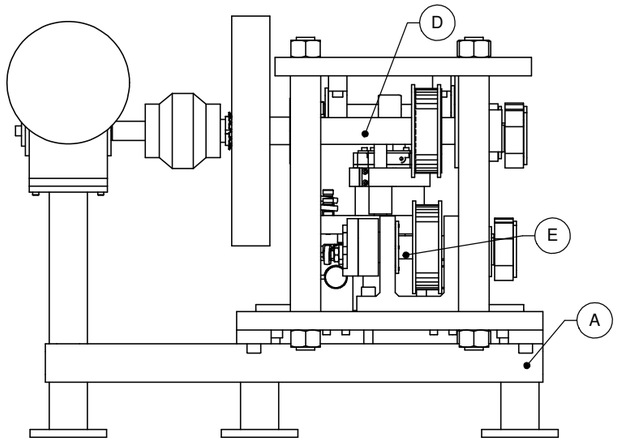

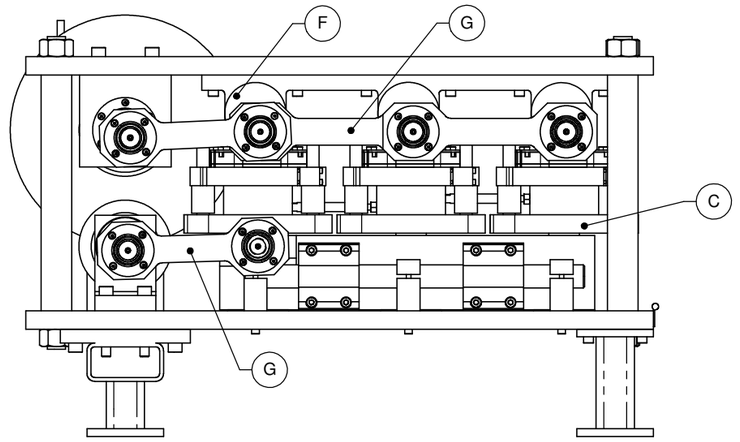

Item	Assembly / Drawing No.	Assembly Name
A	100	Base
B	200	AP Carriage
C	300	Die Set
D	400	Top Shaft
E	500	Bottom Shaft
F	600	FE Crank
G	700	Conrod / Joining Rod
H	800	IE Conrod / IE Joining Rod

General Assembly Orthographic Views

SCALE:1:4 (A1) ALL DIMENSIONS IN mm

UNIVERSITY OF CANTERBURY
MECHANICAL ENGINEERING DEPT NZ

DRAWN : Ben Low	DATE : Oct 04
CHECKED :	DRG. No : 000
APPROVED :	

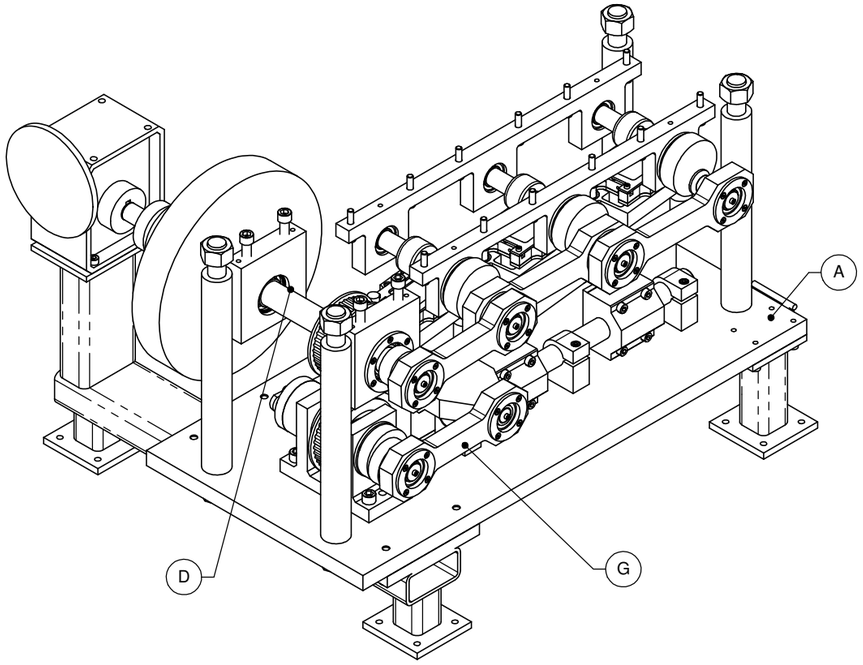

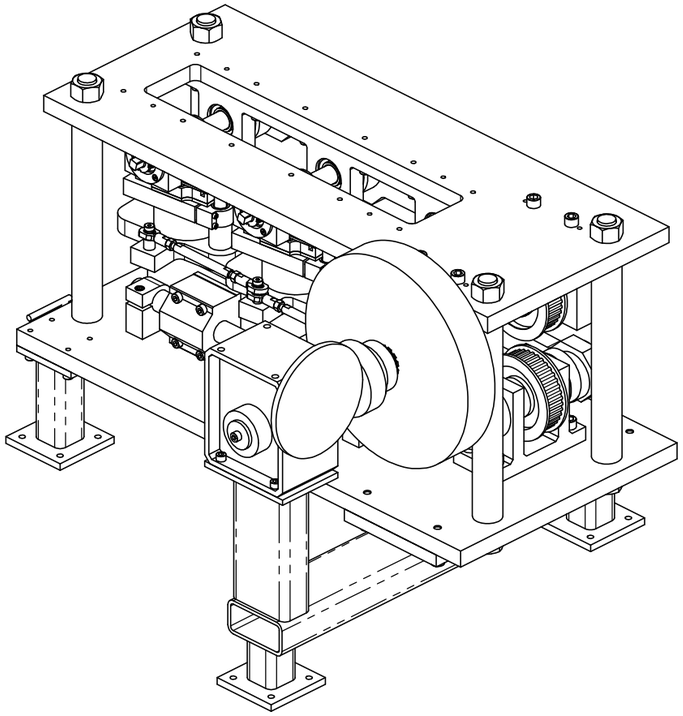

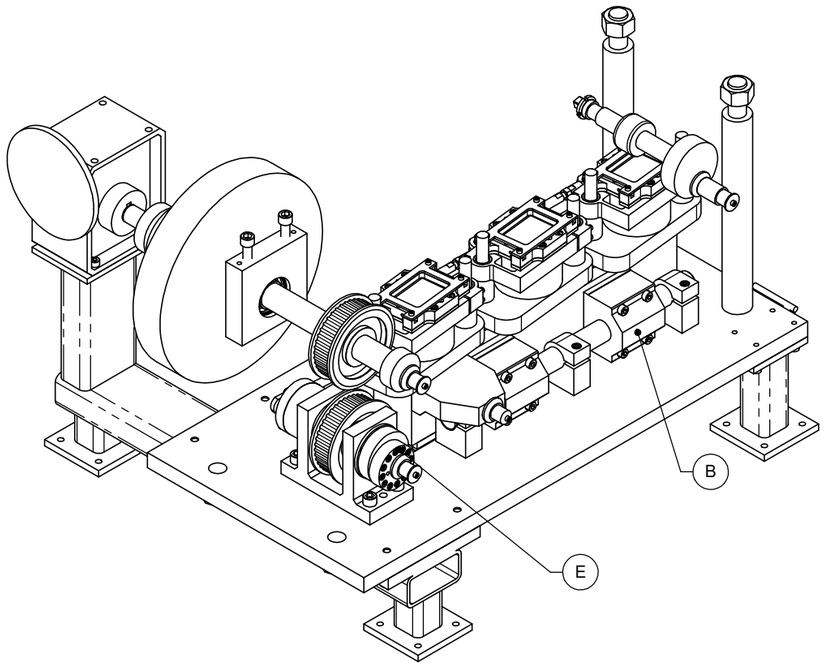

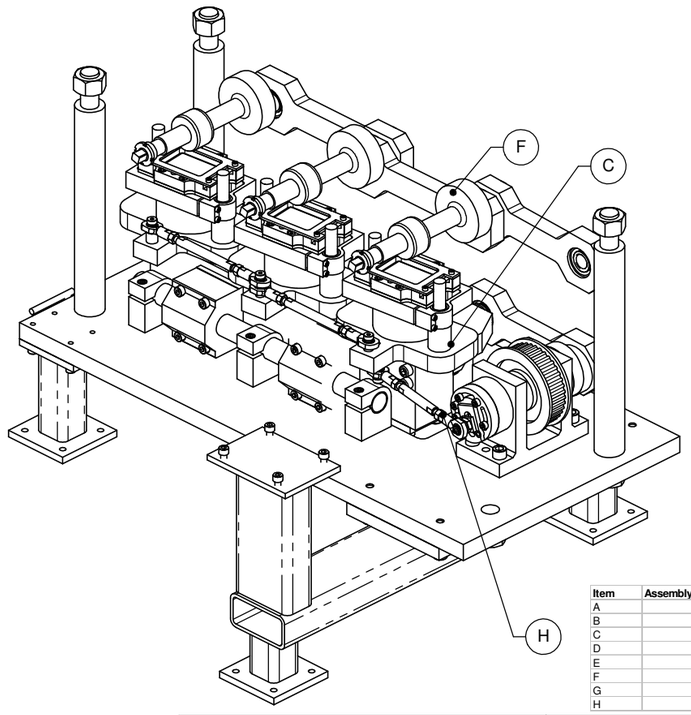

Item	Assembly / Drawing No.	Assembly Name
A	100	Base
B	200	AP Carriage
C	300	Die Set
D	400	Top Shaft
E	500	Bottom Shaft
F	600	FE Crank
G	700	Conrod / Joining Rod
H	800	IE Conrod / IE Joining Rod

General Assembly
Isometric Views

UNIVERSITY OF CANTERBURY
MECHANICAL ENGINEERING DEPT CHCH. N.Z.

DRAWN : Ben Low

DATE : Oct 04

CHECKED :

DRG. No :

SCALE: NTS ALL DIMENSIONS IN mm

APPROVED :

001

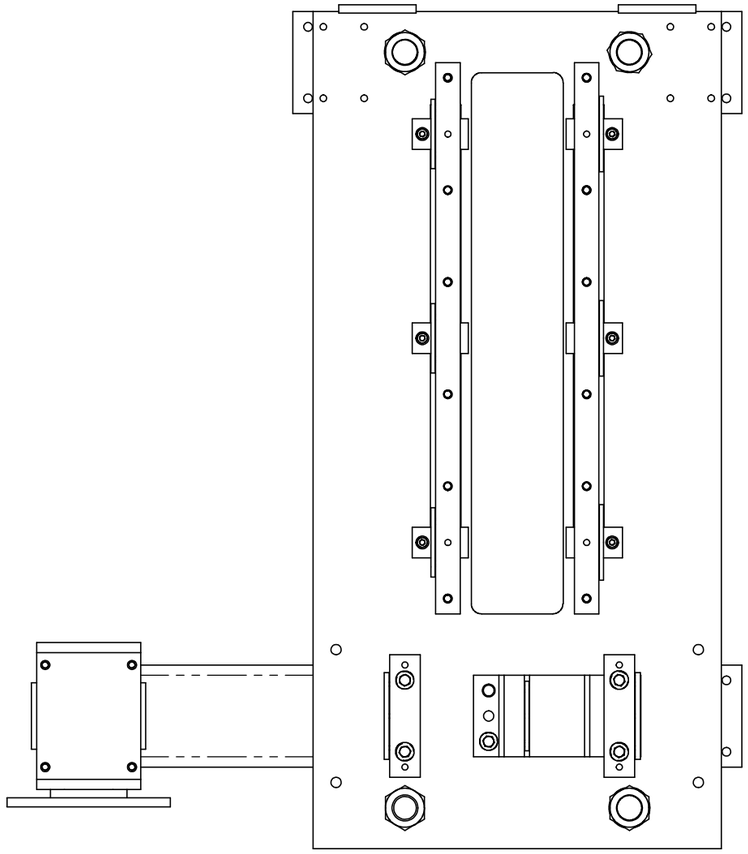

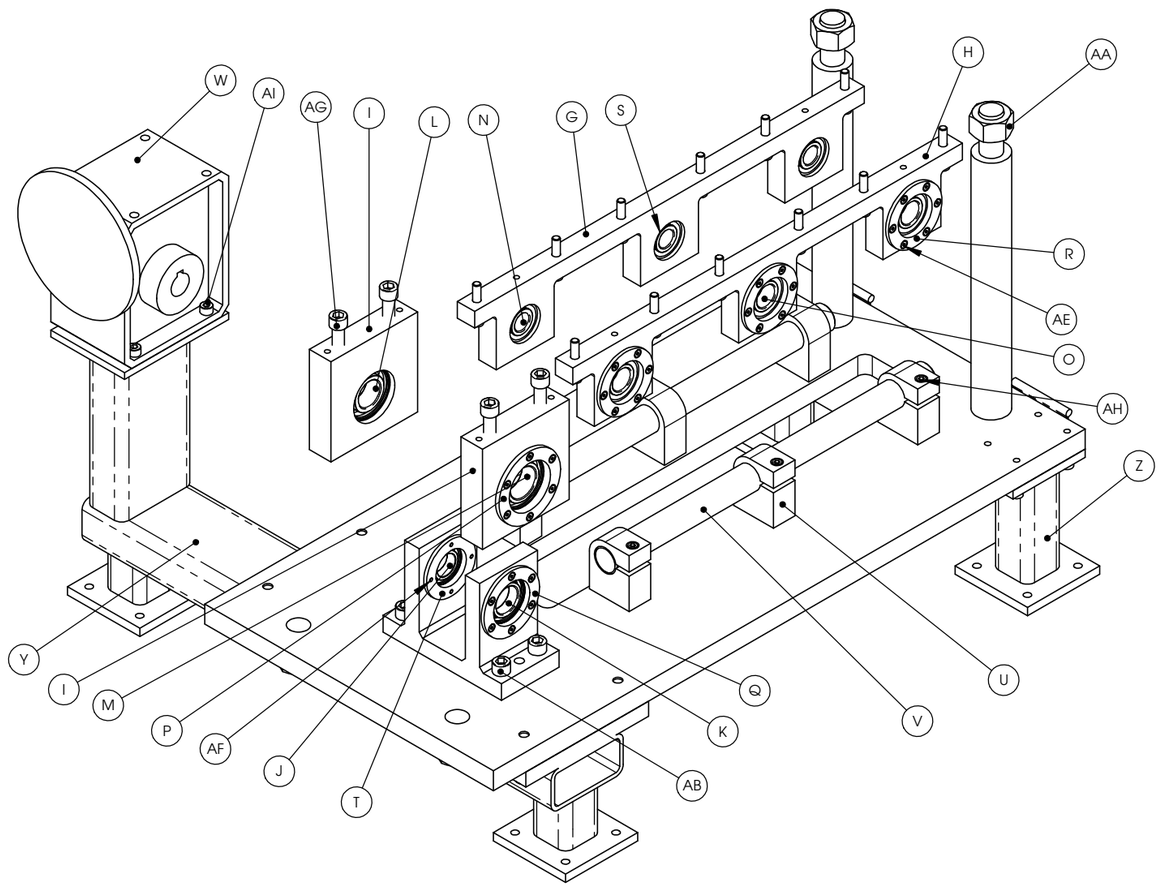

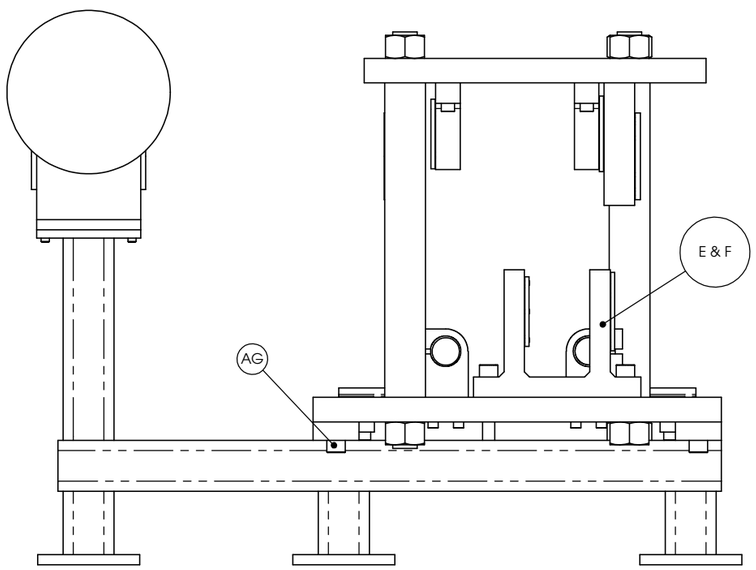

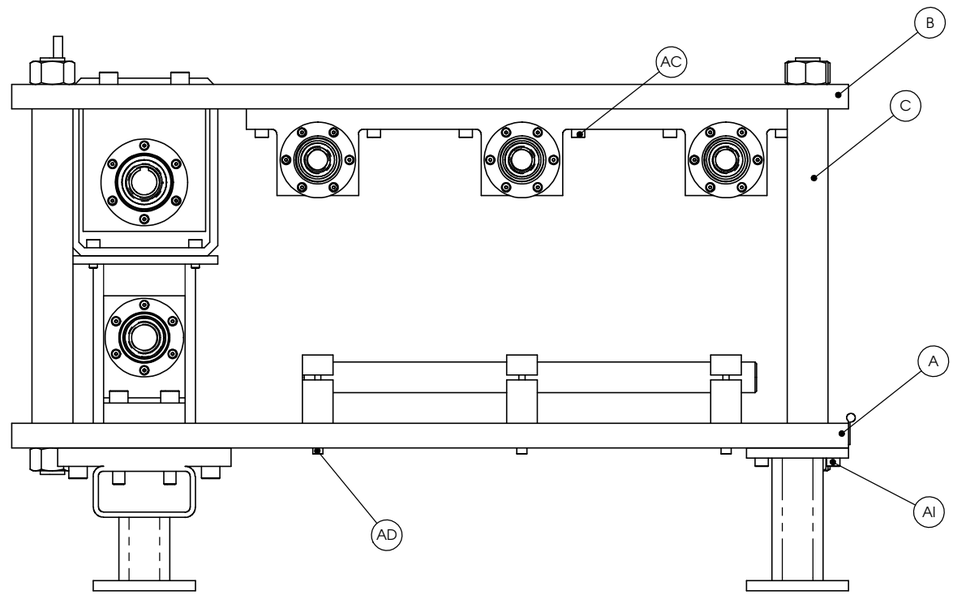

A	110	Bottom	
B	111	Top	
C	112	Upright	
D	120	Guards	Not yet finalised
E	140	Bearing Holder Bottom Shaft	General Assembly
F	141	Bearing Holder Bottom Shaft	
G	142	Bearing Holder FE Shaft LH 47x18	
H	143	Bearing Holder FE Shaft RH 52x18	
I	144	Bearing Holder Top Shaft 62x20	
J	150	Bottom Shaft LH Bearing 6005-2RS1	
K	151	Bottom Shaft RH Bearing 6006-2RS1	
L	152	Top Shaft LH Bearing 62206-2RS1	
M	153	Top Shaft RH Bearing 63007-2RS1	
N	154	FE Shaft LH Bearing 62204-2RS1	
O	155	FE Shaft RH Bearing 62205-2RS1	
P	160	Bearing Retaining Ring 62mm	
Q	161	Bearing Retaining Ring 55mm	
R	162	Bearing Retaining Ring 52mm	
S	163	Bearing Retaining Ring 47mm	Not Visible In This View
T	164	Bearing Retaining Ring 47mm Threaded	
U	170	Rail Support Block	
V	171	30mm Case Hardened Shafting	
W	180	Gearbox 25:1 MU63	
X	181	4 Pole 0.55kW Motor	Not Shown
Y	182	Gearbox Support Arm	
Z	183	Base Support Feet	
AA	190	M24 Nut	
AB	191	M12x80 Cap Screw	
AC	192	M8x40 Cap Screw	
AD	193	M6x35 Cap Screw	
AE	194	M4 x 10 C-Sunk Cap Screw	
AF	195	M4 x 25 C-Sunk Cap Screw	
AG	196	M12 x 40 Cap Screw	
AH	197	M6 x 30 Cap Screw	
AI	198	M8 x 20 Cap Screw	
Item	**Number**	**Description**	

Base
General Assembly
& Bill of Materials

SCALE: 1:3 (A1) ALL DIMENSIONS IN mm

UNIVERSITY OF CANTERBURY
MECHANICAL ENGINEERING DEPT NZ CH. 2

DRAWN : Ben Low	DATE : Oct 04
CHECKED :	DRG. No : 100
APPROVED :	

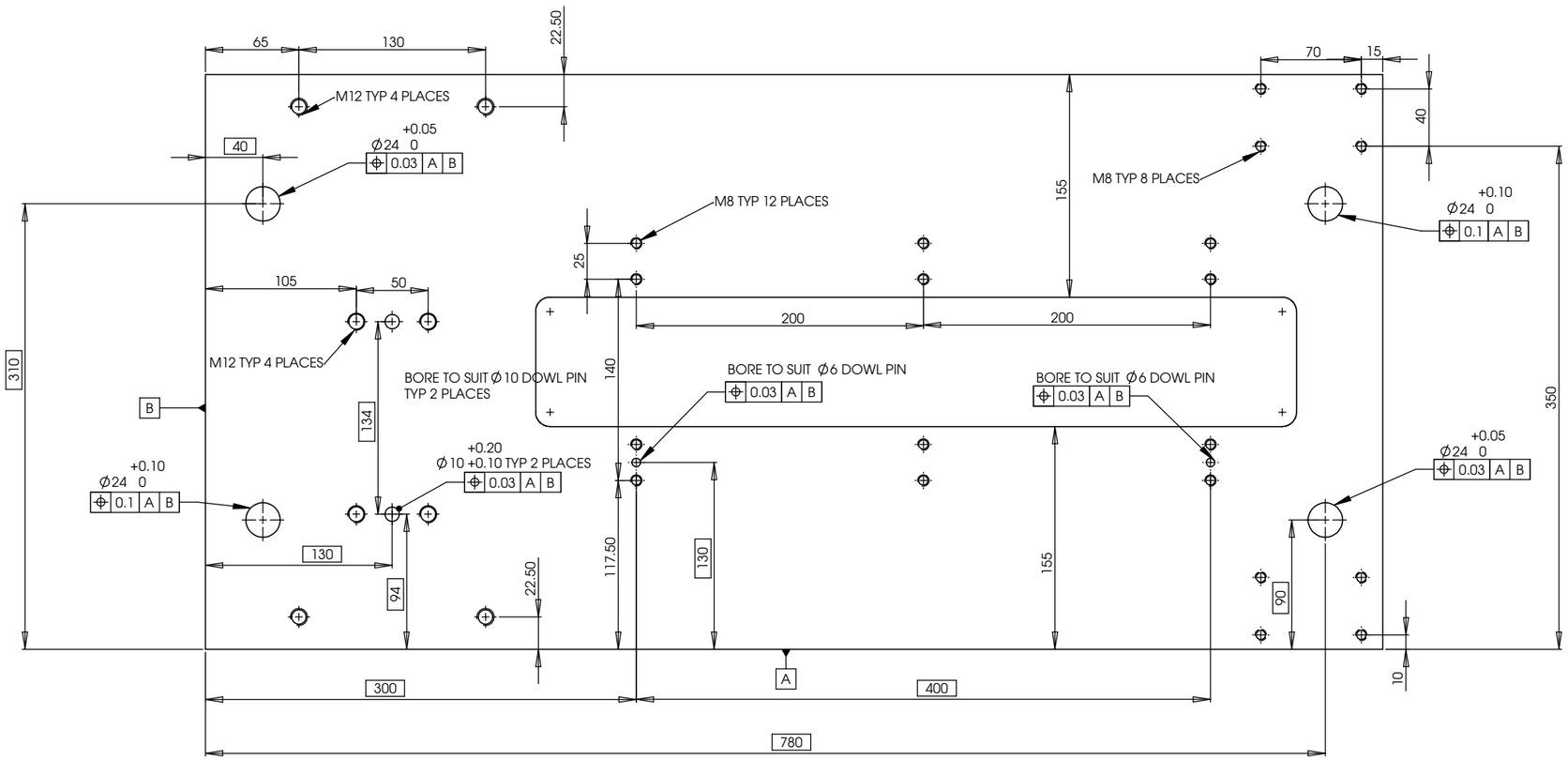

NOTE: THE 14 M4X6mm THREADED HOLES FOR MOUNTING THE SAFETY GUARDS ARE NOT SHOWN FOR CLARITY
THEY ARE SHOWN IN 110 BOTTOM PLATE VER2.DXF

BOTTOM PLATE	UNIVERSITY OF CANTERBURY MECHANICAL ENGINEERING DEPT CHCH. N.Z.	
	DRAWN : Ben Low	DATE : Oct 04
	CHECKED :	DRG. No : 110
SCALE:1 : 2 (A1) ALL DIMENSIONS IN mm	APPROVED :	

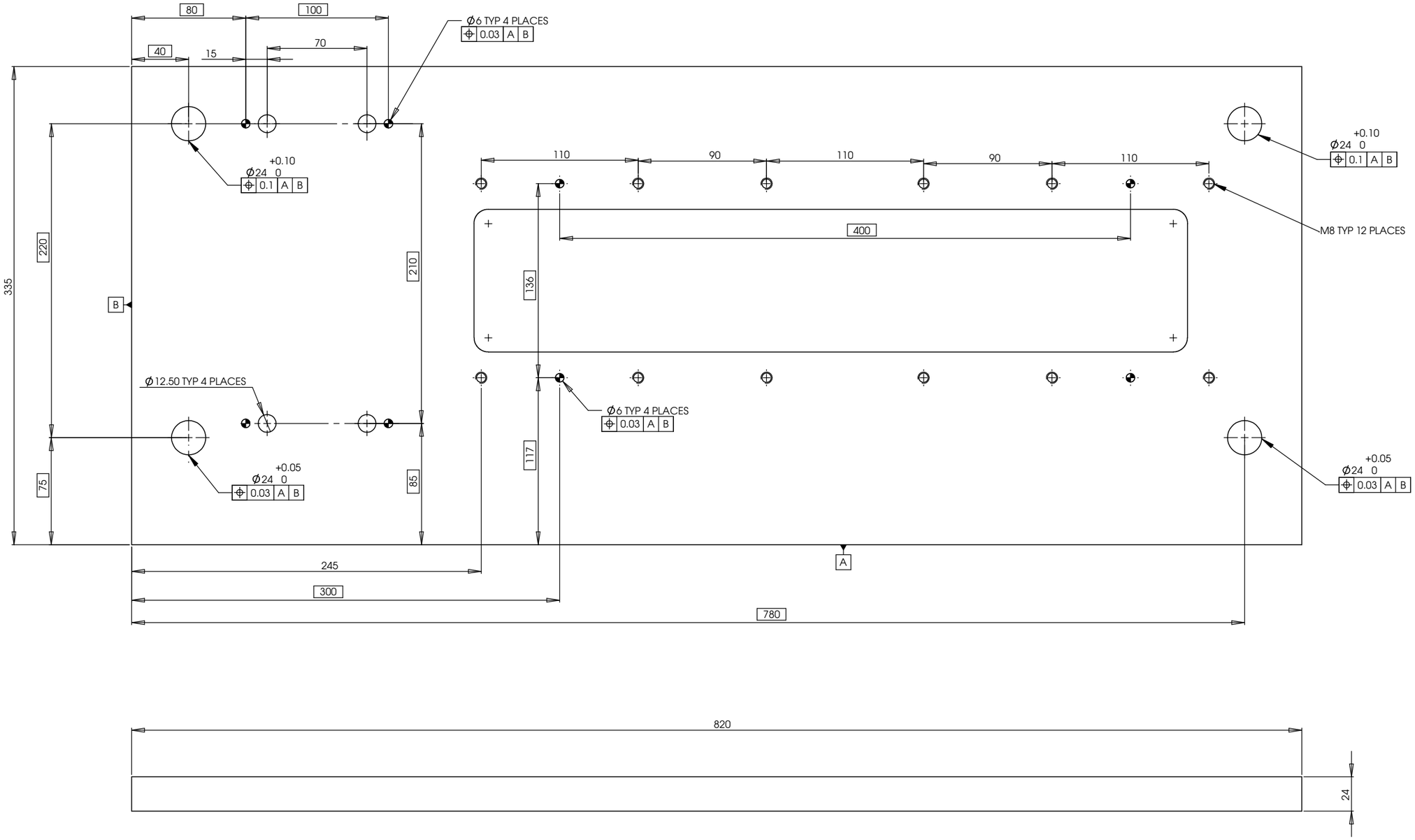

TOP PLATE	**UNIVERSITY OF CANTERBURY** MECHANICAL ENGINEERING DEPT CHCH. N.Z.	
	DRAWN : Ben Low	DATE : Oct 04
	CHECKED :	DRG. No : 111
SCALE: 1 : 1.5 (A1) ALL DIMENSIONS IN mm	APPROVED :	

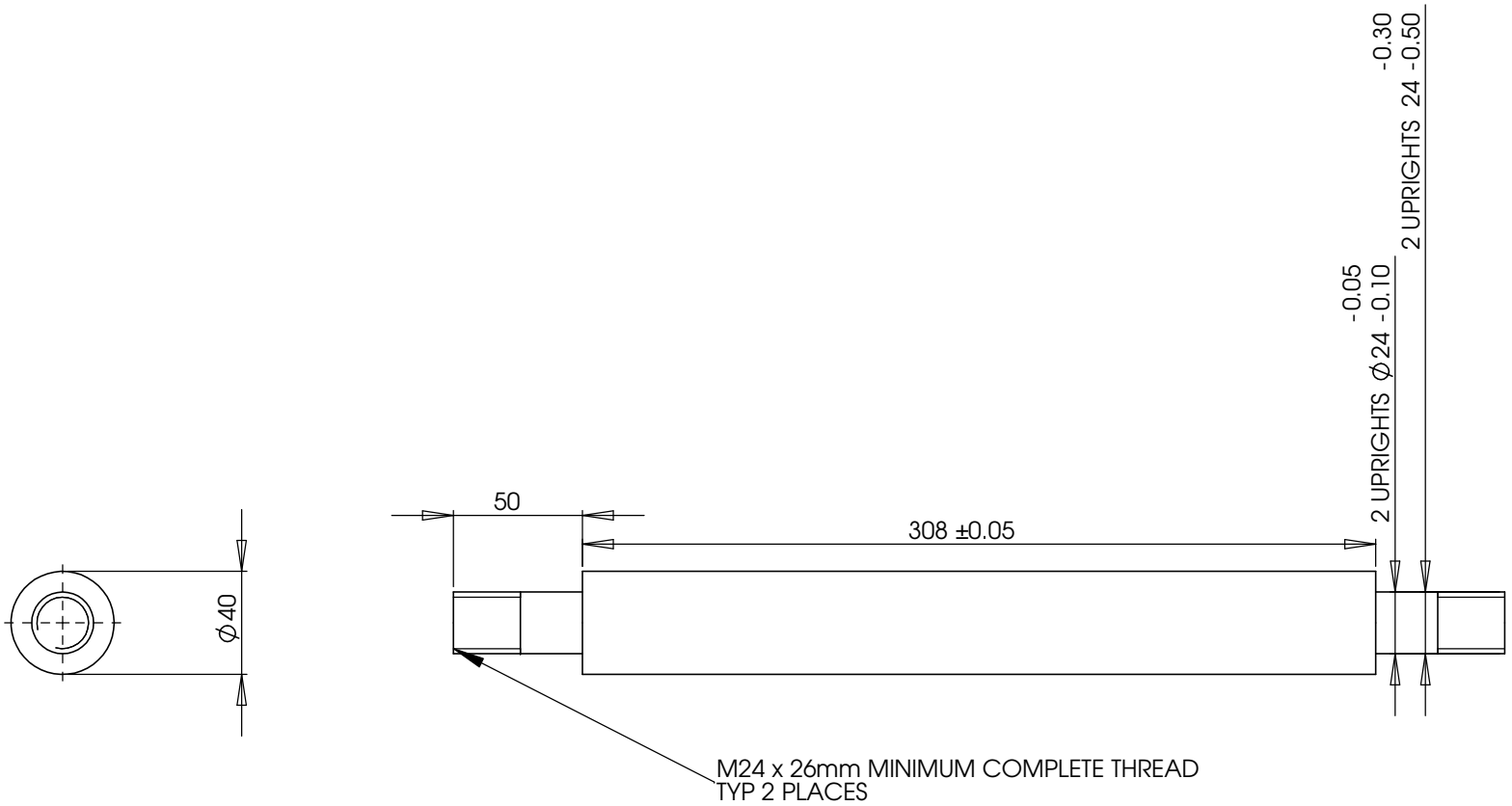

UPRIGHT		SCHOOL OF ENGINEERING MECHANICAL ENGINEERING DEPARTMENT	
		Drawn: Ben Low	Date: Nov 04
No. Required: 4	Material: MILD STEEL	Checked:	DRG No. 112
Scale: 1 : 2 (A3)	All Dimensions in mm	Approved:	

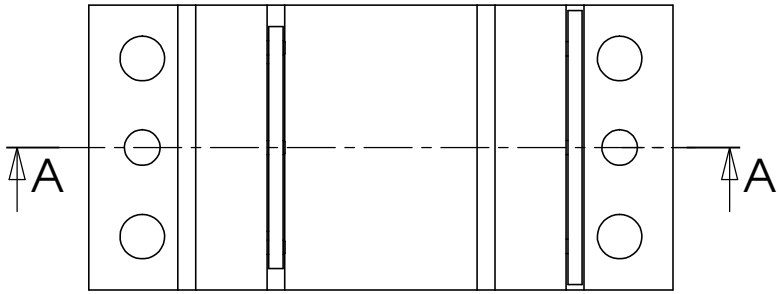

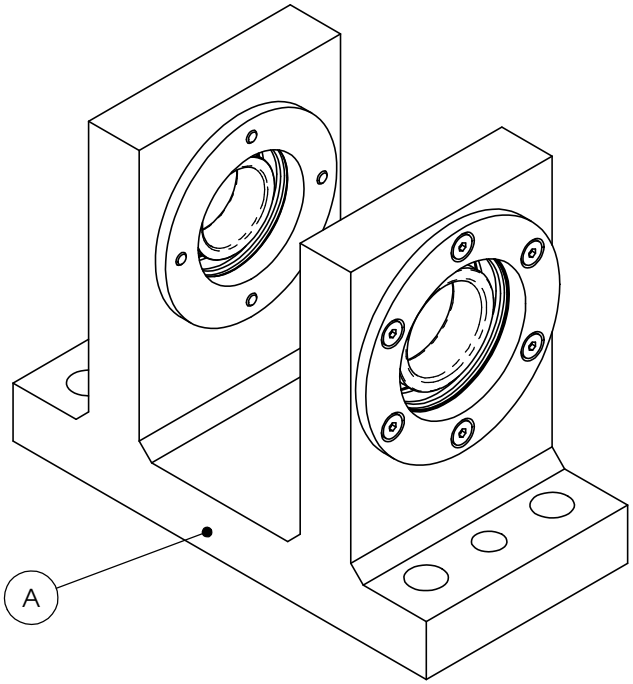

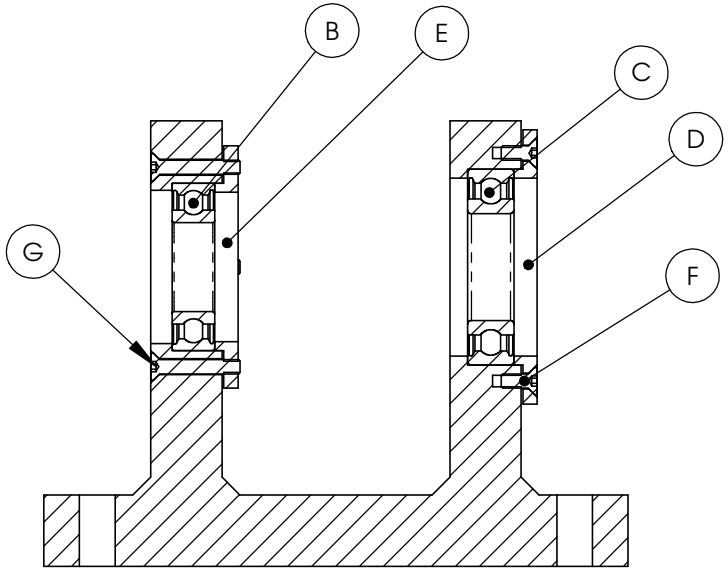

A-A

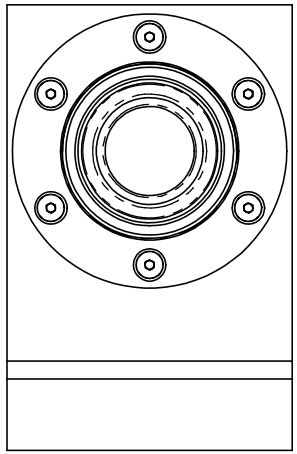

Item	Part No	Description
A	141	Bearing Holder Bottom Shaft
B	150	Bottom Shaft LH Bearing 6005-2RS1
C	151	Bottom Shaft RH Bearing 6006-2RS1
D	161	Bearing Retaining Ring 55mm
E	164	Bearing Retaining Ring 47mm Threaded
F	194	M4 x 10 C-Sunk Cap Screw
G	195	M4 x 25 C-Sunk Cap Screw

BEARING HOLDER BOTTOM SHAFT GENERAL ASSEMBLY & BILL OF MATERIALS

SCHOOL OF ENGINEERING
MECHANICAL ENGINEERING DEPARTMENT

		Drawn: Ben Low	Date: Nov 04
No. Required:	Material:	Checked:	DRG No. 140
Scale: 1 : 1.5 (A3)	All Dimensions in mm	Approved:	

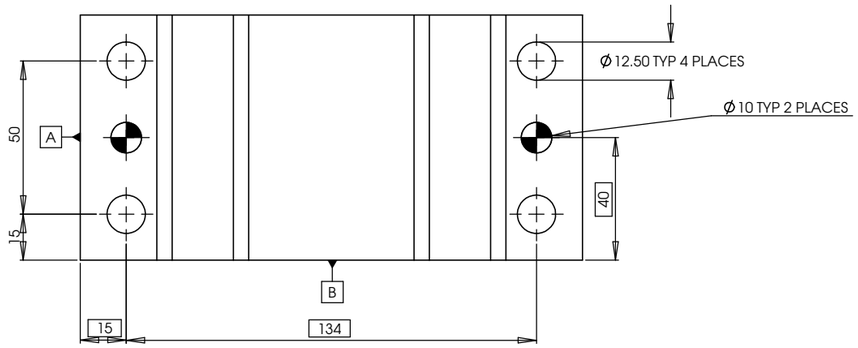

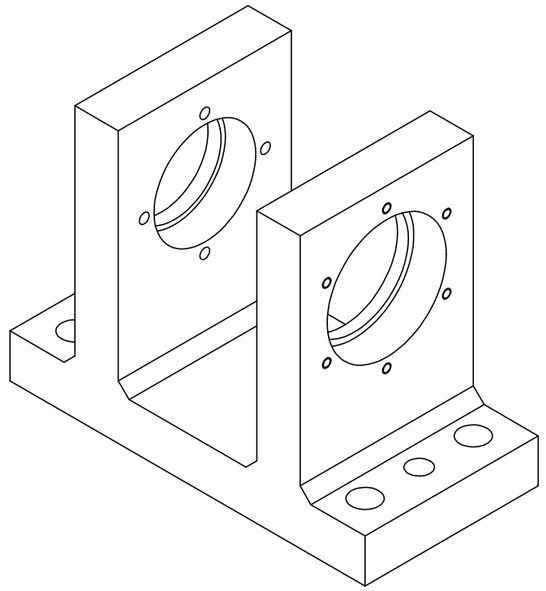

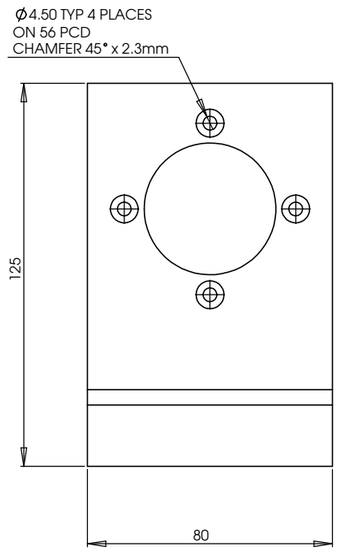

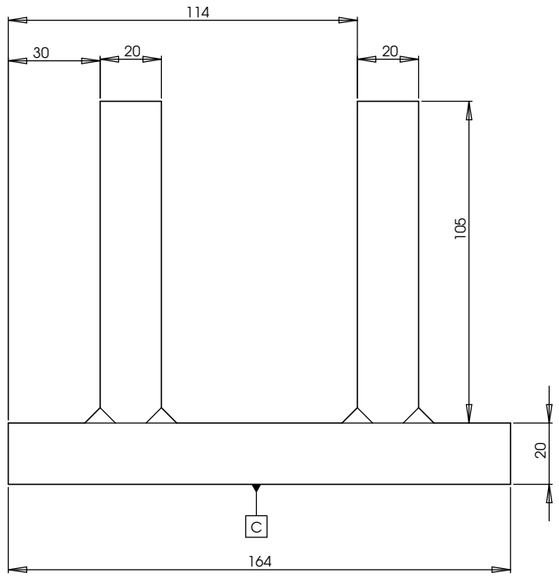

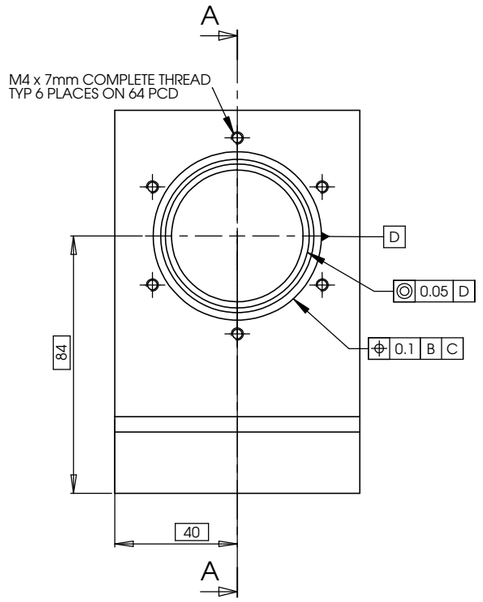

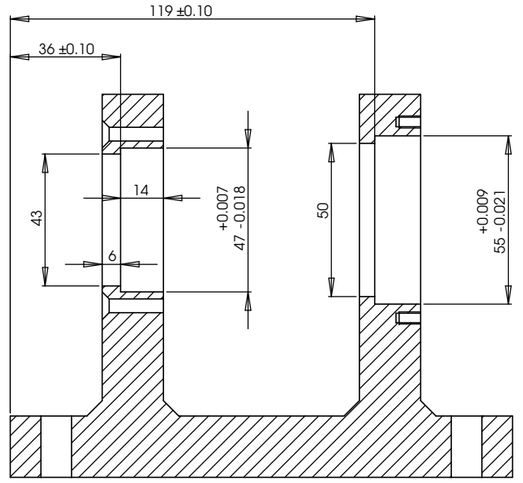

A-A

No. Required: 1

Material: MILD STEEL

BOTTOM SHAFT BEARING HOLDER	**UNIVERSITY OF CANTERBURY** MECHANICAL ENGINEERING DEPT CH.CH. NZ
	DRAWN : Ben Low — DATE : Oct 04
	CHECKED : — DRG. No : 141
SCALE: 1 : 1 (A1) ALL DIMENSIONS IN mm	APPROVED :

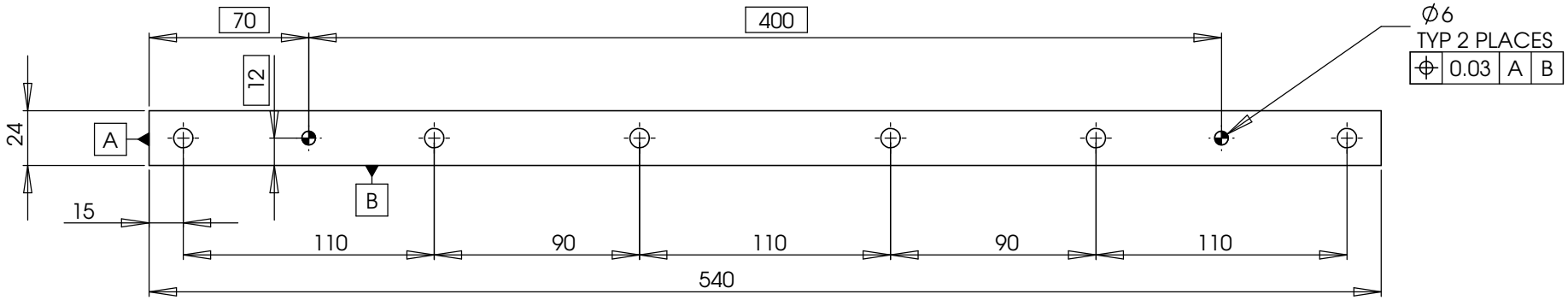

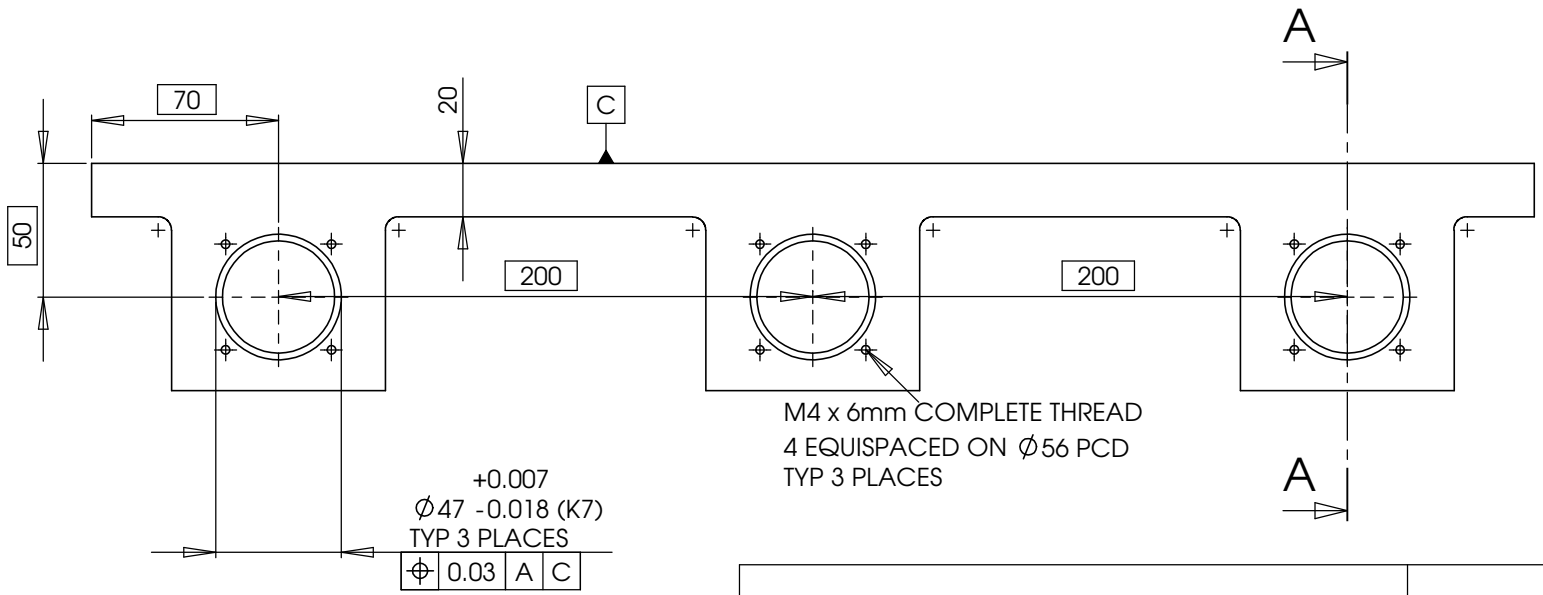

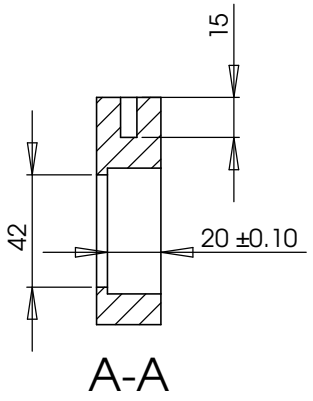

FE BEARING HOLDER - LEFT

SCHOOL OF ENGINEERING
MECHANICAL ENGINEERING DEPARTMENT

		Drawn: Ben Low	Date: Nov 04
No. Required: 1	Material: MILD STEEL	Checked:	DRG No. 142
Scale: 1 : 2 (A3)	All Dimensions in mm	Approved:	

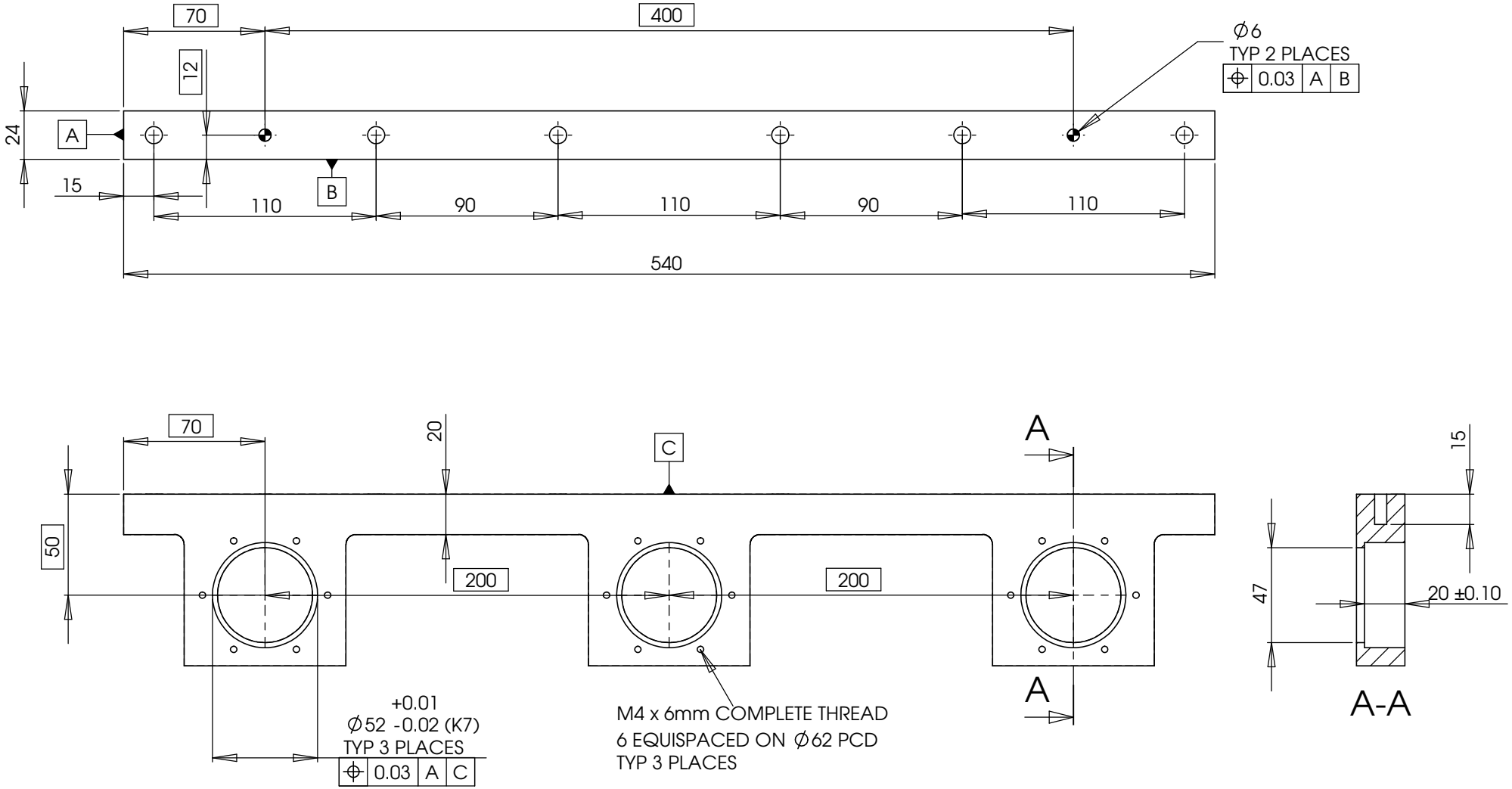

FE BEARING HOLDER - RIGHT		SCHOOL OF ENGINEERING MECHANICAL ENGINEERING DEPARTMENT	
		Drawn: Ben Low	Date: Nov 04
No. Required: 1	Material: MILD STEEL	Checked:	DRG No. 143
Scale: 1 : 2 (A3)	All Dimensions in mm	Approved:	

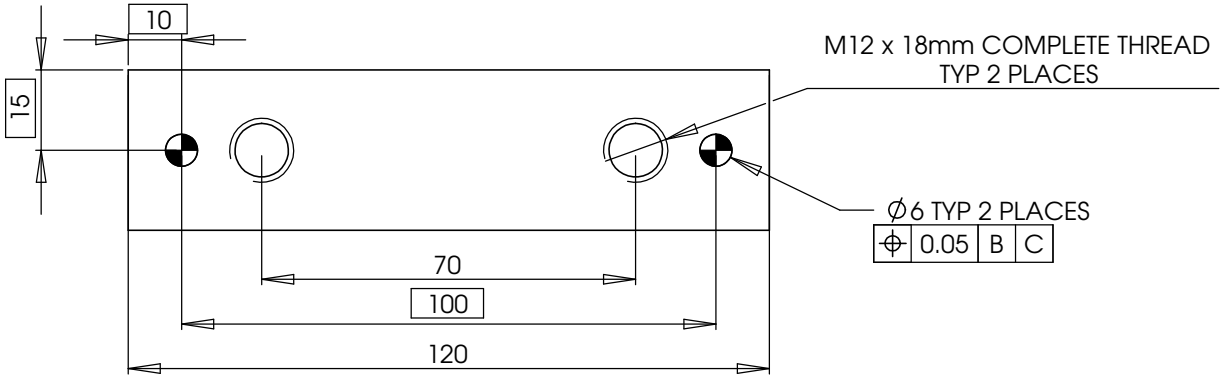

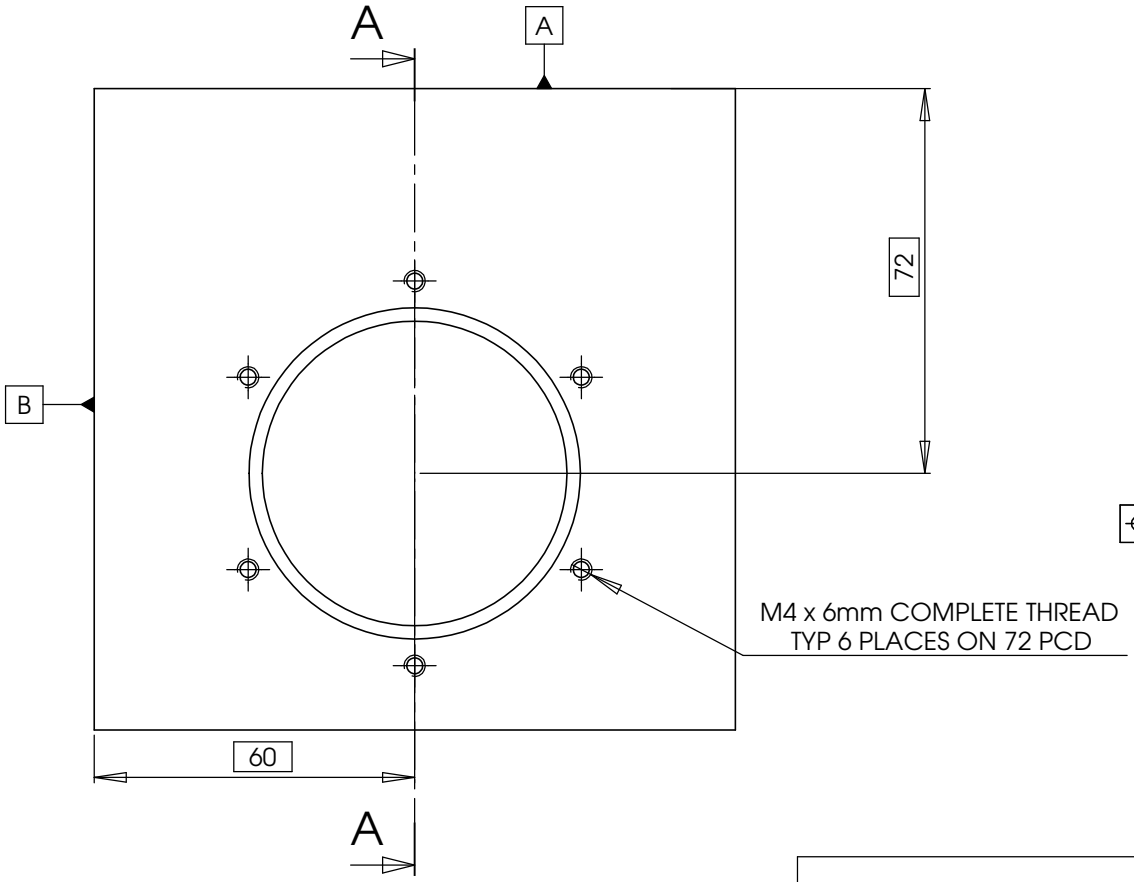

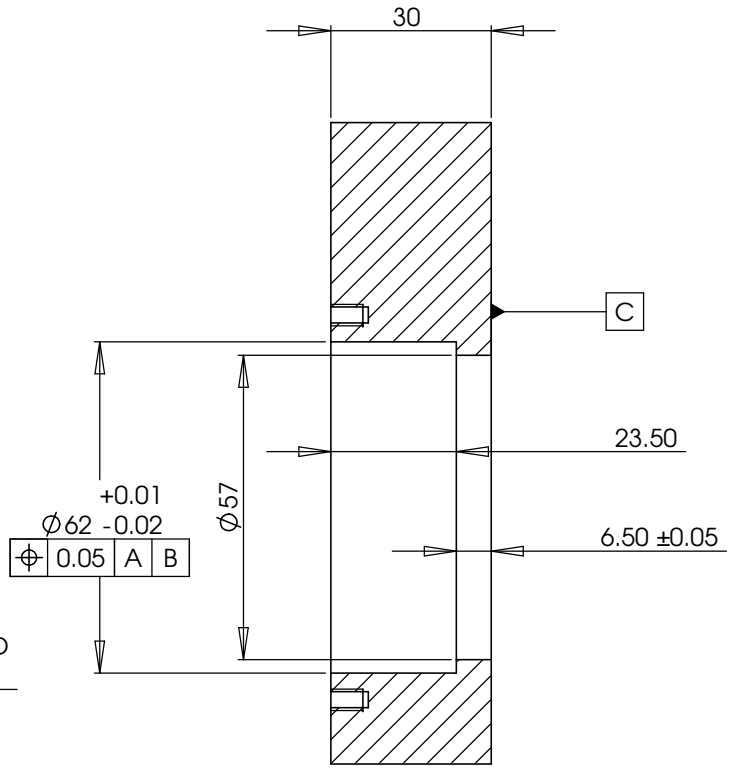

A-A

BEARING HOLDER TOP SHAFT 62 X 20

SCHOOL OF ENGINEERING
MECHANICAL ENGINEERING DEPARTMENT

		Drawn: Ben Low	Date: Nov 04
No. Required: 2	Material: MILD STEEL	Checked:	DRG No. 144
Scale: 1: 1 (A3)	All Dimensions in mm	Approved:	

PART NO. 160
RETAINING RING FOR 62MM OD BEARING
(TOP SHAFT BEARINGS)
NO. REQUIRED: 2

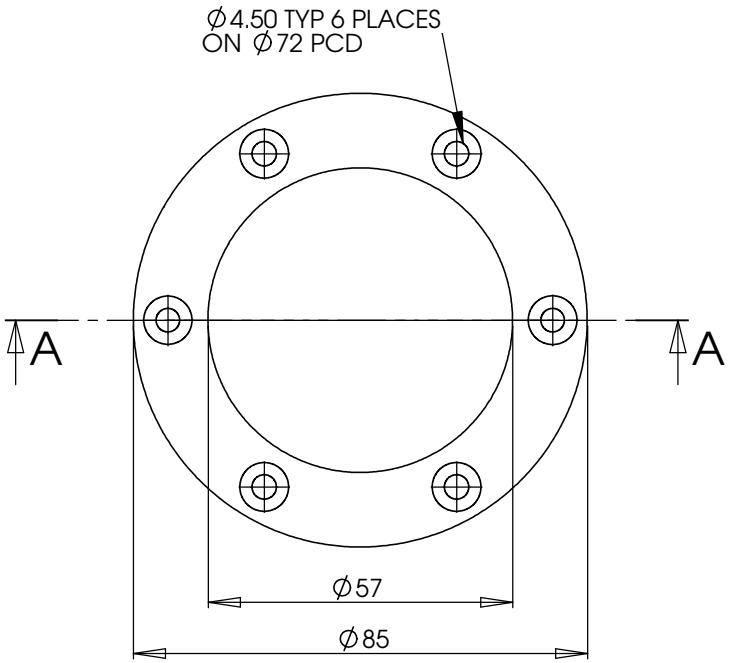

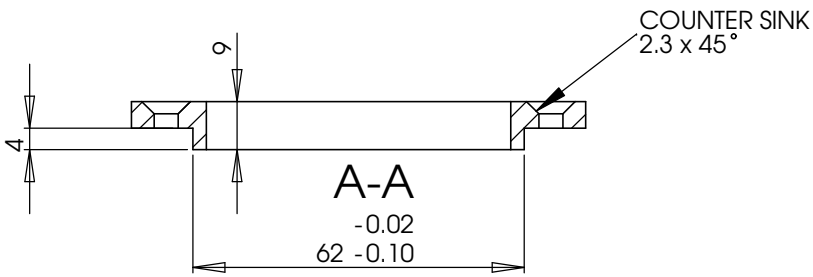

PART NO. 161
RETAINING RING FOR 55MM OD BEARING
(RH BOTTOM SHAFT BEARING)
NO. REQUIRED: 1

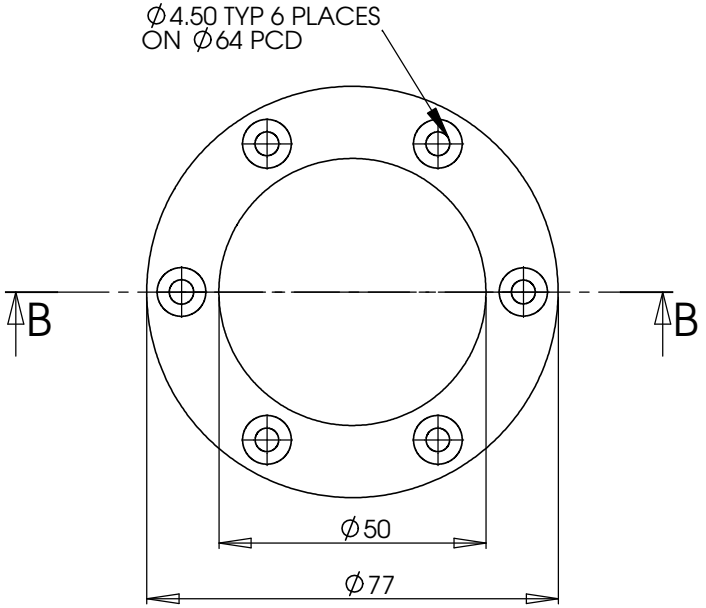

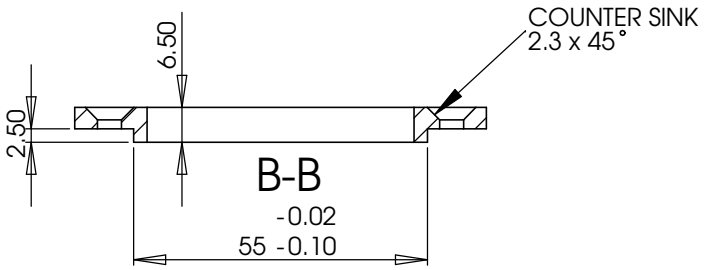

BEARING RETAINING RINGS		SCHOOL OF ENGINEERING MECHANICAL ENGINEERING DEPARTMENT	
		Drawn: Ben Low	Date: Nov 04
No. Required:	Material: MILD STEEL	Checked:	DRG No. 160-161
Scale: 1 : 1 (A3)	All Dimensions in mm	Approved:	

PART NO. 162
RETAINING RING FOR 52mm OD BEARING
(RH FE SHAFT BEARING)
NO. REQUIRED: 3

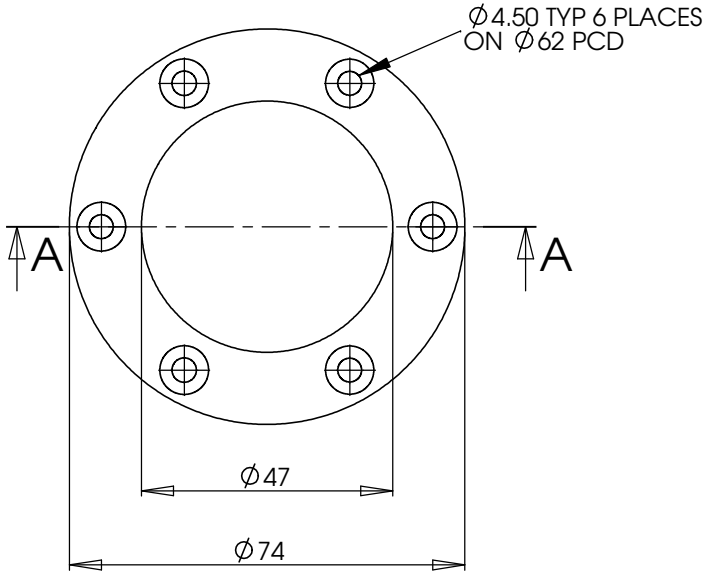

PART NO. 163
RETAINING RING FOR 47mm OD BEARING
(LH FE SHAFT, CONROD & JOINING ROD BEARINGS)
NO. REQUIRED: 11

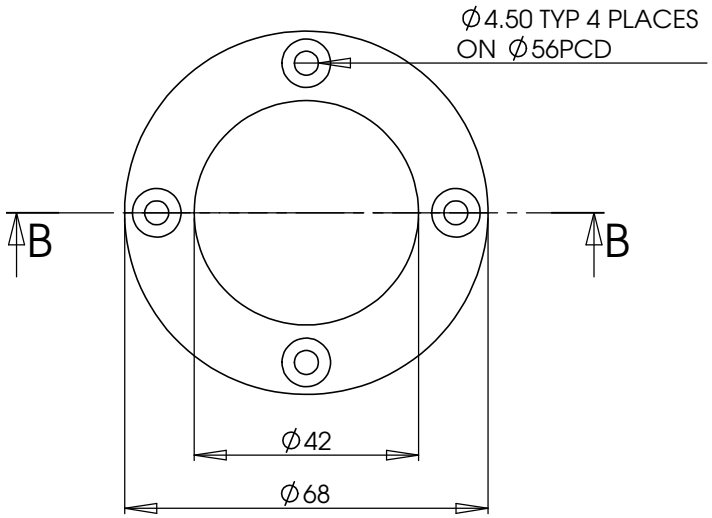

PART NO. 164
RETAINING RING FOR 47mm OD BEARING
(LH BOTTOM SHAFT BEARING)
NO. REQUIRED: 1

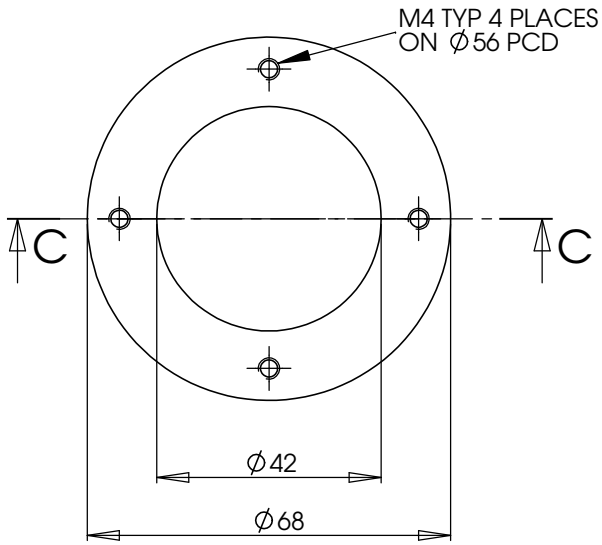

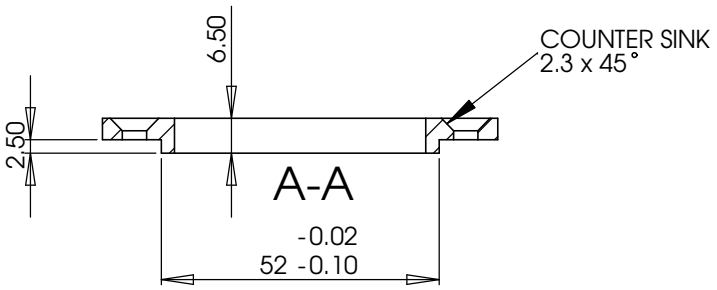

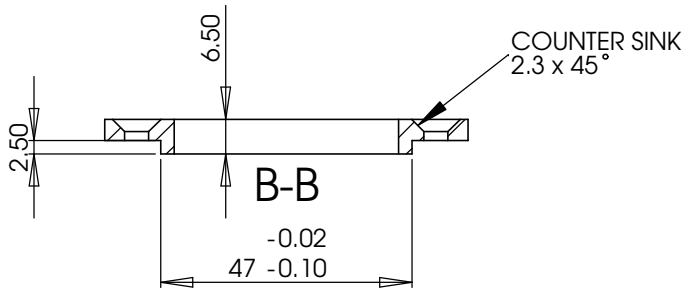

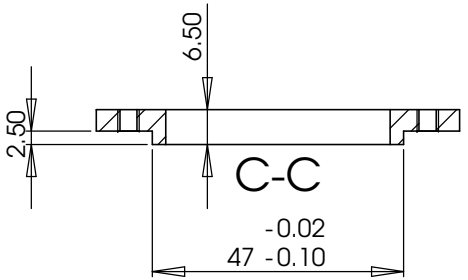

BEARING RETAINING RINGS		SCHOOL OF ENGINEERING MECHANICAL ENGINEERING DEPARTMENT	
		Drawn: Ben Low	Date: Nov 04
No. Required:	Material: MILD STEEL	Checked:	DRG No. 162-164
Scale: 1 : 1 (A3)	All Dimensions in mm	Approved:	

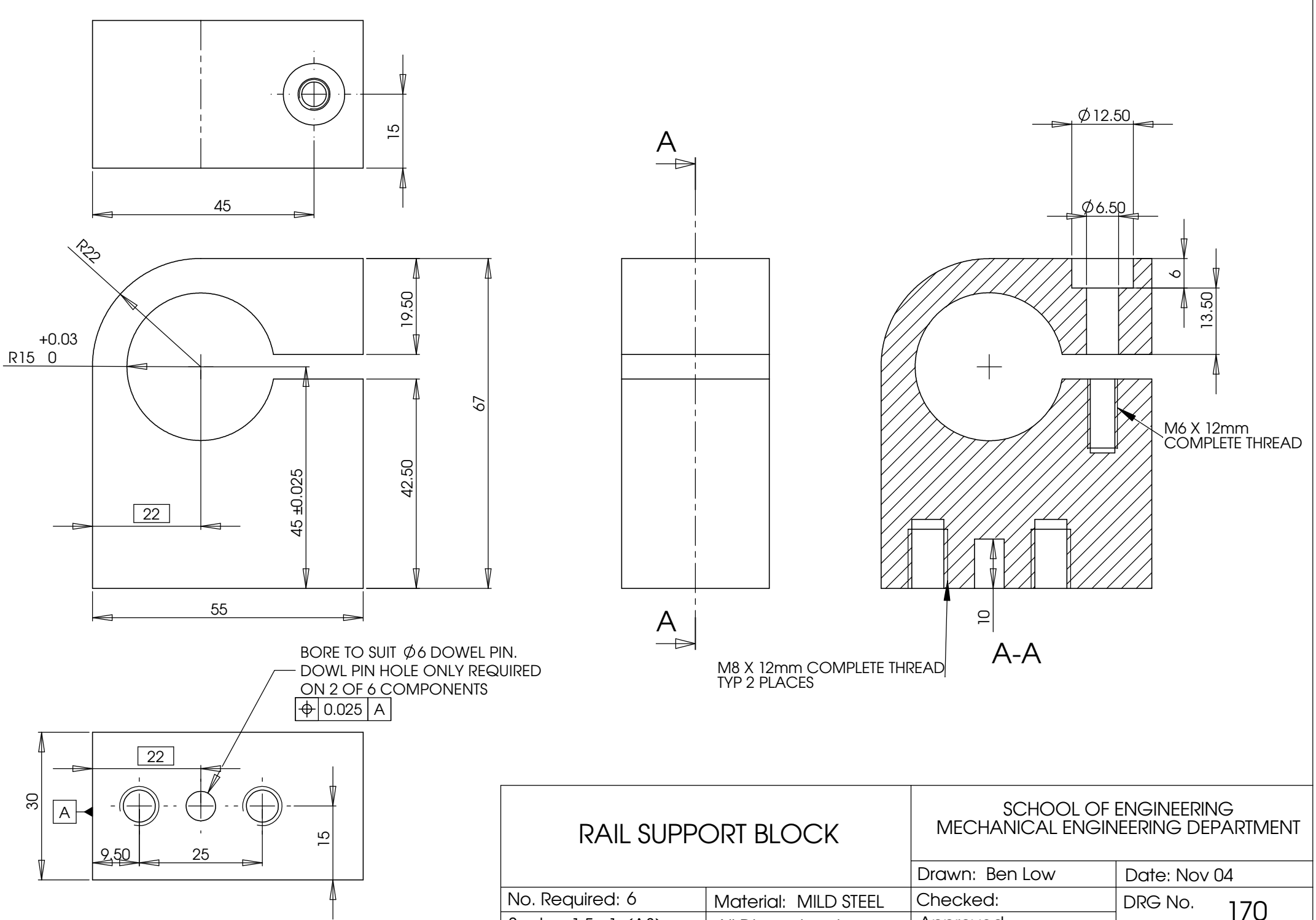

RAIL SUPPORT BLOCK		SCHOOL OF ENGINEERING MECHANICAL ENGINEERING DEPARTMENT	
		Drawn: Ben Low	Date: Nov 04
No. Required: 6	Material: MILD STEEL	Checked:	DRG No. 170
Scale: 1.5 : 1 (A3)	All Dimensions in mm	Approved:	

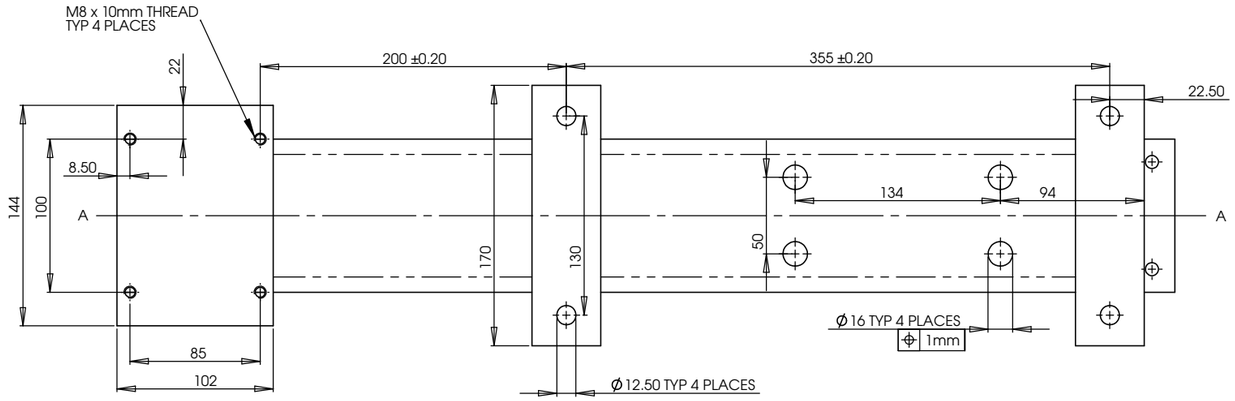

GEARBOX SUPPORT ARM IS SYMMETRIC ABOUT LINE A-A

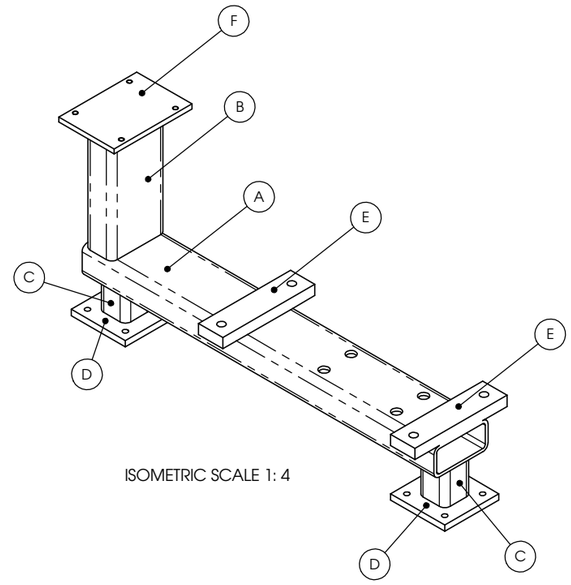

ISOMETRIC SCALE 1: 4

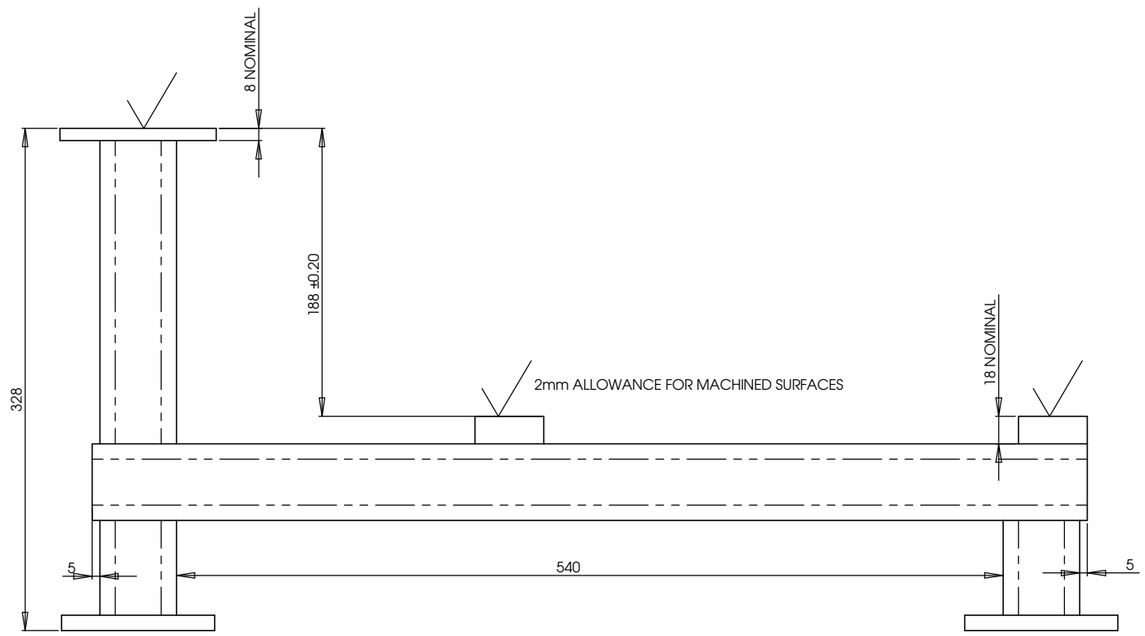

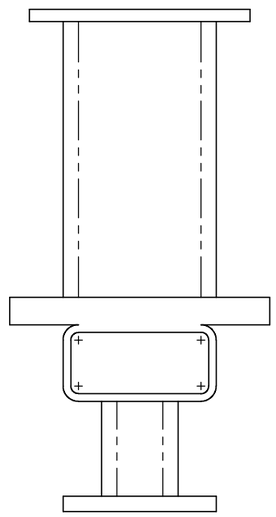

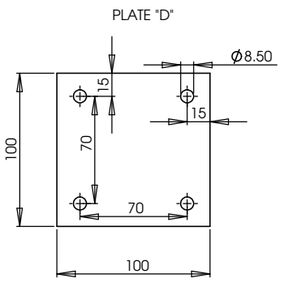

CUTTING LIST		
ITEM	DESCRIPTION	QTY
A	100 x 50 x 5 RHS x 650 LONG	1
B	100 x 50 x 5 RHS x 198 LONG	1
C	50 x 50 x 3 RHS x 62 LONG	2
D	100 x 100 x 10 FLAT	2*
E	45 x 170 x 20 FLAT	2
F	102 x 144 x 10 FLAT	1

* 2 EXTRA OF PLATE D ARE REQUIRED FOR PART NO. 183

GEARBOX SUPPORT ARM

NO. REQUIRED: 1 MATERIAL: RHS & MILD STEEL PLATE

SCALE: 1 : 2 (A1) ALL DIMENSIONS IN mm

UNIVERSITY OF CANTERBURY
MECHANICAL ENGINEERING DEPT CH.CH. N.Z.

DRAWN : Ben Low | DATE : Oct 04

CHECKED :

APPROVED :

DRG. No : 182

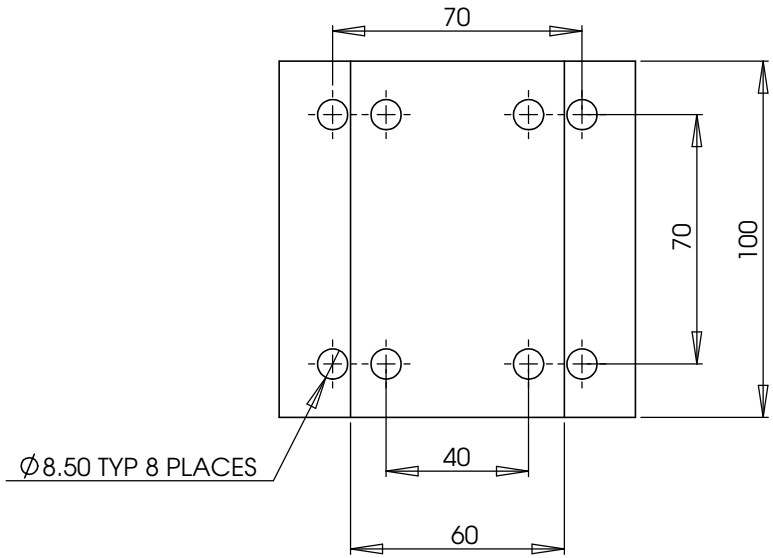

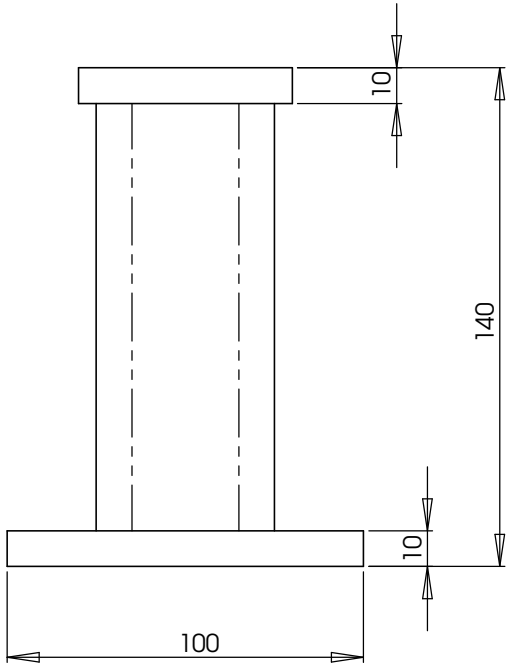

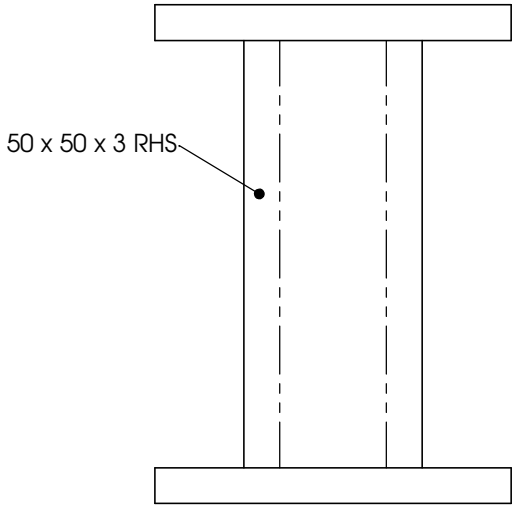

BASE SUPPORT FEET

SCHOOL OF ENGINEERING
MECHANICAL ENGINEERING DEPARTMENT

		Drawn: Ben Low	Date: Nov 04
No. Required: 2	Material: MILD STEEL	Checked:	DRG No. 183
Scale: 1 : 1.5 (A3)	All Dimensions in mm	Approved:	

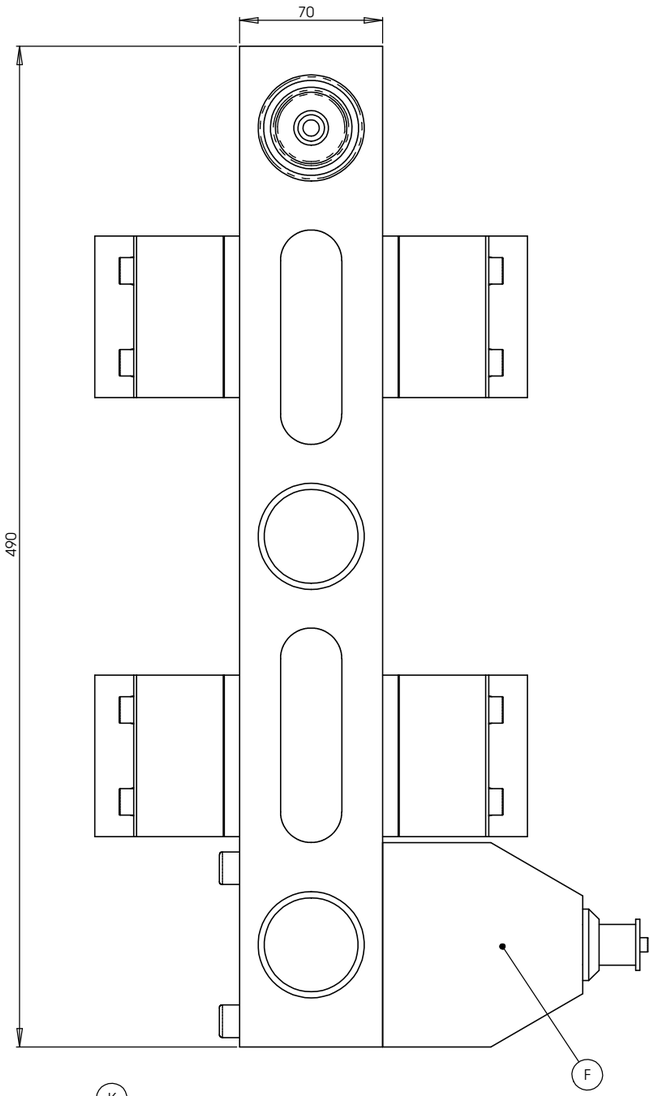

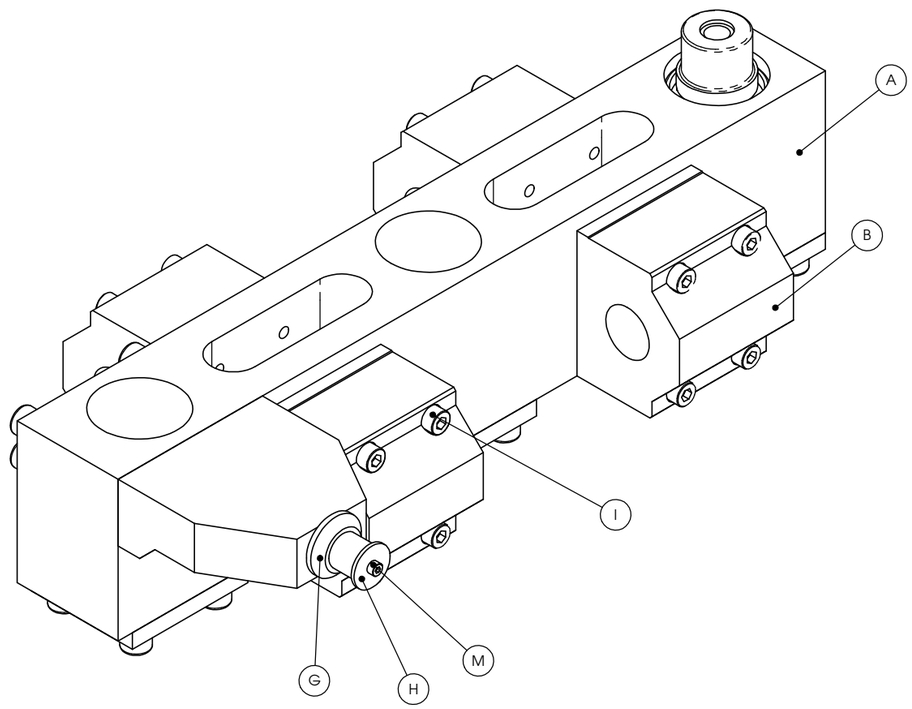

Item	Part No.	Description
A	210	AP Carriage
B	220	Linear Bearing SSEBP M30
C	230	IE Bearings 7205BE
D	231	IE Bearing Spacer
E	232	IE Bearing Retaining Plate
F	240	AP Carriage Conrod Bracket
G	241	Conrod Bearing Spacer 20mm ID
H	242	Washer M4x25x2
I	250	M8 x 70 Cap Screw
J	251	M10 x 30 Cap Screw
K	252	M10 x 90 Cap Screw
L	253	M10 x 80 Cap Screw
M	254	M4 x 8 Cap Screw
N*	320	IE Shaft
O*	323	IE Shaft Lock Nut Spacer
P*	321	M25 Lock Nut
Q*	322	M25 Locking Washer

* = Shown for reference only

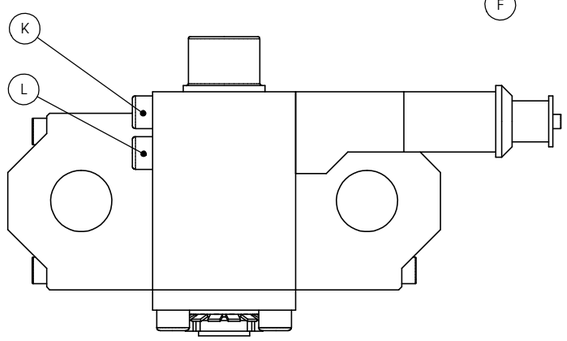

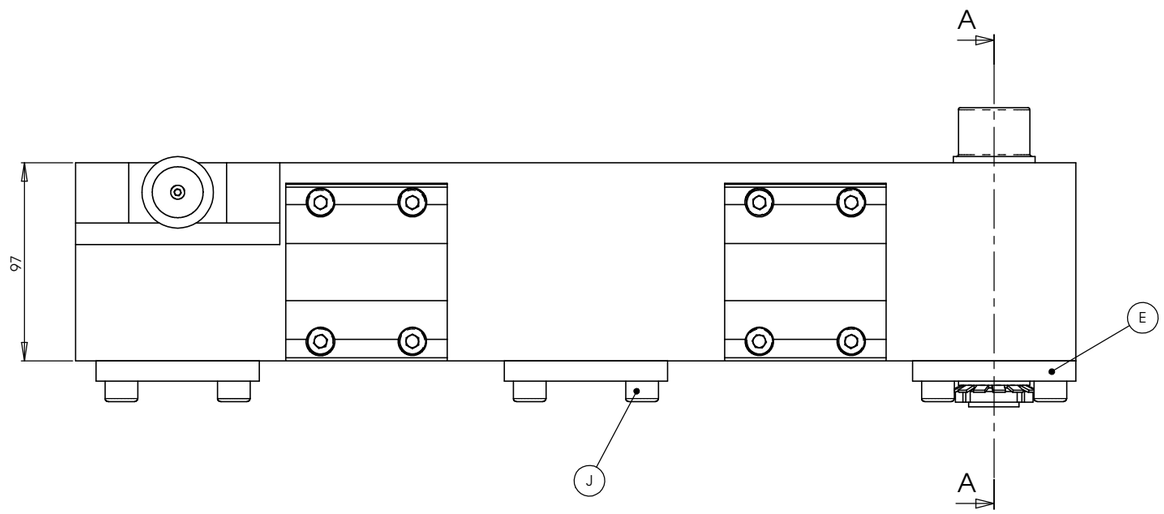

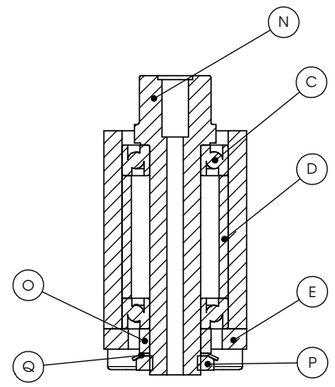

Section A-A

AP Carriage General Assembly & Bill of Materials	**UNIVERSITY OF CANTERBURY** **MECHANICAL ENGINEERING DEPT** CH.CH. N.Z.	
	DRAWN : Ben Low	DATE : Oct 04
	CHECKED :	DRG. No :
SCALE: 1 : 1.5 (A1) ALL DIMENSIONS IN mm	APPROVED :	200

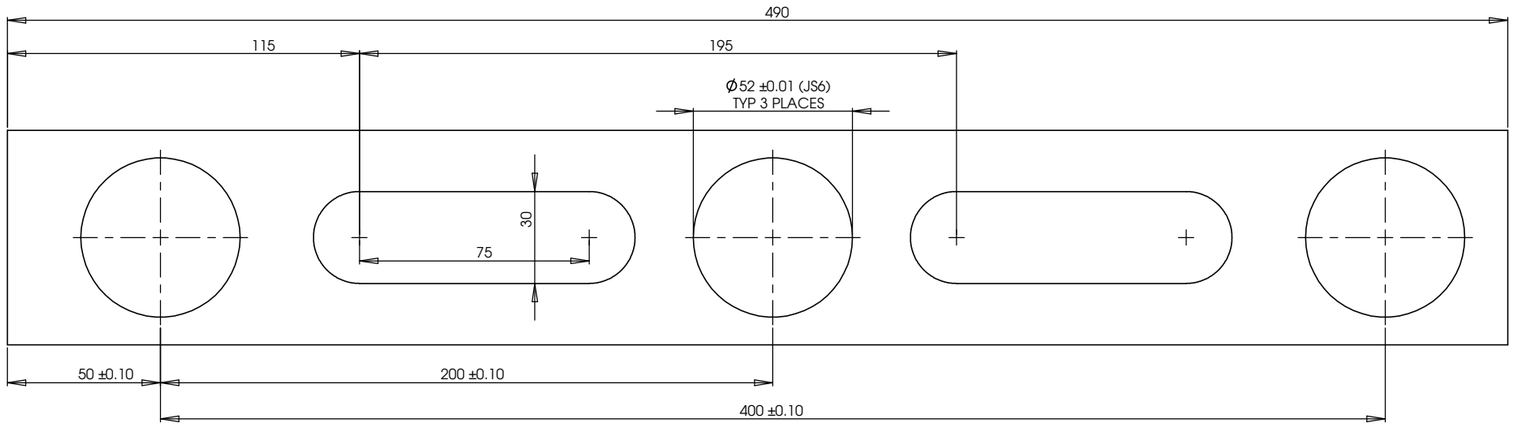

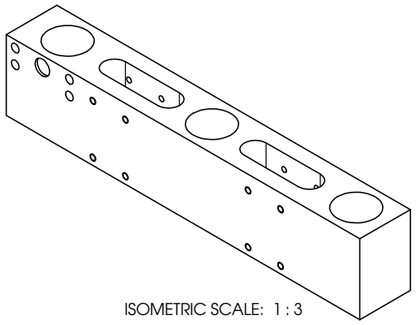

ISOMETRIC SCALE: 1 : 3

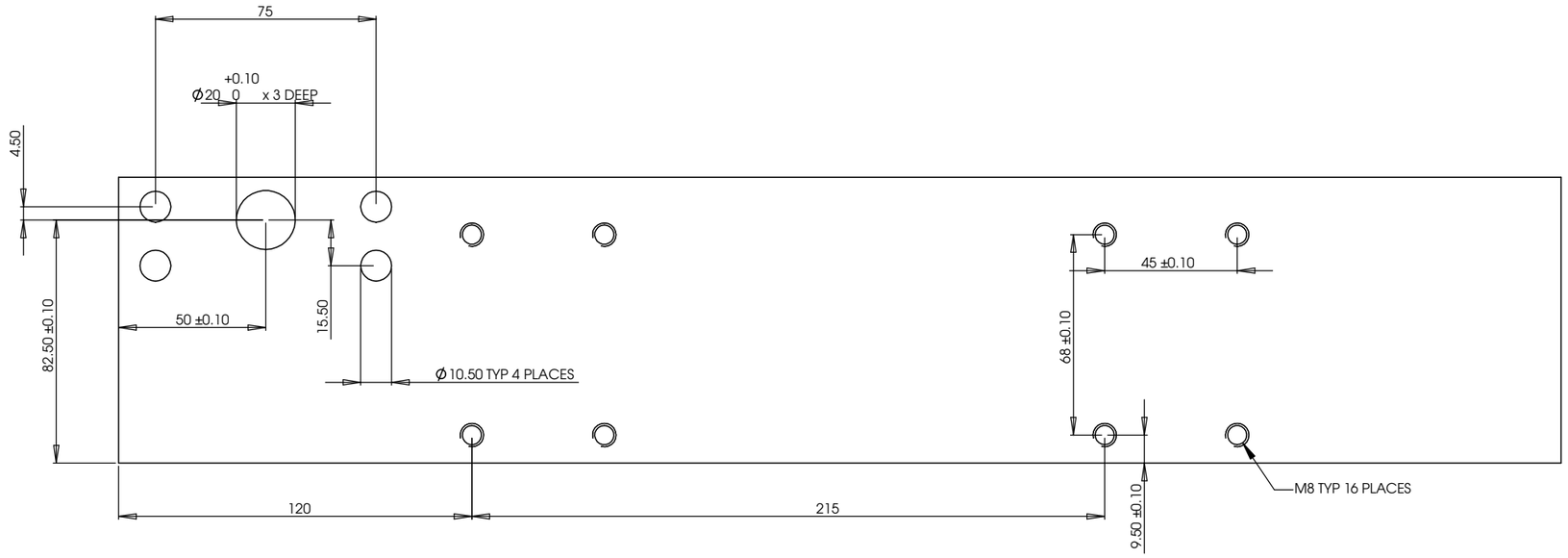

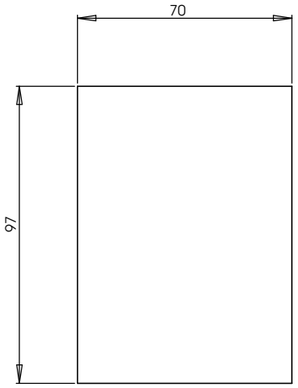

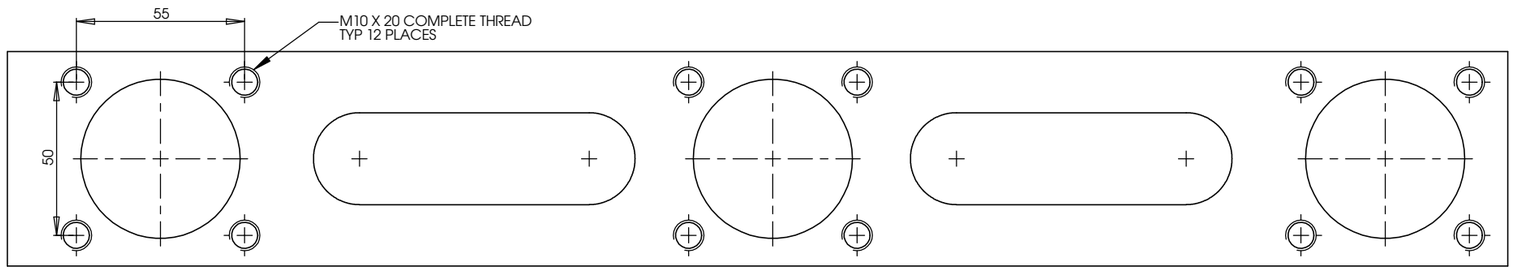

AP CARRIAGE	**UNIVERSITY OF CANTERBURY** MECHANICAL ENGINEERING DEPT. CHCH. N.Z.	
	DRAWN : Ben Low	DATE : Oct 04
MATERIAL: ALUMINIUM TOOLING PLATE	CHECKED :	DRG. No : 210
SCALE: 1 : 1 (A1) ALL DIMENSIONS IN mm	APPROVED :	

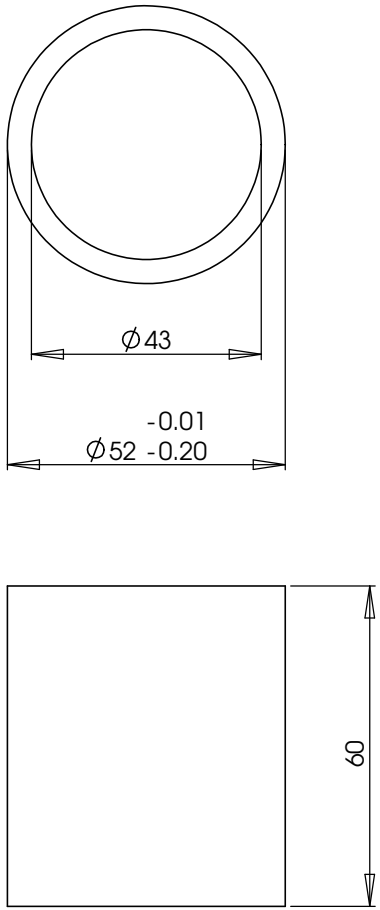

IE BEARING SPACER

SCHOOL OF ENGINEERING
MECHANICAL ENGINEERING DEPARTMENT

		Drawn: Ben Low	Date: Nov 04
No. Required: 3	Material: MILD STEEL	Checked:	DRG No. 231
Scale: 1 : 1 (A3)	All Dimensions in mm	Approved:	

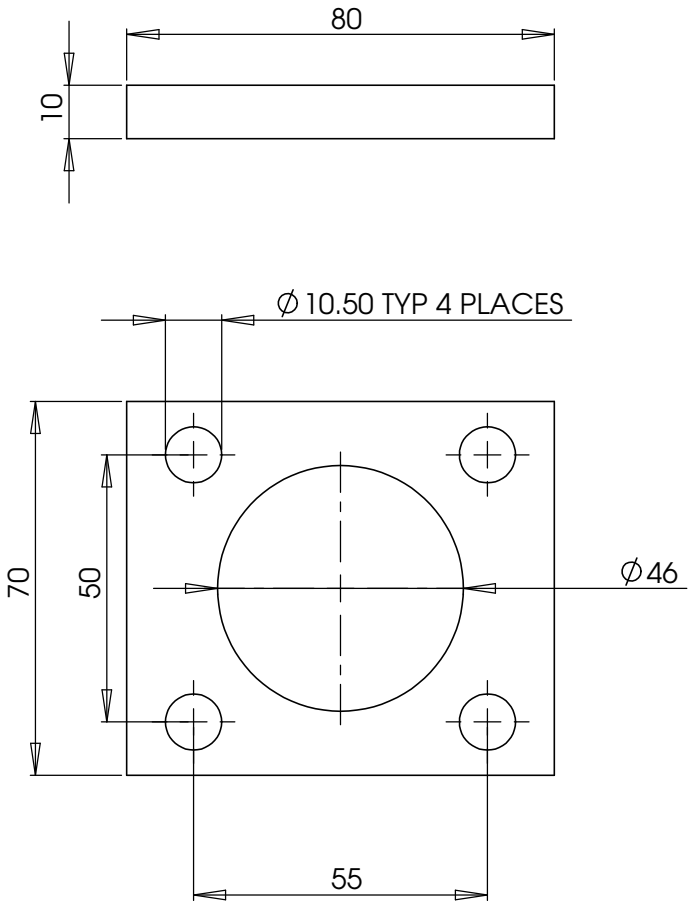

IE BEARING RETAINING PLATE		SCHOOL OF ENGINEERING MECHANICAL ENGINEERING DEPARTMENT	
		Drawn: Ben Low	Date: Nov 04
No. Required: 3	Material: MILD STEEL	Checked:	DRG No. 232
Scale: 1 : 1 (A3)	All Dimensions in mm	Approved:	

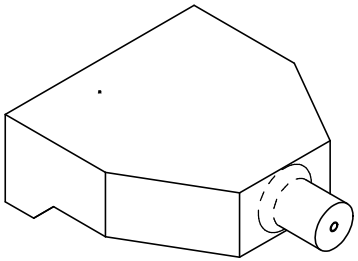

ISOMETRIC SCALE 1 : 2

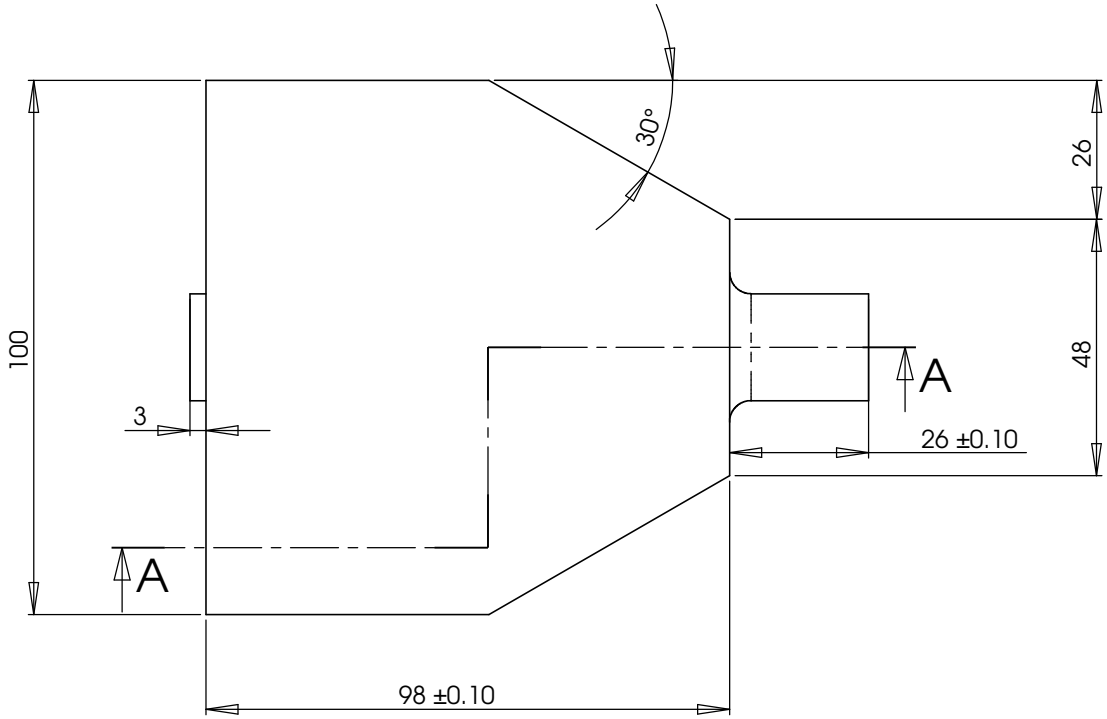

M10 x 22mm COMPLETE THREAD
TYP 2 PLACES

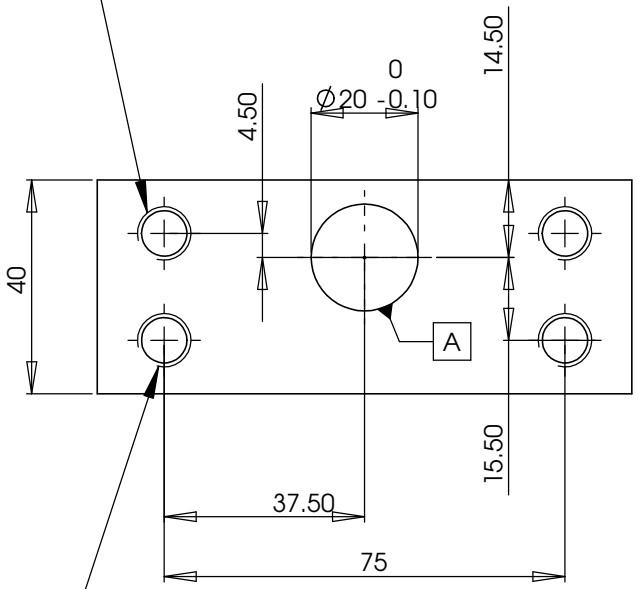

M10 x 12mm COMPLETE THREAD
TYP 2 PLACES

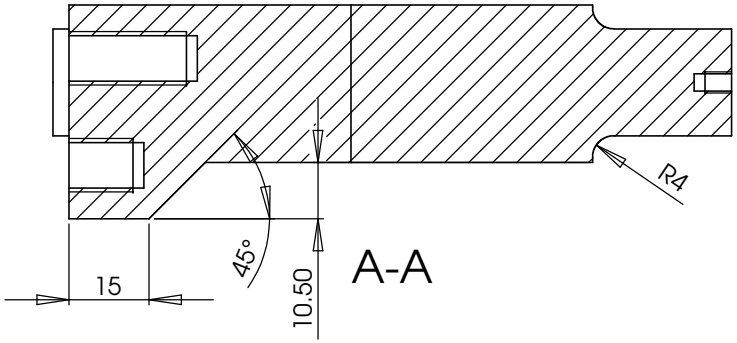

M4 x 7mm COMPLETE THREAD

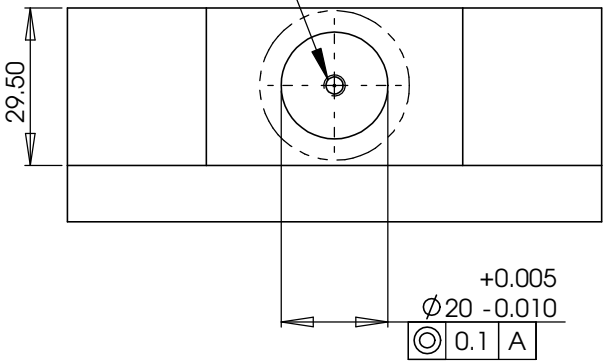

AP CARRIAGE CONROD BRACKET		SCHOOL OF ENGINEERING MECHANICAL ENGINEERING DEPARTMENT	
		Drawn: Ben Low	Date: Nov 04
No. Required: 1	Material: MILD STEEL	Checked:	DRG No. 240
Scale: 1 : 1 (A3)	All Dimensions in mm	Approved:	

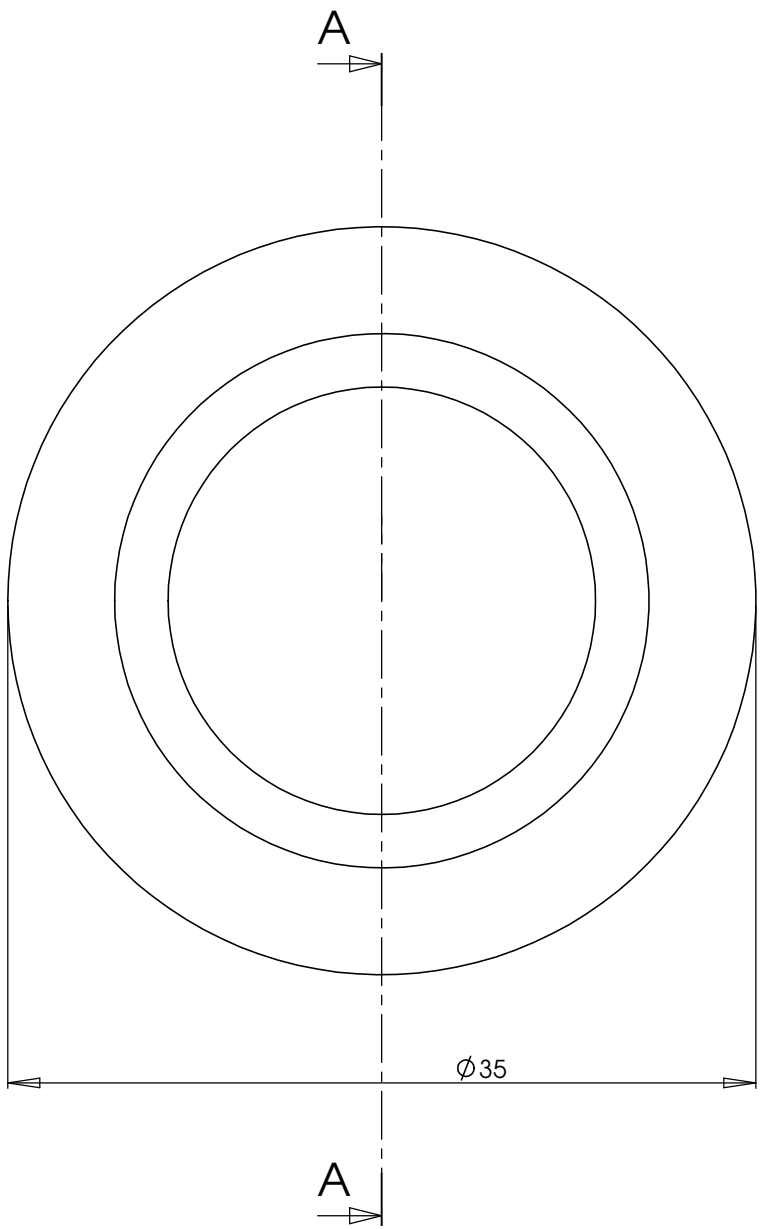

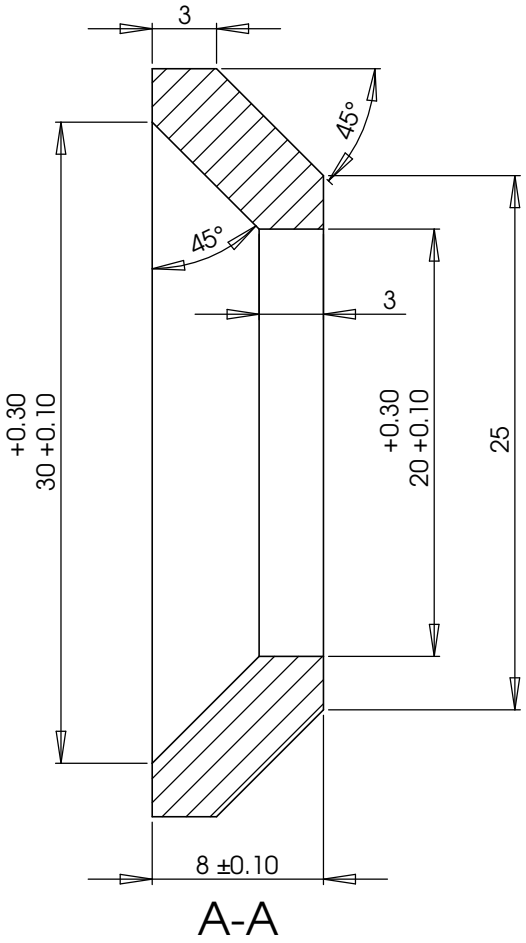

A-A

CONROD BEARING SPACER
20mm ID

SCHOOL OF ENGINEERING
MECHANICAL ENGINEERING DEPARTMENT

		Drawn: Ben Low	Date: Nov 04
No. Required: 6	Material: MILD STEEL	Checked:	DRG No. 241
Scale: 4 : 1 (A3)	All Dimensions in mm	Approved:	

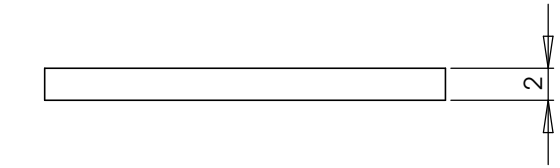

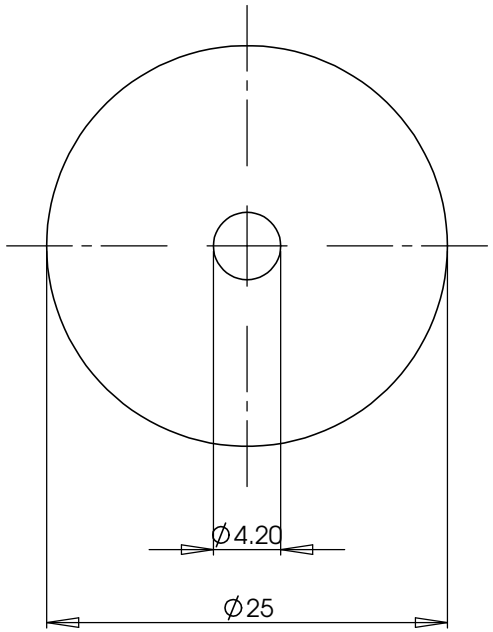

WASHER M4 x 25 x 2

SCHOOL OF ENGINEERING
MECHANICAL ENGINEERING DEPARTMENT

		Drawn: Ben Low	Date: Nov 04
No. Required: 6	Material: MILD STEEL	Checked:	DRG No. 242
Scale: 3 : 1 (A3)	All Dimensions in mm	Approved:	

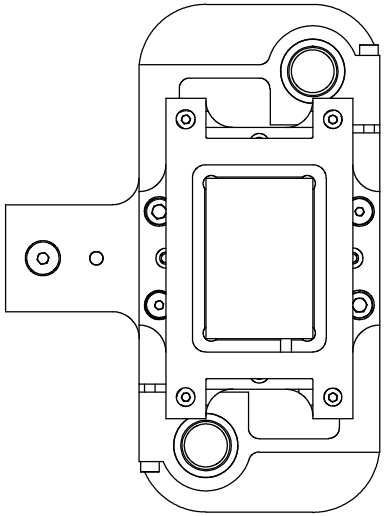

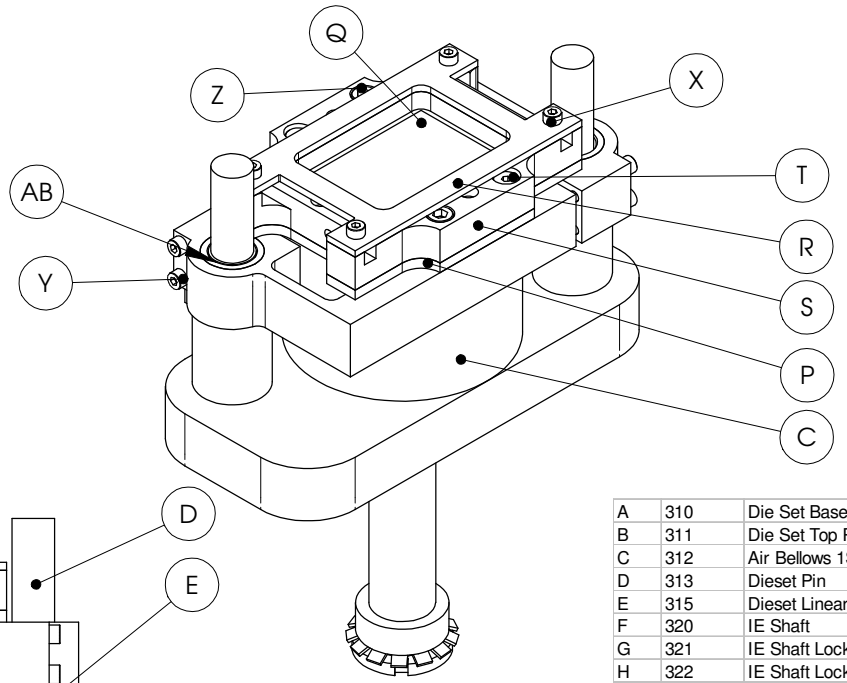

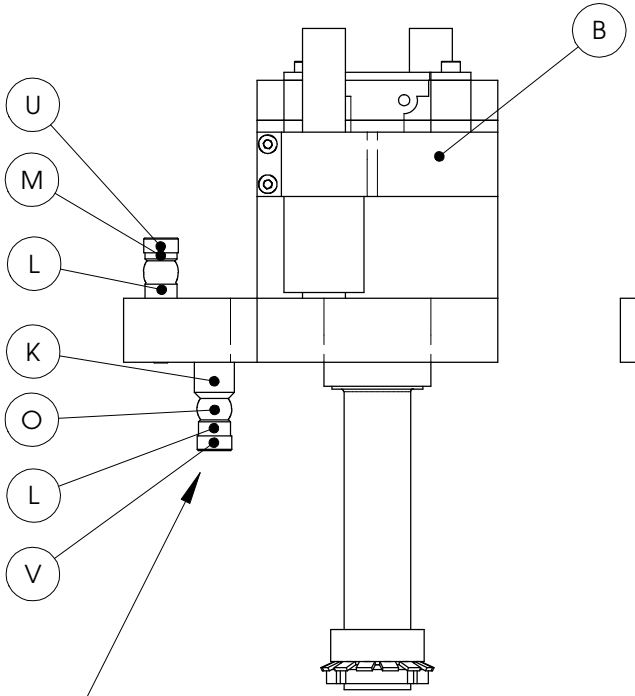

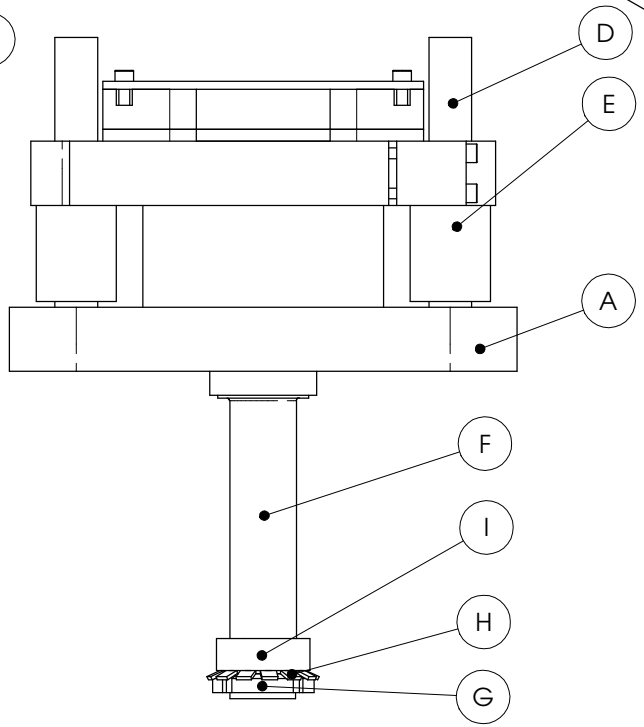

A	310	Die Set Base Plate
B	311	Die Set Top Plate
C	312	Air Bellows 1S3-013
D	313	Dieset Pin
E	315	Dieset Linear Bush Holder
F	320	IE Shaft
G	321	IE Shaft Lock Nut
H	322	IE Shaft Locking Washer
I	323	IE Shaft Lock Nut Spacer
J	330+	IE Balljoint Spacer 17mm
K	331	IE Balljoint Spacer 13.5mm
L	332	IE Balljoint Spacer 6mm
M	333	IE Balljoint Spacer 3mm 1 Chamfer
N	334+	IE Balljoint Spacer 3mm 2 Chamfer
O	811*	IE Balljoint Inner SI 8 E
P	340	SS Tibial Base Plate
Q	341	PE Sample
R	342	Sample Cover Plate
S	344	Polyacetal Sample Holder
T	350	Socket Head Shoulder Screw M6x20
U	351	Socket Head Shoulder Screw M8x30
V	352	Socket Head Shoulder Screw M8x40
W	353	M4 x 20 Cap Screw
X	354	M4 x 25 Cap Screw
Y	355	M4 x 40 Cap Screw
Z	356	M6 x 20 Cap Screw
AA	360#	1/8" Air Fitting M-01AN-6 (SMC) Not Shown
AB	314	Glacier Linear Bearing 1610DU
Item	**Part No.**	**Description**
* = Shown for reference only		
+ = Used in Diesets 2 & 3 - See Drawing 301		

This view shows the balljoint / rod end arrangement for Dieset #1.
For Diesets 2 & 3 see drawing 301

Dieset
General Assembly
& Bill of Materials

Scale: 1: 2 (A3) All Dimensions in mm

SCHOOL OF ENGINEERING
MECHANICAL ENGINEERING DEPARTMENT

Drawn: Ben Low | Date: Oct 04

Checked:

Approved:

DRG No. 300

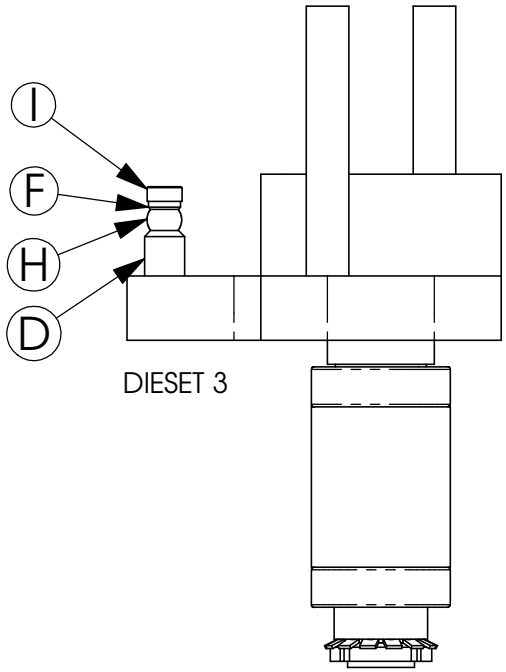

DIESET 3

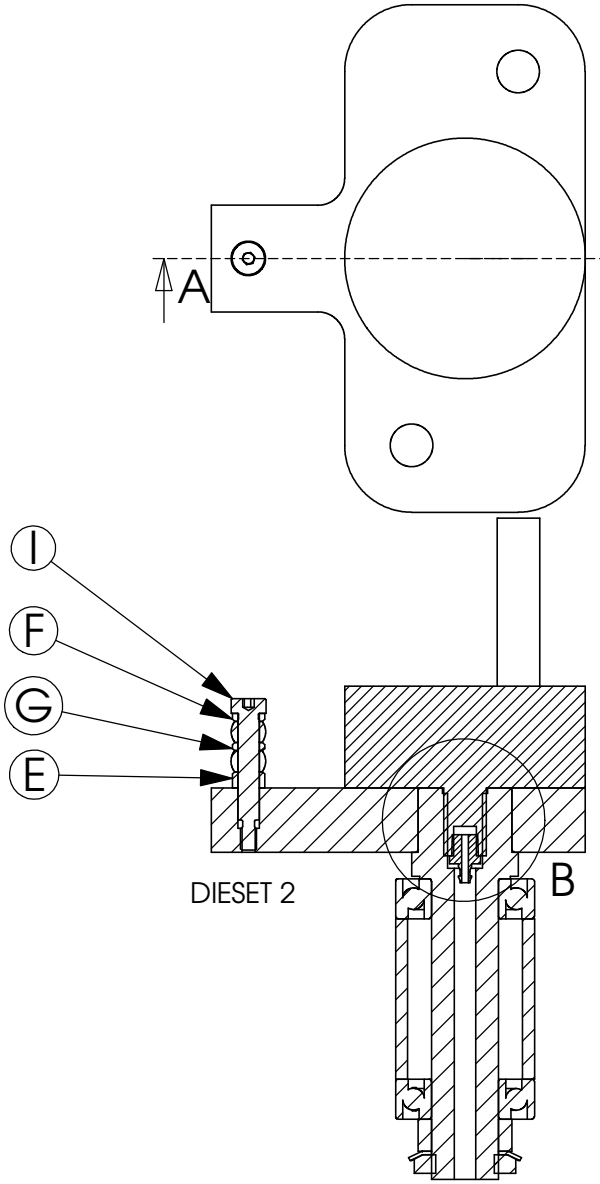

DIESET 2

A-A

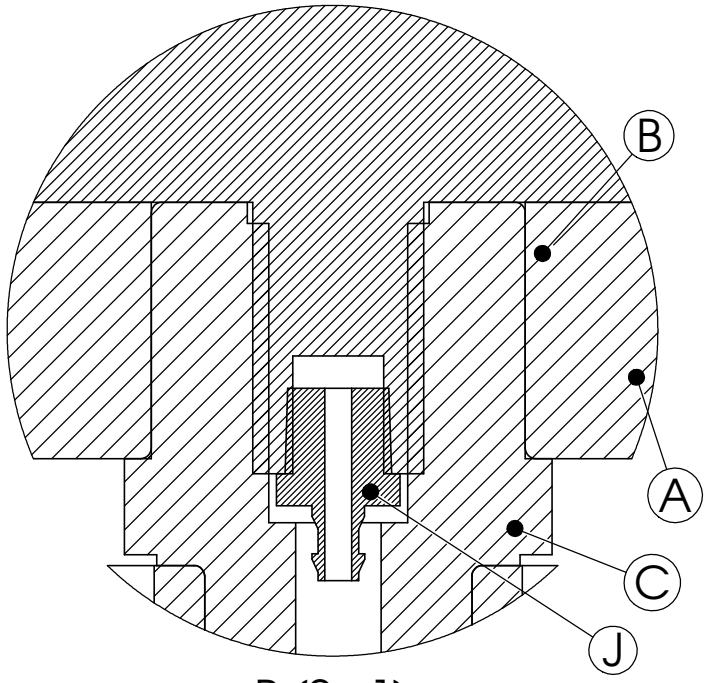

B (2 : 1)

Item	Part No	Description
A	310	Die Set Base Plate
B	312	Air Bellows 1S3-013
C	320	IE Shaft
D	330	IE Balljoint Spacer 17mm
E	332	IE Balljoint Spacer 6mm
F	333	IE Balljoint Spacer 3mm 1 Chamfer
G	334	IE Balljoint Spacer 3mm 2 Chamfer
H	811	IE Balljoint Inner SI 8 E
I	352	Socket Head Shoulder Screw M8x40
J	360	1/8" Air Fitting M-01AN-6 (SMC)

DIESET DETAIL

TO BE VIEWED WITH DRAWING 300

SCHOOL OF ENGINEERING
MECHANICAL ENGINEERING DEPARTMENT

		Drawn: Ben Low	Date: Nov 04
No. Required:	Material:	Checked:	DRG No. 301
Scale: 1 : 2 (A3)	All Dimensions in mm	Approved:	

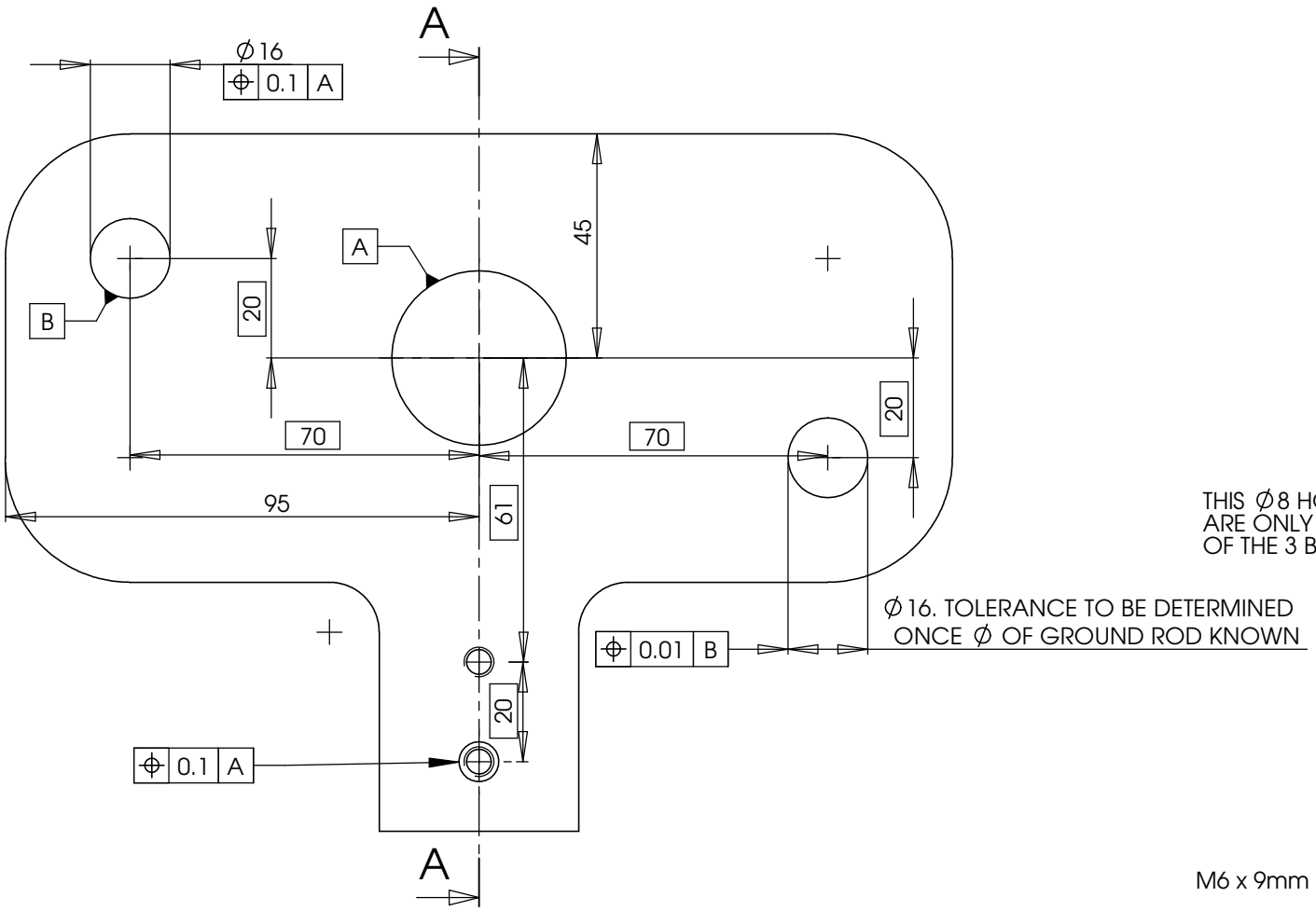

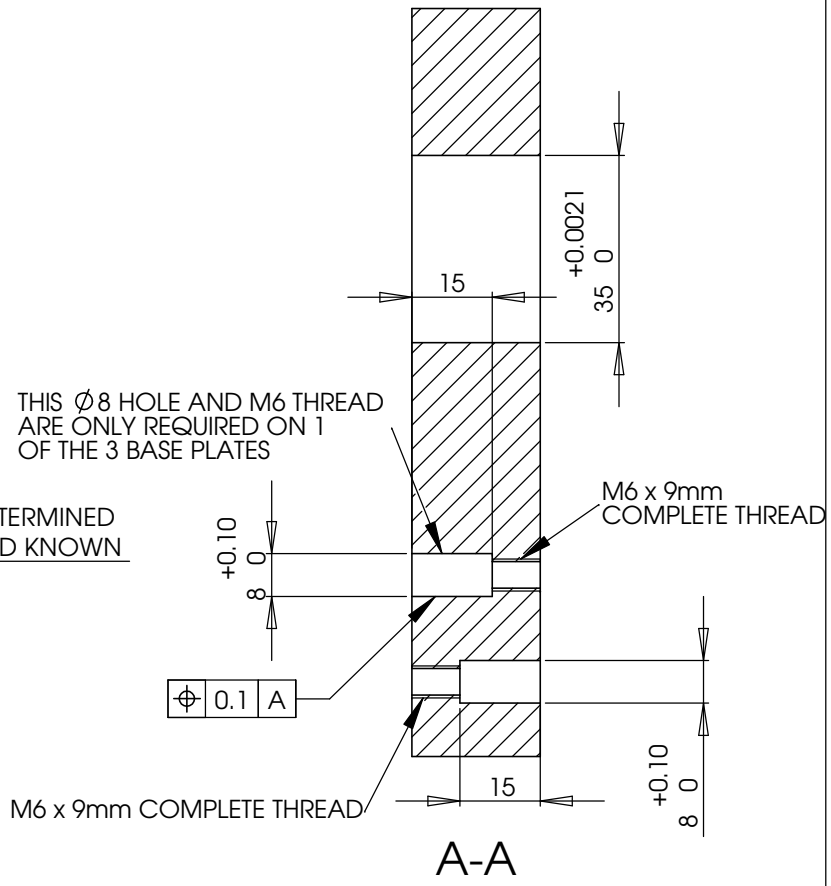

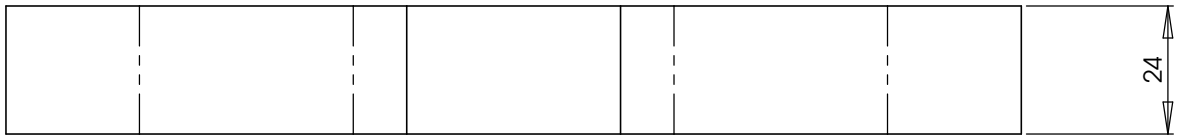

DIE SET BASE PLATE		SCHOOL OF ENGINEERING MECHANICAL ENGINEERING DEPARTMENT	
		Drawn: Ben Low	Date: Nov 04
No. Required: 3	Material: MILD STEEL	Checked:	DRG No. 310
Scale: 1 : 1 (A3)	All Dimensions in mm	Approved:	

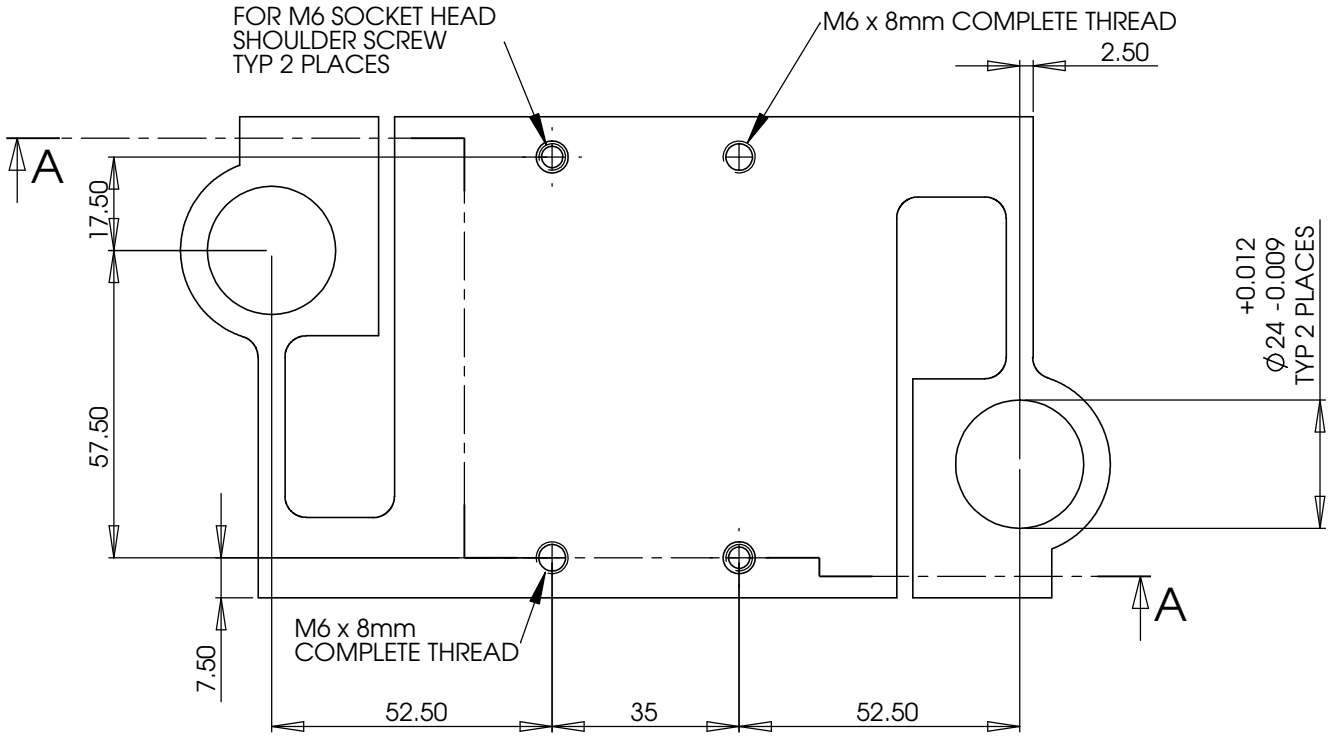

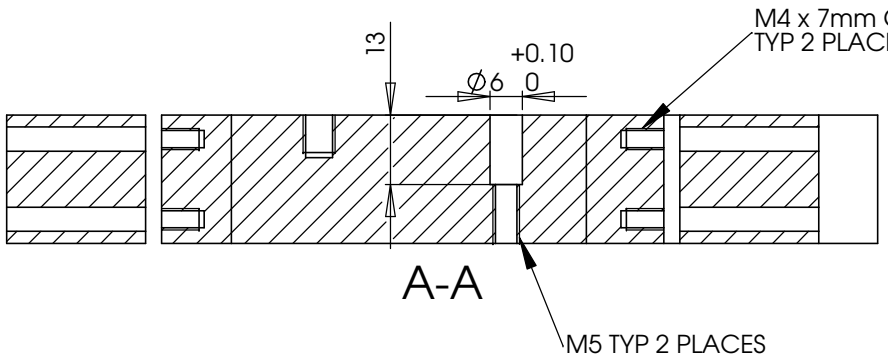

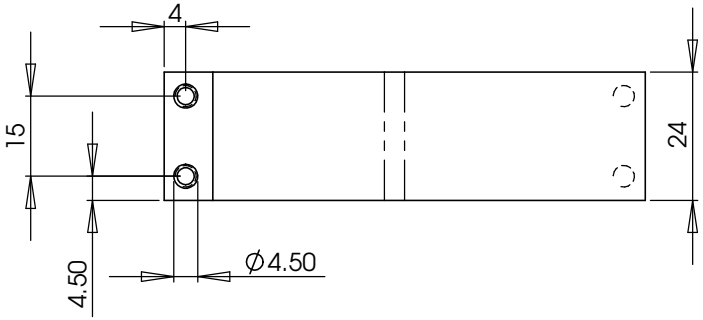

DIESET TOP PLATE

SEE 311.DXF FOR WIRE CUT PROFILE

SCHOOL OF ENGINEERING
MECHANICAL ENGINEERING DEPARTMENT

No. Required: 3	Material: MEDIUM TENSILE STEEL	Drawn: Ben Low	Date: Nov 04
Scale: 1 : 1 (A3)	All Dimensions in mm	Checked:	DRG No. 311
		Approved:	

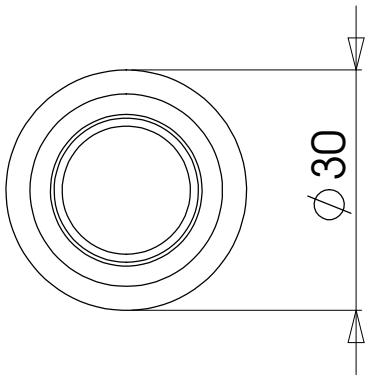

∅24 Tolerance for press fit as discussed

0.8 x 30° CHAMFER
TYP 2 PLACES

GLACIER BUSH
1610DU TYP 2 PLACES

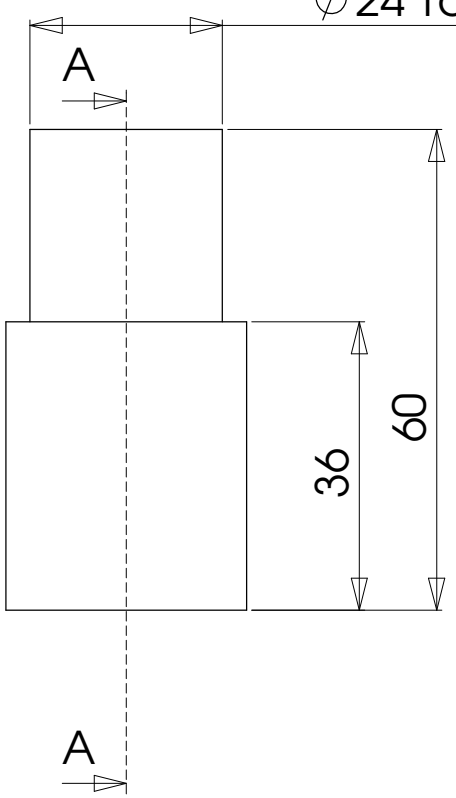

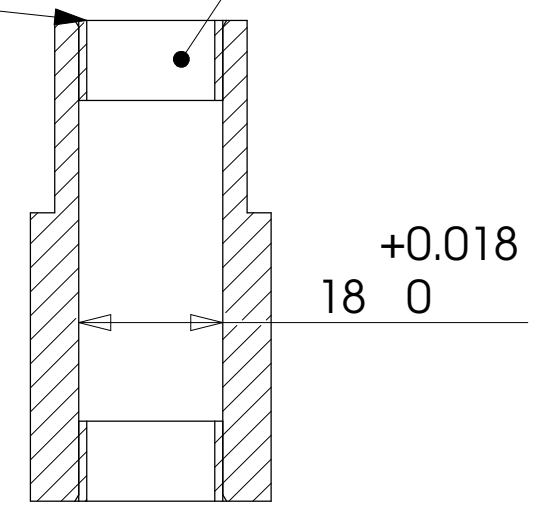

SECTION A-A

DIESET BUSH HOLDER		SCHOOL OF ENGINEERING MECHANICAL ENGINEERING DEPARTMENT	
		Drawn: Ben Low	Date: Nov 04
No. Required: 6	Material: 4140	Checked:	DRG No. 315
Scale: 1.5 : 1 (A3)	All Dimensions in mm	Approved:	

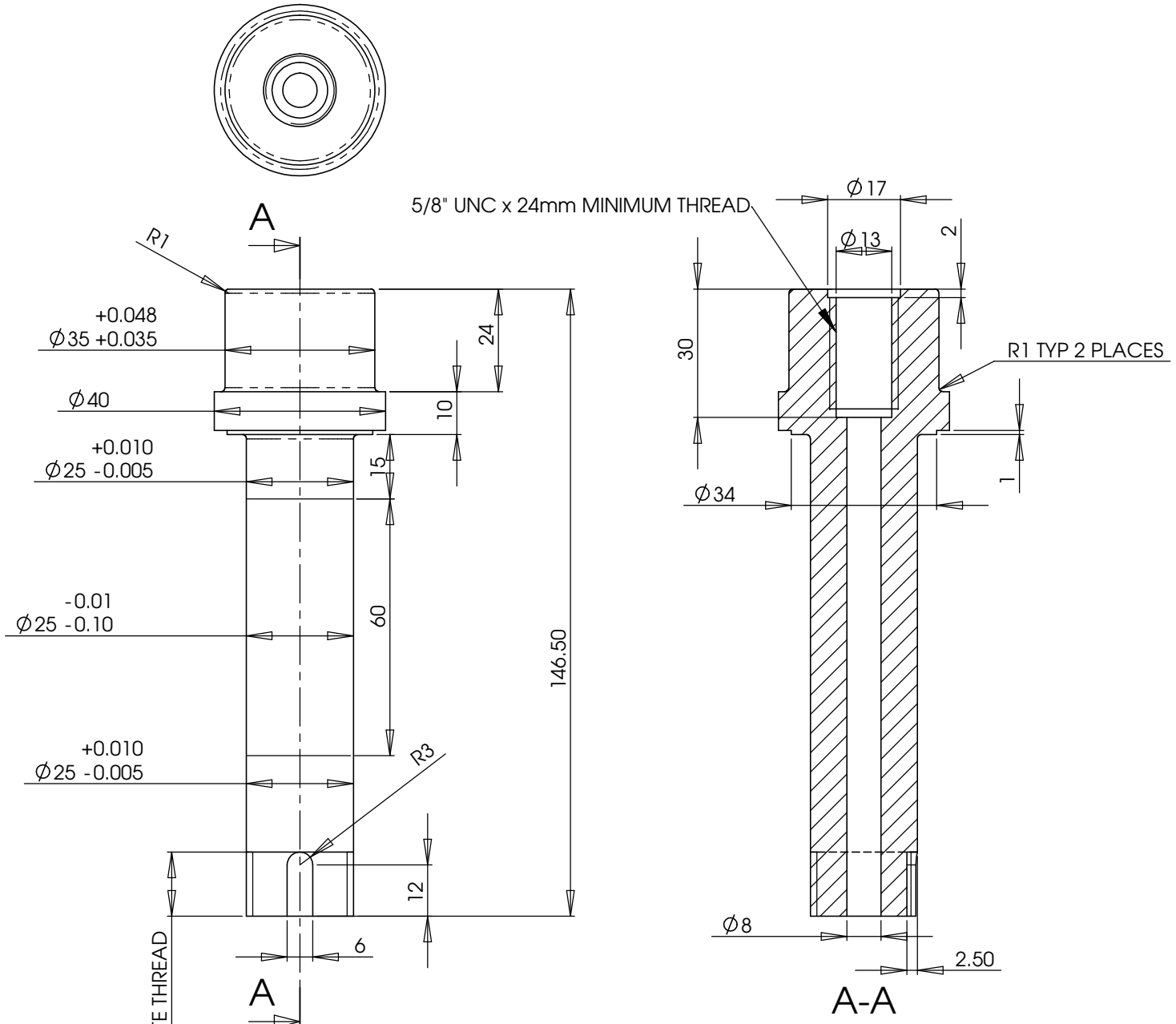

IE SHAFT		SCHOOL OF ENGINEERING MECHANICAL ENGINEERING DEPARTMENT	
		Drawn: Ben Low	Date: Nov 04
No. Required: 3	Material: 4140 STEEL	Checked:	DRG No. 320
Scale: 1 : 1 (A3)	All Dimensions in mm	Approved:	

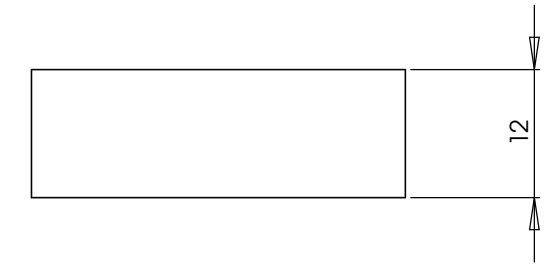

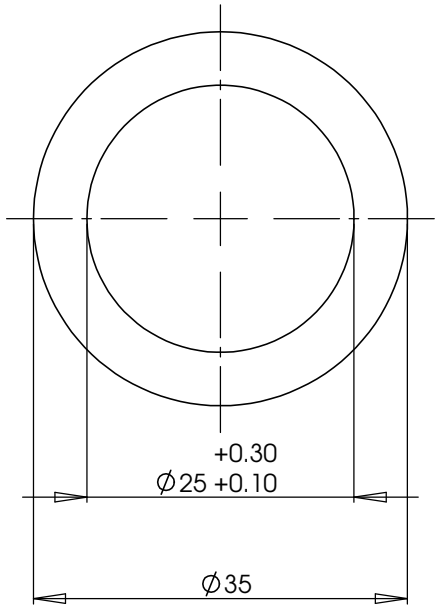

IE SHAFT LOCK NUT SPACER

SCHOOL OF ENGINEERING
MECHANICAL ENGINEERING DEPARTMENT

		Drawn: Ben Low	Date: Nov 04
No. Required: 3	Material: MILD STEEL	Checked:	DRG No. 323
Scale: 2: 1 (A3)	All Dimensions in mm	Approved:	

PART NO: 330
17mm
NO. REQUIRED: 1

PART NO: 331
13.5mm
NO. REQUIRED: 1

PART NO: 332
6mm
NO. REQUIRED: 3

PART NO: 333
3mm 1 CHAMFER
NO. REQUIRED: 3

PART NO: 334
3mm 2 CHAMFER
NO. REQUIRED: 1

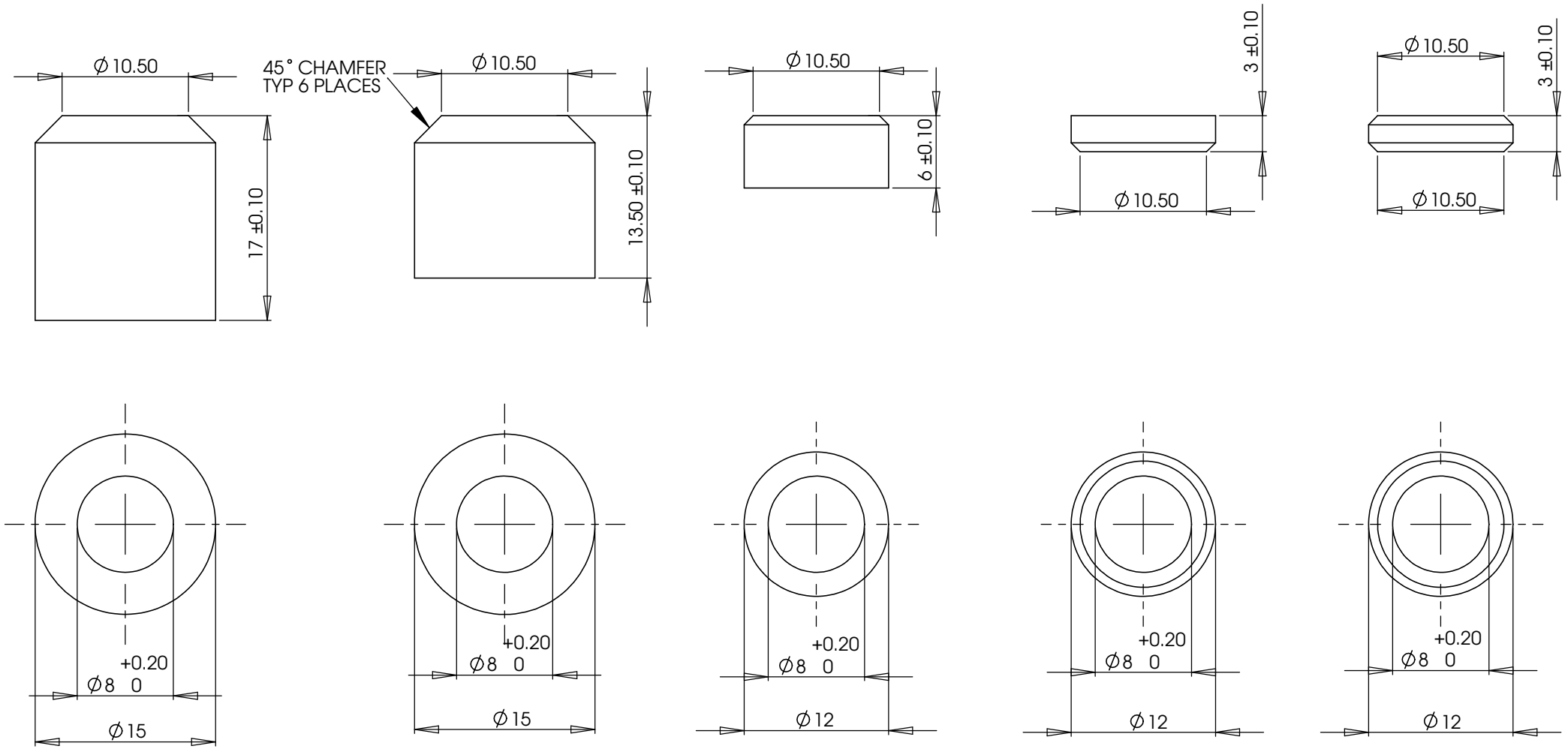

IE BALLJOINT (ROD-END) SPACERS

SCHOOL OF ENGINEERING
MECHANICAL ENGINEERING DEPARTMENT

		Drawn: Ben Low	Date: Nov 04
No. Required:	Material: MILD STEEL	Checked:	DRG No. 330-334
Scale: 3 : 1 (A3)	All Dimensions in mm	Approved:	

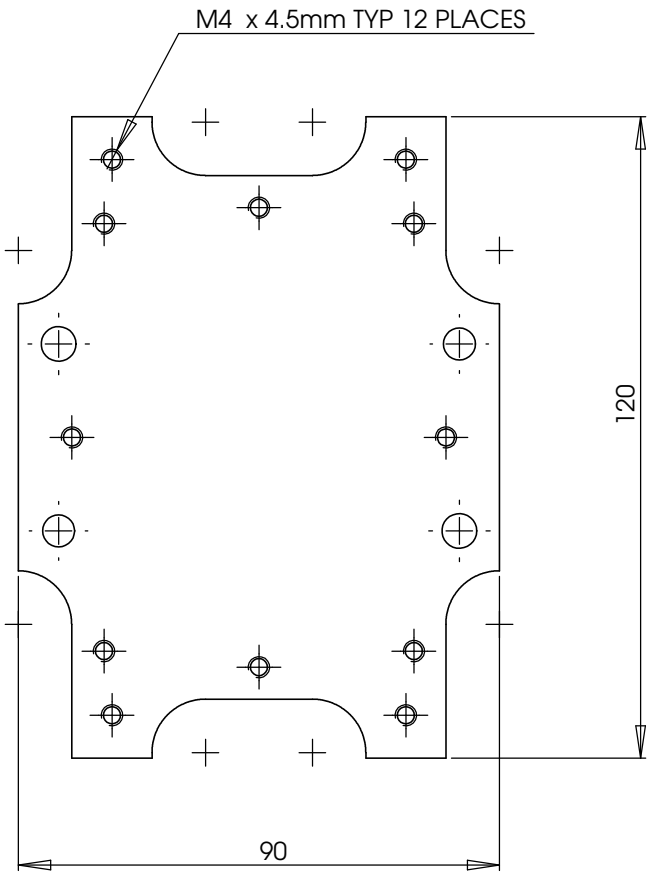

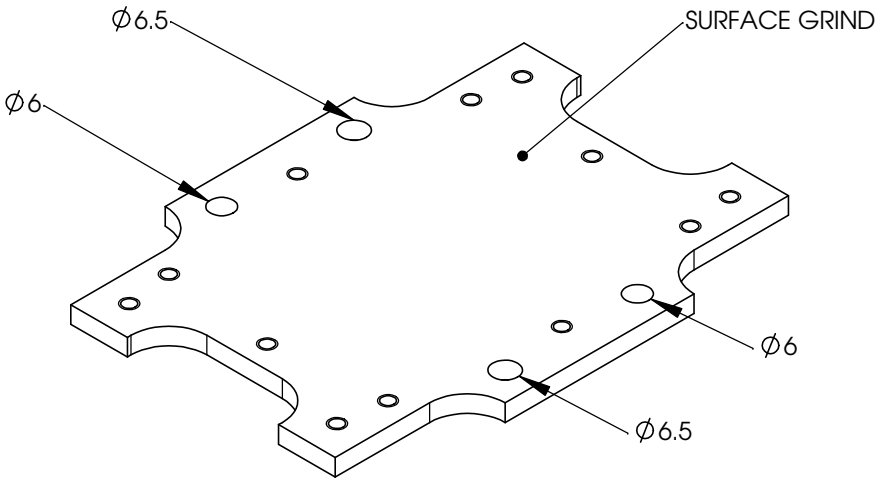

TAKE CARE WITH Ø6 AND Ø6.5 HOLES IN RELATION TO GROUND SURFACE

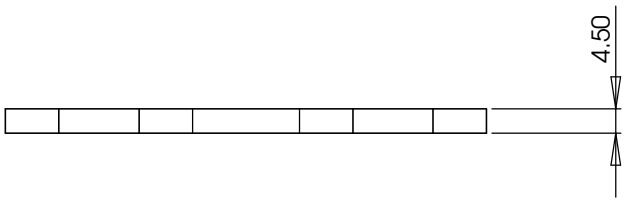

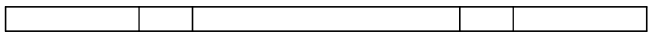

SEE 340 SS TIBIAL BASE PLATE.DXF FOR FULL DETAILS

TIBIAL BASE PLATE		SCHOOL OF ENGINEERING MECHANICAL ENGINEERING DEPARTMENT	
		Drawn: Ben Low	Date: APRIL 05
No. Required: 3	Material: 316L STAINLESS	Checked:	DRG No. 340
Scale: 1 : 1 (A3)	All Dimensions in mm	Approved:	

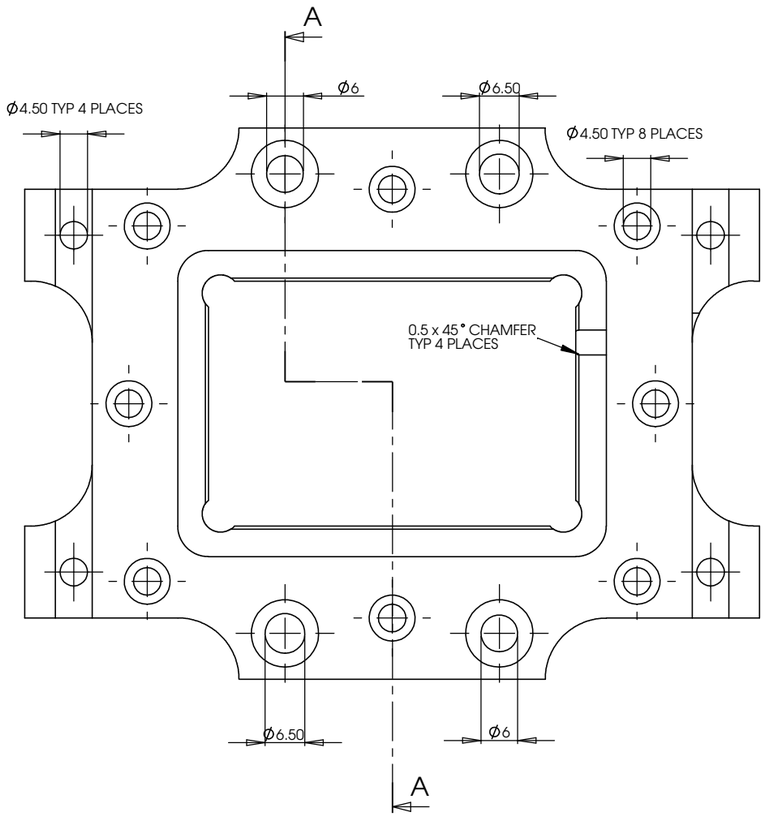

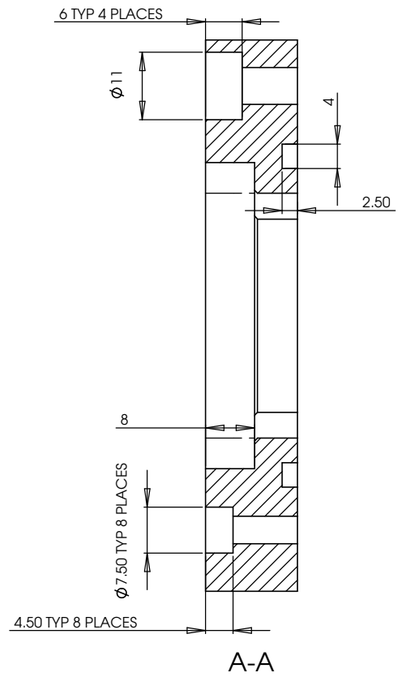

A-A

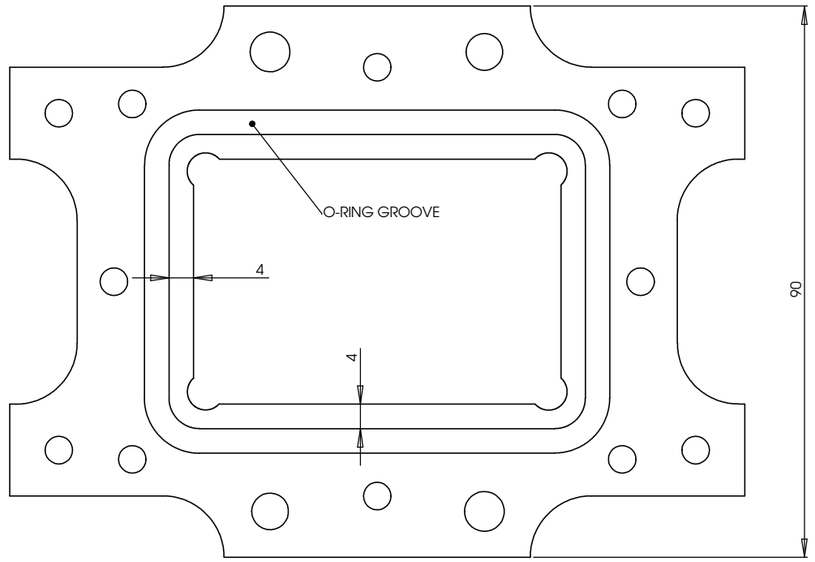

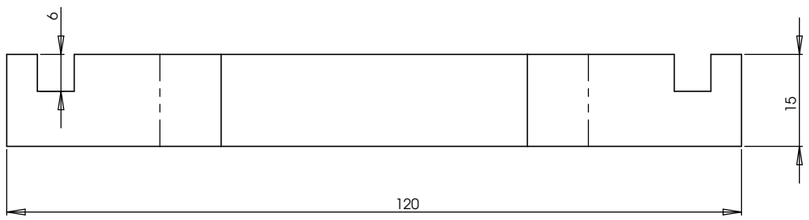

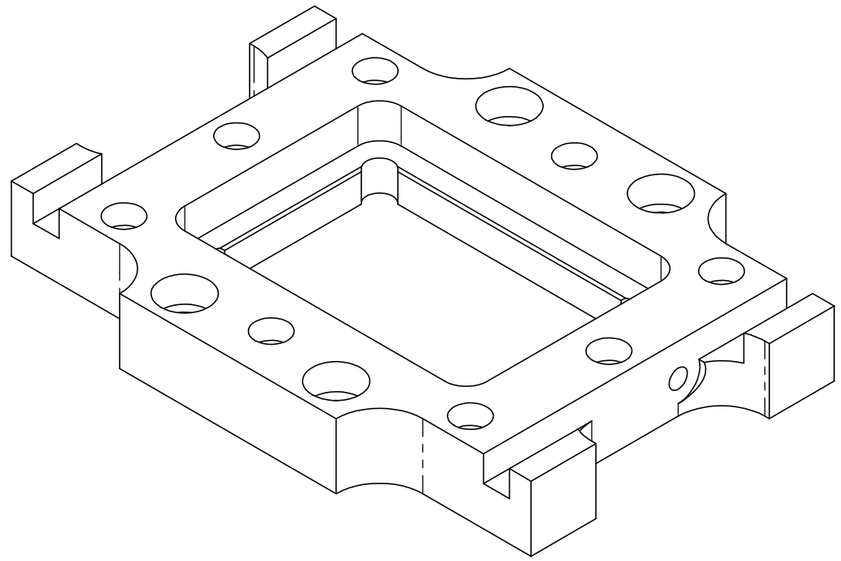

FOR FURTHER DETAILS SEE 344 POLYACETAL SAMPLE HOLDER.DXF
AND 344 POLYACETAL SAMPLE HOLDER.SLDPRT

POLYACETAL SAMPLE HOLDER	**UNIVERSITY OF CANTERBURY** MECHANICAL ENGINEERING DEPT CHCH. N.Z.	
	DRAWN : Ben Low	DATE:April 05
No. REQUIRED: 3 MATERIAL: POLYACETAL	CHECKED :	DRG. No : 344
SCALE: 2 : 1 (A1) ALL DIMENSIONS IN mm	APPROVED :	

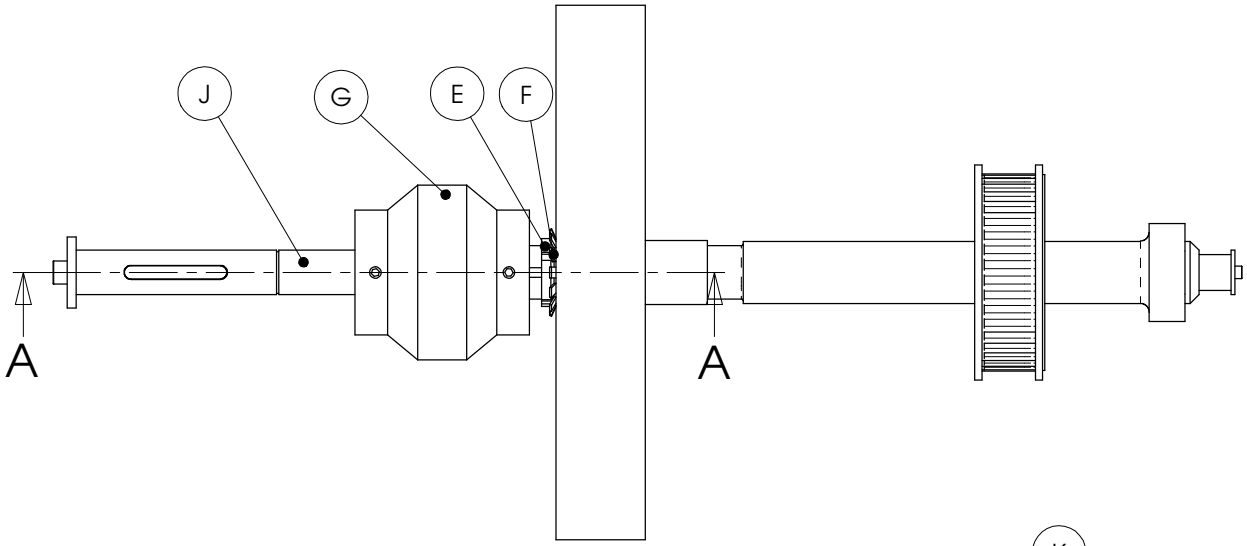

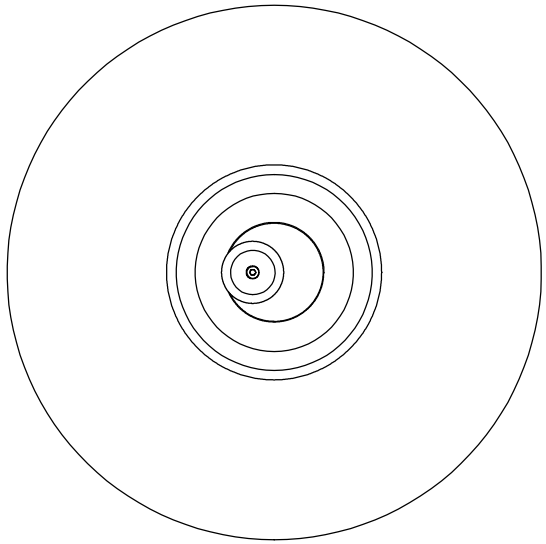

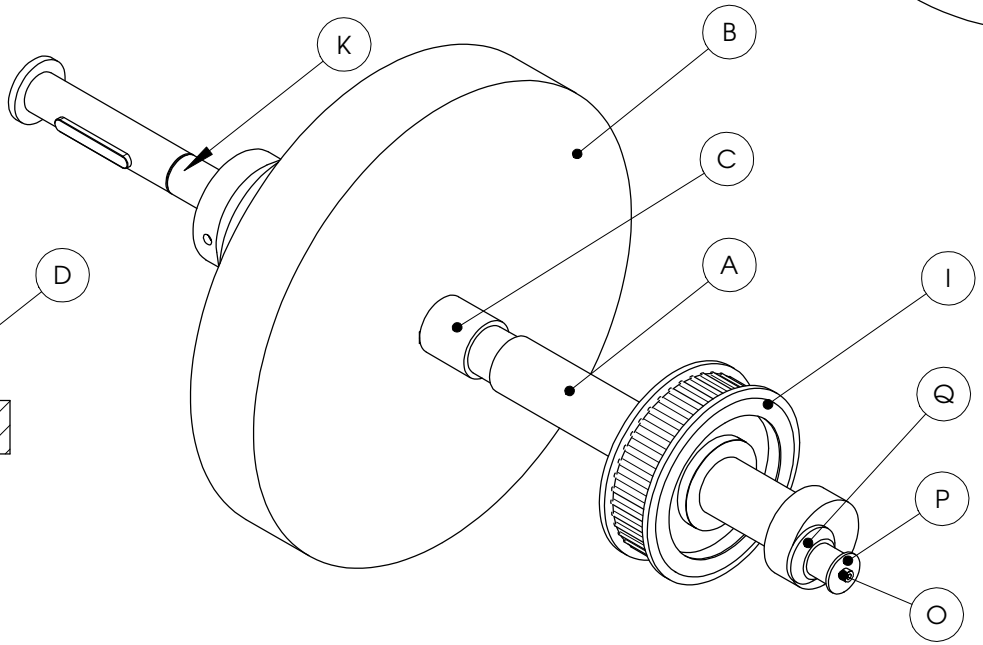

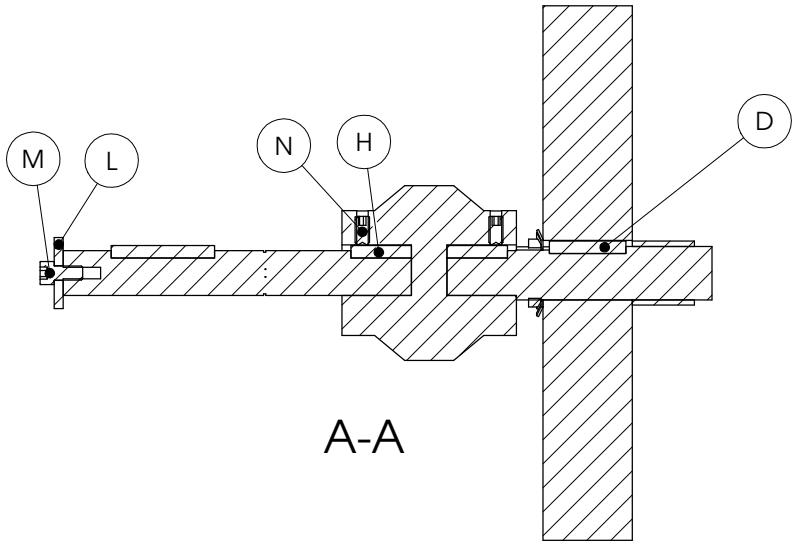

A-A

Item	Part No.	Description
A	410	Top Shaft
B	420	Flywheel
C	421	Flywheel Spacer
D	422	Flywheel Key
E	430	KM6 Lock Nut M30 x 1.5
F	431	MB6 Locking Washer
G	440	Reflex E20 Coupling
H	441	Coupling Key
I	450	8mm x 30mm x 44 tooth Pulley
J	460	Gearbox Shaft
K	461	Retaining Ring B27.7M - 3AM1-25
L	462	Gearbox Shaft Retaining Washer
M	470	M8 x 16 Cap Screw
N	471	Socket Head Set Screw M8 x 16
O	254	M4 x 8 Cap Screw
P	242	Washer M4x25x2
Q	241	Conrod Bearing Spacer 20mm ID

Top Shaft
General Assembly
& Bill of Materials

Scale: 1 : 3 (A3) All Dimensions in mm

SCHOOL OF ENGINEERING
MECHANICAL ENGINEERING DEPARTMENT

Drawn: Ben Low

Checked:

Approved:

Date: Oct 04

DRG No. 400

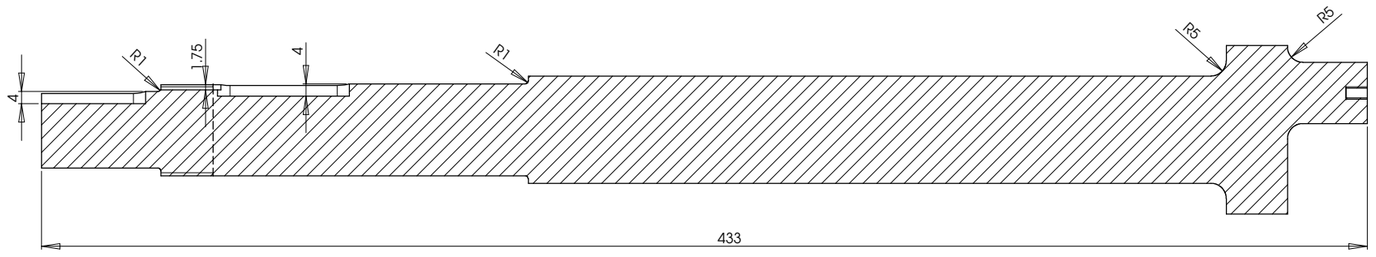

A-A

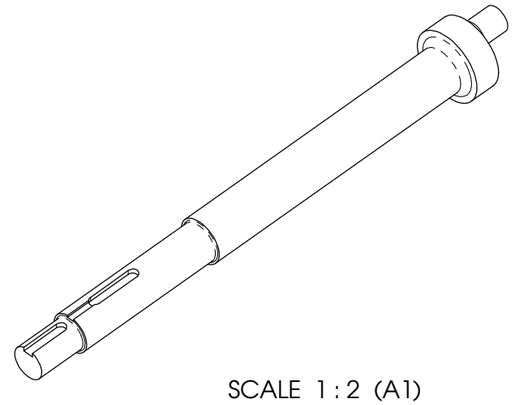

SCALE 1 : 2 (A1)

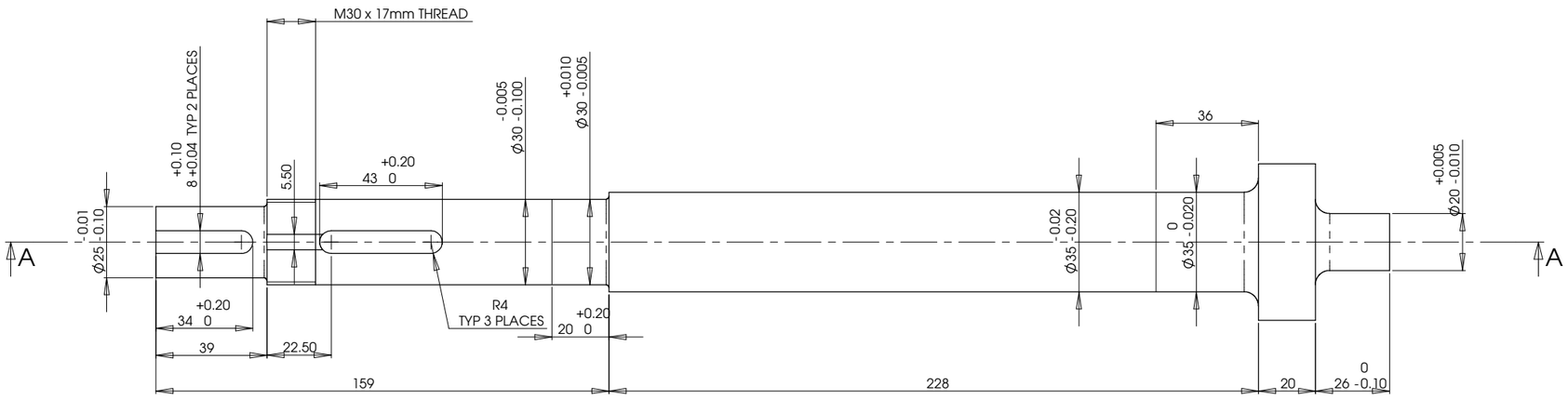

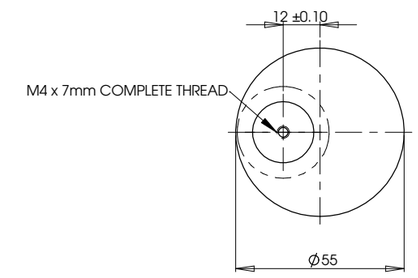

TOP SHAFT	**UNIVERSITY OF CANTERBURY** MECHANICAL ENGINEERING DEPT CHCH. N.Z.	
	DRAWN : Ben Low	DATE : Oct 04
MATERIAL: 4140 STEEL	CHECKED :	DRG. No : 410
SCALE: 1 : 1 (A1) ALL DIMENSIONS IN mm	APPROVED :	

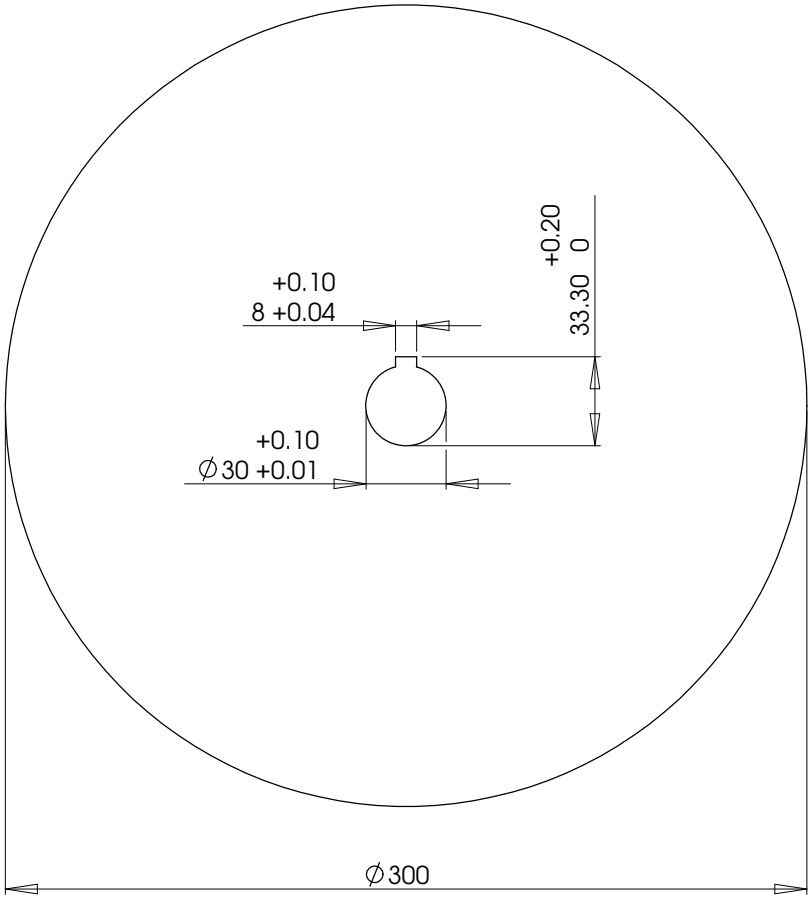

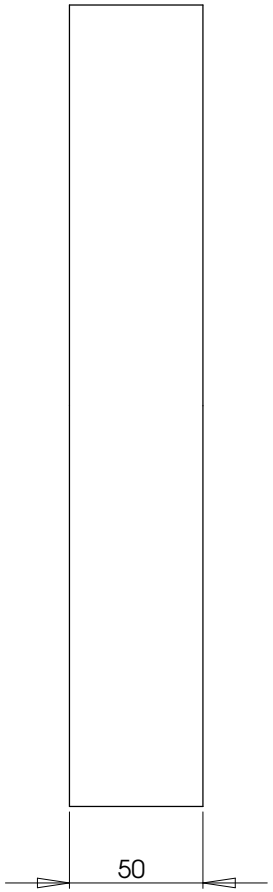

FLYWHEEL		SCHOOL OF ENGINEERING MECHANICAL ENGINEERING DEPARTMENT	
		Drawn: Ben Low	Date: Nov 04
No. Required: 1	Material: MILD STEEL	Checked:	DRG No. 420
Scale: 1 : 2 (A3)	All Dimensions in mm	Approved:	

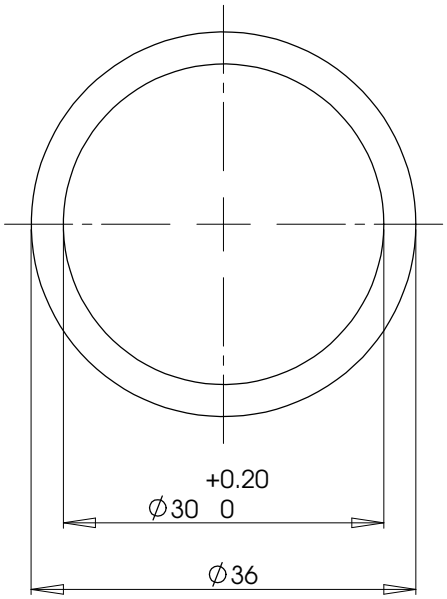

FLYWHEEL SPACER

SCHOOL OF ENGINEERING
MECHANICAL ENGINEERING DEPARTMENT

		Drawn: Ben Low	Date: Nov 04
No. Required: 1	Material: MILD STEEL	Checked:	DRG No. 421
Scale: 2 : 1 (A3)	All Dimensions in mm	Approved:	

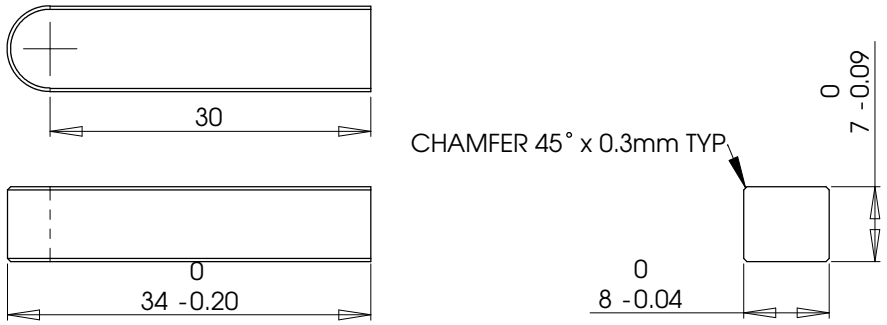

441 COUPLING KEY
NO. REQUIRED: 2

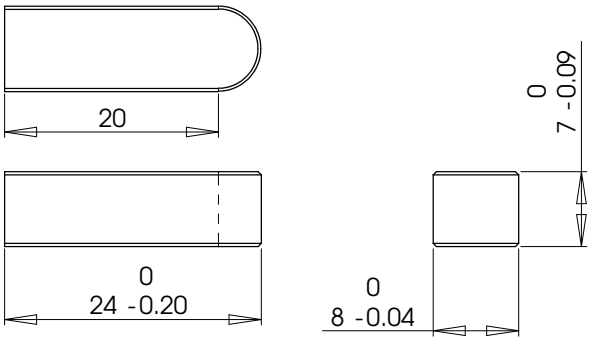

520 IE CRANK KEY (BOTTOM SHAFT)
NO. REQUIRED: 1

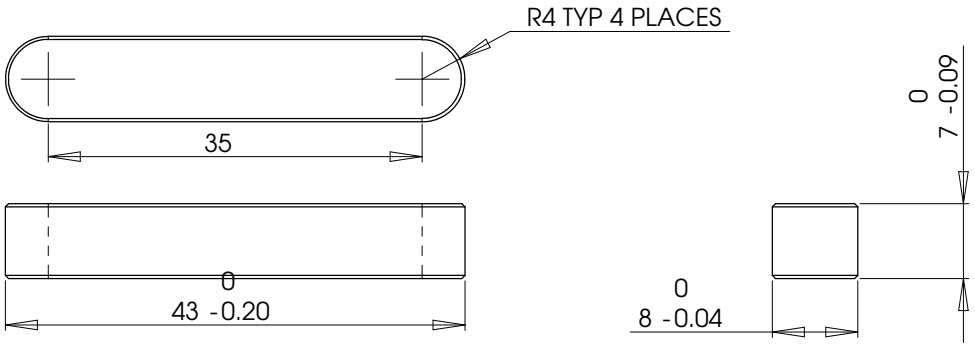

422 FLYWHEEL KEY
NO. REQUIRED: 1

KEYS		SCHOOL OF ENGINEERING MECHANICAL ENGINEERING DEPARTMENT	
		Drawn: Ben Low	Date: Nov 04
No. Required:	Material: KEY STEEL	Checked:	DRG No.
Scale: 2 : 1 (A3)	All Dimensions in mm	Approved:	422, 441 & 520

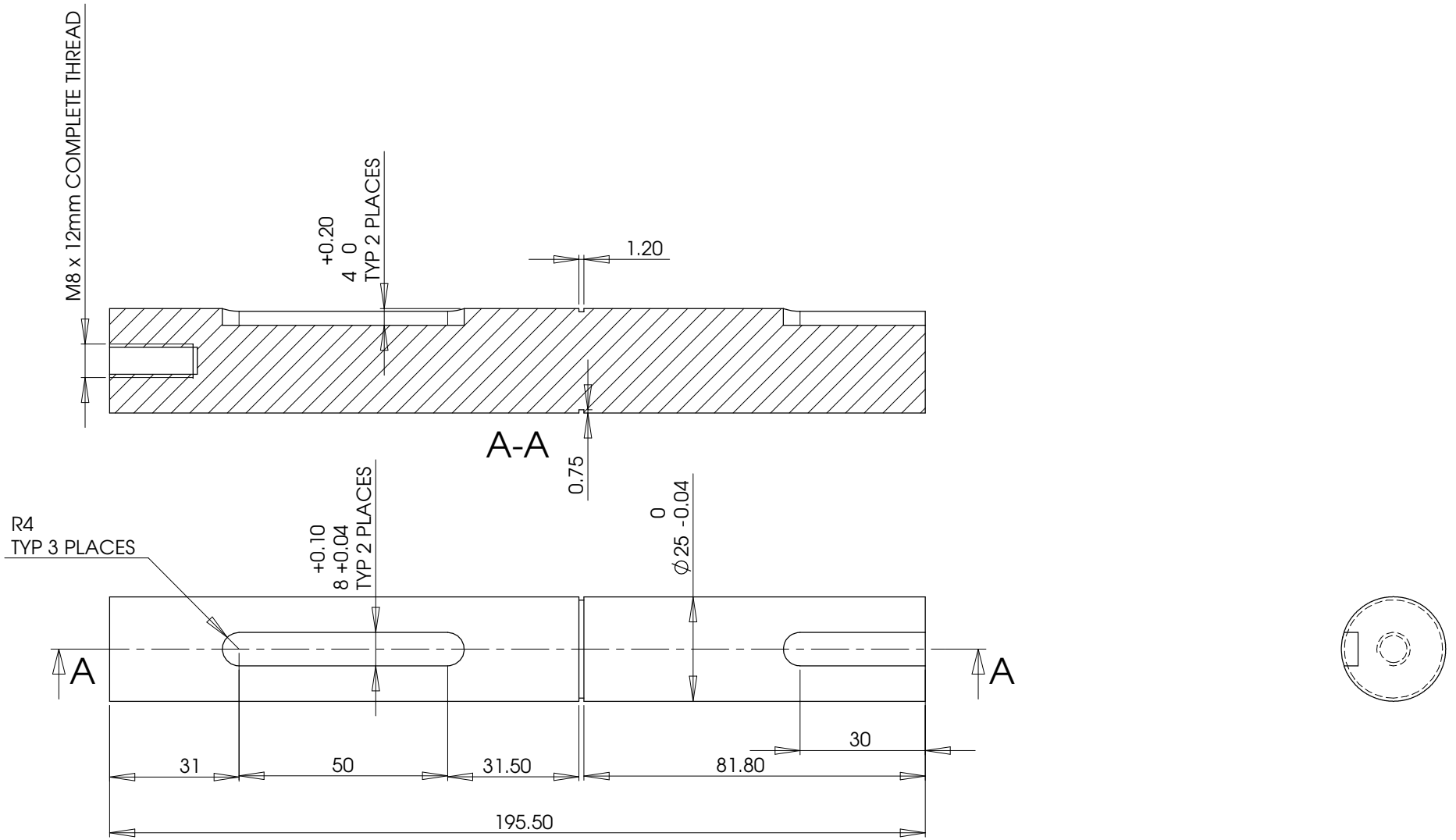

GEARBOX SHAFT		SCHOOL OF ENGINEERING MECHANICAL ENGINEERING DEPARTMENT	
		Drawn: Ben Low	Date: Nov 04
No. Required: 1	Material: 4140 STEEL	Checked:	DRG No. 460
Scale: 1 : 1 (A3)	All Dimensions in mm	Approved:	

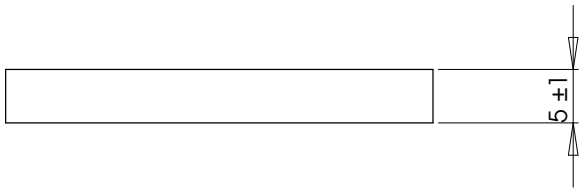

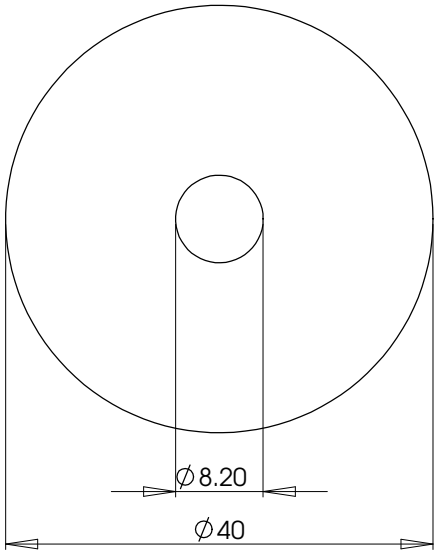

GEARBOX SHAFT RETAINING WASHER

SCHOOL OF ENGINEERING
MECHANICAL ENGINEERING DEPARTMENT

		Drawn: Ben Low	Date: Nov 04
No. Required: 1	Material:MILD STEEL OR AL	Checked:	DRG No. 462
Scale: 2 : 1 (A3)	All Dimensions in mm	Approved:	

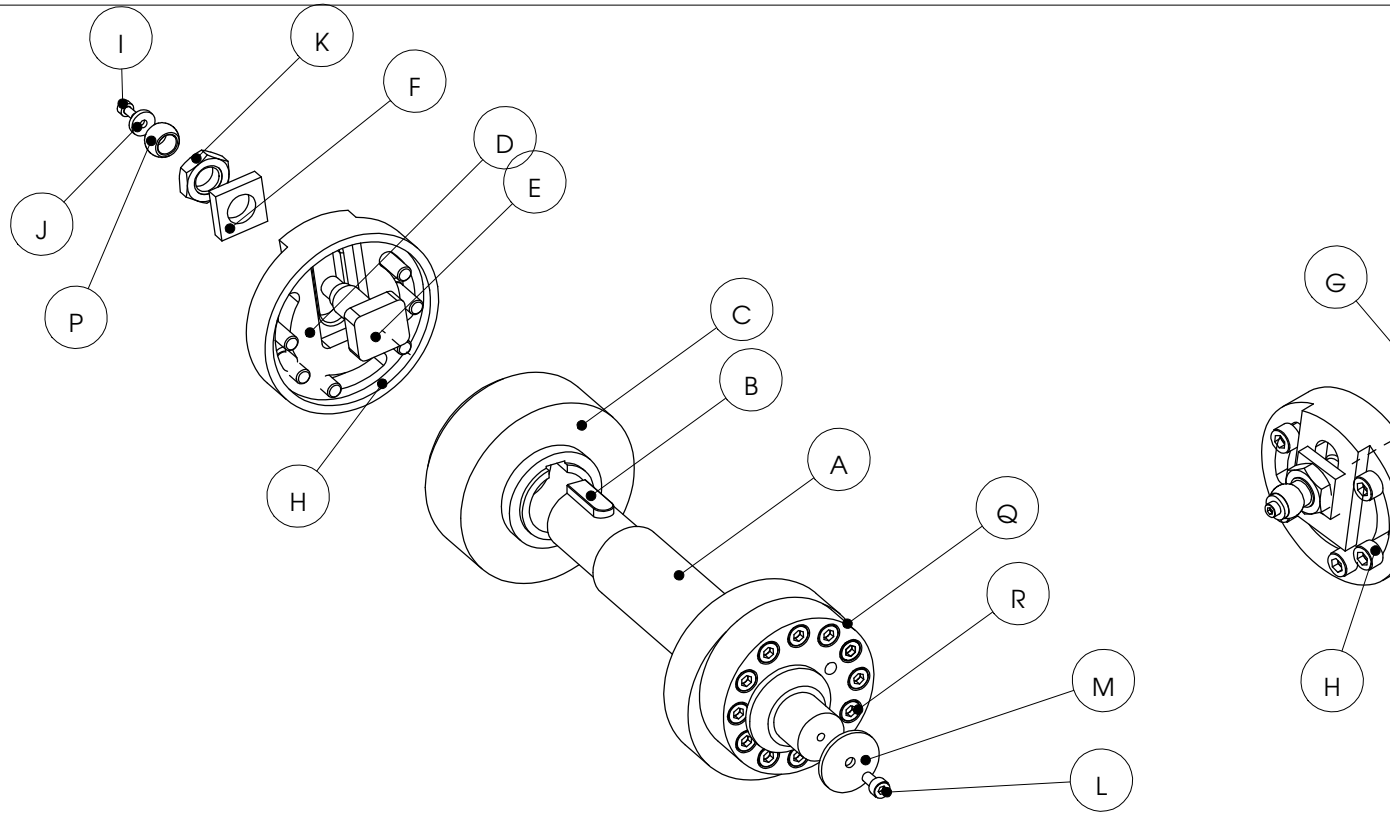

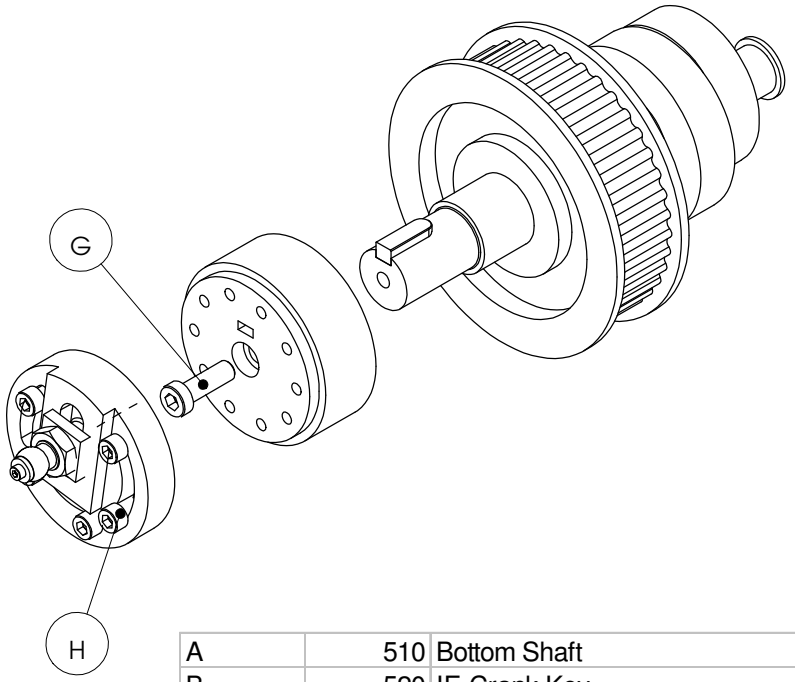

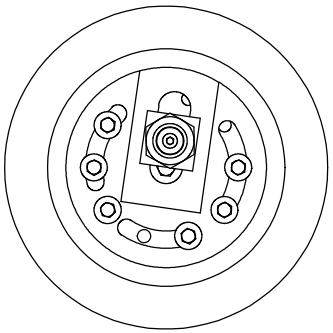

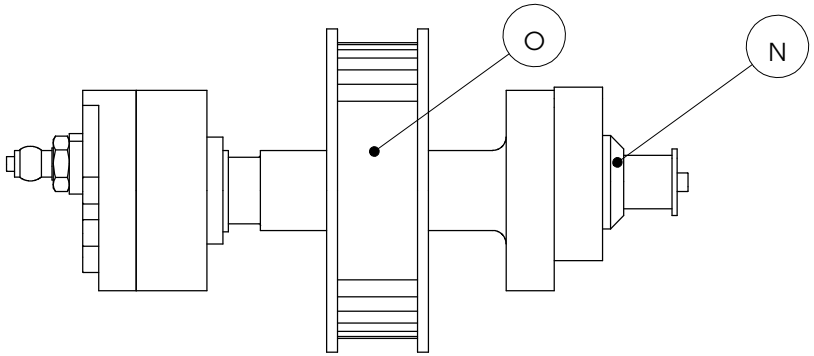

A	510	Bottom Shaft
B	520	IE Crank Key
C	521	IE Crank Mounting Plate
D	522	IE Crank Adjustment Plate
E	523	IE Crank Pin
F	524	IE Crank Pin Washer
G	530	M8 x 16 Low Head Cap Screw
H	531	M6 x 16 Cap Screw
I	532	M3 x 6 Cap Screw
J	536	M3 x 10 Washer
K	534	M12 Nut Thin
L	254	M4 x 8 Cap Screw
M	242	Washer M4x25x2
N	241	Conrod Bearing Spacer 20mm ID
O	450	8mm x 30mm x 44 tooth Pulley
P	811	Ball Joint Inner SI 8 E
Q	511	AP Crank Adjustment Plate
R	533	M5 x 20 Cap Screw

Bottom Shaft General Assembly & Bill of Materials

SCHOOL OF ENGINEERING
MECHANICAL ENGINEERING DEPARTMENT

Drawn: Ben Low | Date: Oct 04

Checked: | DRG No. 500

Scale: 1 : 2 (A3) All Dimensions in mm | Approved:

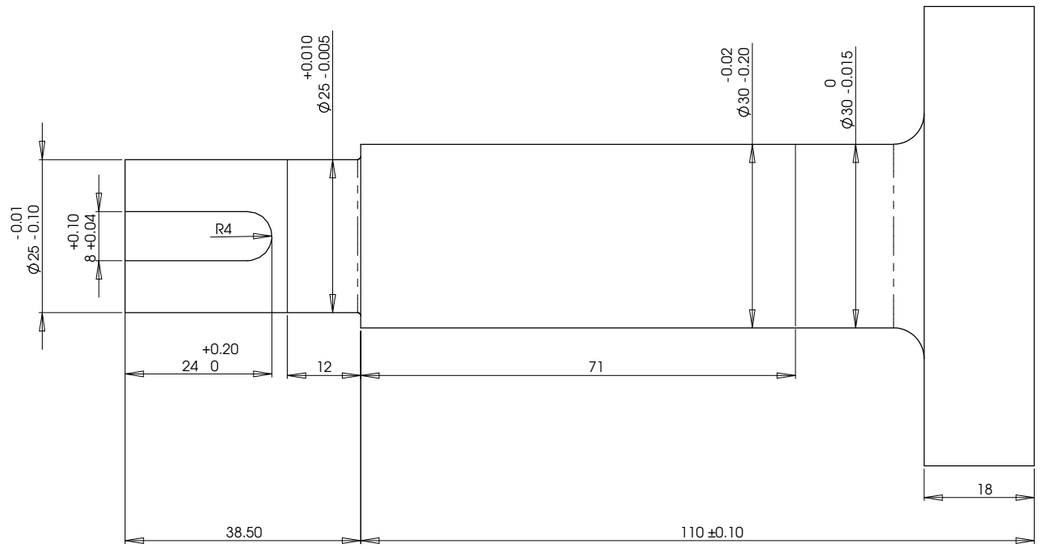

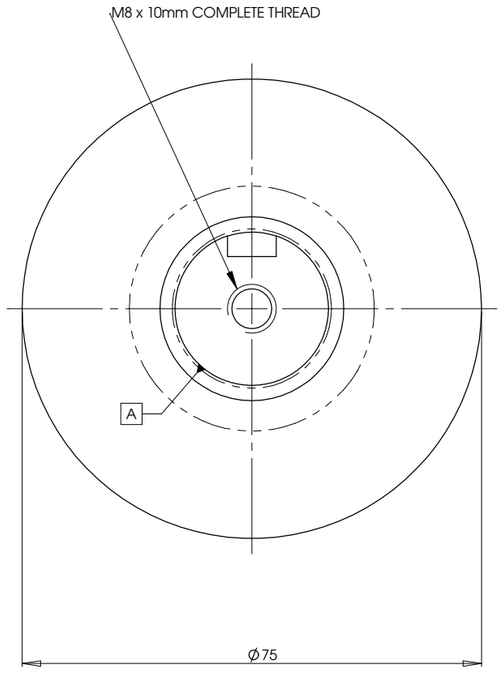

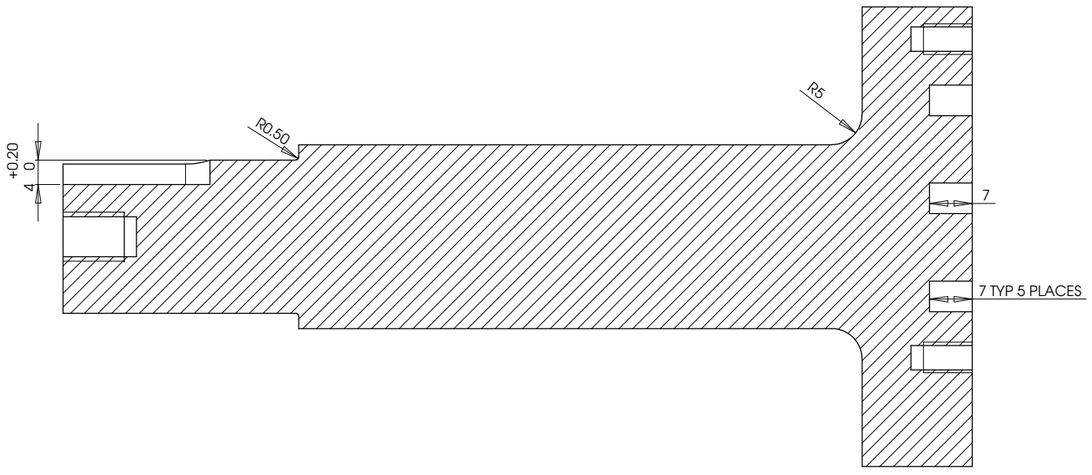

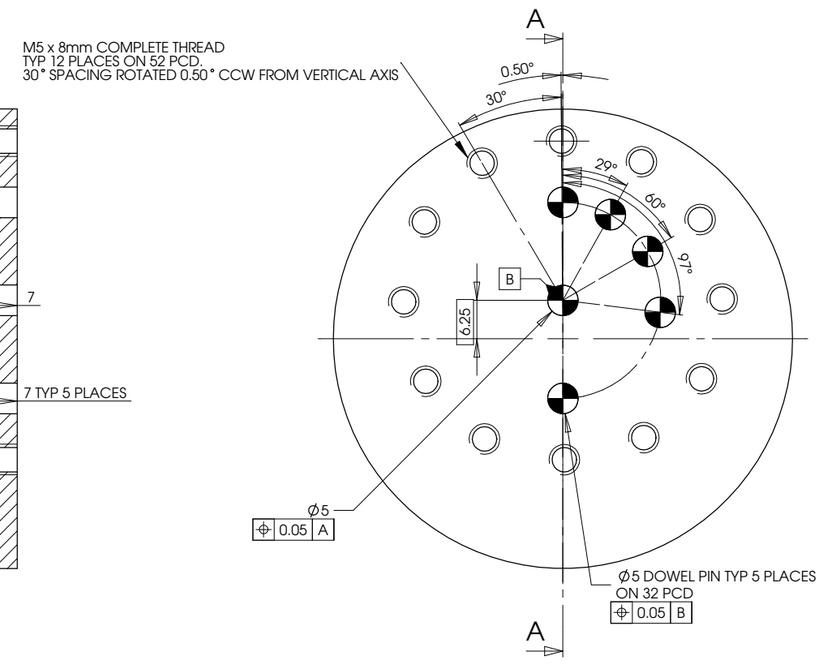

FOR AN ENLARGEMENT SEE DRAWING 510B

BOTTOM SHAFT	**UNIVERSITY OF CANTERBURY** MECHANICAL ENGINEERING DEPT. CH.CH. N.Z.	
	DRAWN : Ben Low	DATE : Oct 04
NO. REQUIRED: 1 MATERIAL: 4140 STEEL	CHECKED :	DRG. No : 510
SCALE:2 : 1 (A1) ALL DIMENSIONS IN mm	APPROVED :	

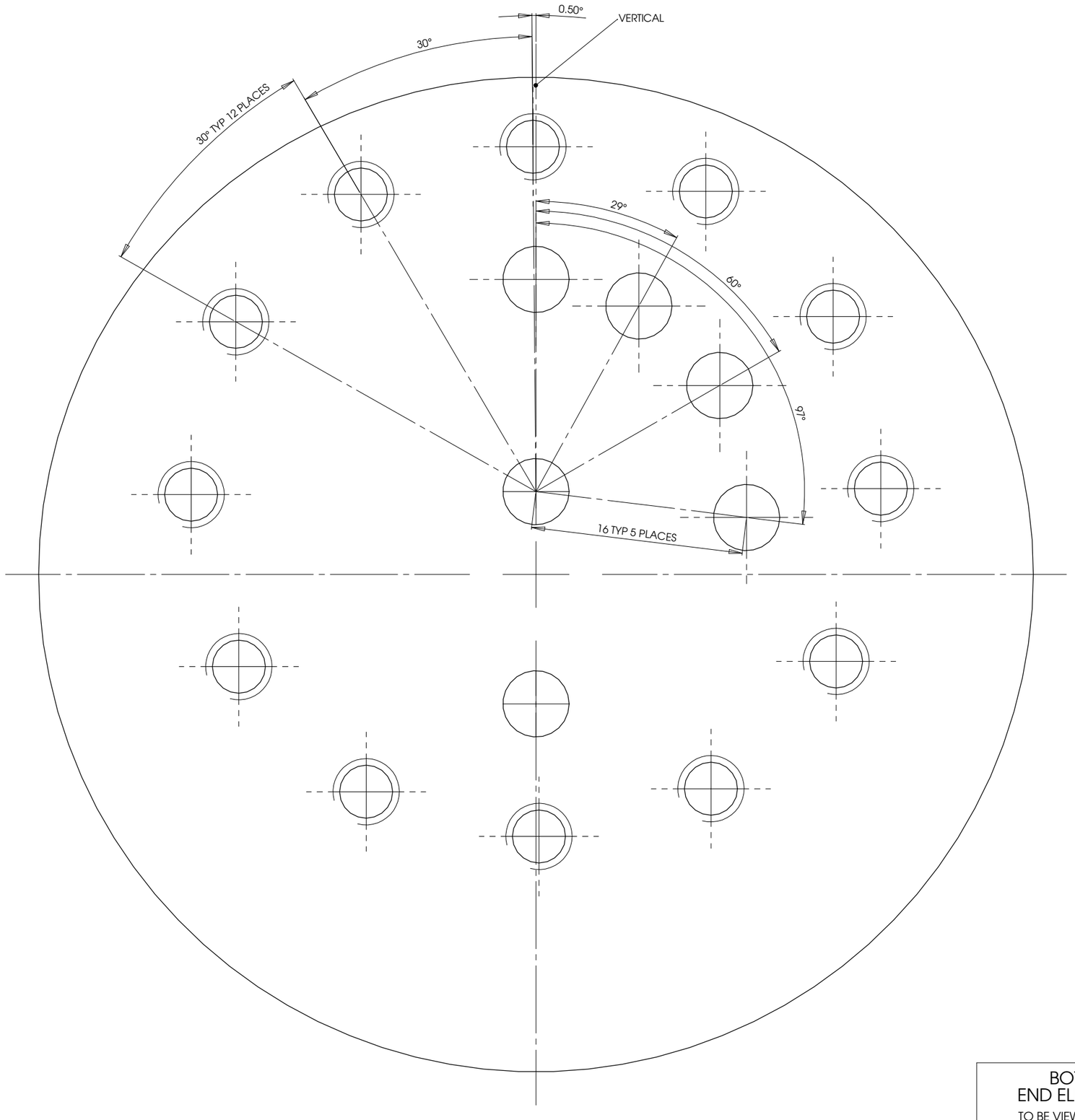

BOTTOM SHAFT
END ELEVATION DETAIL

TO BE VIEWED IN CONJUNCTION WITH DRAWING 510

SCALE: 6 : 1 (A1) ALL DIMENSIONS IN mm

UNIVERSITY OF CANTERBURY
MECHANICAL ENGINEERING DEPT. CHCH. N.Z.

DRAWN : Ben Low	DATE : Oct 04
CHECKED :	DRG. No : 510B
APPROVED :	

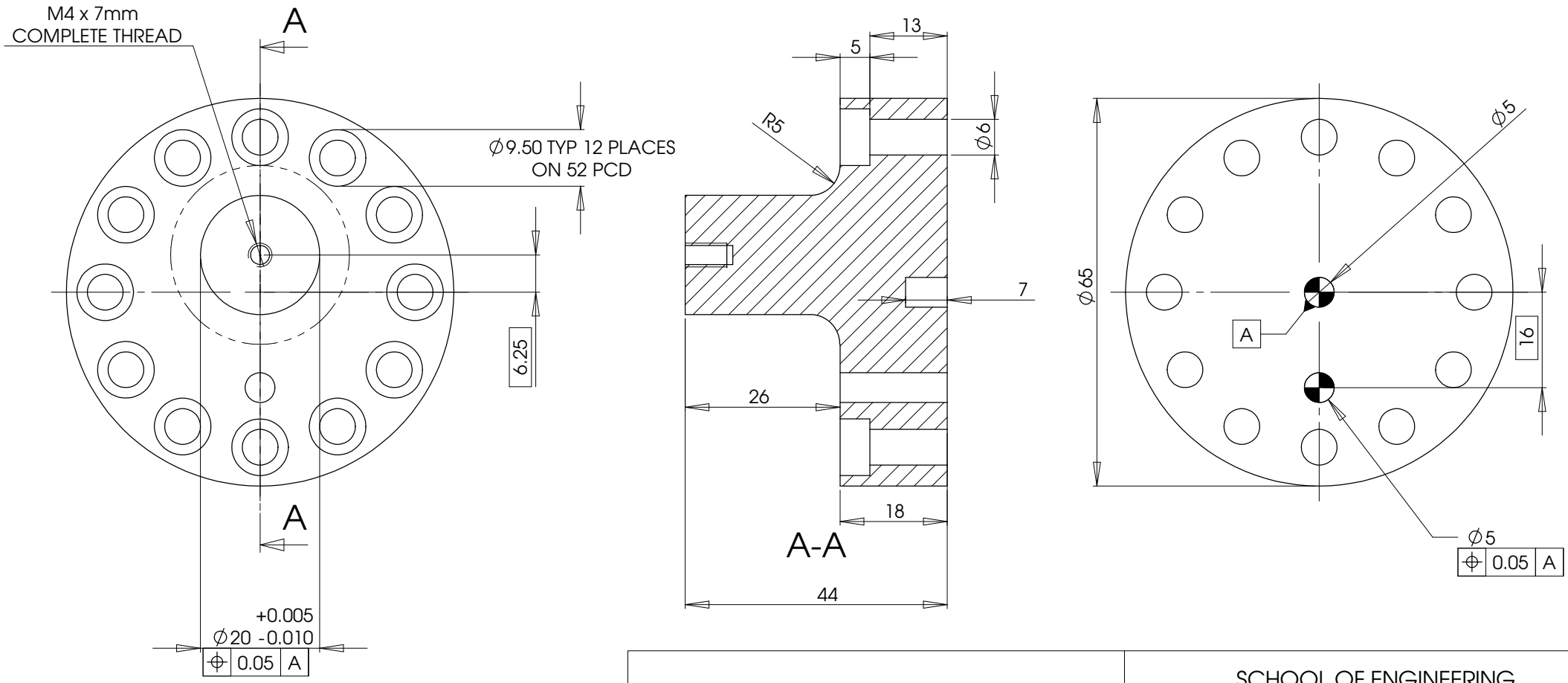

AP CRANK ADJUSTMENT PLATE		SCHOOL OF ENGINEERING MECHANICAL ENGINEERING DEPARTMENT	
		Drawn: Ben Low	Date: Nov 04
No. Required: 1	Material: 4140 STEEL	Checked:	DRG No. 511
Scale: 1.5 : 1 (A3)	All Dimensions in mm	Approved:	

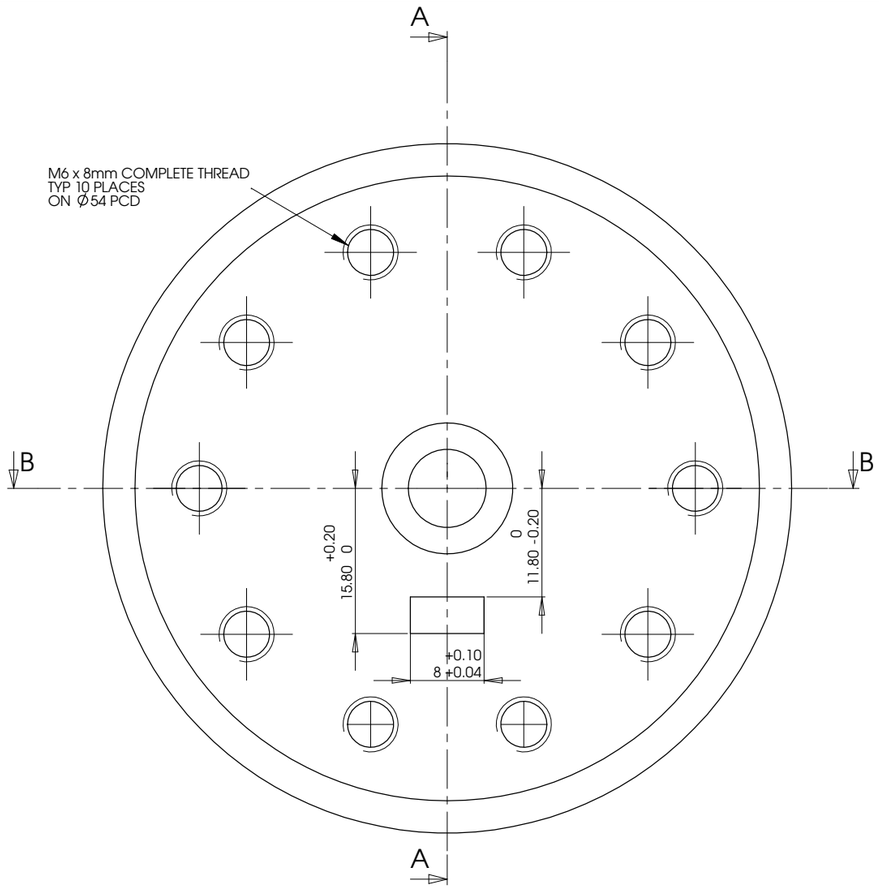

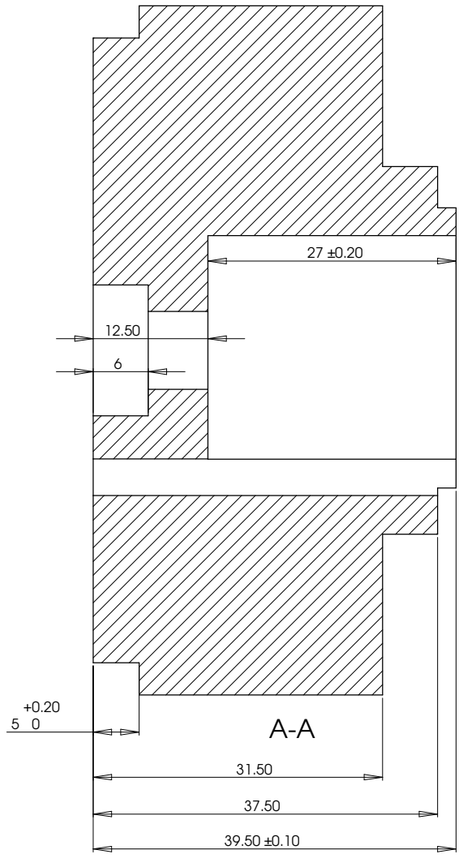

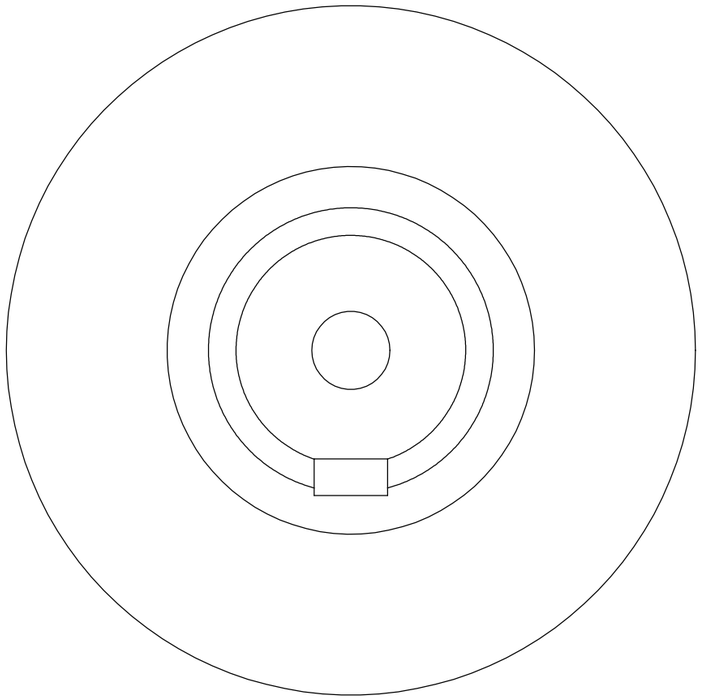

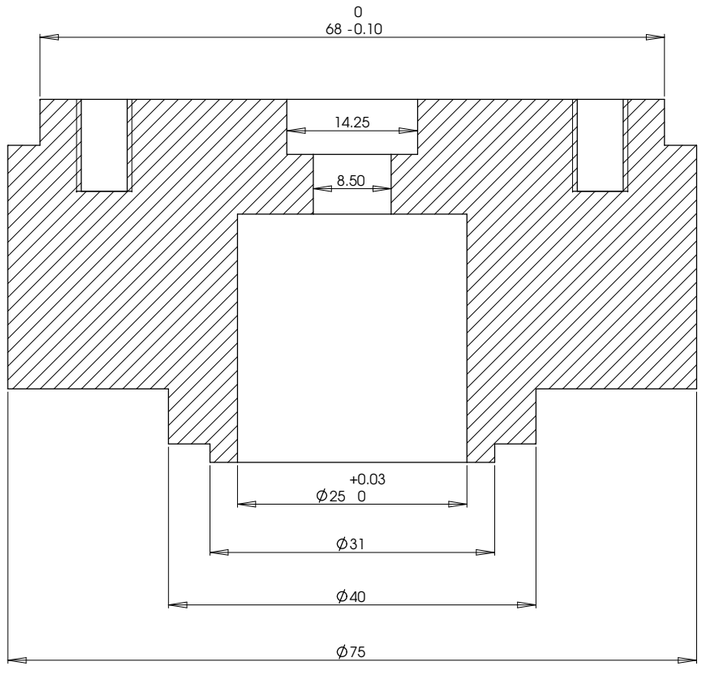

B-B

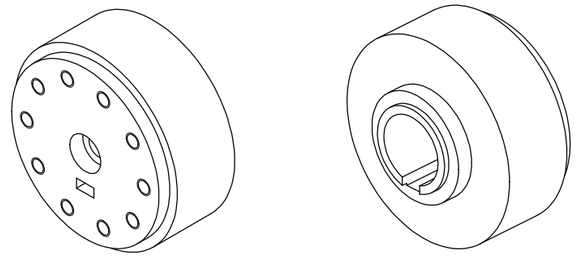

ISOMETRIC VIEWS SCALE 1 : 1 (A1)

No. Required: 1

Material: 4140 STEEL

IE CRANK MOUNTING PLATE	**UNIVERSITY OF CANTERBURY** MECHANICAL ENGINEERING DEPT. CH.CH. N.Z.	
	DRAWN : Ben Low	DATE : Oct 04
	CHECKED :	DRG. No : 521
SCALE: 3 : 1 (A1) ALL DIMENSIONS IN mm	APPROVED :	

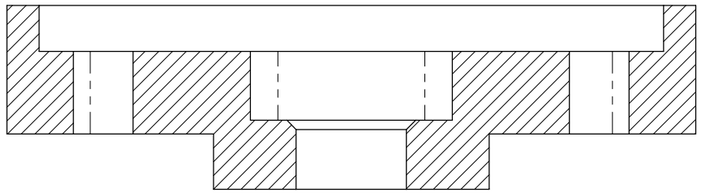

B-B

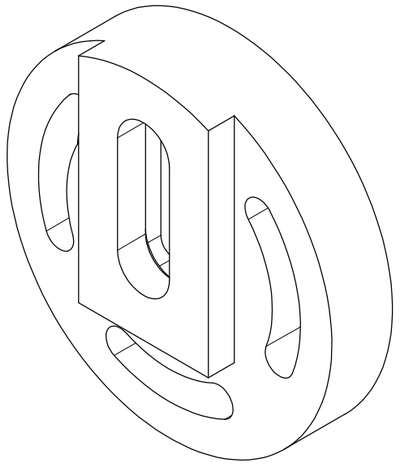

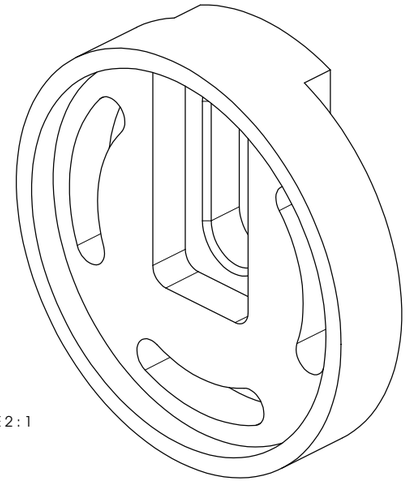

ISOMETRIC SCALE 2 : 1

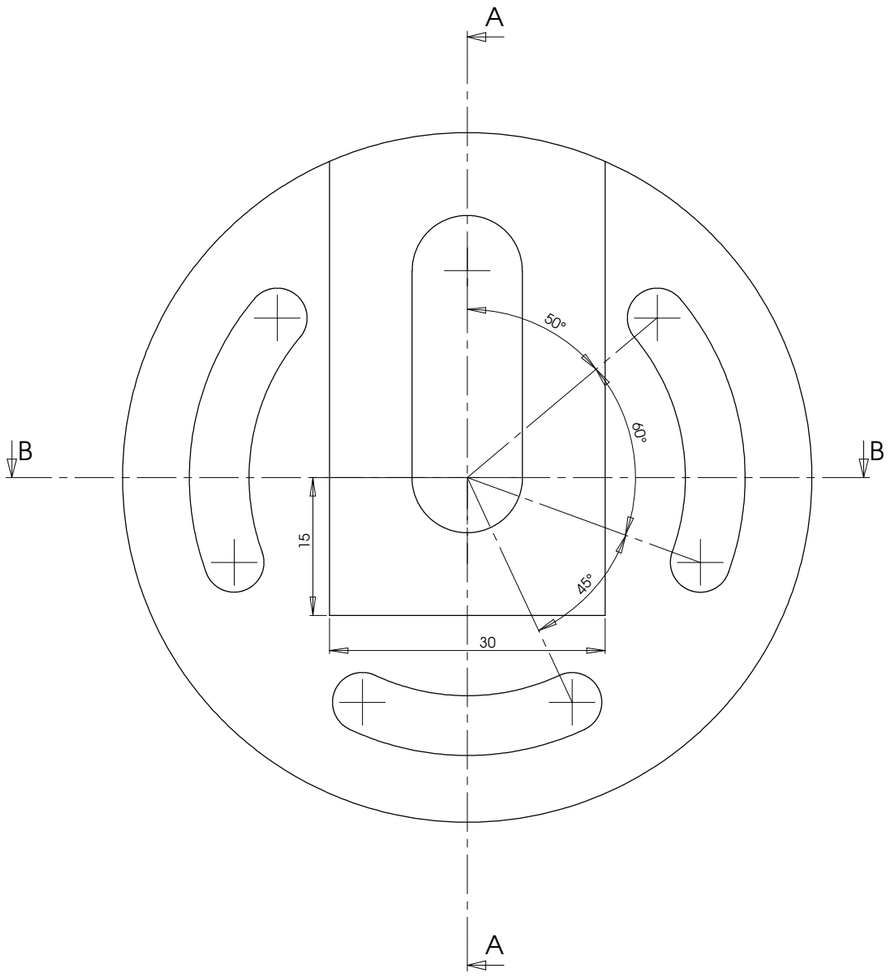

COMPONENT IS SYMMETRIC ABOUT A-A

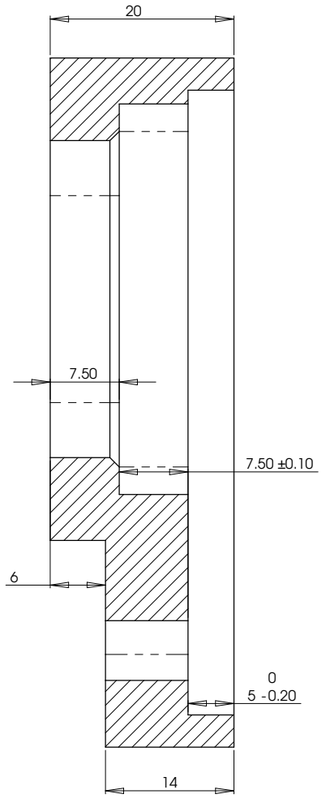

A-A

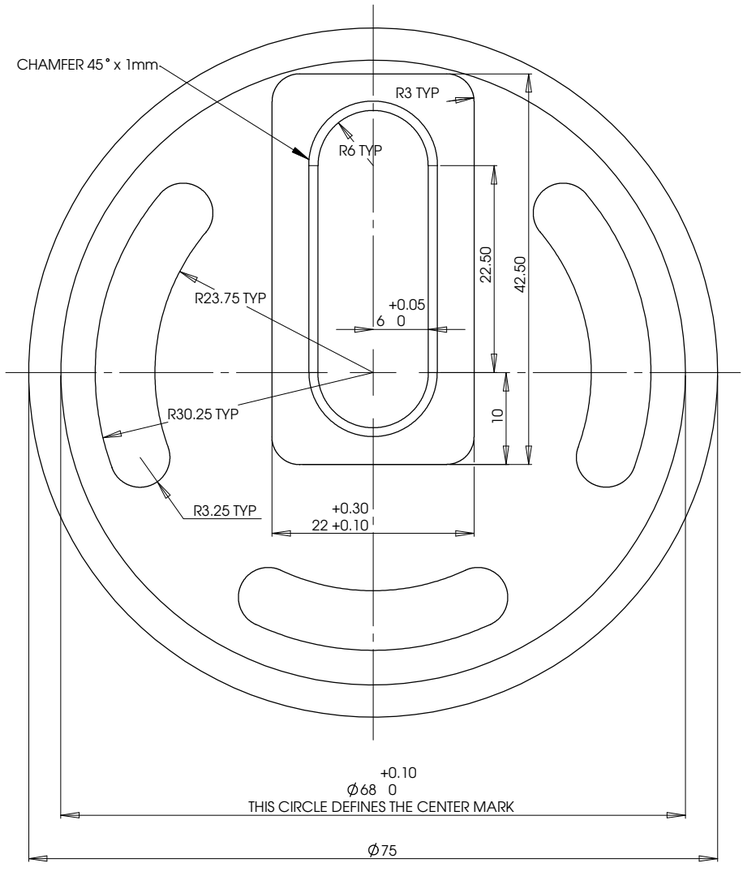

No. Required: 1 Material: 4140 STEEL

IE CRANK ADJUSTMENT PLATE	**UNIVERSITY OF CANTERBURY** MECHANICAL ENGINEERING DEPT. CH.CH. N.Z.
	DRAWN : Ben Low — DATE : Oct 04
	CHECKED : — DRG. No : 522
SCALE: 3 : 1 (A1) ALL DIMENSIONS IN mm	APPROVED :

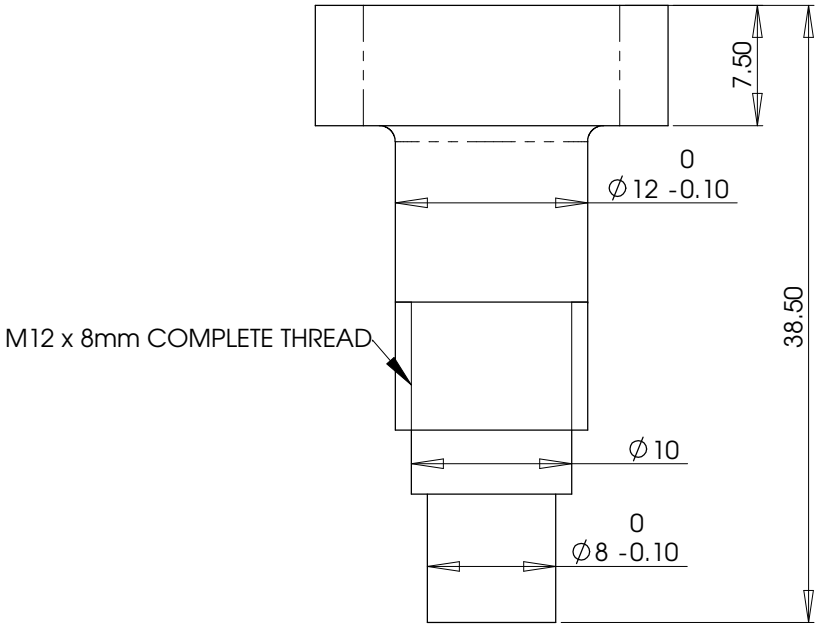

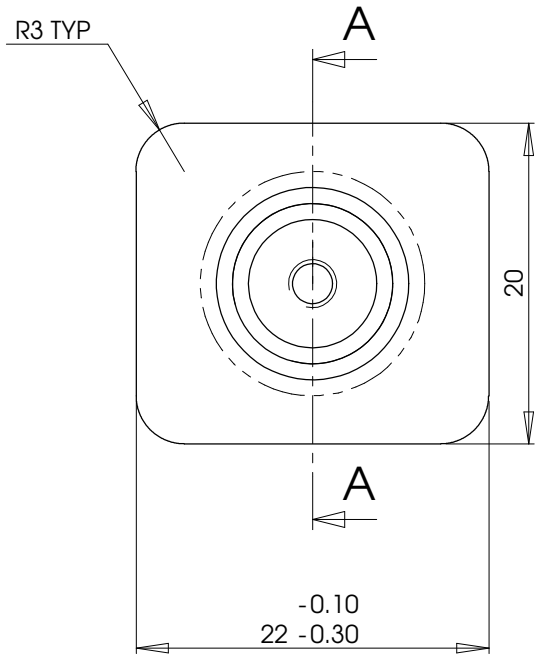

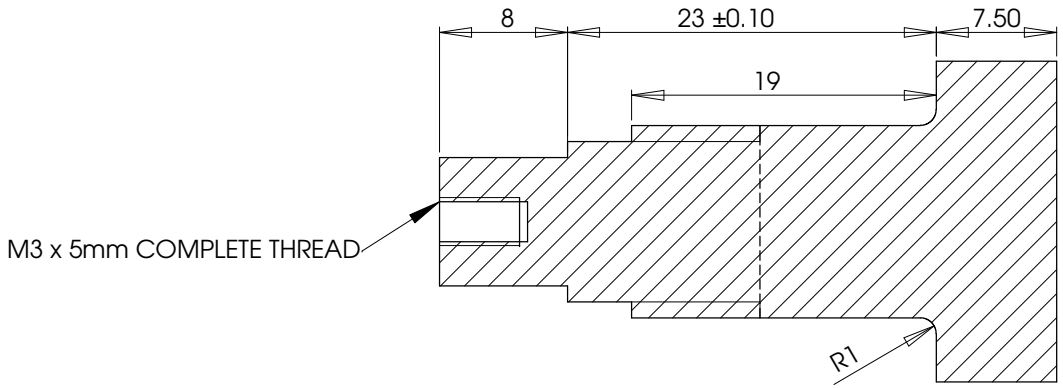

A-A

IE CRANK PIN		SCHOOL OF ENGINEERING MECHANICAL ENGINEERING DEPARTMENT	
		Drawn: Ben Low	Date: Nov 04
No. Required: 1	Material: 4140 STEEL	Checked:	DRG No. 523
Scale: 3: 1 (A3)	All Dimensions in mm	Approved:	

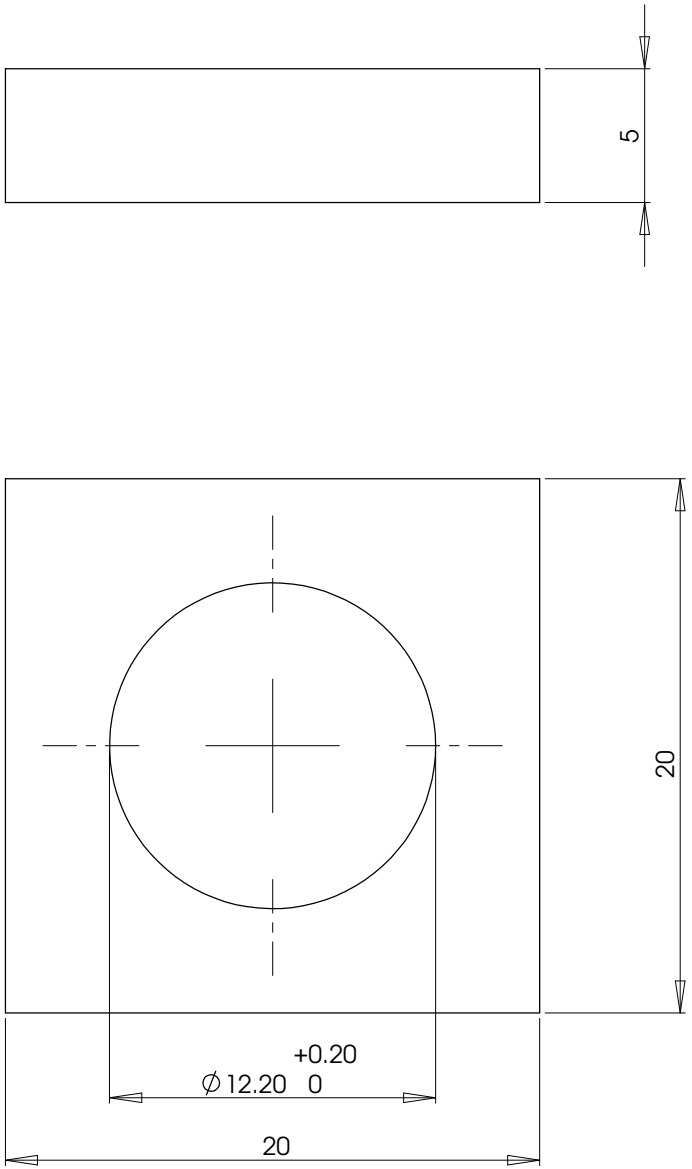

IE CRANK PIN WASHER

SCHOOL OF ENGINEERING
MECHANICAL ENGINEERING DEPARTMENT

		Drawn: Ben Low	Date: Nov 04
No. Required: 1	Material: MILD STEEL	Checked:	DRG No. 524
Scale: 5 : 1 (A3)	All Dimensions in mm	Approved:	

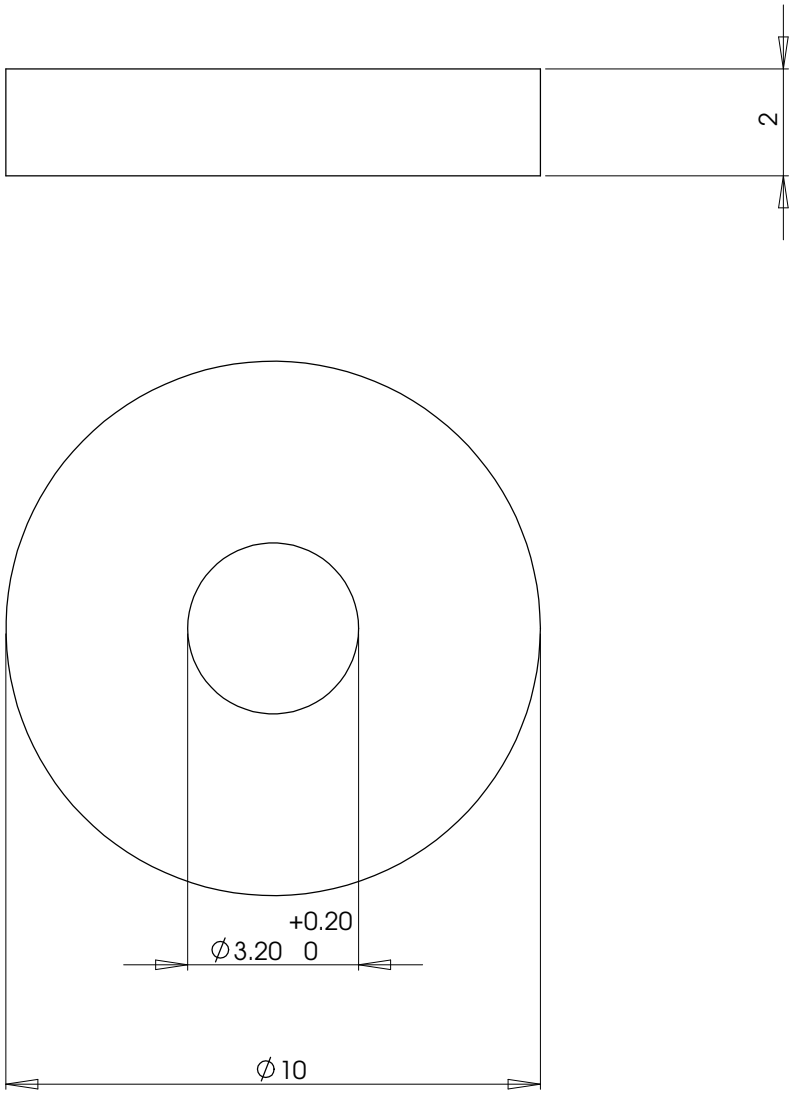

M3 x 10 x 2 WASHER

SCHOOL OF ENGINEERING
MECHANICAL ENGINEERING DEPARTMENT

		Drawn: Ben Low	Date: Nov 04
No. Required: 1	Material: MILD STEEL	Checked:	DRG No. 536
Scale: 10 : 1 (A3)	All Dimensions in mm	Approved:	

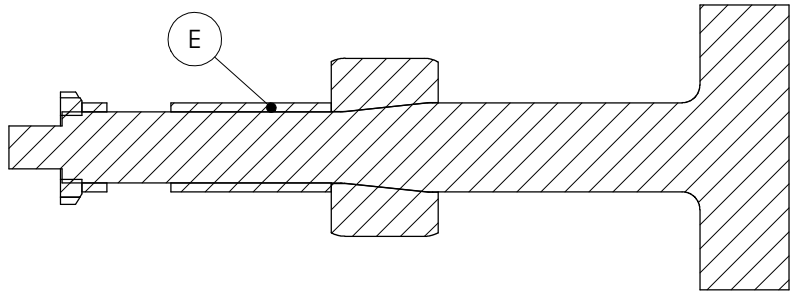

Section A-A

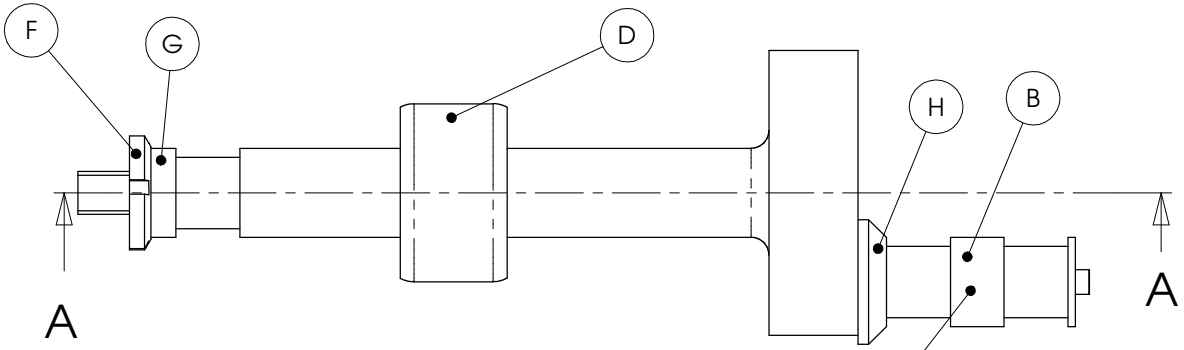

Crank Arm Configuration
for Station 1 & 2 *

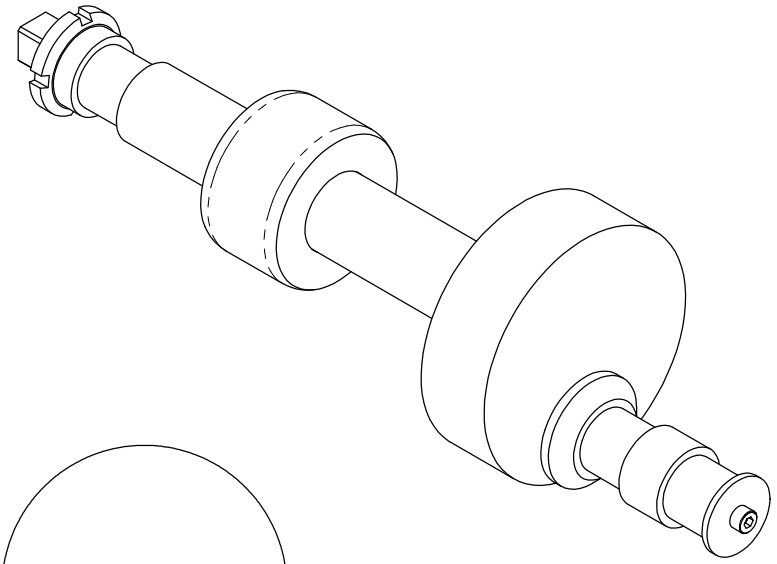

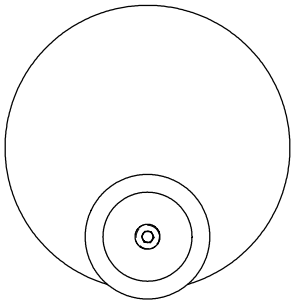

Crank Arm Configuration
for Station 3

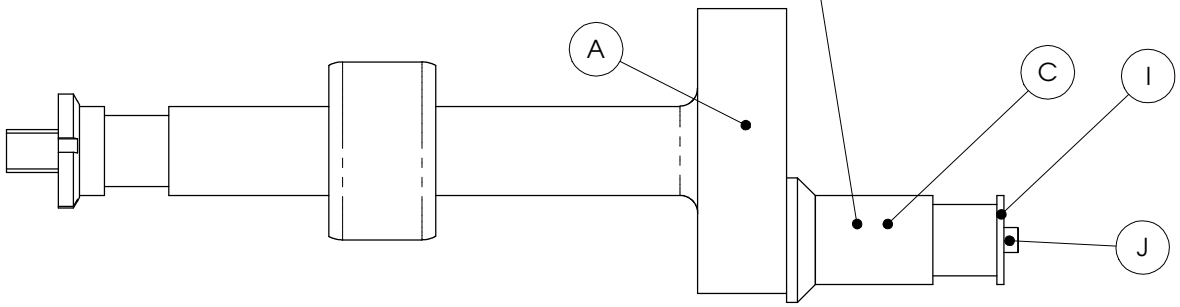

Item	Part No.	Description
A	610	FE Crank Shaft
B	620	FE Crank Arm Spacer Short
C	621	FE Crank Arm Spacer Long
D	630	CoCr Cylinder
E	631	CoCr Cylinder Retaining Sleeve
F	632	KM4 Lock Nut M20x1
G	633	FE Lock Nut Spacer
H	241	Conrod Bearing Spacer 20mm ID
I	242	Washer M4x25x2
J	254	M4 x 8 Cap Screw

FE Crank Shaft
General Assembly
& Bill of Materials

SCHOOL OF ENGINEERING
MECHANICAL ENGINEERING DEPARTMENT

Drawn: Ben Low | Date: Oct 04

Checked: | DRG No. 600

Approved:

Scale: 1 : 1.5 (A3) All Dimensions in mm

* Station 1 is the closest to the motor / gearbox

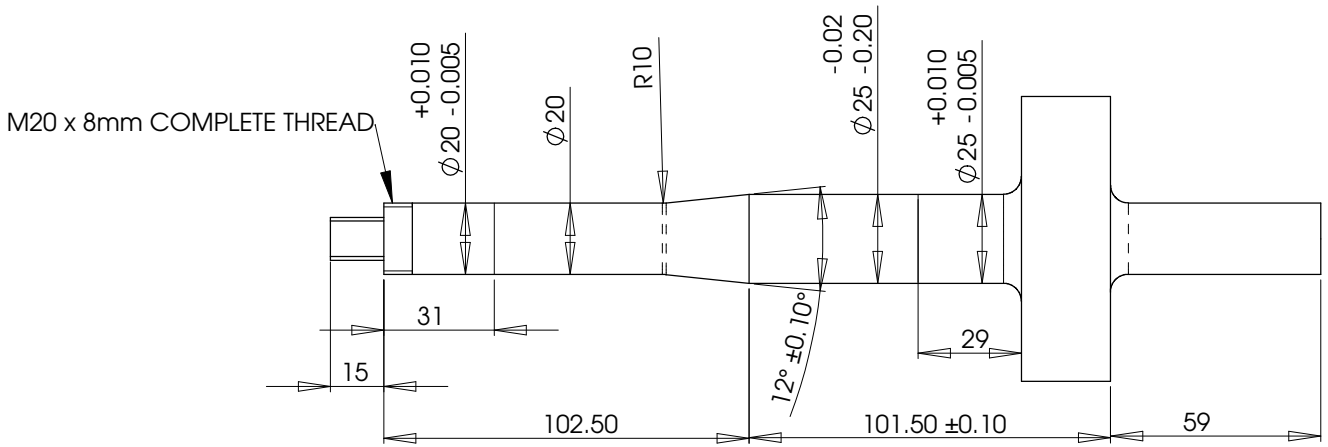

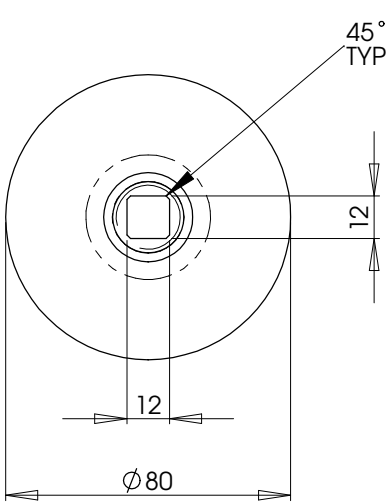

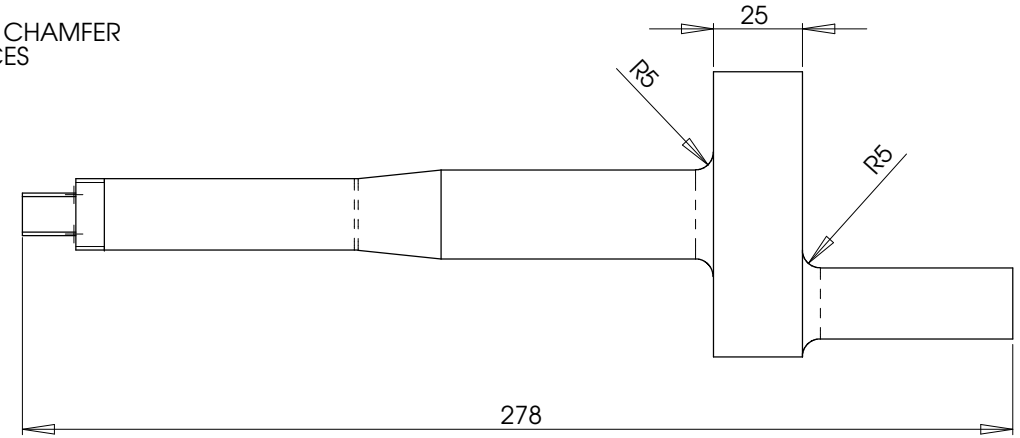

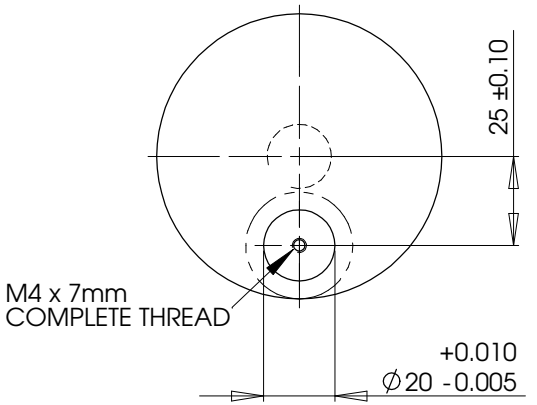

FE CRANKSHAFT		SCHOOL OF ENGINEERING MECHANICAL ENGINEERING DEPARTMENT	
		Drawn: Ben Low	Date: Nov 04
No. Required: 3	Material: 4340 STEEL	Checked:	DRG No. 610
Scale: 1 : 1.5 (A3)	All Dimensions in mm	Approved:	

FE CRANK ARM SPACER - SHORT
PART NO: 620
NO REQUIRED: 2

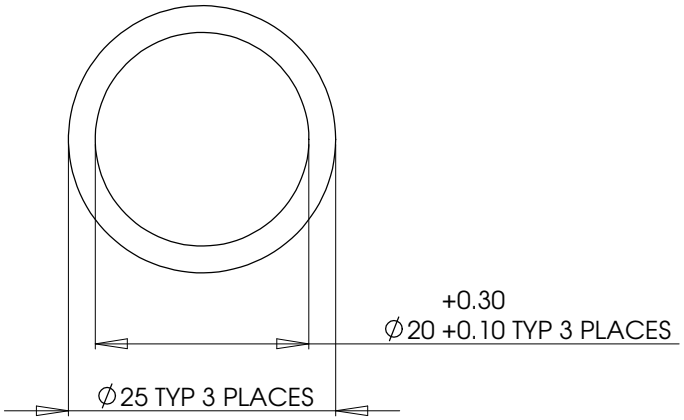

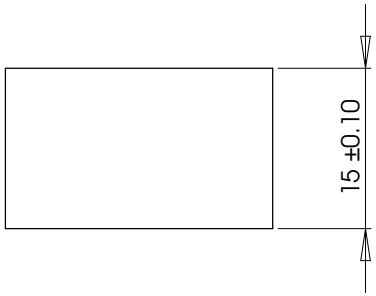

FE CRANK ARM SPACER - LONG
PART NO: 621
NO REQUIRED: 1

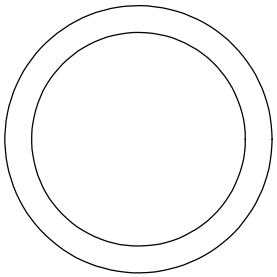

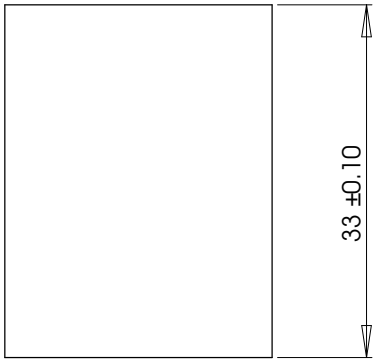

FE LOCK NUT SPACER
PART NO: 633
NO REQUIRED: 3

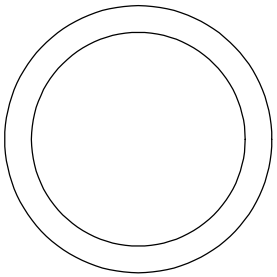

FE SHAFT SPACERS		SCHOOL OF ENGINEERING MECHANICAL ENGINEERING DEPARTMENT	
		Drawn: Ben Low	Date: Nov 04
No. Required:	Material: MILD STEEL	Checked:	DRG No.
Scale: 2 : 1 (A3)	All Dimensions in mm	Approved:	620, 621 & 633

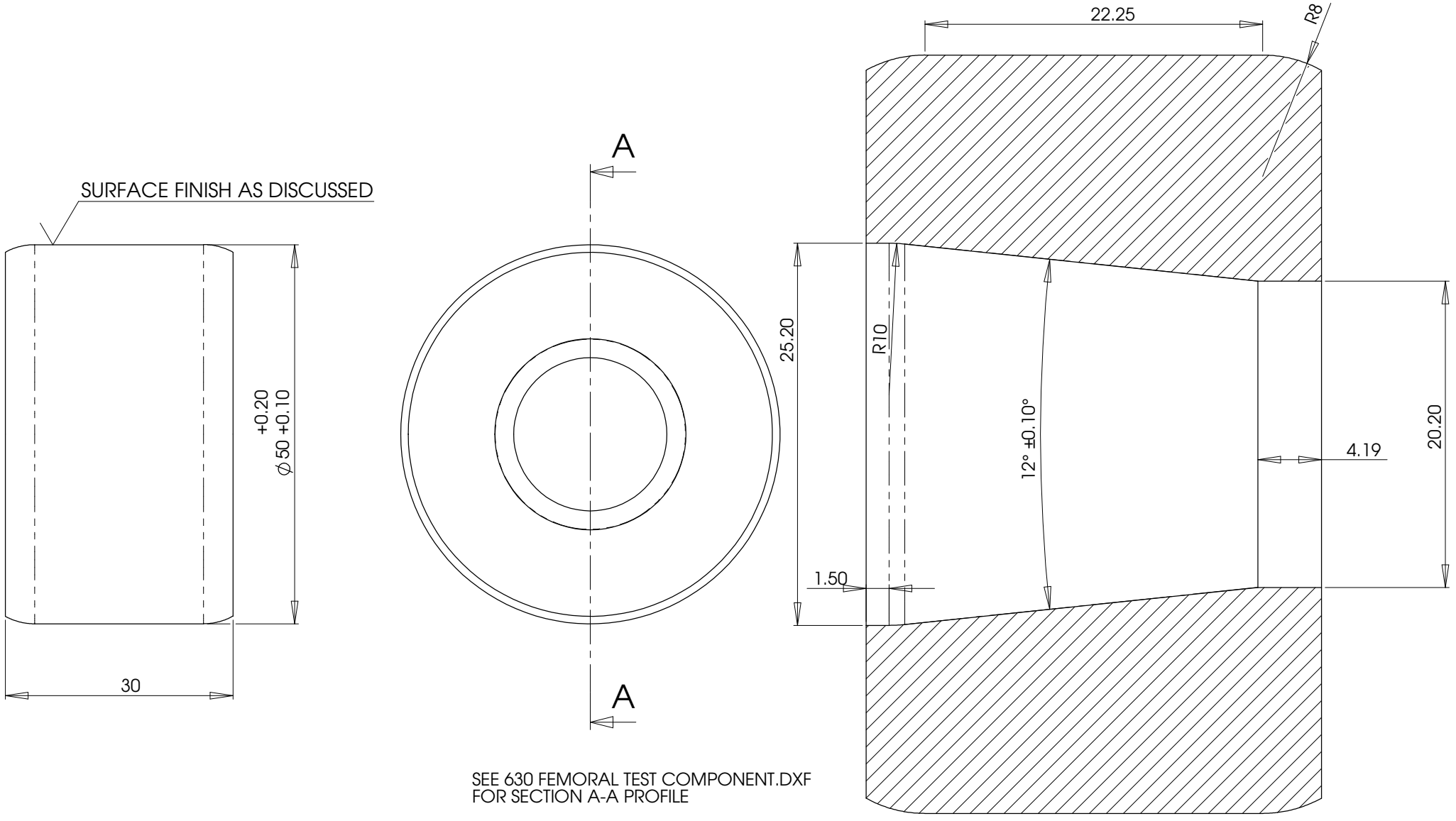

SEE 630 FEMORAL TEST COMPONENT.DXF
FOR SECTION A-A PROFILE

A-A (4 : 1)

FEMORAL TEST COMPONENT

PREVIOUSLY COCR TEST COMPONENT

SCHOOL OF ENGINEERING
MECHANICAL ENGINEERING DEPARTMENT

		Drawn: Ben Low	Date: April 05
No. Required: 3	Material: 316L Stainless	Checked:	DRG No. 630
Scale: 2 : 1 (A3)	All Dimensions in mm	Approved:	

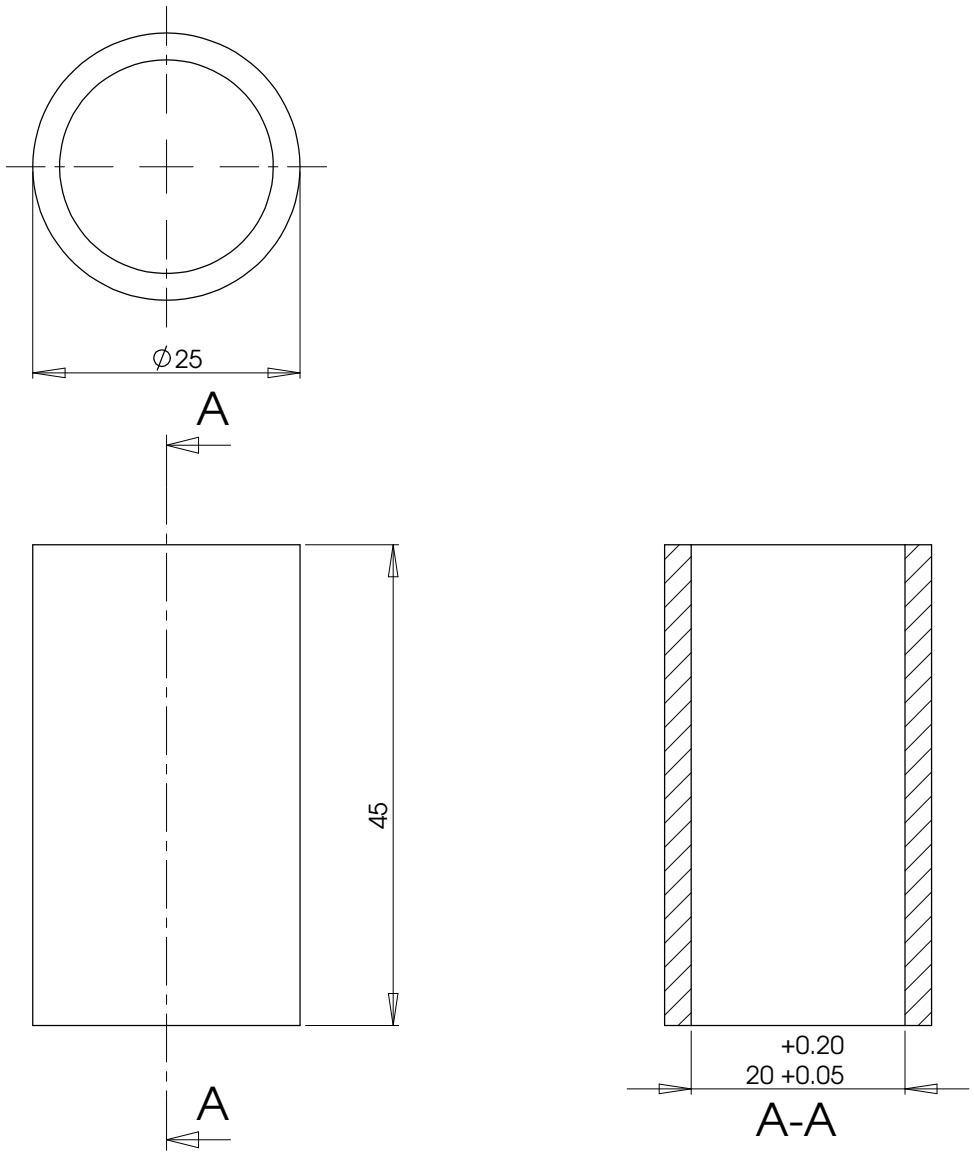

CoCr RETAINING SLEEVE		SCHOOL OF ENGINEERING MECHANICAL ENGINEERING DEPARTMENT	
		Drawn: Ben Low	Date: Nov 04
No. Required: 3	Material: 316 STAINLESS	Checked:	DRG No. 631
Scale: 2 : 1 (A3)	All Dimensions in mm	Approved:	

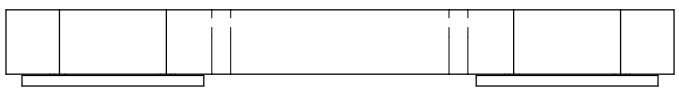

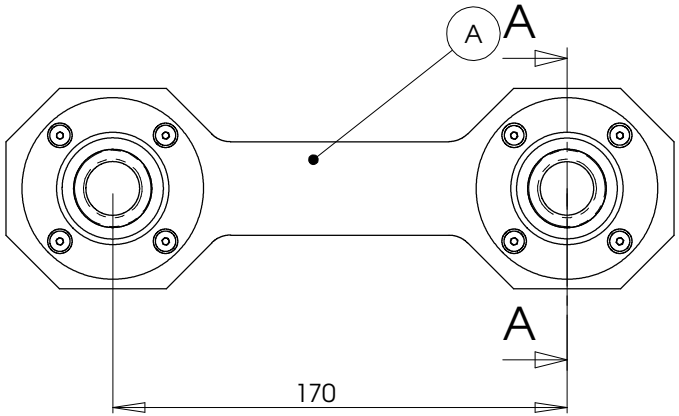

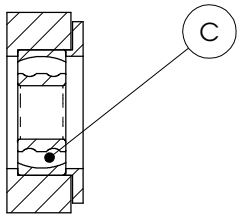

A-A

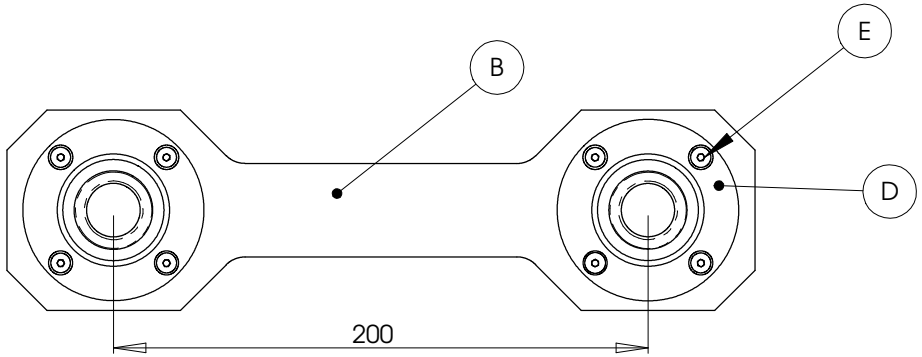

Item	Part No.	Description
A	710	Conrod
B	711	Joining Rod
C	712	2204-2RS1 Self Aligning Bearing
D	163	Bearing Retaining Ring 47mm
E	194	M4 x 10 C-Sunk Cap Screw

CONROD & JOINING ROD ARE IDENTICAL
APART FROM CENTER DISTANCE

CONROD & JOINING ROD GENERAL ASSEMBLY & BILL OF MATERIALS

SCHOOL OF ENGINEERING
MECHANICAL ENGINEERING DEPARTMENT

		Drawn: Ben Low	Date: Nov 04
No. Required:	Material:	Checked:	DRG No. 700
Scale: 1 : 1.5 (A3)	All Dimensions in mm	Approved:	

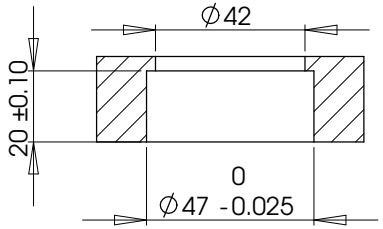

A-A

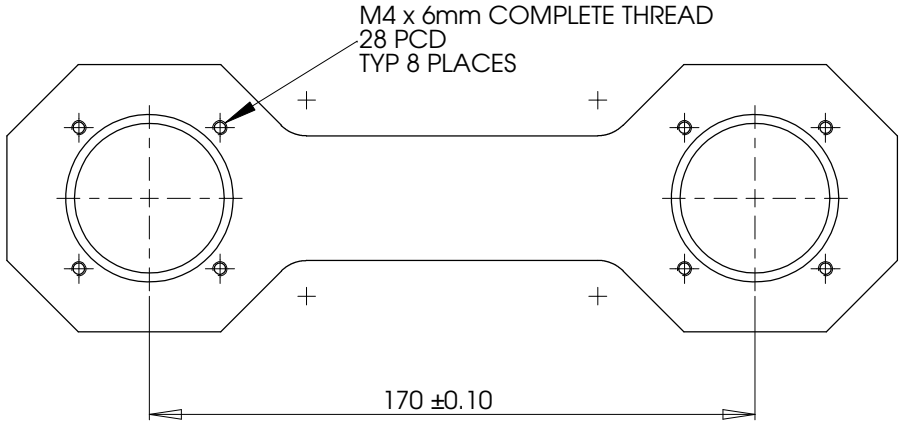

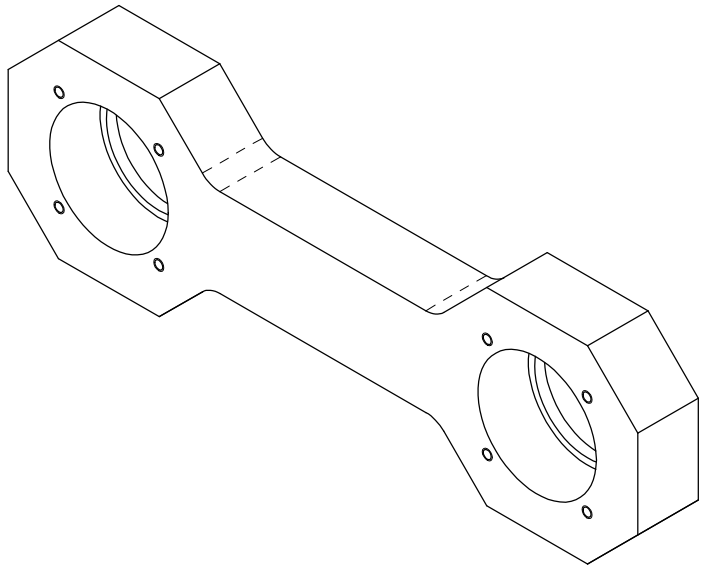

CONROD		SCHOOL OF ENGINEERING MECHANICAL ENGINEERING DEPARTMENT	
		Drawn: Ben Low	Date: Nov 04
No. Required: 2	Material: MILD STEEL	Checked:	DRG No. 710
Scale: 1 : 1.5 (A3)	All Dimensions in mm	Approved:	

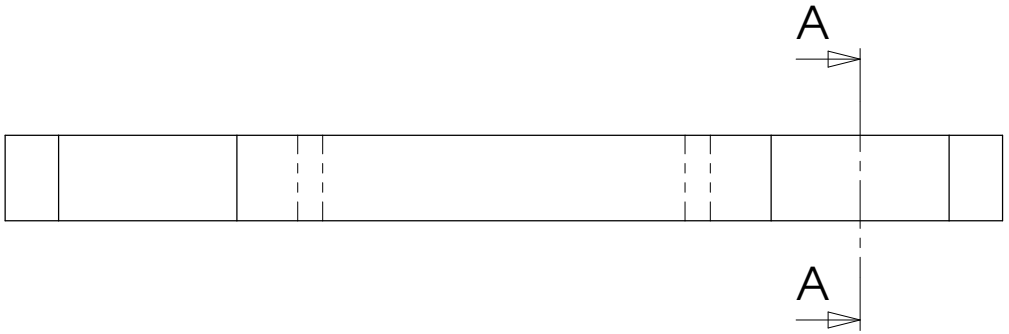

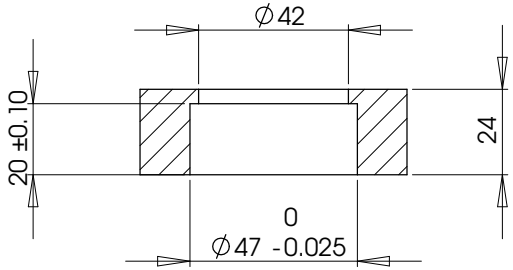

A-A

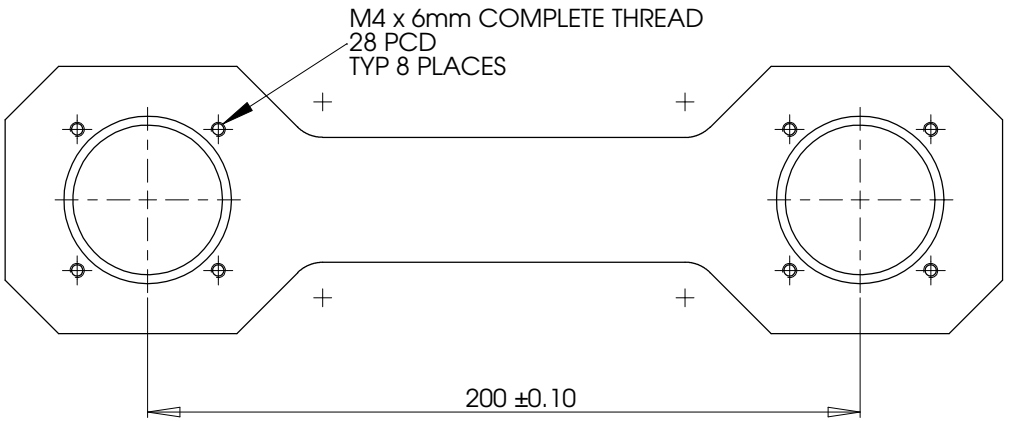

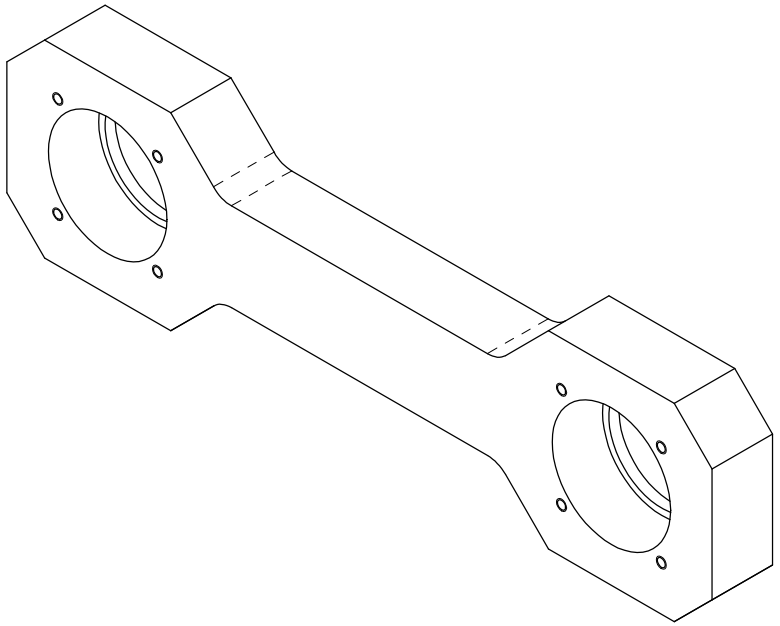

JOINING ROD		SCHOOL OF ENGINEERING MECHANICAL ENGINEERING DEPARTMENT	
		Drawn: Ben Low	Date: Nov 04
No. Required: 2	Material: MILD STEEL	Checked:	DRG No. 711
Scale: 1 : 1.5 (A3)	All Dimensions in mm	Approved:	

IE CONROD
PART NO: 810
NO. REQUIRED: 1

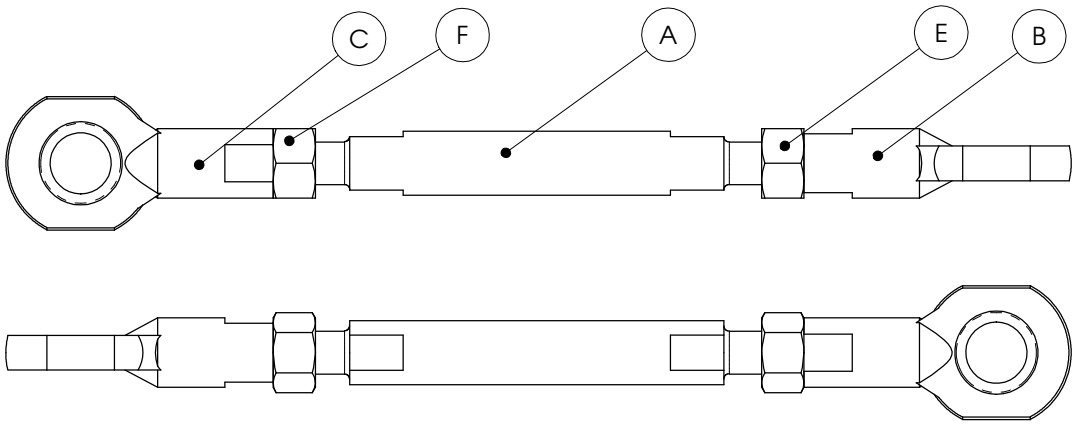

IE JOINING ROD
PART NO: 820
NO. REQUIRED: 2

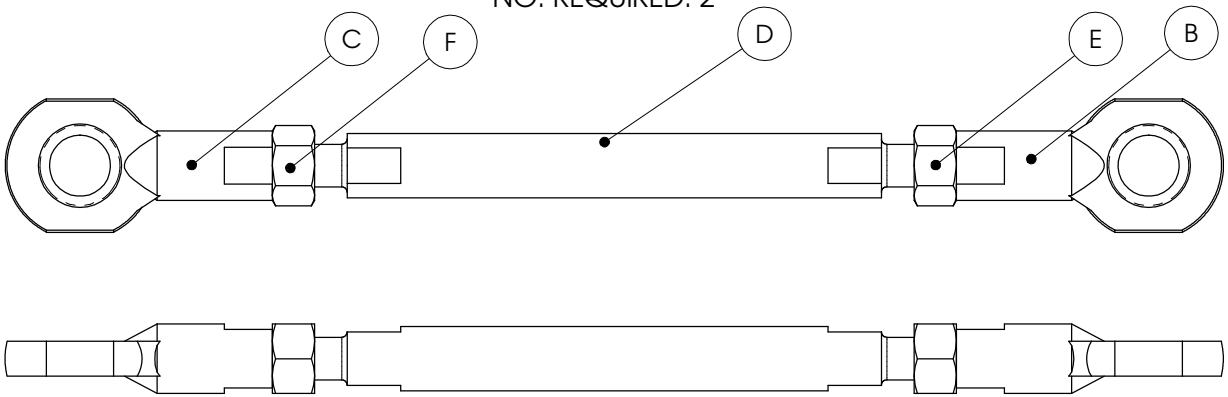

Item	Part No.	Description
A	810	IE Conrod
B	811	Rod End SI_8_E
C	812	Rod End SIL_8_E
D	820	IE Joining Rod
E	830	M8 Nut
F	831	LH M8 Nut

IE CONROD & JOINING ROD GENERAL ASSEMBLY & BILL OF MATERIALS

SCHOOL OF ENGINEERING
MECHANICAL ENGINEERING DEPARTMENT

		Drawn: Ben Low	Date: Nov 04
No. Required:	Material:	Checked:	DRG No. 800
Scale: 1: 1 (A3)	All Dimensions in mm	Approved:	

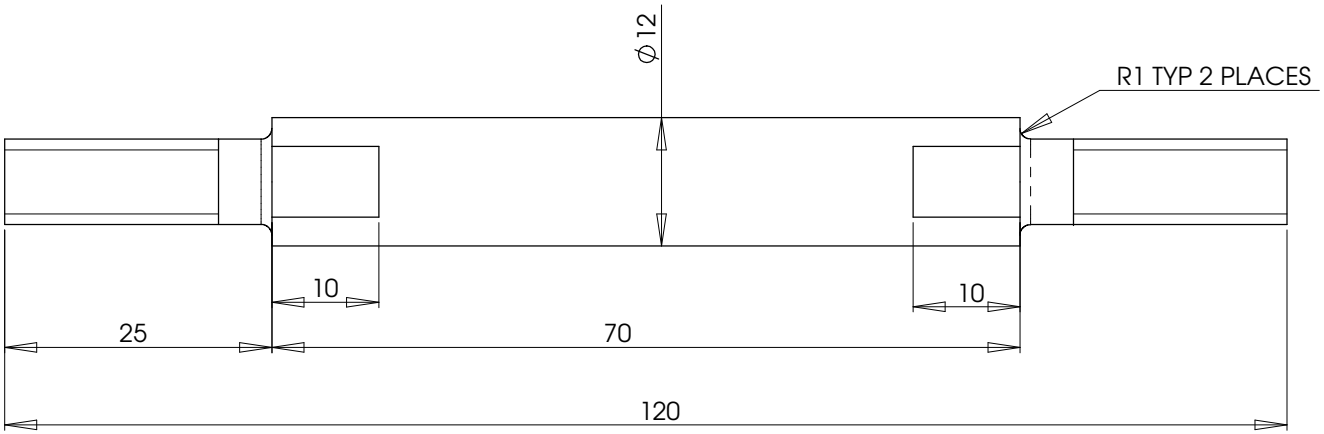

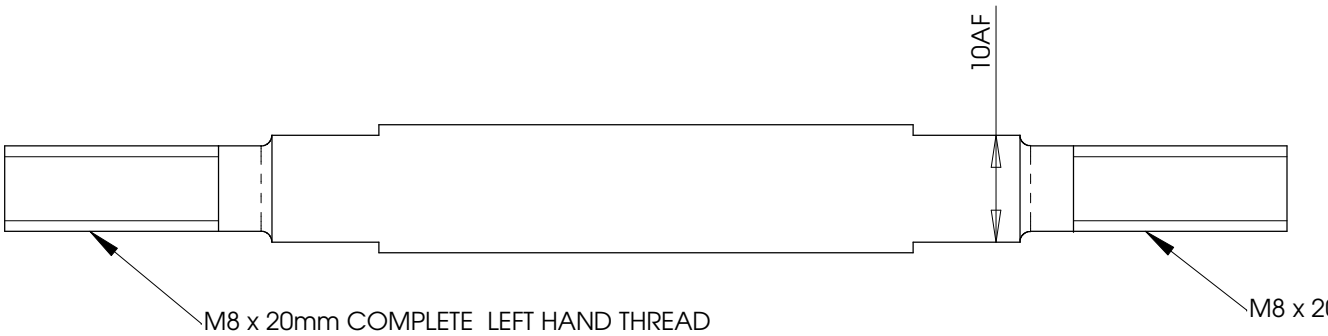

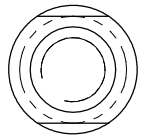

IE CONROD		SCHOOL OF ENGINEERING MECHANICAL ENGINEERING DEPARTMENT	
		Drawn: Ben Low	Date: Nov 04
No. Required: 1	Material: MILD STEEL	Checked:	DRG No. 810
Scale: 2 : 1 (A3)	All Dimensions in mm	Approved:	

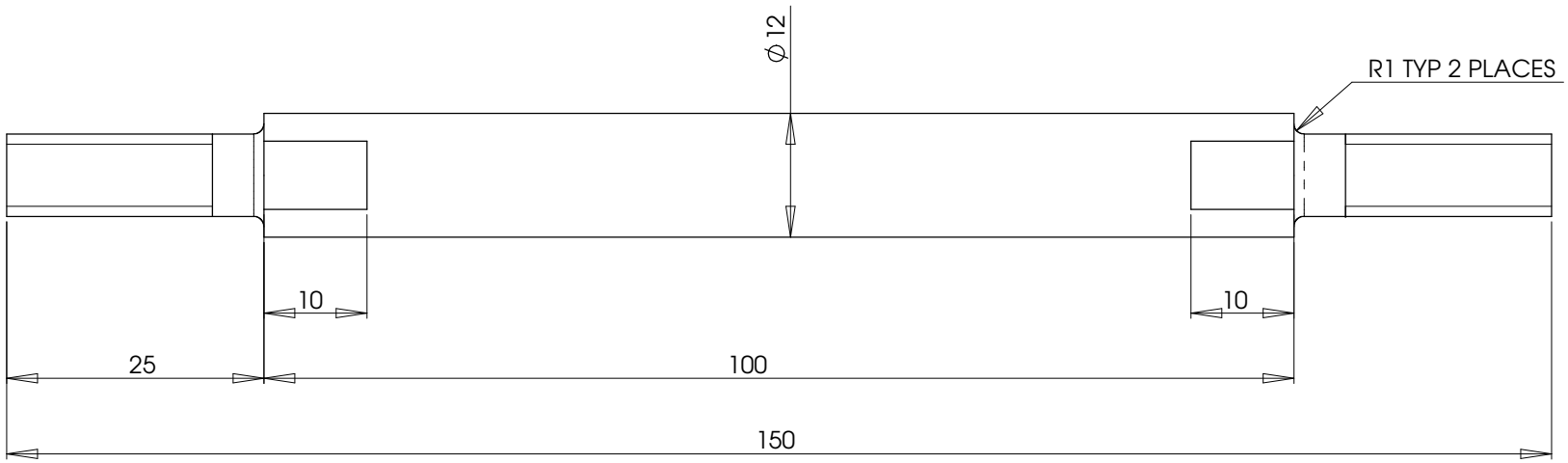

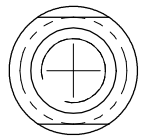

IE JOINING ROD

SCHOOL OF ENGINEERING
MECHANICAL ENGINEERING DEPARTMENT

		Drawn: Ben Low	Date: Nov 04
No. Required: 2	Material: MILD STEEL	Checked:	DRG No. 820
Scale: 2 : 1 (A3)	All Dimensions in mm	Approved:	

Cutting List			
Material: 1" x 1" RHS			
Item	Length	No. Required	
A	1090	2	
B	900	1	
C	400	6	
D	610	1	
E	85	1	
F	154.2	1	
G	115	2	
H	140.4	1	
I	265	1	
J	410	4	

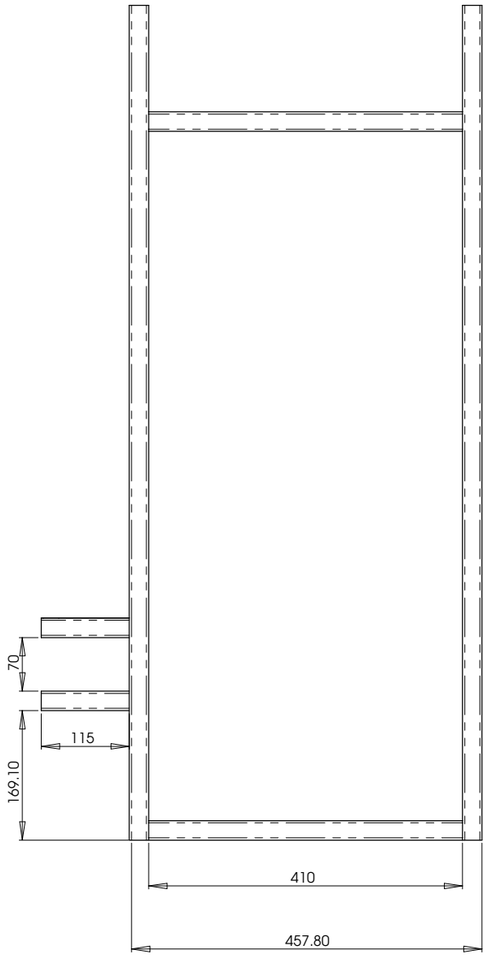

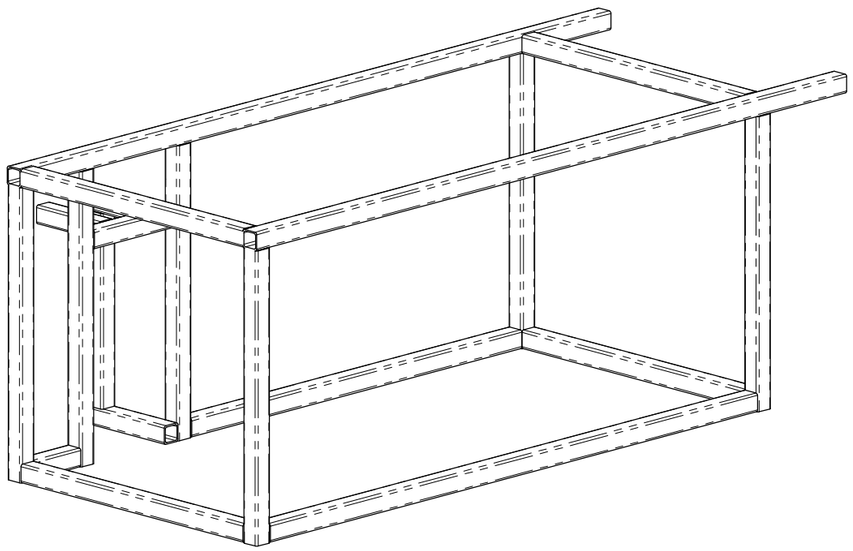

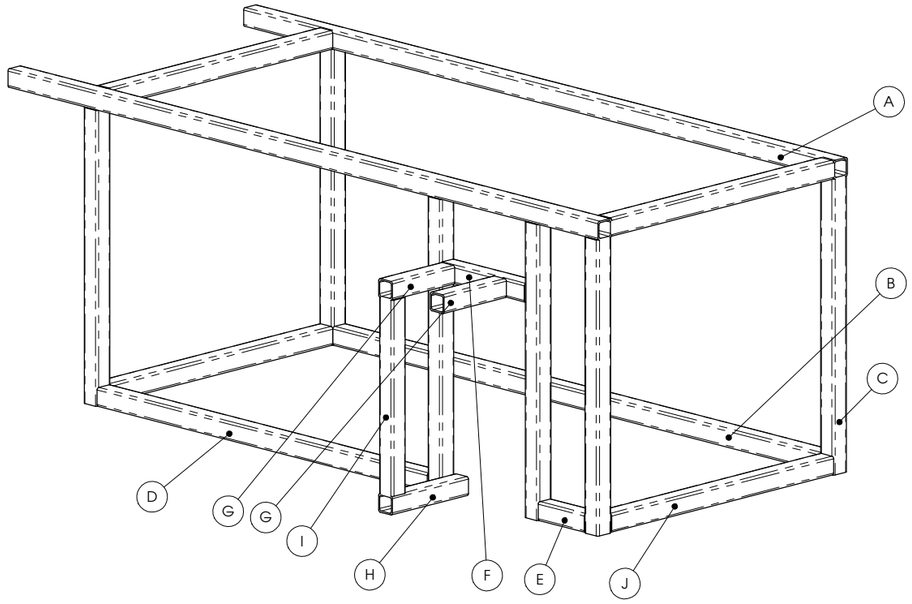

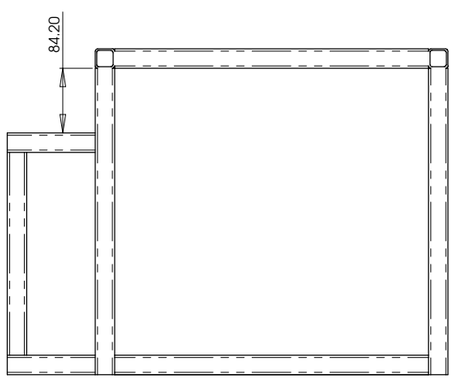

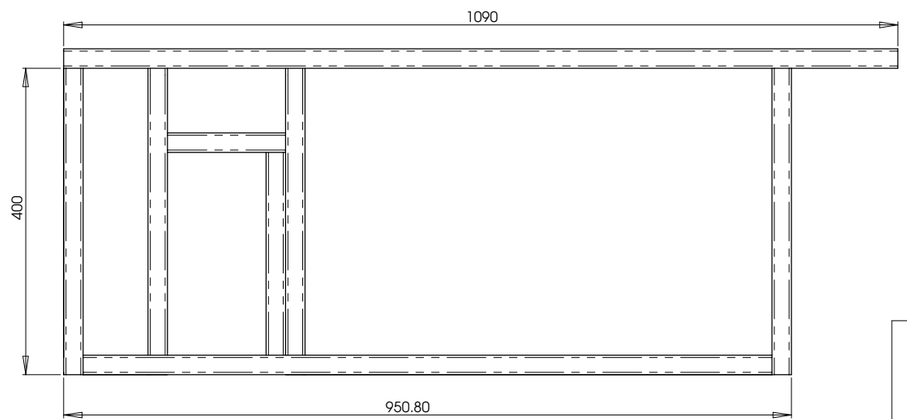

SAFETY GUARD FRAME	UNIVERSITY OF CANTERBURY MECHANICAL ENGINEERING DEPT. CH.CH. N.Z.	
	DRAWN : Ben Low	DATE : May05
	CHECKED :	DRG. No : 910
SCALE:1 : 4 (A1) ALL DIMENSIONS IN mm	APPROVED :	

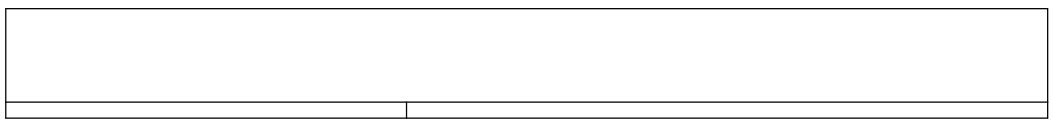

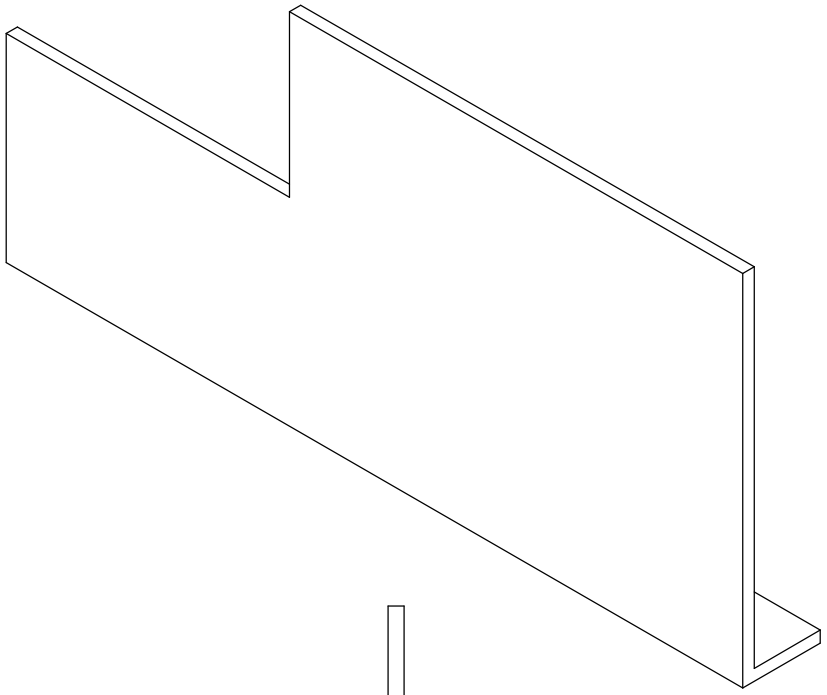

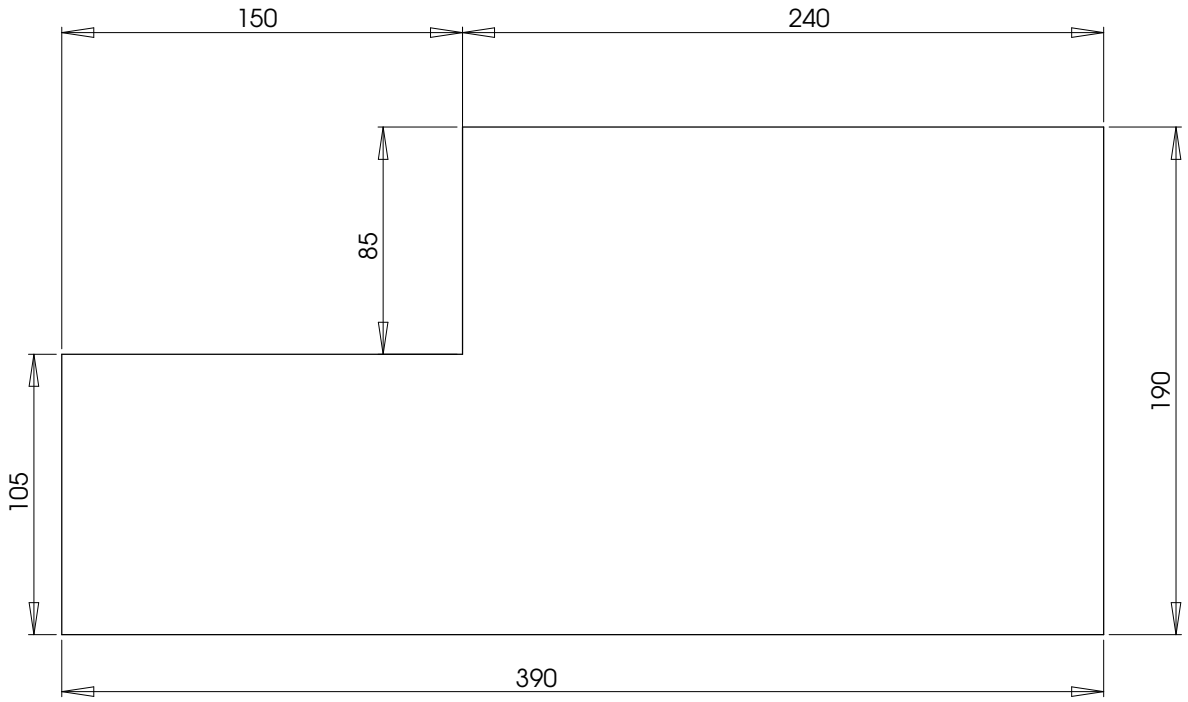

		SCHOOL OF ENGINEERING MECHANICAL ENGINEERING DEPARTMENT	
		Drawn: Ben Low	Date: Nov 04
No. Required:	Material: Perspex	Checked:	DRG No. 920
Scale:	All Dimensions in mm	Approved:	